THE UNIVERSITY *of* EDINBURGH

Rare semi-leptonic B meson decays

James Lyon

Doctor of Philosophy
University of Edinburgh
2013

Declaration

I declare that this thesis was composed by myself and that the work contained therein is my own, except where explicitly stated otherwise in the text.

(*James Lyon*)

Abstract

In this thesis, novel corrections to $B \to X\gamma$ and $B \to Xl^+l^-$ decays, where X is a pseudoscalar or vector meson, are presented. These are the chromomagnetic matrix element, weak annihilation in a general four-quark operator basis and a long-distance charm loop contribution.

The calculation of the chromomagnetic matrix element completes the calculation of matrix elements for all relevant effective weak operators in $B \to V\gamma$ decays, removing an infrared divergence which previous computations had treated in a very approximate way. It also encounters an interesting technical obstacle not previously seen in sum rule calculations, which is likely to be encountered regularly in future once higher order loop diagrams are calculated. The potential for this term to contribute to the CP asymmetry in $D \to V\gamma$ in the presence of new physics is discussed.

The improved computation of weak annihilation diagrams is applied to the analysis of isospin asymmetries in radiative and semi-leptonic $B \to (\rho, K^{(*)})$ decays, and the computation of long-distance charm bubble terms is applied to produce an improved prediction for time-dependent CP asymmetries in various $B \to V\gamma$ decays.

Contents

Chapter 1

Introduction

One of the goals of science is to explain the behaviour of complex systems in terms of simpler components, and to infer underlying principles which explain as wide a range as possible of observations. The pursuit of ever simpler building blocks led to the discoveries that chemicals are comprised of atoms, atoms of electrons and nuclei, and nuclei of protons and neutrons. Subsequently a number of other particles which are not constituents of normal matter were discovered, and the study of these, along with the smallest building blocks of normal matter, is what came to be known today as elementary particle physics.

Elementary particle physics was undoubtedly hugely successful throughout the second half of the 20^{th} century, culminating in the introduction of the Standard Model (SM) in the 1960s and '70s [1–9], which explained all observations in particle physics at that time as well as predicting the existence of a number of then unobserved fundamental particles. Subsequent experiments have identified all of the predicted particles, although some at considerably different masses to those expected, culminating in the experimental discovery of the Higgs boson in 2012 [10, 11]. In all this time, the only modification made to the SM has been the inclusion of neutrino mass following the observation of solar neutrino oscillation at the Sudbury Neutrino Observatory and Kamiokande experiments in the 1990s [12, 13].

For all of this success, the SM still leaves a number of questions unanswered. Unification with general relativity has been a long-standing goal of theoretical physicists but has so far proven technically difficult, and since the reach of particle physics experiments is unlikely to allow small scale observation of gravitational effects for the foreseeable future, this is likely to remain a largely mathematical exercise. Aside from this, the SM itself contains several open problems, most notably the hierachy problem and the puzzle of its matter content and couplings. The hierarchy problem is enticing since it suggests that the Higgs boson mass should be unstable against quantum corrections, and therefore it is hoped that new particles exist at masses not much larger than that of the Higgs to resolve this problem. The leading theoretical candidate

for these new particles today is supersymmetry, although lack of experimental discovery so far at the Large Hadron Collider (LHC) has somewhat dampened optimism that it should be within easy reach.

As for the particle content and couplings of the SM, there are two essentially orthogonal puzzles. First, the cancellation of gauge anomalies between quarks and leptons within a family, which would seem to imply that the SM charge assignments arise from some underlying structure. Second, the question of why there are three families and why they appear to have a hierarchical mass structure. Experiments at the Large Electron-Positron collider indicated that if a fourth family exists, it is unlike the three already known since the Z boson only appears to decay to three types of neutrino [14]. As for the mass hierarchy, although much theoretical work has been done [15], there is presently no conclusive evidence of physics beyond the SM.

So then, what is B physics and what role does it play in all of this? The answer to the first question is straightforward: B physics studies the decays of the b quark, which are measured indirectly through the decays of heavy mesons containing b quarks. As for the second, these decays are particularly interesting because they probe the flavour sector of the SM, which contains the only known CP violating phase. Thorough experimental understanding of this sector is therefore desirable since it is believed that the amount of CP violation in the SM is not nearly sufficient to account for the observed baryon asymmetry of the universe [16, 17].

Aside from the top quark, the b is the heaviest quark in the standard model, but unlike the top it is sufficiently long lived to hadronise. Still, the fact that the b quark mass is much larger than the scale of quantum chromodynamics (QCD) means that perturbation theory remains an effective tool for computing B meson processes; non-perturbative effects can be separated from short distance physics and grouped by inverse powers of the B meson mass. Since the QCD aspects of B mesons can be handled well within perturbation theory, decay rates can be predicted directly in terms of the SM electroweak sector and a small number of non-perturbative QCD parameters, allowing indirect tests of the electroweak sector. The large number of different decay channels enables many independent tests of the SM to be performed, and likewise many independent constraints on its parameters, and deviations in any channel would be a likely indication of new physics. This complements the results of high energy collision experiments which aim to produce new particles on or near the mass shell. The study of B meson decays has been ongoing since the exclusive lifetime was measured at the Large Electron-Positron collider [18,19]; subsequently the dedicated B physics experiments BaBar and Belle were performed, and today the LHCb experiment is continuing to provide more precise measurements of B decays as part of the LHC experimental programme [20]. As with the other LHC experiments, although some tantalising hints of non-SM physics have been seen [21, 22], it is still likely as not that better statistics will confirm the SM picture.

This thesis will focus on semi-leptonic heavy-to-light B meson decays. Various new contributions to these decays are computed, and their importance to isospin and CP asymmetries

will be analysed. The remainder of this thesis is organised as follows:

Chapter 2 General theoretical background and methods used to perform calculations in B physics are discussed, and conventions are established. The ultra-relativistic approximation is introduced and evaluated in light of the results for the isospin asymmetry in Chapter 5.

Chapter 3 The contribution of the chromomagnetic operator to semi-leptonic B decays is calculated. The differences between the light cone sum rules and QCD factorisation approaches are highlighted, and the infrared singularities are discussed. This calculation runs into a significant technical obstacle due to the need to separate states with B meson quantum numbers from light states in the sum rule. The details of this problem are presented, and the resulting implications for constructing multi-loop sum rules are pondered.

Chapter 4 A scenario for sizeable CP asymmetry in D meson decays, through the chromomagnetic operator whose matrix elements are calculated in Chapter 3, is presented.

Chapter 5 The isospin asymmetry in $B \to (K, K^*, \rho) l^+ l^-$ is calculated using light cone sum rules (LCSRs) for all four-quark operators up to dimension 6. This is applied to the SM operator basis to obtain a prediction for this asymmetry and loose constraints on beyond-SM operators. Selection rules for operators in each process are discussed which allow deviations from the SM prediction to appear much more strongly in specific channels if beyond-SM physics does not couple to $V - A$ currents.

Chapter 6 The contribution of charm loops with soft gluon emission to $B \to V l^+ l^-$ decay is calculated. It is analysed in the context of other non-factorisable charm bubble terms and its contribution to the right-handed decay amplitude in the SM, where it appears to dominate since the parity conserving and violating amplitudes are not related in this case.

Chapter 7 A summary of the results of each chapter is given, along with concluding remarks on how the calculations in this thesis may be further improved in future.

Chapter 2

Preliminaries

In this chapter the basic techniques used throughout this thesis to compute heavy meson decays will be discussed.

2.1 Conventions

The process of writing down a quantum field theory usually involves a certain amount of freedom of choice, where signs and basis conventions can be changed without affecting any observables of the theory. It is rather unfortunate although perhaps inevitable that some of these choices have not developed universally accepted conventions, and so comparison between results of different papers can occasionally be rather laborious if it is not made clear what the effects of conventions are.

In this thesis, the covariant derivative is taken to be

$$D_\mu = \partial_\mu - ieQA_\mu - ig\frac{\lambda^a}{2}A^a_\mu \quad , \tag{2.1}$$

which leads to interaction vertices with fermions of the form $+ie\gamma^\mu$ and $ig\gamma^\mu\frac{\lambda^a}{2}$, where λ^a are the Gell-Mann matrices and Q is the particle charge, either $+2/3$ or $-1/3$ for quarks and -1 for leptons. The gauge charges e and g are both taken to be positive. This agrees with [23][1].

The totally antisymmetric Levi-Civita tensor is defined to satisfy $\epsilon_{0123} = +1$, which follows [24] but not [23]. This enters Dirac traces through

$$\mathrm{Tr}\{\gamma^\mu\gamma^\nu\gamma^\rho\gamma^\sigma\gamma_5\} = 4i\epsilon^{\mu\nu\rho\sigma} \ . \tag{2.2}$$

Note that this definition is only meant to imply the sign of the traces involving γ_5 and not its

[1] Somewhat confusingly [23] sometimes absorbs the electron charge $Q = -1$ into this definition to give $D_\mu = \partial_\mu + ieA_\mu$.

D-dimensional extension, which will be discussed in Section 2.4. This convention also disagrees with the default choice of FeynCalc[2] [25].

2.2 The Standard Model (SM)

The SM is the long standing and highly successful model underpinning the current state of theoretical particle physics developed during the 1960s and '70s [1–9]. Its basic ingredients are well known: it has three generations of fermions, each containing quarks and leptons, and a single scalar Higgs field, which interact via Yukawa couplings and a gauged $SU(3) \times SU(2)_L \times U(1)_Y$ symmetry. Putting all of these ingredients together (e.g. [23]), the Lagrangian density for the matter and Higgs sectors may be written

$$\begin{aligned}\mathcal{L} = &-\frac{1}{4}F^a_{\mu\nu}F^a_{\mu\nu} + \sum_i i\bar{Q}^i_L \not{D} Q^i_L + \sum_i \left[i\bar{u}^i_R \not{D} u^i_R + i\bar{d}^i_R \not{D} d^i_R\right] + (D_\mu H)^\dagger (D^\mu H) \\ &+ \mu^2 H^\dagger H - \lambda (H^\dagger H)^2 - \sum_{i,j} \bar{Q}^i_L \left[y^{ij}_u \tilde{H} u^j_R + y^{ij}_d H d^j_R\right] + \text{h.c.} + \text{leptons} \quad ,\end{aligned} \tag{2.3}$$

where $Q^i_L = (u^i_L, d^i_L)$ are left-handed $SU(2)$ quark doublets and u_R, d_R are right-handed quark fields, $\tilde{H}^a \equiv \epsilon^{ab} H^\dagger_b$ is the Higgs field transformed to the $SU(2)$ anti-fundamental representation, and the covariant derivative D_μ implies inclusion of all gauge fields necessary for the field it acts on. The lepton sector has not been written out in full since its dynamics will play no role in this thesis. The "Mexican hat" shape of the Higgs potential $\lambda|H|^4 - \mu^2|H|^2$ implies a non-trivial minimum of the effective action and therefore that $\langle H \rangle \neq 0$ in the vacuum. For interactions at scales small compared to the Higgs vacuum expectation value (VEV), the basis of fields used in (2.3) is therefore inappropriate as there will be large bilinear mixing terms. This is of course the scenario of interest for B meson decays.

Rewriting (2.3) accounting for the non-zero Higgs VEV has several consequences. The first of these is that the quarks, leptons and W and Z bosons become massive. Since the solar neutrino oscillation experiments of the '90s, neutrinos are also known to have mass [12,13], but their masses are too small to have an effect in accelerator experiments. The mass terms for the quarks are then given by

$$\bar{Q}^i_L y^{ij}_u \langle \tilde{H} \rangle u^j_R \equiv y^{ij}_u m_0 \bar{u}^i_L u^j_R \qquad\qquad \bar{Q}^i_L y^{ij}_d \langle H \rangle d^j_R \equiv m_0 y^{ij}_d \bar{d}^i_L d^j_R \quad , \tag{2.4}$$

where the up/down type of the left-handed quarks is defined by the direction of the Higgs VEV. The mass basis for the quarks is given by the singular value decomposition (e.g. [26]) of the matrices $y_{u,d}$ as

$$y_{u,d} = U_{u,d} \Sigma_{u,d} W^\dagger_{u,d} \quad . \tag{2.5}$$

[2] This convention can be changed; see appendix A.

The diagonal matrix $m_0\Sigma_{u,d}$ then gives the quark masses. The $W_{u,d}$ matrices can be absorbed into the definitions of the right-handed fields u_R, d_R without affecting any other terms in the SM Lagrangian and are thus unphysical. The same cannot be said of the U matrices: after the change of basis

$$u_L = U_u u'_L \qquad\qquad d_L = U_d d'_L \quad , \tag{2.6}$$

the gauge interaction with the $SU(2)_L$ field, labelled B_μ, after expanding the Pauli matrix components becomes

$$\begin{aligned}\frac{1}{\sqrt{2}}\begin{pmatrix} \bar{u}'_L U_u^\dagger & \bar{d}'_L U_d^\dagger \end{pmatrix}\gamma_\mu \begin{pmatrix} B_\mu^3 & B_\mu^1 - iB_\mu^2 \\ B_\mu^1 + iB_\mu^2 & -B_\mu^3 \end{pmatrix}\begin{pmatrix} U_u u'_L \\ U_d d'_L \end{pmatrix} \\ = \frac{1}{\sqrt{2}}\begin{pmatrix} \bar{u}'_L & \bar{d}'_L \end{pmatrix}\gamma_\mu \begin{pmatrix} B_\mu^3 & V(B_\mu^1 - iB_\mu^2) \\ V^\dagger(B_\mu^1 + iB_\mu^2) & -B_\mu^3 \end{pmatrix}\begin{pmatrix} u'_L \\ d'_L \end{pmatrix} \quad ,\end{aligned} \tag{2.7}$$

where $V = U_u^\dagger U_d$ is the Cabibbo–Kobayashi–Maskawa (CKM) matrix [27, 28]. Two of the $SU(2)_L$ boson degrees of freedom therefore induce transitions between up- and down-type quarks, while the other is diagonal. The matrix V is unitary since it is the product of two unitary matrices. A 3×3 unitary matrix has nine degrees of freedom: five of these may be eliminated by phase rotations on the six quark flavours (the sixth global phase has no effect) leaving four physically relevant parameters.

Both the fact that the CKM matrix does not appear in the B^3 interaction term and its unitarity are important in the SM. The B^3 component of the $SU(2)_L$ gauge field mixes with the $U(1)_Y$ gauge field to form the photon and the Z boson, and the absence of the CKM matrix here means that there are no tree-level flavour-changing neutral currents (FCNCs) in the SM, so any FCNC process is loop suppressed and expected to be small. Although neutral current decays are rare in comparison with charged current decays and thus correspondingly more difficult to measure precisely, they are interesting objects of study since it may be the case that contributions from beyond-SM physics are significant. The unitarity of the CKM matrix again leads to a suppression of flavour-changing neutral processes: neutral flavour-changing loop processes will take the form $V^\dagger M V$ as seen in Figure 2.1, and thus would be flavour-diagonal were it not for the fact that the interaction matrix M depends on the mass of the intermediate quark. This is known as the Glashow–Iliopoulos–Maiani (GIM) mechanism [29]. It leads to a rather different structure of FCNC decays for heavy up- and down- type quarks since the top quark is so much heavier than the bottom: $b \to s$ and $b \to d$ decays contain large logarithms $\sim \log m_t^2/m_b^2$ but the corresponding logarithms for the charm quark are much smaller $\sim \log m_b^2/m_c^2$. This point will be returned to in Chapter 4.

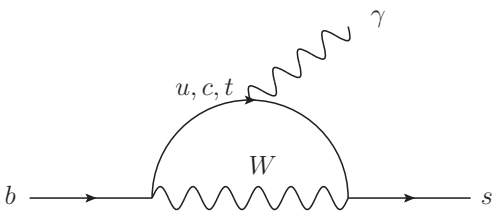

Figure 2.1: Example of a flavour-changing neutral loop process. The appearance of the CKM matrix twice in this diagram in the form $V^\dagger V$ would mean that off-diagonal flavour-changing terms such as $b \to s$ transitions would be zero were it not for the different masses of the up-type quarks.

The standard choice for parametrisation of the CKM matrix is in terms of three Euler angles and a CP violating phase [30]. In this thesis a widespread alternative parametrisation due to Wolfenstein [31] and its all-order extension [32] will be employed. The full expressions are rather lengthy so are not reproduced; however the approximate expression for the CKM matrix in this parametrisation is

$$V = \begin{pmatrix} V_{ud} & V_{us} & V_{ub} \\ V_{cd} & V_{cs} & V_{cb} \\ V_{td} & V_{ts} & V_{tb} \end{pmatrix} = \begin{pmatrix} 1 - \frac{\lambda^2}{2} & \lambda & A\lambda^3(\rho - i\eta) \\ -\lambda & 1 - \frac{\lambda^2}{2} & A\lambda^2 \\ A\lambda^3(1 - \rho - i\eta) & -A\lambda^2 & 1 \end{pmatrix} , \tag{2.8}$$

which is accurate up to $O(\lambda^4)$ corrections. This expansion in a small parameter $\lambda \approx 0.23$ reveals that the CKM matrix exhibits some structure; it is nearly diagonal and the coefficients for transitions between different quark generations have considerably different magnitudes. The origin of this structure is not yet well understood, though many proposed models exist [15].

2.3 The Renormalisation Group (RG)

As is well known, calculations beyond tree-level in quantum field theory often lead to the appearance of divergent integrals. In order to produce finite predictions, the procedure of renormalisation was developed, where the divergent parts are absorbed into unphysical parameters of the theory. The problem then is that it is not clear that absorbing divergences of all possible diagrams is possible when there are only a finite number of parameters into which to absorb them. In fact the divergences can only be absorbed for a specific class of renormalisable theories – non-renormalisable theories are also common such as the effective electroweak theory, which will be described in Section 2.4, but in that case calculations must be restricted to a fixed perturbative order.

The problem of renormalisation was largely solved by the Bogoliubov–Parasiuk–Hepp–Zimmermann (BPHZ) scheme [33–35] which gives an algorithm for systematically subtracting the divergences of a given Feynman graph. It does not however solve a second problem: quantum field theories usually contain symmetries, notably, as far as the SM is concerned, Yang-

Mills theory, and symmetries are easiest to deal with when they are manifestly preserved. The situation with regard to non-Abelian gauge theories was vastly improved by the introduction of dimensional regularisation under which the gauge symmetry is preserved [36]. This is not entirely without a price: Lorentz invariance must be broken to deal correctly with *chiral* gauge theories in this approach, although problems in chiral gauge theories are virtually inevitable owing to the Adler-Bell-Jackiw anomaly [37, 38].

The effect of regularisation and renormalisation is that the couplings of a quantum field theory acquire a dependence on the regularisation parameter. Since the goal of renormalisation is to eliminate that parameter it is replaced by another parameter using some renormalisation conditions. This parameter is massive, which is in general unavoidable since as it will turn out the divergent integrals correspond to anomalous breaking of scale invariance [39, 40]. The introduction of a new parameter raises the question of whether the theory indeed has more parameters than originally intended or not. In fact, the original coupling and the newly introduced mass scale can be related to each other, and this relation is known as the renormalisation group.

Since at hadronic scales the QCD gauge coupling is much larger than the electromagnetic coupling, it is most common to deal only with loop corrections in α_s and to neglect those in α_{em} and the Fermi coupling G_F. In this case in dimensional regularisation the bare coefficient of an operator c_0 may be written (e.g. [41])

$$c_0(\epsilon) = \mu^{-n\epsilon} Z_c(\epsilon, g(\mu)) c(\mu) \quad , \tag{2.9}$$

where $\epsilon = \frac{4-D}{2}$ and n is found by fixing c to its engineering dimension in the Lagrangian and Z to be dimensionless. c can be a mass, or more usefully in the case of weak decays the coefficient of an effective operator. The renormalisation constant Z_c only depends on the renormalisation scale μ indirectly through the gauge coupling $g(\mu)$ in minimal schemes[3]. The independence of the left-hand side of (2.9) on μ can be exploited to eventually give

$$\mu \frac{dc}{d\mu} = c\left[\gamma_c(g) + n\epsilon\right] \qquad\qquad \mu \frac{dg}{d\mu} = -g\left[\beta(g) + \epsilon\right] \quad , \tag{2.10}$$

where the definition of the β function for the running of the gauge coupling has also been included. It is interesting to note that in order for (2.10) to hold it must be the case that the residue of the $1/\epsilon$ pole in $Z_c(\epsilon, g(\mu))$ carries all information about the scale dependence of c; all more singular poles must be defined in terms of this one, which can provide a non-trivial check on the formalism. (2.10) is, without a perturbative expansion, as much as can be done for the gauge coupling g; however in the case of c it is usual to remove the dependence of c on

[3] The extension to theories with multiple gauge couplings is straightforward since the scale μ can be chosen separately for each coupling.

μ entirely in favour of a dependence on g, which gives

$$\frac{dc}{d\alpha} = -\frac{\gamma_c(\alpha)}{2\alpha\beta(\alpha)} c \xrightarrow[\beta(\alpha)\to\alpha\beta_0/4\pi]{\gamma_c\to\alpha\gamma_c^{(0)}/4\pi} \left(-\frac{\gamma_c^{(0)}}{2\beta_0}\right)\frac{c}{\alpha} \quad , \tag{2.11}$$

where a change of variables to $\alpha \equiv \frac{g^2}{4\pi}$ has been introduced, and this is the form of the renormalisation group equation useful in dealing with effective theories. The factor $-\gamma_0/2\beta_0$ is the result of definitions used to reach (2.10) and this convention shall be used to define the one loop anomalous dimension γ_0 of an operator in this thesis[4], but it is not a universal convention. The leading order solution to (2.11) is then

$$c(\mu_1) = \left(\frac{\alpha(\mu_1)}{\alpha(\mu_2)}\right)^{-\gamma_c^{(0)}/2\beta_0} c(\mu_2) \quad . \tag{2.12}$$

The question that has not yet been addressed is the usefulness of (2.11) and (2.12), which allow the renormalisation scale μ to be varied without affecting physical observables since the bare coupling is held fixed. In practice this relation is not exact since, as in (2.12), it is usual to work at a finite order of perturbation theory and therefore changing the renormalisation point only keeps the physical results fixed up to a certain perturbative order. Although the behaviour of uncalculated terms is in principle unknown, the RG can be exploited to choose the renormalisation point such that the perturbative series should be expected to converge as rapidly as possible. In practical terms loop calculations in quantum field theory result in the appearance of logarithms of the ratio of the external scale q^2, as well as particle masses, to the renormalisation point, that is $\sim \log q^2/\mu^2$. An RG improved calculation will then set $\mu^2 \sim q^2$, so that such logarithms are small.

In a theory with multiple couplings the situation is slightly more complicated: (2.10) must be replaced by

$$\mu\frac{dc_i}{d\mu} = \gamma_{ij}(g)c_j \tag{2.13}$$

in order to account for mixing between different operators. γ_{ij} is known as the anomalous dimension matrix (ADM). If the convention $\gamma_{ij} = \alpha\gamma_{ij}^{(0)}/4\pi$ is adopted at leading order following (2.11), (2.13) can then be rewritten as

$$\frac{dc_i}{d\alpha_s} = -\frac{\gamma_{ij}^{(0)}c_j}{2\alpha_s\beta_0} \quad . \tag{2.14}$$

In order to extend the solution (2.12) to the case of multiple couplings the ADM is diagonalised by

$$c_i^D = V_{ij}c_j \qquad\qquad \gamma_{ij}^D = V_{ik}\gamma_{kl}^{(0)}V_{lj}^{-1} \tag{2.15}$$

[4] Anomalous dimensions are listed for some relevant operators in appendix B.5.

and then the solution takes a very similar form to (2.12):

$$c_i(\mu_1) = \sum_{j,k} V_{ij}^{-1} \left(\frac{\alpha_s(\mu_1)}{\alpha_s(\mu_2)}\right)^{-\gamma_{jj}^D/2\beta} V_{jk} c_k(\mu_2) \quad . \tag{2.16}$$

For higher order calculations it is necessary to solve the flow equation (2.13) beyond the leading order in α_s; sadly in this case an exact analytic solution cannot be found and the differential equation may either be solved numerically or by an expansion in $\alpha_s(\mu_1) - \alpha_s(\mu_2)$. The expansion in the latter case is given in the appendix of [42] and this is the method that will be employed to compute the effective Wilson coefficients for $b \to s$ decays below.

2.4 Effective Hamiltonian for $b \to s l^+ l^-$

The scale of B meson decays is $\sim 5\,\text{GeV}$, far below the electroweak scale characterised by $M_W \sim 80\,\text{GeV}$. A description of electroweak interactions in terms of W bosons and including the top quark will therefore lead to large logarithms in the resulting calculations $\sim \log m_b^2/M_W^2$ when loop corrections are included. The appearance of large logarithms indicates that a perturbative series is likely to show poor convergence. In cases where large logarithms are due to a choice of the renormalisation scale far from the interaction scale, the appropriate solution is to use the RG to change the renormalisation point and re-sum the leading large logarithms. In the present case, the large scale is due to the presence of heavy particles rather than a large renormalisation scale, so this cannot immediately be done.

The way to avoid this problem however is simple: since the W boson mass is large compared to the momentum scales being studied, an expansion in $1/M_W^2$ can be performed. In the simplest case, a W boson exchange between two quark lines can be replaced by a four-quark operator

$$\frac{g_W^2}{2} V_{cs}^* V_{cb} \bar{s}\gamma_\mu \frac{1-\gamma_5}{2} c \frac{g^{\mu\nu}}{p^2 - M_W^2} \bar{c}\gamma_\nu \frac{1-\gamma_5}{2} b = -\frac{G_F}{\sqrt{2}} V_{cs}^* V_{cb} \bar{s}\gamma_\mu(1-\gamma_5)c\ \bar{c}\gamma^\mu(1-\gamma_5)b + O\left(\frac{p^2}{M_W^4}\right), \tag{2.17}$$

as illustrated in Figure 2.2. The implication of (2.17) is that an effective Hamiltonian

$$H_{\text{eff}} = \frac{G_F}{\sqrt{2}} V_{cs}^* V_{cb} \bar{s}\gamma_\mu(1-\gamma_5)c\ \bar{c}\gamma^\mu(1-\gamma_5)b \tag{2.18}$$

will produce the same results as the full theory at low momentum scales. In fact owing to the structure of the CKM matrix (2.8) this is the largest flavour-changing neutral term.

This illustrates the general procedure rather well: all operators below a certain dimension consistent with the symmetries of the full theory are written down and then their coupling constants are fixed, so that their effect matches that of the full ultraviolet theory up to corrections suppressed by heavy masses, e.g. [43]; in this case, the W and Z boson masses and the top quark mass. The Higgs boson mass is in fact not relevant because the Higgs boson does not

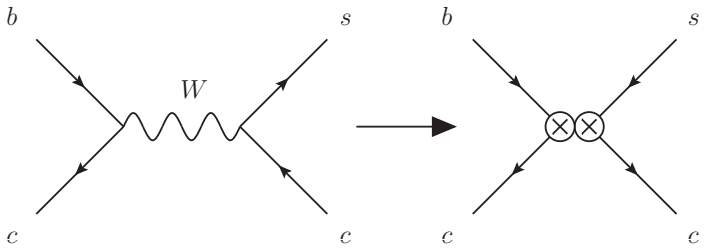

Figure 2.2: Replacement of W boson by a local four quark effective operator

mediate flavour-changing processes, although the Z manages to circumvent this for technical reasons.

So far, the question of renormalisation has not been addressed. It is well known that the Fermi theory of weak interactions is non-renormalisable; since G_F has negative dimension, an infinite number of dimensionless operators can be constructed. In contrast to the case of a renormalisable field theory, multiple insertions of a four-quark operator would be renormalised by a higher dimension operator appearing at a higher power of G_F which must be separately matched to the ultraviolet theory. In practice however the higher dimension operators associated with higher powers of G_F are expected to be heavily suppressed since they would carry more powers of $1/M_W^2$ and thus a calculation at leading order is sufficient.

By contrast, loop corrections in the strong coupling constant α_s are crucial, since these will generate large logarithms that must be resummed to get accurate results. Integrating out the heavy degrees of freedom is done with the renormalisation scale $\mu^2 \sim M_W^2$, so that logarithms appearing in the couplings of the effective theory are small. Since the heavy particle masses have been traded for a large renormalisation point in the effective theory, renormalisation group evolution may then be used to bring that scale down to the interaction scale of interest, and only small logarithms appear. This is the power of the effective theory approach: it allows interactions with heavy particles to be computed accurately, where the corresponding calculation in the full ultraviolet theory could require high order loop corrections to achieve the same results.

The inclusion of α_s loop corrections in constructing the effective theory for $b \to s l^+ l^-$ processes introduces a number of new operators. The relevant infrared symmetry constraint is unitarity of the CKM matrix (2.8). Since renormalisation constants are purely a property of the theory at short distances particle masses do not appear, and thus GIM cancellation in the divergent parts of loop diagrams is exact, which reduces the number of operators required. The full effective Hamiltonian needs ten operators, given by [44]

$$H_{\text{eff}} = \frac{G_F}{\sqrt{2}} \left[\sum_{i=1}^{2} (\lambda_u C_i \mathcal{O}_i^u + \lambda_u C_i \mathcal{O}_i^u) - \lambda_t \sum_q \sum_{i=3}^{6} C_i \mathcal{O}_i^q - \lambda_t \sum_{i=7}^{10} C_i \mathcal{O}_i \right] \quad , \tag{2.19}$$

where the index q runs over all active quark flavours (u, d, s, c, b), and $\lambda_q = V_{qs}^* V_{qb}$ is a commonly

used shorthand for CKM matrix elements. The operators appearing in the effective Hamiltonian are:

Current-current operators

$$\mathcal{O}_1^q = (\bar{s}_i q_j)_{V-A}(\bar{q}_j b_i)_{V-A} \qquad \mathcal{O}_2^q = (\bar{s}_i q_i)_{V-A}(\bar{q}_j b_j)_{V-A} \quad ;$$

QCD penguin operators

$$\mathcal{O}_3^q = (\bar{s}_i b_i)_{V-A}\sum_q(\bar{q}_j q_j)_{V-A} \qquad \mathcal{O}_4^q = (\bar{s}_i b_j)_{V-A}\sum_q(\bar{q}_j q_i)_{V-A}$$
$$\mathcal{O}_5^q = (\bar{s}_i b_i)_{V-A}\sum_q(\bar{q}_j q_j)_{V+A} \qquad \mathcal{O}_6^q = (\bar{s}_i b_j)_{V-A}\sum_q(\bar{q}_j q_i)_{V+A} \quad ;$$

Magnetic penguin operators

$$\mathcal{O}_7 = -\frac{e m_b}{8\pi^2}\bar{s}\sigma\cdot F(1+\gamma_5)b \qquad \mathcal{O}_8 = -\frac{g_s m_b}{8\pi^2}\bar{s}\sigma\cdot G(1+\gamma_5)b \quad ;$$

Semileptonic operators

$$\mathcal{O}_9 = \frac{\alpha_{\rm em}}{2\pi}(\bar{l}\gamma^\mu l)(\bar{s}\gamma_\mu(1-\gamma_5)b) \qquad \mathcal{O}_{10} = \frac{\alpha_{\rm em}}{2\pi}(\bar{l}\gamma^\mu\gamma_5 l)(\bar{s}\gamma_\mu(1-\gamma_5)b) \quad .$$

The notation for quark currents is $\bar{q}q_{V\pm A} \equiv \bar{q}\gamma^\mu(1\pm\gamma_5)q$, where the vector index is implicitly contracted. Small corrections proportional to the s-quark mass that appear in $\mathcal{O}_7$ and $\mathcal{O}_8$, which are identical to the terms given under the replacement $m_b(1+\gamma_5) \to m_s(1-\gamma_5)$, have been neglected. The operator $\mathcal{O}_{10}$ arises due to intermediate Z bosons, which might seem to be forbidden because the relevant diagram contains both a W and Z boson; however, this is circumvented because the Z boson coupling is a mixture of the weak and electromagnetic couplings and thus it can appear at $O(\alpha_{\rm em}G_F)$. To include higher order loop corrections in α_s properly, it turns out to be convenient to go over to an alternative basis containing fewer instances of γ_5 [45]; closed loops with odd numbers of γ_5 matrices complicate loop calculations in dimensional regularisation since γ_5 is strictly a four-dimensional object.

A particular issue that arises in electroweak interactions is the presence of γ_5. It is well known that the extension of the γ_5 matrix away from $D = 4$ is not straightforward, because it is not possible simultaneously to satisfy [46]

$$\mathrm{Tr}\{\gamma_5\gamma^\mu\gamma^\nu\gamma^\rho\gamma^\sigma\} \propto \epsilon^{\mu\nu\rho\sigma} \qquad \text{and} \qquad \{\gamma_5,\gamma_\mu\} = 0 \tag{2.20}$$

in $D \neq 4$. There are two well-known schemes for dealing with occurrences of γ_5, known as the 't Hooft–Veltman (HV) scheme [36] and the naive dimensional regularisation (NDR) scheme [47],

defined through

$$\gamma_5 = \frac{i}{4!}\epsilon_{\mu\nu\rho\sigma}\gamma^\mu\gamma^\nu\gamma^\rho\gamma^\sigma \qquad \text{and} \qquad \{\gamma_5, \gamma_\mu\} = 0 \tag{2.21}$$

respectively. Both schemes have significant difficulties: the HV scheme breaks D-dimensional Lorentz invariance and thus the counterterms needed to renormalise the theory do not respect gauge symmetry [47]. The NDR scheme is internally inconsistent, since it can be shown without assumptions on γ_5 that

$$\mathrm{Tr}[\{\gamma_\alpha, \gamma_5\}\gamma^\alpha\gamma_\mu\gamma_\nu\gamma_\rho\gamma_\sigma] = 2(D-4)\,\mathrm{Tr}[\gamma_5\gamma_\mu\gamma_\nu\gamma_\rho\gamma_\sigma] \quad , \tag{2.22}$$

which is obviously inconsistent with $\{\gamma_\alpha, \gamma_5\} = 0$ in $D \neq 4$ dimensions, and therefore closed fermion loops with odd numbers of γ_5 matrices cannot be calculated [48]. However it turns out that $b \to s$ decays do not require computing closed loops with odd numbers of γ_5 matrices, and in this situation the NDR scheme is perfectly consistent and far simpler than the HV scheme.

In the context of the effective Hamiltonian (2.19), the choice of γ_5 scheme affects the Wilson coefficients (WCs) $C_{7,8,9}$, because these operators at tree level are at the same order of α_s or α_{em} as loop corrections arising from the four-quark operators $\mathcal{O}_{1-6}$. It is therefore common to absorb these loop corrections into effective coefficients $C_{7,8}^{\mathrm{eff}}$ [49], which are scheme independent at leading order. They are given, for the effective Hamiltonian (2.19) in the NDR scheme, by:

$$C_7^{\mathrm{eff}} = C_7 - \frac{4}{9}C_3 - \frac{4}{3}C_4 + \frac{1}{9}C_5 + \frac{1}{3}C_6\,, \qquad C_8^{\mathrm{eff}} = C_8 + \frac{4}{3}C_3 - \frac{1}{3}C_5 \quad . \tag{2.23}$$

The situation with C_9 is slightly different: the corrections from the four-quark operators are not local. However, since C_9 couples to a lepton pair which does not couple to gluons at leading order in α_{em}, $b \to sll$ through C_9 can be factorised, and therefore it makes sense to include the complete one-loop corrections into an effective operator $C_9^{\mathrm{eff}}(q^2)$, which can be combined with the exclusive form factors. The relevant form factors will be described in Section 2.9. The function $C_9^{\mathrm{eff}}(q^2)$ is given in the NDR scheme by

$$C_9^{\mathrm{eff}}(q^2) = C_9 + Y(q^2) \quad , \tag{2.24}$$

where the loop corrections $Y(q^2)$ are [50]:

$$\begin{aligned} Y(q^2) =& h(q^2, m_c)\left(-\frac{\lambda_c}{\lambda_t}(3C_1 + C_2) + 3C_3 + C_4 + 3C_5 + C_6\right) \\ &- \frac{h(q^2, m_b)}{2}(4C_3 + 4C_4 + 3C_5 + C_6) \\ &- h(q^2, 0)\left(\frac{\lambda_u}{\lambda_t}(3C_1 + C_2) + \frac{1}{2}(C_3 + 3C_4)\right) + \frac{4}{27}(C_3 + 3C_4 + 8C_5) \quad . \end{aligned} \tag{2.25}$$

	$\mu = m_b$		$\mu = \sqrt{m_b \Lambda_H}$	
	CMM	BBL	CMM	BBL
C_1	-0.2622	-0.1311	-0.5636	-0.2818
C_2	1.0087	1.0524	1.0299	1.1238
C_3	-0.0051	0.0110	-0.0175	0.0194
C_4	-0.0778	-0.0316	-0.1718	-0.0524
C_5	0.0003	0.0087	0.0012	0.0132
C_6	0.0009	-0.0371	0.0042	-0.0775
C_7^{eff}	-0.2975		-0.3351	
C_8^{eff}	-0.1569		-0.1828	
C_9	4.0354		4.4207	
C_{10}	-4.2496		-4.2496	

Table 2.1: WCs at $\mu = m_b$ and $\mu = \sqrt{m_b \Lambda_H}$ at NNLL order for $m_b = 4.7\text{GeV}$, $M_W = 80.4\text{GeV}$, $\sin^2\theta_W = 0.23$, $m_t = 177\text{GeV}$, $\Lambda_H = 0.5\text{GeV}$ and $\Lambda^{(5)}_{\text{QCD}} = 214\text{MeV}$ in two different bases. Three-loop running for α_s is used. The BBL basis used is that defined in [42]; it is equivalent to the traditional basis defined in [44] at leading order. The CMM basis [45] is used for loop calculations; however, all results are presented in the BBL basis and all references to WCs C_{1-6} elsewhere in the text are in that basis.

The function h is the standard quark vacuum polarisation function (this form from [51])

$$h(s,m) = -\frac{4}{9}\left(\log\frac{m^2}{\mu^2} - \frac{2}{3} - z - (2+z)\frac{\Delta}{2}\right) - \frac{4}{9}(2+z)\sqrt{|z-1|}\begin{cases}\arctan\dfrac{1}{\sqrt{z-1}} & z>1\\ \log\dfrac{1+\sqrt{1-z}}{\sqrt{z}} - \dfrac{i\pi}{2} & z\le 1\end{cases} \tag{2.26}$$

where $z \equiv \frac{4m^2}{s}$ and the renormalisation scheme dependent term Δ [52] has been included for later convenience. It is given by

$$\Delta = \frac{2}{4-D} - \gamma_E + \log 4\pi \quad , \tag{2.27}$$

which is set to zero in the $\overline{\text{MS}}$ scheme.

2.4.1 Wilson coefficients (WCs) for $b \to s l^+ l^-$

The calculation of the WCs of the Hamiltonian for $b \to s$ decay is rather involved, so this intermediate result of the calculations in chapters 5 and 6 is included so that the results can be more easily reproduced. The renormalisation group flow procedure is applied as described in Section 2.3 up to three-loop order, specifically using the solution of the flow equation to this order in the appendix of [42]. Rather than the operator basis defined below (2.19) this calculation is done in the CMM basis [45] since it is in this basis that the higher order anomalous dimensions have been computed, as its construction was designed to ease automated calculation.

The complete ADM to three loops is taken from [53], and the expressions for the Wilson coefficients C_i at the electroweak scale are take from [54] for C_{1-6} and $C_{9,10}$ and [55] for $C^{\text{eff}}_{7,8}$. These are always employed at $\mu = M_W$ to set the initial conditions for the RG flow; that is

to say the uncertainty owing to α_s^4 terms at this scale is ignored, although uncertainty of the masses of the W boson and top quark is accounted for. Since $\alpha_s(M_W) \approx 0.11$ is small this should have a negligible effect on the overall uncertainty of our calculations.

After computing coefficients at the chosen low scale in the CMM basis, they are then transformed into the pseudo-BBL basis defined in [42, eq. 79], which is equivalent to the BBL basis at leading order in α_s. The results of this procedure are given in table 2.1.

2.5 The Operator Product Expansion (OPE)

Perturbation theory in the SM is expected to be valid at short distances, or equivalently at energies large compared to the masses of hadronic resonances arising from QCD. An important question in addressing SM phenomenology is therefore how pure perturbation theory breaks down and whether longer distance correlations can be addressed. The OPE provides a means to address these problems.

The OPE, introduced by Wilson [56], proposes that at short distances a product of two operators A and B may be expanded

$$A(x)B(0) = \sum_i c_i(x)\mathcal{O}_i(0) \quad , \tag{2.28}$$

where $\mathcal{O}_i$ are local operators and $c_i(x)$ are c-number coefficient functions, and the sum in principle runs over all operators $\mathcal{O}_i$ whose quantum numbers are the same as those of the product AB. Under perturbation theory at sufficiently short distances it might be hoped from dimensional analysis that

$$A(\lambda x)B(0) = \sum_i c_i(\lambda x)\mathcal{O}_i(0) \xrightarrow{\lambda \to 0} \sum_i \lambda^{d_{\mathcal{O}_i} - d_A - d_B} c_i(x)\mathcal{O}_i(0) \tag{2.29}$$

holds, where $d_{\mathcal{O}}$ is the engineering dimension of the operator $\mathcal{O}$, up to logarithmic corrections. Since fields in a quantum field theory in more than two dimensions will have positive dimension it would then be expected that only a finite number of operators $\mathcal{O}_i$ with $d_{\mathcal{O}_i} < d_n$ for some d_n can be written down. This would imply that at sufficiently short distances only a finite number of terms in the OPE (2.28) need to be considered, as higher dimension operators are suppressed by powers of the distance. The claim of the OPE [56] is that this holds quite generally: as $\lambda \to 0$ in (2.29), only a finite number of coefficient functions are more singular than λ^{d_n} for some d_n, even beyond perturbation theory.

Of course, the practical utility of the OPE arises from the fact that the coefficient functions $c_i(x)$ can be computed within perturbation theory, and then the expectation values of local operators in vacuum and on different particle states can be derived from experiment. Rigorously it has been shown that coefficient functions can be derived by computing divergences in $L + 1$

loop graphs [57], which amounts to considering the action of the Callan–Symanzik equation on both sides of (2.28) [41]. This procedure is rather cumbersome, however, since it involves computing diagrams involving one more loop than the final result and is not what is normally done, rather the usual interaction–picture perturbation theory using a Dyson series is performed followed by Wick contraction, e.g. [23]. In contrast to the usual perturbative approach, in which normal ordered operator products are dropped because their expectation values are zero in the perturbative vacuum, all terms are retained since the same cannot be guaranteed for the full vacuum. It then follows that the most singular short distance term in the OPE is exactly the perturbative part, since it is associated with the dimension 0 identity operator.

This procedure can be somewhat better justified by considering the Dyson–Schwinger equations (DSEs) [58–60], which provide genuinely non-perturbative constraints between different time-ordered operator products[5]. In the usual case, this means starting from the Gaussian solution to the free field theory and recovering standard perturbation theory. In the OPE case as discussed above, the recovery of the coefficient functions of operators whose perturbative expectation value is zero is also sought. The appropriate zero order solution is given by Wick's theorem [61] followed by Taylor expanding the x coordinates on the normal ordered operators [41], e.g.

$$\mathcal{T}\{A(x)B(0)\} = \Delta_F^{AB}(x)\cdot\mathbb{I} + \sum_n \frac{1}{m!}x^{\mu_1\cdots\mu_m}{:}(\partial_{\mu_1\ldots\mu_m}A)B{:} \quad , \tag{2.30}$$

where $\mathbb{I}$ is the identity operator, $\Delta_F^{AB}(x)$ the bare Feynman propagator and $:AB:$ a normal ordered local operator. It has been assumed that A and B are fields rather than composite operators which would necessitate the inclusion of many more operators arising from commuting the constituent fields.

This naturally raises the question of the connection of the operators on the right-hand side of (2.28) to those in (2.30). Wilson's argument for (2.28) [56] constructs the right-hand side by systematically extracting the most singular part of $A(x)B(0)$ at short distances, subtracting this singularity and then repeating. At each step in such a construction only the most singular term in the most singular remaining coefficient function is recovered, and for subsequent steps an extension of that coefficient function away from $x = 0$ must be made. This means that the operators appearing on the right-hand side of (2.28) in general are expected to be scheme dependent. The right-hand side of (2.30) however is scheme independent, except insofar as an arbitrary scale Λ could have been introduced and Λ^2x^2 terms included in the coefficient functions. These was no reason to do this, however, as is well known divergences occur in interacting quantum field theories which must be regularised by the explicit introduction of an arbitrary mass scale and renormalisation conditions. The extension of normal ordered products to all perturbative orders of an interacting field theory was solved by Zimmermann through the

[5] See appendix C for a brief discussion.

BPHZ regularisation scheme [62].

Further, in contrast to the case of renormalisable local actions, OPE calculations may contain infrared divergences [63–65]. Since the SM is infrared finite, it is expected that infrared divergences should cancel in observable processes in the spirit of the Kinoshita–Lee–Nauenberg theorem [66, 67]. Infrared divergences in Feynman diagrams with massless particles are expected, however, and in OPE calculations must be absorbed into operator expectation values; in particular for external bound states in QCD, infrared divergences must cancel between short and long distance physics in order for perturbation theory to be useful. Separation of scales in this way is the subject of factorisation theorems [68]. In principle this means that OPE condensates can depend on a separate UV and IR renormalisation point; however, under normal circumstances they would be fixed to the same value since the usual goal of RG running is to make logarithms small and both the IR and UV renormalisation scales are compared to the same hard scale.

It might be wondered whether in calculating OPE coefficient functions perturbatively crucial non-perturbative information might be missed. Given the practical impossibility of performing non-perturbative OPE calculations on phenomenologically interesting theories, this question cannot truly be answered; however, it has at least been shown that the coefficient functions respect all symmetries of the underlying theory [69], that is to say all symmetry-breaking contributions must come from expectation values of local operators. Since the OPE is an expansion in terms of operators rather than correlation functions this is rather to be expected, as symmetry-breaking terms would usually be dependent on external parameters such as temperature and density which the OPE cannot see. Indeed, although the OPE is practically useful where there is a substantial difference between the interaction scale and the scale of non-perturbative physics, conceptually it is a separation between the behaviour of a theory arising from commutation relations of operators and that from external states.

Finally, there is the question of what role symmetries and equations of motion play in the OPE. Since the coefficient functions are nothing but Feynman diagrams with certain external kinematics, there must be relations between some of them. In order to produce consistent results, symmetry constraints must therefore be satisfied by OPE expectation values such that the combination of the short and long distance parts is free of residual gauge dependence. The simplest example of such a constraint is in the quark condensate

$$\langle\bar{\psi}(i\not{D}-m)\psi\rangle=0 \implies i\langle\bar{\psi}\not{\partial}\psi\rangle=m\langle\bar{\psi}\psi\rangle+O(\alpha_s)\,, \tag{2.31}$$

and generalisations of this equation of motion constraint play a crucial role in the construction of light meson distribution amplitudes (DAs) [70]. The equation (2.31) also has an additional implication: the OPE may not be strictly truncated at a given external operator dimension since equations of motion may relate condensates of different dimension. The higher dimension

condensate may be excluded by other means, however, as in this case neglecting the light quark mass implies $\langle\bar{\psi}\not{\partial}\psi\rangle \sim m \to 0$.

Of course, none of this necessitates that the OPE actually converges for a particular process, that is to say that the coefficient functions relevant to a particular process at physical external momenta will in fact suppress higher dimension condensates. It turns out that in common cases this cannot be guaranteed, and this is the subject of the next section.

2.6 Correlation functions near the light cone

The mathematical objects of interest to particle physics are S-matrix elements, which, as is well known, may be related to Fourier transforms of correlation functions via Lehmann–Symanzik–Zimmermann (LSZ) reduction [71]. This means that the behaviour of a correlation function at all spatial coordinates is used in computing a physical result and it must be shown that the use of an expansion such as (2.28) is justified, i.e. that the short distance contribution is dominant.

The dominant contribution is best illustrated by way of example. A scattering process producing a pion will, after evaluating the operator product expansion for the short distance part, contain a contribution from the two quark operator, which may be generally expressed as

$$\mathcal{M} = \int d^d x \int \frac{d^d l}{(2\pi)^d}\, e^{i(k+l)\cdot x} \sum_P \langle 0|{:}\bar{\psi}(x)\Gamma_P(l,q_i)\psi(0){:}|\pi(p)\rangle \quad , \tag{2.32}$$

where Γ_P are projections of the short distance part onto the basis of Dirac matrices, q_i are the external momenta of the process and k is some linear combination of q_i. From Lorentz invariance it follows that the required pion expectation values are

$$\langle 0|{:}\bar{\psi}(x)\Gamma\psi(0){:}|\pi(p)\rangle = \tilde{\phi}_\Gamma(p\cdot x, m_\pi^2 x^2) \quad , \tag{2.33}$$

where Γ is a specific component of a Dirac projector. Plugging this into (2.32) and removing the x-coordinate via a Taylor expansion gives

$$\mathcal{M} = \sum_P \phi_{\Gamma_P}\left(ip\cdot\frac{\partial}{\partial l}, -m_\pi^2\frac{\partial^2}{\partial l^2}\right)\Gamma_P(l,q_i)\Big|_{l=-k} \quad . \tag{2.34}$$

The key to whether or not the OPE converges is now held by Γ_P. These derivatives may be rewritten in terms of Lorentz scalar quantities as:

$$p\cdot\frac{\partial}{\partial l} \to 2(p\cdot l)\frac{\partial}{\partial l^2} + \sum_i p\cdot q_i \frac{\partial}{\partial(l\cdot q_i)} + m_\pi^2\frac{\partial}{\partial(l\cdot p)} \tag{2.35}$$

$$m_\pi^2\frac{\partial^2}{\partial l^2} \to m_\pi^2\left[2D\frac{\partial}{\partial l^2} + 4l^2\frac{\partial^2}{\partial(l^2)^2} + 4(l\cdot q_i)\frac{\partial^2}{\partial(l^2)\partial(l\cdot q_i)} + q_i\cdot q_j\frac{\partial^2}{\partial(l\cdot q_i)\partial(l\cdot q_j)} + \dots\right] \quad , \tag{2.36}$$

where the dots are all terms including invariants in p and are identical in structure to those in q_i, since p is not singled out in (2.36), unlike in (2.35). In order to proceed further, it is necessary to assume that the action of the derivatives on the short distance function Γ_P is to suppress it by a large scale. This will typically be the case except in the vicinity of singularities of Γ_P, and in perturbative correlation functions amounts to the requirement that propagators are off-shell.

If the hard scale of the interaction is Q^2, the scaling assumptions

$$\frac{\partial}{\partial(l^2)} \sim \frac{\partial}{\partial(l\cdot q_i)} \sim \frac{\partial}{\partial(l\cdot p)} \sim \frac{1}{Q^2} \qquad\qquad l^2 \sim l\cdot q_i \sim p\cdot q_i \sim Q^2 \tag{2.37}$$

combined with (2.35) and (2.36) lead to the conclusion that

$$p\cdot\frac{\partial}{\partial l} \sim 1 \qquad\qquad m_\pi^2\frac{\partial^2}{\partial l^2} \sim \frac{m_\pi^2}{Q^2} \tag{2.38}$$

and hence it would seem that the expansion in terms of powers of the derivative (2.36) is convergent but the expansion in terms of (2.35) is not. It is also possible to reach this conclusion by considering the oscillation of the exponential $e^{ik\cdot x}$ appearing in (2.32) in a certain reference frame, e.g. [41]. It should be mentioned at this point that particle masses have largely been ignored in this argument: the presence of very massive particles does not spoil light-cone convergence since derivatives will introduce additional powers of $1/M^2$ and it is assumed that $M^2 \gg Q^2$, and in fact were this always the case then (2.35) would scale as Q^2/M^2 and be a valid basis for expansion.

Since the derivative (2.36) corresponds to a series expansion in x^2, a process is light-cone dominated when this expansion converges, as is expected to be the case when the short distance kernel Γ_P is away from any thresholds. However x^μ (through $p\cdot x$) is not a good expansion parameter, and therefore the full $p\cdot x$ dependence must be retained.

The final step in treating external hadrons is then to characterise the function $\tilde{\phi}_\Gamma$ (2.33) near $x^2 = 0$. The classic OPE would expand the left-hand side of (2.33) in terms of operators of increasing dimension

$$\bar{\psi}(x)\psi(0) = \partial_{\mu_1\ldots\mu_m}\left[\bar{\psi}\overleftrightarrow{D}_{\nu_1\ldots\nu_n}\psi\right] \quad , \tag{2.39}$$

where $\overleftrightarrow{D}_\mu = \overleftarrow{D}_\mu - \overrightarrow{D}_\mu$, and characterise the pion state in terms of expectation values of these local operators. Unfortunately such an approach will lead to sums which do not converge [72], and in fact the correct approach is to keep the full $p\cdot x$ dependence and write

$$\langle 0|\bar{\psi}(x)\Gamma\psi(x)|\pi(p)\rangle = \int_0^1 \phi_\Gamma(u)e^{iup\cdot x}du \quad . \tag{2.40}$$

The function ϕ_Γ is then known as a distribution amplitude (DA). It is somewhat interesting that the integral is over the range $[0,1]$; physically the interpretation is that a configuration in

which one of the quarks has negative energy is extremely unlikely. Mathematically, however, it has an entirely different origin: in a non-interacting conformal theory (which QCD) is at leading order) the free OPE may be explicitly summed to give a result of the form [73]

$$\bar{\psi}(x)\Gamma\psi(0) \simeq \int_0^1 \sum_n f_n(u, p\cdot x, x^2)\mathbb{O}_n(ux)du \tag{2.41}$$

and hence in a perturbative construction of the OPE it follows that the general form (2.40) has the correct momentum flow structure. In contrast to the local OPE discussed in the previous section, this leads to a situation where an infinite number of parameters may enter into the function ϕ_Γ without any suppression in the hard scale of the process. This then presents the problem of how to capture an infinite number of parameters in a useful way. This problem is solved by exploiting the approximate conformal symmetry of QCD and categorising operators on the light cone in terms of twist rather than dimension [74], and then the contribution of higher twist operators are expected to be suppressed by the Borel parameter in sum rules [75].

An issue that has not been discussed throughout this section is gauge invariance of distribution amplitudes such as (2.40). The solution to this problem is usually to construct DAs in the Fock-Schwinger gauge $x\cdot A = 0$ so that a matrix element $\bar{\psi}(0)\psi(x)$ may be interpreted in a gauge invariant way by joining the two quark operators with a straight Wilson line. In other gauges infinite resummations must be performed in order to separate "physical" gluon emission from terms purely associated with cancelling gauge dependence [76].

2.7 Calculating with distribution amplitudes

The light-cone OPE in non-vacuum external states manifests itself through DAs, which provide a systematic way of approximating non-perturbative states through a small number of parameters. The full listing of DAs used in this thesis is given in appendix B; in this section some details of performing calculations with these objects will be discussed.

Light-cone distribution amplitudes are developed in terms of a conformal basis at light-like distances, e.g. [75]. As discussed in Section 2.6, for S-matrix elements knowledge of the correlation functions away from the light cone is also required. This can be recovered by matching Lorentz invariant structures order by order in the external state mass, which implies that the light-cone expansion is also a small mass expansion, and that results must be truncated at a certain order in light-external meson masses in order to be consistent. This does not apply to B meson distribution amplitudes in which light-cone dominance arises via a rather different mechanism due to the $1/m_b$ expansion, which will be discussed in Section 5.4.5.

A nice example to illustrate the above point occurs in weak annihilation (WA), which contributes to the isospin asymmetry and will be discussed in Section 5.3. In that case, the matrix

element

$$(p+q)_\mu \langle K^*(p,\eta)\gamma^*(q)|\bar{s}\gamma^\mu q|0\rangle = \langle K^*(p,\eta)\gamma^*(q)|i\partial_\mu[\bar{s}\gamma^\mu q]|0\rangle \tag{2.42}$$

must be computed. Owing to the derivative operator acting on the weak current this matrix element may be computed exactly using a Ward identity, up to light quark mass corrections $O(m_s, m_q)$. This was the procedure used in the first sum rule calculations of WA [77, 78] and expounded in more detail in [79].

The Ward identity procedure gives

$$\begin{aligned}(p+q)_\mu \langle K^*\gamma|\bar{s}\gamma^\mu q|0\rangle =& ie(p+q)_\mu\epsilon_\nu \int_x e^{-ip_B\cdot x}\langle K^*|T\bar{s}\gamma^\mu q(x)J^\nu_{\text{em}}(0)|0\rangle \\ =& ie\epsilon_\nu\int_x e^{-ip_B\cdot x}\langle K^*|i\partial_\mu\left\{T\bar{s}\gamma^\mu q(x)J^\nu_{\text{em}}(0)\right\}|0\rangle \\ =& e(Q_q-Q_s)\epsilon_\nu\langle K^*(p,\eta)|\bar{s}\gamma^\nu q(0)|0\rangle \\ =& e(Q_q-Q_s)f_{K^*}m_{K^*}(\eta\cdot\epsilon)\end{aligned} \tag{2.43}$$

and indeed the hadronic part of the matrix element only requires the identity $\langle K^*(p,\eta)|\bar{s}\gamma^\nu q(0)|0\rangle = f_{K^*}m_{K^*}\eta^\nu$ and no knowledge of the K^* Bethe–Salpeter wave function is necessary. Indeed, the result (2.43) is accurate to all orders in QCD subject to neglecting the quark masses.

The result (2.43) may also be computed using the K^* DA, although the calculation is rather more involved. The relevant terms in the K^* DA are [80]

$$\begin{aligned}&\langle K^*(p,\eta)\,|\,\bar{s}(x)_a[x,0]q(0)_b\,|\,0\rangle = \int_0^1 du\, e^{iup\cdot x}\left\{\frac{f_{K^*}^\perp}{4N_c}(\not\eta\not p)_{ba}\phi_\perp(u)\right. \\ &\left.+\frac{m_{K^*}f_{K^*}}{4N_c}\left[(\not p)_{ba}\frac{\eta\cdot x}{p\cdot x}\left(\phi_\parallel(u)-g_\perp^{(v)}(u)\right)+(\not\eta)_{ba}g_\perp^{(v)}(u)+\frac{1}{4}\epsilon_{\mu\nu\rho\sigma}\eta^\nu p^\rho x^\sigma\left(\gamma^\mu\gamma_5\right)_{ba}g_\perp^{(a)}(u)\right]\right\}\end{aligned} \tag{2.44}$$

where $[x,0]$ indicates a Wilson line to make the expression gauge invariant. A fuller version is given in appendix B. A curious property of this expression is that an odd number of powers of the K^* mass appears on the right-hand side, which implies that it cannot obviously be expected to be suppressed by $m_{K^*}^2/Q^2$ with respect to the first term. As an example, it in fact turns out that in the leading electromagnetic penguin amplitude for $B\to K^*\gamma$, all terms in (2.44) occur at the same order in the $1/m_b$ expansion, e.g. [81]. This situation can arise because the binding energy of the initial state B meson in that process is $\sim m_B - m_b \sim 0.5\text{GeV}$, providing a scale comparable to m_{K^*}, and would presumably also be the case in many other processes with external QCD bound states. The form of the DA also presents a problem which does not occur in normal perturbation theory: how to deal with the presence of coordinates when working in momentum space is preferable? Fortunately the answer is straightforward, since

$$x^\mu e^{iup\cdot x} = -\frac{i}{u}\frac{\partial}{\partial p_\mu}e^{iup\cdot x} \qquad \frac{1}{p\cdot x}e^{iup\cdot x} = i\int_0^u e^{ivp\cdot x}dv + \frac{1}{p\cdot x} \tag{2.45}$$

and for practical purposes the DA (2.44) is rewritten

$$\langle K^*(p,\eta)\,|\,\bar{s}(x)_a[x,0]q(0)_b\,|\,0\rangle = \int_0^1 du \left\{ \frac{f_{K^*}^{\perp}}{4N_c}(\not{\eta}\not{p})_{ba}\phi_\perp(u) \right.$$

$$\left. + \frac{m_{K^*}f_{K^*}}{4N_c}\left[-(\not{p})_{ba}\frac{\Phi(u)}{u}\eta_\mu\frac{\partial}{\partial p_\mu} + (\not{\eta})_{ba}g_\perp^{(v)}(u) - \frac{i}{4}\epsilon_{\mu\nu\rho\sigma}\eta^\nu p^\rho\,(\gamma^\mu\gamma_5)_{ba}\,\frac{g_\perp^{(a)}(u)}{u}\frac{\partial}{\partial p^\sigma}\right]\right\} e^{iup\cdot x} \quad , \tag{2.46}$$

where the function $\Phi(u)$ is defined as

$$\Phi(u) = \int_0^u \phi_\parallel(v) - g_\perp^{(v)}(v)dv \quad . \tag{2.47}$$

Thus all coordinates are removed from (2.44) at the expense of the introduction of derivatives in the external momentum. Unfortunately the computer algebra package FeynCalc has no facilities to deal with vector derivatives, so a certain amount of creative trickery is required if one does not wish to perform all calculations by hand; performing the derivative manually by introducing an additional vector and Taylor expanding in its coefficient works, provided that it does not exhaust the computer's memory.

The coefficient functions $\phi_{\perp,\parallel}(u)$ and $g_\perp^{(v,a)}(u)$ are somewhat confusingly also known as distribution amplitudes. The functions $\phi_{\perp,\parallel}(u)$ are expanded in terms of Gegenbauer polynomials [80, 82]

$$\phi_{\perp,\parallel}(u) = 6\bar{u}u\left(1 + \sum_{n=1}^{\infty} a_n^{\perp,\parallel}C_n^{3/2}(2u-1)\right) \quad , \tag{2.48}$$

which is directly connected to the fact that QCD is conformally invariant, although the specific form arises because Gegenbauer polynomials $C_n^{3/2}(2u-1)$ form an orthogonal basis on $[0,1]$ with the weight $\bar{u}u$ [83], so the coefficients of the DA are the expectation values of operators of specific collinear twist acting on the K^* state [73]. The functions $g_\perp^{(v,a)}(u)$ are not independent but are are given in terms of other DAs by equations of motion [75].

Finally, the matrix element (2.42) can be evaluated using (2.46) and taking into account the equation of motion[6] [70, 84]

$$\Phi(u) = \bar{u}\left(g_\perp^{(v)}(u) - \frac{g_\perp^{(a)\prime}(u)}{4}\right) - \frac{g_\perp^{(a)}(u)}{4} \tag{2.49}$$

[6] This equation is derived from (4.15/16) of [70], and a nearly identical equation with $u \leftrightarrow \bar{u}$ appears in [84].

and the result is

$$(p+q)_\mu \langle K^*(p,\eta)\gamma(q,\epsilon)|\bar{s}\gamma^\mu q|0\rangle$$
$$= e\epsilon_\nu f_{K^*} m_{K^*} \int_0^1 du \Bigg\{ Q_q \Bigg[\eta^\nu \left(g_\perp^{(v)}(u) - \frac{u^2 p^2}{(\bar{u}p+q)^2} \left(g_\perp^{(v)}(u) + \frac{1}{4} g_\perp^{\prime(a)}(u) \right) \right)$$
$$- (\bar{u}p+q)^\nu \frac{2up^2(\eta\cdot q)}{(\bar{u}p+q)^4} \left(\Phi(u) + \frac{1}{4} g_\perp^{(a)}(u) \right) \Bigg] - Q_s \left[\bar{u} \leftrightarrow u \right] \Bigg\} \quad , \quad (2.50)$$

which agrees with (2.43) since $\int_0^1 g_\perp^{(v)}(u)du = 1$ up to factors of $p^2 = m_{K^*}^2$. These terms must be neglected since they occur at a higher order in $m_{K^*}^2$ than the DA (2.44) is complete to, that is to say they are identified with twist-4 terms and would cancel with terms arising from the twist-3 and twist-4 DAs, which are detailed in [85]. However, the requirement to truncate to a certain order in m_{K^*} to get consistent results is not strictly connected to the twist expansion; higher Gegenbauer moments in DAs also have higher twist but are in no way connected to the expansion in m_{K^*}, rather the equations of motion link terms at different powers of m_{K^*}, appearing in the meson DA whose lowest twist part is different.

2.8 Sum rules

The principal tool used to compute B meson transitions in this thesis is light cone sum rules (LCSRs). This is really two distinct techniques, the combination of which is sufficiently advantageous to merit its own name. The light cone part of this method refers to the light cone OPE and is described in Section 2.6; this section will describe the calculation of hadronic processes through sum rules.

A typical matrix element for a semi-leptonic B meson decay is

$$\langle l^+ l^- M | H_{\text{eff}} | B(p_B) \rangle \quad . \quad (2.51)$$

This may be related to a matrix element with the external B meson replaced by a local operator with appropriate quantum numbers:

$$\Pi(p_B) \equiv i \int d^4x e^{-ip_B\cdot x} \langle l^+ l^- M | H_{\text{eff}} J_B(x) | 0 \rangle = \frac{\langle l^+ l^- M | H_{\text{eff}} | B(p_B) \rangle \langle B(p_B) | J_B(0) | 0 \rangle}{m_B^2 - p_B^2} + \dots \quad (2.52)$$

This is nothing other than the LSZ reduction formula [71]. The dots include both poles at masses other than m_B and the continuum contribution arising from multi-particle states. The current J_B is given by

$$J_B = i m_b \bar{b}\gamma_5 q \qquad \langle B(p_B)|J_B(0)|0\rangle = m_B^2 f_B \quad . \quad (2.53)$$

The correlation function Π cannot be perturbatively computed at $p_B^2 = m_B^2$ since QCD perturbation theory is not reliable near resonances, which is hardly surprising as bound states are an intrinsically non-perturbative effect. It can however be reliably computed sufficiently far below the perturbative threshold, i.e. $p_B^2 \ll (m_b - \Lambda_{\rm QCD})^2$. The method of sum rules [86, 87] then relies on the following observation: in the region in which $\Pi(p_B^2)$ may be reliably computed, Cauchy's theorem can be used to say that

$$\Pi(p_B^2) = \frac{1}{2\pi i} \oint_\Gamma \frac{\Pi(s)}{s - p_B^2} ds \quad . \tag{2.54}$$

The integration contour Γ separates the point p_B^2 from all other singularities and branch cuts in $\Pi(s)$ in the complex plane. If the function $\Pi(s)$ falls off sufficiently quickly for $|s| \to \infty$ in all directions then the contour Γ may be taken to infinity, so that only parts of the contour surrounding the singularities remain. If it does not vanish sufficiently quickly at infinity then subtractions may be performed so that the function to which Cauchy's theorem is applied has the right asymptotic properties. A common example which does not converge is given by the two point Passarino–Veltman function B_0 [88]. Importantly these subtractions will drop out of the final form of the sum rule, as will be shown shortly.

(2.54) is already a sum rule; however, it is not yet of a form useful to estimate the contribution of a single particle. To do this, (2.52) and (2.54) are combined to give

$$\Pi(p_B^2) = \frac{1}{2\pi i} \oint_\Gamma \frac{\Pi(s)}{s - p_B^2} ds = \frac{f_B m_B^2}{m_B^2 - p_B^2} \langle l^+ l^- M | H_{\rm eff} | B(p_B) \rangle + \frac{1}{2\pi i} \oint_{\Gamma_C} \frac{\Pi(s)}{s - p_B^2} ds \quad , \tag{2.55}$$

where the contour Γ_C encloses all complex singularities except the B meson pole, and the integral term may therefore be considered to arise from excited and multi-particle states. At this stage the equation (2.55) is exact. For the integral over the contour Γ the correlation function $\Pi(s)$ may be computed perturbatively, and provided p_B^2 is sufficiently far from thresholds QCD, perturbation theory will produce an accurate result. This is known as *global duality* between the hadronic and partonic pictures and it is exact owing to Cauchy's theorem. In order to calculate the transition matrix element, an estimate of the continuum contribution Γ_C is therefore required. The approximation used [87] is again to calculate $\Pi(s)$ perturbatively inside this integral and take the contour Γ_C to enclose all complex singularities above $\mathrm{Re}(s) = s_0$ on the real line. Singularities off the real line may also occur; these will be discussed in Section 3.2.4. This is known as the *semi-global duality* approximation. s_0 is an effective threshold parameter and is chosen somewhere in the vicinity of the lowest-lying multi-particle state in the same channel, which in the case of the current J_B implies a B meson with either two pions or a rho meson, so $s_0 \sim (m_B + 2m_\pi)^2 \sim (m_B + m_\rho)^2$. Applying this approximation to (2.55) gives

$$\frac{f_B m_B^2}{m_B^2 - p_B^2} \langle l^+ l^- M | H_{\rm eff} | B(p_B) \rangle = \frac{1}{2\pi i} \oint_{\Gamma_P} \frac{\Pi^{\rm pert}(s)}{s - p_B^2} ds \quad , \tag{2.56}$$

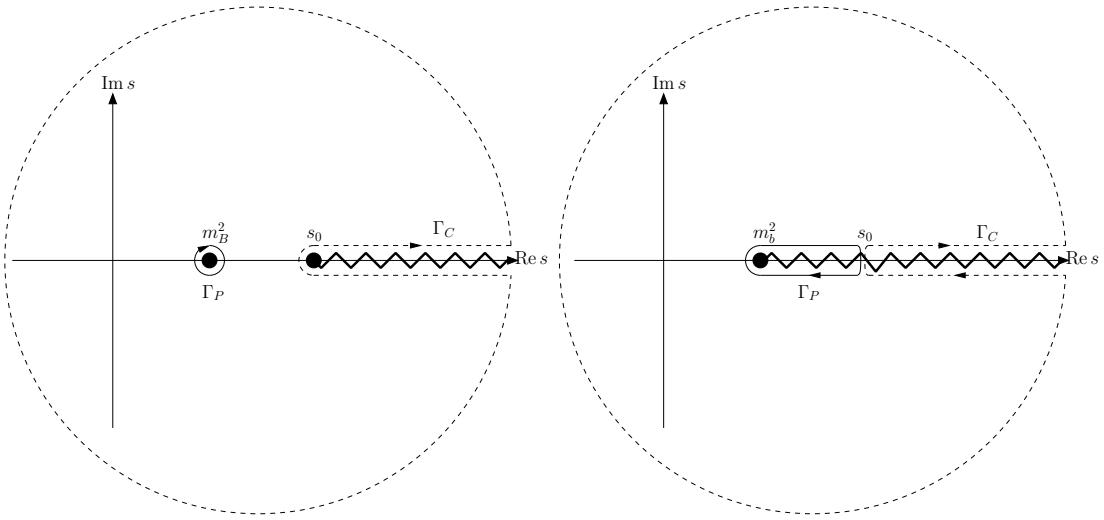

Figure 2.3: Illustration of contours used in a B meson sum rule. The left-hand diagram shows the complex structure of the full theory, and the right-hand diagram shows the structure of the perturbative approximation. The semi-global duality approximation relies on the continuum contribution Γ_C computed perturbatively being a good approximation to the contour Γ_C in the full theory, and therefore the contour Γ_P in a perturbative calculation is a good approximation to the pole residue in the full theory.

where the contour Γ_P is the difference between the contours Γ and Γ_C and therefore encloses the B meson pole. This process is illustrated in Figure 2.3. Note that although this formula is approximate and the contour integral is exactly over the low-lying resonance region in which perturbation theory cannot be trusted, the exactness of global duality implies that this approximation is reasonable provided that perturbation theory is reliable over the contour Γ_C, which surrounds higher resonance and multi-particle contributions. Finally, a Borel transform in the variable p_B^2, related to the inverse Laplace transform is applied. Since the dependence of (2.56) on p_B^2 has a simple functional form, only a single formula for the Borel transform is required

$$\mathcal{B}_{p_B^2 \to M^2}\left[\frac{1}{s - p_B^2}\right] = \frac{1}{M^2} e^{-s/M^2} \,, \tag{2.57}$$

and thus p_B^2 is eliminated in favour of a mass M^2, known as the Borel parameter. The Borel transform eliminates subtractions required in constructing the relation (2.54), since terms which are polynomial in p_B^2 transform into $\delta(M^2)$ and its derivatives, and such terms do not contribute for $M^2 > 0$. The final form of the sum rule is therefore:

$$\begin{aligned} \langle l^+ l^- M | H_{\text{eff}} | B(p_B) \rangle &= \frac{1}{f_B m_B^2} \frac{1}{2\pi i} \oint_{\Gamma_P} \exp\left(\frac{m_B^2 - s}{M^2}\right) \Pi^{\text{pert}}(s) ds \\ &\equiv \frac{1}{f_B m_B^2} \int_{m_b^2}^{s_0} \exp\left(\frac{m_B^2 - s}{M^2}\right) \rho(s) ds \quad . \end{aligned} \tag{2.58}$$

The function $\rho(s)$ arises since it is assumed that the contour Γ_P lies along the real line and therefore the contour integration can be traded for an integral of a density function $\rho(s)$. The

Borel parameter in this formula must be selected to satisfy two requirements simultaneously: that the OPE (either the local or light-cone version) converges, i.e. that contributions from operator condensates of higher dimension or twist are suppressed, and that the contribution from the continuum is small; or to put it another way, that the sensitivity to s_0 is minimized [86]. If these conditions cannot both be fulfilled, then the sum rule estimate of the matrix element (2.58) cannot be trusted.

Although the use of sum rules as they are applied to B meson decays has been illustrated, their original development was in the context of two-point Green's functions [86], where they have a very clean theoretical interpretation owing to the Källén–Lehmann spectral representation [89, 90], which states that for a general two-point function

$$\langle \mathcal{T}\{\phi(x)\phi(y)\}\rangle = \int_0^\infty \rho(s)\Delta(x-y,s)\frac{ds}{2\pi} \quad , \tag{2.59}$$

where $\Delta(x-y,s)$ is the Feynman propagator for a free particle of mass $\sqrt{s}$, and a Fourier transform will take this exactly to the form (2.55). Therefore in the case of two-point functions Figure 2.3 is completely general and there can be no branch cuts except on the positive real axis. The optical theorem and Cutkosky cutting rules [91] rather imply that this can be generalised to $2n$-point forward scattering amplitudes. It cannot however be extended to three- and higher n-point functions as will be seen in Chapter 3.

2.9 Decomposition of $B \to V$ and $B \to P$ matrix elements

Matrix elements for $B \to V$ and $B \to P$ transitions are expanded in terms of scalar functions; in order to do this the basis tensors must be specified to fix the normalisation of these functions. The $B \to P$ case is simple since there is only a single meson polarisation and hence only the normalisation is required, whereas in the $B \to V$ case the presence of three polarisations means that the optimal way to separate these must also be taken into account.

Following the conventions of [92], the matrix elements of $B \to M l^+ l^-$ in either the vector or pseudoscalar final state case may be written at leading order in $\alpha_{\rm em}$, i.e. assuming single photon exchange, as

$$\begin{aligned} &{}_{\rm out}\langle M(p) l^+(l_1) l^-(l_2)|B(p+q)\rangle_{\rm in} \\ &= \frac{G_F}{\sqrt{2}}\lambda_t \frac{\alpha_{\rm em} m_b}{q^2\pi}\left(\bar{u}(l_1)\gamma_\mu v(l_2)\sum_i P_i^\mu \mathcal{T}_i^V(q^2) + \bar{u}(l_1)\gamma_\mu\gamma_5 v(l_2)\sum_i P_i^\mu \mathcal{T}_i^A(q^2)\right)\delta^{(4)}(q-l_1-l_2) \quad , \end{aligned} \tag{2.60}$$

where λ_t is as defined below (2.19), and $\bar{u}$ and v are lepton polarisation spinors of mass dimension

1/2. The case $B \to V\gamma$ is closely related and given by:

$$ {}_{\text{out}}\langle V(p)\gamma(q,\epsilon)|B(p_B)\rangle_{\text{in}} = \frac{G_F}{\sqrt{2}}\lambda_t \frac{g_{\text{em}} m_b}{4\pi^2} \sum_i \epsilon_\mu P_i^\mu \mathcal{T}_i^V(0)\delta^{(4)}(p_B - p - q) \quad . \tag{2.61} $$

The corresponding pseudoscalar decay $B \to P\gamma$ does not exist owing to angular momentum conservation. For the same reason, only two of the three possible vector meson polarisations occur in the decay $B \to V\gamma$ since angular momentum conservation requires that the vector meson and photon helicities are the same, and the physical photon has no longitudinal polarisation. The tensors P_i are the standard choice for penguin form factors, e.g. [81, 93]:

$$ \begin{aligned} P_1^\mu =& 2\epsilon^{\mu\nu\rho\sigma}\eta_\nu p_\sigma q_\rho \\ P_2^\mu =& i\left[(m_B^2 - m_V^2)\eta^\mu - (\eta\cdot q)(2p+q)^\mu\right] \\ P_3^\mu =& i(\eta\cdot q)\left[q_\mu - \frac{q^2}{m_B^2 - m_V^2}(2p+q)^\mu\right] \\ P_T^\mu =& \frac{1}{m_B + m_P}\left[(m_B^2 - m_P^2)q^\mu - q^2(2p+q)^\mu\right] \quad . \end{aligned} \tag{2.62} $$

The functions $\mathcal{T}_i$ are usually broken down into contributions from each operator in (2.19), although this is only valid at leading order in α_s, since at higher orders the scale dependence of the Wilson coefficients in (2.19) partially cancels the scale dependence of the matrix elements of each individual operator, and hence only matrix elements which may be factorised in a scale-independent way can be truly considered separate contributions to (2.60). The contribution of the semi-leptonic operators $\mathcal{O}_9$ and $\mathcal{O}_{10}$ are conventionally written in terms of the form factors [81, 93]

$$ \begin{aligned} \langle P(p)|\bar{s}\gamma_\mu b|B(p_B)\rangle =& f_+(q^2)\left((p_B+p)_\mu - \frac{m_B^2 - m_P^2}{q^2}q_\mu\right) + \frac{m_B^2 - m_P^2}{q^2}F_0(q^2)q_\mu \\ \langle V(p,\eta)|\bar{s}\gamma_\mu b|B(p_B)\rangle =& \epsilon_{\mu\nu\rho\sigma}\eta^\nu p_B^\rho p^\sigma \frac{2V(q^2)}{m_B + m_V} \\ \langle V(p,\eta)|\bar{s}\gamma_\mu\gamma_5 b|B(p_B)\rangle =& i\eta_\mu(m_B + m_V)A_1(q^2) - i(p_B+p)_\mu(\eta\cdot p_B)\frac{A_2(q^2)}{m_B + m_V} \\ & - iq_\mu(\eta\cdot p_B)\frac{2m_V}{q^2}\left(A_3(q^2) - A_0(q^2)\right) \quad , \end{aligned} \tag{2.63} $$

where $q \equiv p_B - p$, and

$$ A_3(q^2) = \frac{m_B + m_V}{2m_V}A_1(q^2) - \frac{m_B - m_V}{2m_V}A_2(q^2) \, . \tag{2.64} $$

The additional relations $A_3(0) = A_0(0)$ and $f_+(0) = F_0(0)$ ensure that the matrix elements are free of kinematical singularities at $q^2 = 0$. Likewise, the electromagnetic operator $\mathcal{O}_7$

contribution is written in terms of the form factors

$$\langle P(p)|\bar{s}\sigma_{\mu\nu}q^\nu b|B(p_B)\rangle = i\left((p_B+p)_\mu q^2 - q_\mu(m_B^2-m_P^2)\right)\frac{f_T(q^2)}{m_B+m_P} \tag{2.65}$$

$$\langle V(p,\eta)|\bar{s}\sigma_{\mu\nu}q^\nu b|B(p_B)\rangle = 2i\epsilon_{\mu\nu\rho\sigma}\eta^\nu p_B^\rho p^\sigma T_1(q^2) \tag{2.66}$$

$$\begin{aligned}\langle V(p,\eta)|\bar{s}\sigma_{\mu\nu}q^\nu\gamma_5 b|B(p_B)\rangle =& T_2(q^2)\left(\eta_\mu(m_B^2-m_V^2)-(\eta\cdot p_B)(p_B+p)_\mu\right)\\ &+T_3(q^2)(\eta\cdot p_B)\left(q_\mu-\frac{q^2}{m_B^2-m_V^2}(p_B+p)_\mu\right)\quad,\end{aligned} \tag{2.67}$$

and Dirac algebra implies that $T_1(0)=T_2(0)$.

The matrix element parametrisation in (2.60) is chosen such that $\mathcal{T}_i^V \sim C_7 T_i + \ldots$. The axial lepton amplitude $\mathcal{T}^A$ arises entirely from the $\mathcal{O}_{10}$ operator, and in terms of the standard form factors (2.63) is

$$\mathcal{T}^A_{1,2,3} = C_{10}H_{1,2,3}(q^2) \qquad \mathcal{T}^A_T = C_{10}h_T(q^2)\quad, \tag{2.68}$$

where the functions H_i and h_T are defined to capture the conversion factors

$$\begin{aligned} H_0(q^2) &= (\eta\cdot q)\frac{m_V}{m_b}A_0(q^2) & H_1(q^2) &= \frac{q^2V(q^2)}{2m_b(m_B+m_V)}\\ H_2(q^2) &= \frac{q^2A_1(q^2)}{2m_b(m_B-m_V)} & H_3(q^2) &= -\frac{m_V}{m_b}A_3(q^2)\\ h_0(q^2) &= -\frac{m_B^2-m_P^2}{2m_b}f_0(q^2) & h_T(q^2) &= \frac{m_B+m_P}{2m_b}f_+(q^2)\,. \end{aligned} \tag{2.69}$$

for later convenience. The vector lepton amplitudes $\mathcal{T}^V$ are expanded as:

$$\begin{aligned}\mathcal{T}_i^V(q^2) &= C_9^{\text{eff}}(q^2)H_i(q^2) + C_7^{\text{eff}}T_i(q^2) + C_8^{\text{eff}}G_i(q^2) + W_i(q^2) + S_i(q^2) + L_i(q^2) \quad i=1,2,3\\ \mathcal{T}_T^V(q^2) &= C_9^{\text{eff}}(q^2)h_T(q^2) + C_7^{\text{eff}}f_T(q^2) + C_8^{\text{eff}}G_T(q^2) + W_T(q^2) + S_T(q^2)\end{aligned} \tag{2.70}$$

For readers unfamiliar with this particular subject area, T_i, f_T and all functions appearing on the right-hand side of (2.69) are standard: the functions $\mathcal{T}_i$ defined here are similar in spirit and notation to those used in [42] but are not equivalent owing to $\mathcal{O}_{9,10}$ contributions being included here but treated separately there, and the remaining functions G_i, W_i, S_i and L_i are not used outside this thesis and the papers on which it is based.

The form factor functions T_i, f_T and those in (2.69) are taken where required from [81, 93]. The functions G_i were calculated in [94] and this calculation is detailed further in Chapter 3. The functions W_i and S_i arise from the four-quark operators, and are an arbitrary separation convenient for examining the isospin asymmetry in $B\to K^*ll$. These functions were calculated in [92] and this calculation is described in Chapter 5. The functions L_i arise from a charm bubble emitting a soft gluon into the final state meson and are calculated in Chapter 6 [95]. The effective Wilson coefficients $C_{7,8,9}^{\text{eff}}$ are explained in Section 2.4.

The standard choice of basis tensors (2.62) is however less than ideal in the vector meson case, because it does not uniquely separate the contribution of longitudinally polarised mesons. It is advantageous to separate this contribution for two reasons: first, it clearly separates the terms that do not appear at $q^2 = 0$, and second, the vector meson distribution amplitudes nicely separate into transverse and longitudinal terms at leading and next-to-leading twist. In [92], the basis used was

$$\begin{aligned} P_V^\mu &= 2\epsilon^{\mu\nu\rho\sigma}\eta_\nu p_\rho q_\sigma \\ P_A^\mu &= \frac{i}{\sqrt{\hat{\lambda}_V}}\left(\hat{\lambda}_V m_B^2 \eta^\mu - 2(\eta\cdot q)\left((1-\hat{m}_V^2-\hat{q}^2)p^\mu - 2\hat{m}_V^2 q^\mu\right)\right) \\ P_0^\mu &= \frac{4i\hat{m}_V}{\sqrt{2\hat{q}^2\hat{\lambda}_V}}(\eta\cdot q)\left[2\hat{q}^2 p^\mu - (1-\hat{m}_V^2-\hat{q}^2)q^\mu\right] \quad , \end{aligned} \tag{2.71}$$

where hatted quantities are dimensionless and normalised to the B meson mass ($\hat{q}^2 = q^2/m_B^2$ and $\hat{m}_V = m_V/m_B$), and

$$\lambda_V \equiv \lambda(1, \hat{m}_V^2, \hat{q}^2) = ((1+\hat{m}_V)^2 - \hat{q}^2)((1-\hat{m}_V)^2 - \hat{q}^2) \tag{2.72}$$

is the Källén function, again with normalised entries. P_V and P_A are the tensors associated with transverse meson polarisations since $p \cdot P_{V,A} = 0$, and P_0 is the longitudinal, or zero helicity, polarisation. P_V and P_A are labelled as such since they arise from the vector and axial vector part of the weak current respectively; it is also convenient to define positive and negative helicity coefficient tensors by

$$P_\pm^\mu = \frac{1}{\sqrt{2}}\left[P_V^\mu \mp P_A^\mu\right] \quad , \tag{2.73}$$

since the left-handed structure of weak decays means that $\mathcal{T}_-$ is expected to be zero up to quark mass-type corrections[7]. Subscripts attached to T, $\mathcal{T}$ and other functions defined in (2.70) indicate that the subscripted symbol is the coefficient of that tensor, so that there are three possible bases:

$$\begin{aligned} \mathcal{T}_1(q^2)P_1^\mu + \mathcal{T}_2(q^2)P_2^\mu + \mathcal{T}_3(q^2)P_3^\mu &= \mathcal{T}_V(q^2)P_V^\mu + \mathcal{T}_A(q^2)P_A^\mu + \mathcal{T}_0(q^2)P_0^\mu \\ &= \mathcal{T}_+(q^2)P_+^\mu + \mathcal{T}_-(q^2)P_-^\mu + \mathcal{T}_0(q^2)P_0^\mu \quad . \end{aligned} \tag{2.74}$$

[7] Specifically, either non-zero quark masses or chiral odd vacuum condensates such as $\langle\bar{q}q\rangle$, $\langle\bar{q}Gq\rangle$, etc.

The conversion formulae between these bases are:

$$\mathcal{T}_{\pm}(q^2) = \frac{1}{\sqrt{2}}[\mathcal{T}_V(q^2) \mp \mathcal{T}_A(q^2)] \tag{2.75}$$

$$\mathcal{T}_0(q^2) = \frac{1}{\hat{m}_V}\sqrt{\frac{\hat{q}^2}{8}}\left[\frac{1+3\hat{m}_V^2-\hat{q}^2}{\sqrt{\hat{\lambda}_V}}\mathcal{T}_2(q^2) - \frac{\sqrt{\hat{\lambda}_V}}{1-\hat{m}_V^2}\mathcal{T}_3(q^2)\right] \tag{2.76}$$

$$\mathcal{T}_V(q^2) = \mathcal{T}_1 \tag{2.77}$$

$$\mathcal{T}_A(q^2) = \frac{1-\hat{m}_V^2}{\sqrt{\hat{\lambda}_V}}\mathcal{T}_2(q^2) \quad . \tag{2.78}$$

Note that for $m_V \to 0$ this reproduces the heavy quark form factors, for example comparing to the notation $\mathcal{T}_{\perp,\parallel}$ of [42]

$$\mathcal{T}_{V,A}(q^2) \xrightarrow{m_V\to 0} \mathcal{T}_\perp(q^2) \qquad \mathcal{T}_0(q^2) \xrightarrow{m_V\to 0} -\sqrt{\frac{q^2}{m_V^2}}(1-\hat{q}^2)\mathcal{T}_\parallel(q^2) \quad , \tag{2.79}$$

where $\mathcal{T}_V(q^2) = \mathcal{T}_A(q^2)$ in the heavy quark limit [96,97].

Writing the decay rate in terms of the $\mathcal{T}_i$ functions leads to simple expressions for the total $B \to V$ and $B \to P$ decay rates:

$$\frac{d\Gamma}{dq^2}[B \to V l^+ l^-] = \left[\frac{\hat{\lambda}_V^{3/2}}{q^2}\right]\left(\frac{\alpha_{\rm em}}{4\pi}\right)^2 c_H \sum_{i=V,A}\left[\left|\mathcal{T}_V^i(q^2)\right|^2 + \left|\mathcal{T}_A^i(q^2)\right|^2 + \left|\mathcal{T}_0^i(q^2)\right|^2\right] \tag{2.80}$$

$$\frac{d\Gamma}{dq^2}[B \to P l^+ l^-] = \left[\frac{\hat{\lambda}_P^{3/2}}{2(m_B+m_K)^2}\right]\left(\frac{\alpha_{\rm em}}{4\pi}\right)^2 c_H \sum_{i=V,A}\left|\mathcal{T}_T^i(q^2)\right|^2 \tag{2.81}$$

$$\Gamma[B \to V\gamma] = \left[\frac{3}{4}\hat{\lambda}_V^{3/2}\right]\left(\frac{\alpha_{\rm em}}{4\pi}\right) c_H \left[\left|\mathcal{T}_V^V(0)\right|^2 + \left|\mathcal{T}_A^V(0)\right|^2\right] \quad , \tag{2.82}$$

where

$$c_H \equiv \frac{G_F^2|\lambda_t|^2 m_b^2 m_B^3}{12\pi^3} \tag{2.83}$$

arises from the weak effective Hamiltonian and meson phase space factors and the lepton mass has been neglected. The normalisation of the tensors (2.71) is chosen such that each of the $\mathcal{T}$ functions has the same effect on the decay rate (2.80). The decay rates (2.80) and (2.81) have had the integration over the final state angular distribution performed, since that was the quantity of interest in studying the isospin asymmetry in Chapter 5. However, a set of optimized angular observables for $B \to V l^+ l^-$ has been developed in [98–100], one of which will be discussed in Chapter 6.

2.10 The ultra-relativistic approximation

There is a well-known approximation in light-cone physics relating longitudinally polarised vector meson results to those for pseudoscalar mesons. The reason for this arises from a term

in the K^* DA [81][8]

$$\langle K^*(p,\eta)|\bar{s}(x)_a[x,0]q(0)_b|0\rangle = \int_0^1 du\, e^{iup\cdot x}\frac{m_{K^*}f_{K^*}}{4N_c}(\not{\eta})_{ba}\frac{\eta\cdot x}{p\cdot x}\phi_\parallel(u) + \dots \tag{2.84}$$

which is strikingly similar to the leading twist term in the K DA [93]

$$\langle K(p)|\bar{s}(x)_a[x,0]q(0)_b|0\rangle = \int_0^1 du e^{iup\cdot x} i\frac{f_K}{4N_c}[\not{p}\gamma_5]_{ba}\phi_K(u) + \dots \tag{2.85}$$

apart from the $\frac{\eta\cdot x}{p\cdot x}$ term and having opposite parity. The fact that it has opposite parity is normally irrelevant for weak decays since the γ_5 matrix can usually be eliminated by $\gamma_5(1-\gamma_5) = -(1-\gamma_5)$ up to quark mass-type corrections, which are expected to be small. For a two-body decay, the polarisation vector may be separated into $\eta^\mu = \eta^\mu_\perp + \eta^\mu_\parallel$, where $\eta_\perp \cdot q = 0$ gives the transverse component perpendicular to the plane of the decay. This is done fully in 5.12; however, in the limit $m^2_{K^*} \to 0$, it is straightforward to show that

$$\eta^\mu_\parallel = \frac{p}{m_{K^*}} + O(m^*_K) \quad , \tag{2.86}$$

which allows the inconvenient factor $\frac{\eta\cdot x}{p\cdot x}$ to be eliminated in this limit. It therefore follows that

$$\langle K^*(p,\eta_\parallel)|\bar{s}(x)_a[x,0]q(0)_b|0\rangle \sim \langle K(p)|\bar{s}(x)_a[x,0](i\gamma_5 q(0))_b|0\rangle + O(m^2_{K,K^*}) \quad , \tag{2.87}$$

subject to replacement of masses, decay constants and Gegenbauer moments in the DA. This replacement will be used in Chapter 3 to calculate the chromomagnetic form factor of longitudinally polarised mesons.

The conventional wisdom that longitudinally polarised vector mesons are equivalent to pseudoscalar mesons is however incorrect. Aside from the fact that it is dependent on the $V-A$ structure of SM weak interactions to eliminate the parity difference, which invalidates the approximation beyond the SM, it also does not hold beyond the leading twist DA. It is apparent from (2.86) that $O(m^2_{K^*})$ corrections to the approximation should be expected, however in fact there are also corrections at the first subleading order $O(m_{K^*})$. This can be seen from the selection rules for WA in table 5.1, since the pseudoscalar meson couples to an operator that the vector meson does not, which is what brought it to our attention [92].

At next-to-leading order in m_{K^*}, there are two types of new term appearing in the K^* DAand one in the K DA. In the case of the $g_\perp^{(v,a)}$ DAs in the K^*, the ultra-relativistic approximation holds, because these contribute to the perpendicular polarisation amplitude at $O(m_{K^*})$ and thus do not interfere with the longitudinal polarisation. An example of this is given by the operators $O^{\text{WA}}_{6,8}$ in WA in Section 5.3. The other new terms at $O(m_{K,K^*})$ are the $h_\parallel^{(s,t)}$ and $\phi_{p,\sigma}$ in the K^* and K respectively. These do not respect the ultra-relativistic approximation and

[8] See appendix B for more complete DAs and an explanation of terms involved

thus it breaks down at $O(m_{K,K^*})$.

Two points about this breakdown are worth noting: first, it is small in heavy-to-light decays owing to power counting in $1/m_B$: the $\phi_\perp$ and $g_\perp^{(v,a)}$ terms are both leading in $1/m_B$ for perpendicular polarisations so are both included [101]; however, for longitudinal polarisation only $\phi_\parallel$ is leading and so the effects of $h_\parallel^{(s,t)}$ can be neglected. This means that the violation of the ultra-relativistic approximation is small. The second point is the origin of the breakdown: the K and K^* are fundamentally different particles and in fact the subleading twist DAs $\phi_{p,\sigma}$ and $h_\parallel^{(s,t)}$ have entirely different origins. The twist-3 K^* DAs $h_\parallel^{(s,t)}$ are related by Wandzura-Wilczek type equations of motion to $\phi_\perp$[9] [70] and are thus not independent degrees of freedom. The twist-3 K DAs $\phi_{p,\sigma}$ are also constrained by equations of motion but there is no equivalent to $\phi_\perp$ for the K, and in fact the leading contribution to $\phi_{p,\sigma}$ is from chiral symmetry breaking [93]. This can be seen from the appearance of the coefficient $\mu_K^2 = f_K m_K^2/(m_s + m_q)$, which is approximately $\mu_K^2 \sim \langle \bar{q}q \rangle / f_K$ according to the Gell-Mann–Oakes–Renner relation [102].

[9] Neglecting three particle contributions.

Chapter 3

The chromomagnetic operator in heavy-to-light FCNCs

This chapter will describe the calculation of the matrix elements

$$\langle M(p)\gamma^*(q)|\mathcal{O}_8|H(p_B)\rangle \tag{3.1}$$

where $p_B = p+q$. The operator $\mathcal{O}_8$ is the chromomagnetic operator of the electroweak effective Hamiltonian discussed in Section 2.4, given by:

$$\mathcal{O}_8 = -\frac{g}{8\pi^2} m_b \bar{s}\sigma \cdot G(1+\gamma_5)b \equiv \left[-\frac{g m_b}{8\pi^2}\right]\tilde{\mathcal{O}}_8 \quad . \tag{3.2}$$

This operator also contains a small term proportional to the strange quark mass which couples to the right- rather than left-handed s quark, but this will be neglected as the strange quark mass is neglected throughout this calculation. H is a pseudoscalar heavy meson, principally the B meson, but results will also be provided for the D meson albeit with considerably larger uncertainty. M is a pseudoscalar or vector meson and γ^* is a photon, which may be off-shell so that both the decays to a photon and a lepton pair can be accessed.

The calculation of the chromomagnetic matrix elements has been previously published in [103].

3.1 Matrix element and sum rule

For definiteness, throughout this chapter the initial state meson shall be taken to be a B meson and the final state meson shall be taken to be a vector meson. The replacement of B with D is straightforward and the replacement of the final state vector meson with a pseudoscalar is

in this case closely related to the longitudinal degree of freedom of the vector, as discussed in Section 2.10. The amplitude of the transition induced by the chromomagnetic operator reads:

$$\mathcal{A}^{*\rho}(V) \equiv \langle \gamma^*(q,\rho)V(p,\eta)|\tilde{O}_8|\bar{B}(p_B)\rangle = i\int \langle V|Tj^\rho_{\rm em}(x)\tilde{\mathcal{O}}_8(0)|\bar{B}\rangle\, e^{iq\cdot x}d^4x + \dots \quad (3.3)$$

The dots stand for higher twist contributions not captured by perturbation theory; in the case of the on-shell photon the leading twist photon DA will be discussed in Section 3.4.1. For a sufficiently off-shell photon the local OPE would be more appropriate; however, only the leading perturbative term will be considered here as higher dimension operators should be substantially suppressed for $q^2 > 1\,\text{GeV}^2$. The intermediate region $0 < q^2 < 1\,\text{GeV}^2$ is too close to the vicinity of the ρ meson intermediate state to be computable perturbatively. The external momenta are $p_B = p+q$ and η is the vector meson polarisation. The photon polarisation is left as the uncontracted index ρ here. The operator $\tilde{\mathcal{O}}_8 = \bar{s}\sigma\cdot G(1+\gamma_5)b$ is the operator $\mathcal{O}_8$ (3.2) after dropping the constant prefactor.

Four scalar functions are defined corresponding to the three polarisations of the vector meson and the one of the pseudoscalar:

$$\begin{aligned} c_V\,\mathcal{A}^{*\rho}(V) &= k_G\left(G_1(q^2)P_1^\rho + G_2(q^2)P_2^\rho + G_3(q^2)P_3^\rho\right) \\ \mathcal{A}^{*\rho}(P) &= k_G\left(G_T(q^2)P_T^\rho\right) \quad . \end{aligned} \quad (3.4)$$

The Lorentz structures P_i^ρ are defined in Section 2.9, and importantly are the same as those used in the definition of the standard $B\to V$ and $B\to P$ tensor form factors. The factor c_V is included to absorb factors arising from coupling only to one valence state of a meson, which occurs in the case of $\rho^0 \sim (\bar{u}u - \bar{d}d)/\sqrt{2}$ and $\omega \sim (\bar{u}u + \bar{d}d)/\sqrt{2}$, where a $b\to d$ transition will only couple to the $\bar{d}d$ component. This means that $c_V = -\sqrt{2}$ for $B\to\rho^0$, $c_V = \sqrt{2}$ for $B\to\omega$ and $c_V = 1$ in all other transitions. The constant $k_G \equiv -2e/g$ is chosen so that the functions G_ι parallel the standard form factors T_i and f_T[1]:

$$\begin{aligned} \langle \gamma^*(q,\rho)V(p,\eta)|H_{\rm eff}|\bar{B}\rangle &\propto \sum_i (C_7T_i(q^2) + C_8G_i(q^2))P_i^\rho + \dots \\ \langle \gamma^*(q,\rho)P(p)|H_{\rm eff}|\bar{B}\rangle &\propto (C_7f_T(q^2) + C_8G_T(q^2))P_T^\rho + \dots \end{aligned} \quad (3.5)$$

For semi-leptonic decays, the physical domain of these functions is $4m_l^2 < q^2 < (m_B - m_{P,V})^2$; however, lepton masses do not directly enter this calculation except through q^2. The validity of these results will be futher discussed in Section 3.4.1.

Since the weak interaction is localised through the effective Hamiltonian, the transition matrix element for $\mathcal{O}'_8$, which is $\mathcal{O}_8$ with opposite chirality $(1+\gamma_5)\to(1-\gamma_5)$ can be inferred directly. Under exchange of chirality $(1+\gamma_5)\to(1-\gamma_5)$ in $\mathcal{O}_8$ (3.2), the G_ι-functions transform

[1] See Section 2.9 for their definitions.

as follows:

$$\{G_1, G_2, G_3, G_T\} \xrightarrow{(1+\gamma_5)\to(1-\gamma_5)} \{G_1, -G_2, -G_3, G_T\} \quad . \tag{3.6}$$

Note however that this calculation cannot be used to compute the effect of $\mathcal{O}_8'$ in the SM since it is proportional to m_s which is taken to be zero. Beyond–SM applications where $\mathcal{O}_8'$ has a larger coefficient are the intended use of (3.6), and one such application will be discussed in Chapter 4.

3.1.1 The sum rule

The matrix elements (3.1) are extracted from the correlation function

$$\Pi^V(q^2, p_B^2) = \epsilon^{*\rho}(q)\Pi_\rho^V(q^2, p_B^2) = i\int \langle \gamma^*(q)V(p)|TJ_B(x)\tilde{O}_8(0)|0\rangle\, e^{-ip_B\cdot x}d^4x \tag{3.7}$$

where the B meson figures as an interpolating current:

$$J_B = im_b\bar{b}\gamma_5 q\ , \qquad \langle B(p_B)|J_B|0\rangle = m_B^2 f_B \quad . \tag{3.8}$$

In the equation above $q = u, d$ are light flavoured quarks and f_B is the standard B meson decay constant. The techniques for extracting the matrix element (3.3) from (3.7) are discussed in Section 2.8. In the present case, however, a major complication will arise: it will not be possible to write the perturbative computation of (3.7) in the form

$$\Pi^V(q^2, p_B^2) = \int_{m_b^2}^{\infty} \frac{\rho(q^2, s)}{s - p_B^2} ds \tag{3.9}$$

as in (2.54), where the integral is taken along the real line. The situation that will occur is depicted in Figure 3.5, which shows the presence of a complex singularity off the real line. As will be shown later, the presence of this singularity is the result of analytic continuation from the Euclidean momentum region to the physical one and cannot be avoided by a different choice of Riemann sheet. This complex singularity is the result of an anomalous threshold in the three-point Green's function (3.7) and the key point in relation to constructing a sum rule in the presence of such an anomalous threshold is that its real part is above the duality threshold. Therefore, the anomalous threshold and the associated branch cut are taken to be part of the continuum of excited and multi-particle states, and thus the final sum rule will still be in the form of an integral along the real line and may be interpreted as a density function in the sense of the Källén-Lehmann spectral representation [89, 90] below the duality threshold.

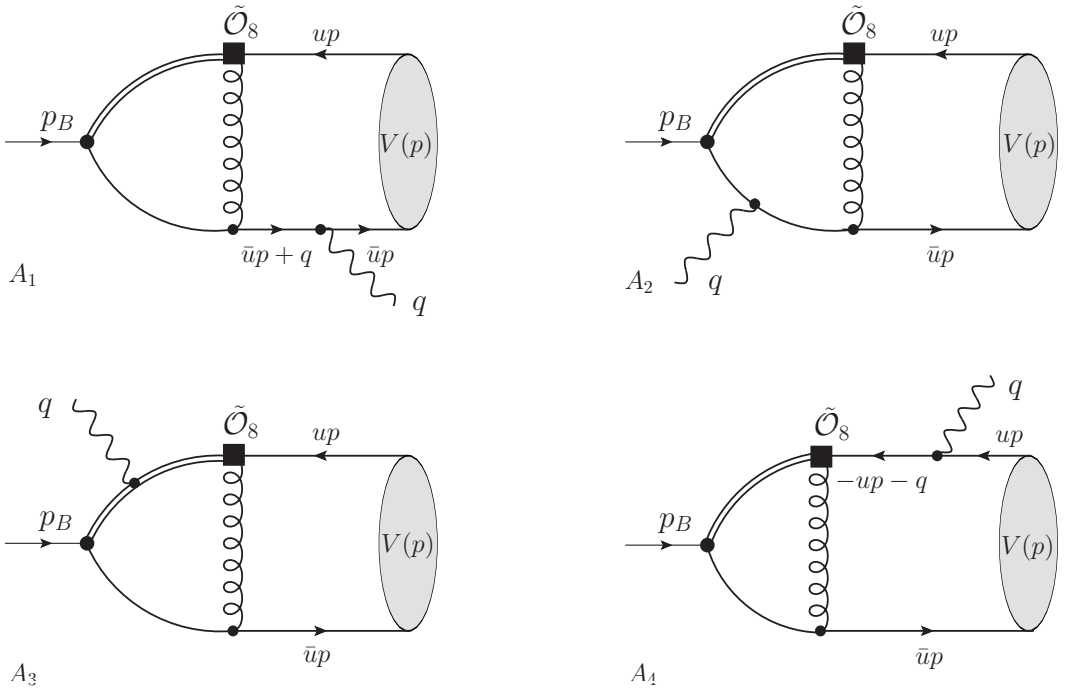

Figure 3.1: Chromomagnetic spectator scattering diagrams. $V(p)$ is the external meson distribution amplitude, which may be a vector or pseudoscalar meson. The pseudoscalar meson case is related to the longitudinal polarisation of the vector meson when using the ultra-relativistic approximation so no additional computation is required. See Section 2.10 for discussion.

3.2 Computation of G_ι

At leading order in α_s there are twelve graphs contributing to G_ι. They can be separated into two groups as shown in figures 3.1 and 3.2:

$$G_\iota(q^2) = G_\iota^{(s)}(q^2) + G_\iota^{(ns)}(q^2) \quad . \tag{3.10}$$

$G_\iota^{(ns)}$ contains six graphs in which the gluon from the chromomagnetic operator connects to the b- or s-quark line, henceforth known as non-spectator graphs. $G_\iota^{(s)}$ contains four graphs in which the gluon connects to the light quark line, known as spectator graphs. The two remaining graphs in which the gluon connects to the heavy quark line and the photon is radiated from the spectator quark line are neglected; they are expected to be suppressed since none of the energy from the heavy quark decay is transferred to the light quark.

The non-spectator graphs (Figure 3.1) may be computed in an inclusive approach [104] and then convoluted with vector and magnetic penguin form factors to produce an exclusive result. This procedure is described in Section 3.2.5. The main part of this chapter is devoted to the computation of the spectator graphs $G_\iota^{(s)}$ and a discussion of the complications outlined in Section 3.1.1.

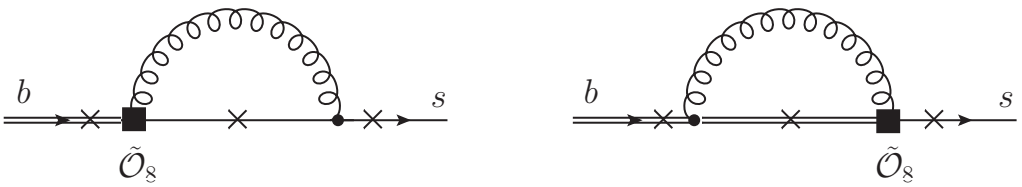

Figure 3.2: Non-spectator contributions to G_ι. The contribution from these graphs can be computed via a convolution of the inclusive result of [104] with the vector and magnetic penguin form factors described in 2.9.

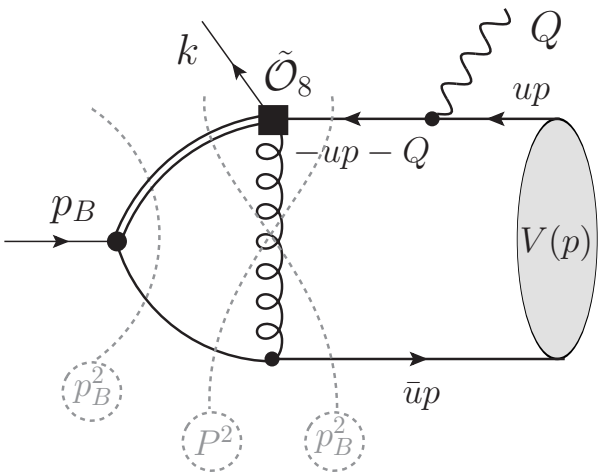

Figure 3.3: Cuts in the presence of the extended external momentum configuration. The momentum insertion k at the weak operator introduces the new momentum invariant $P^2 \equiv (p_B - k)^2$. The cut in P^2 should not be included in the dispersion representation since, as is clear from the diagram, it cuts the s rather than the b quark line and hence has the wrong quantum numbers for a B meson state. The two cuts in p_B^2 both have the right quantum numbers and indicate that this sum rule includes both two- and three- particle B meson states, and thus both hard gluon scattering and contribution from initial state soft gluons are included.

3.2.1 Parasitic cuts

The discussion of sum rules in Section 2.8 does not touch upon the technical details of the analytic structure of correlations such as (3.7). The analytic structure of two-point functions is known from the Källén-Lehmann spectral representation [89, 90], and correspondingly sum rules derived from correlation functions with the same initial and final state are expected to have simple structure. This situation arises for example in the case of the cross-section for $e^+e^- \to$ hadrons, e.g. [105], and such sum rules are known as diagonal.

The correlation function (3.7) is however non-diagonal. The analytic structure of this correlation function can be partially examined through Cutkosky rules [91]. The cuts corresponding to the momentum from the J_B current insertion are shown for diagram A_4 in Figure 3.3. Of the three cuts shown, only two cut the b quark line. The third instead cuts the s quark line: this cut should not enter the sum rule for a B meson initial state since it has the wrong quantum numbers and it also leads to a cut starting at $p_B^2 = 0$ rather than $p_B^2 = m_b^2$, as would be

expected from a perturbative approximation to a B meson state. This additional cut may be considered to arise from alternative time orderings in (3.7), since the matrix element may be written

$$\begin{aligned} & i\,\langle\gamma^*(q)V(p)|TJ_B(x)\tilde{O}_8(0)|0\rangle\,e^{-ip_B\cdot x} \\ & = \sum_\psi \Big[\langle\gamma^*(q)V(p)|\tilde{O}_8(0)|\psi\rangle\,\langle\psi|J_B(x)|0\rangle\,\theta(-x_0) + \langle\gamma^*(q)V(p)|\psi\rangle\,\langle\psi|J_B(x)\tilde{O}_8(0)|0\rangle\,\theta(x_0)\Big] \quad , \end{aligned} \tag{3.11}$$

with appropriate normalisation of the complete set of inserted states $|\psi\rangle$. For $x_0 < 0$ only those states $|\psi\rangle$ with $\bar{b}q$ quantum numbers contribute, whereas for $x_0 > 0$ only those with $\bar{s}q$ do so. Unfortunately this observation, while interesting, does not lead to an apparent method to select only the B meson-like cuts, since inserting the Heaviside step function into the expression (3.7) breaks manifest Lorentz invariance, which it would seem wise to avoid.

The method used to circumvent this problem was introduced by Khodjamirian for $B \to \pi\pi$ in [106]; similar approaches have also been used previously outside B physics [107, 108]. The approach is to consider the three external momenta p_B, p and q to be independent, or equivalently to introduce a spurious momentum k flowing into the chromomagnetic operator $\tilde{\mathcal{O}}_8$. The sum is then based on a four-point rather than a three-point correlation function, so there are three additional momentum invariants which are taken to be the squares of the vectors

$$P \equiv p_B - k \qquad\qquad Q \equiv q - k \tag{3.12}$$

and the spurious momentum k itself. The effect of this modification on the diagram A_4 is shown in Figure 3.3, where it can be seen that the sq state now has momentum P rather than p_B and therefore does not contaminate the analytic structure in p_B^2. To recover the correlation function (3.1) from the sum rule with the extended external momentum configuration, the five invariants P^2, q^2, Q^2, p^2, k^2 are set on-shell:

$$P^2 = m_B^2 \qquad q^2 = Q^2 \qquad k^2 = 0 \qquad p^2 = m_{V,P}^2 \quad . \tag{3.13}$$

The approximation $m_{V,P}^2 = 0$ is used throughout this calculation, which is required for consistency with the level of twist approximation of the final state meson[2]. This choice is not unique: as is well known the kinematics of a four-point function may be described in terms of Mandelstam variables [109], and the seven kinematic invariants that can be constructed are reduced to six by a constraint. In the present case the invariant $(p+k)^2 = (p_B - Q)^2 = p_B^2 - P^2$ may be considered the seventh momentum square, and under the choice (3.13) it is not on shell where it would be zero. However $p_B^2 - P^2 = O(m_b\Lambda_{\rm QCD})$ is in fact not off-shell in the dispersion

[2] Corrections due to the non-zero mass of the vector or pseudoscalar meson first enter at twist 4.

integral by more than the width of the duality window, and hence this problem should be considered part of the intrinsic uncertainty of the semi-global duality approximation. The quantity $p_B^2 - P^2$ does however contain the invariant p_B^2 used to construct the dispersion relation where it arguably should not, and hence this may be expected to affect the complex structure of the dispersion representation, which, as it turns out, is what happens.

The addition of an external momentum k means that the P_ι basis described in Section 2.9 is no longer adequate. Instead an extended basis with an additional tensor structure in each of the pseudoscalar and vector meson cases is used. The correlation function (3.7) is expanded in terms of functions g_ι, where $\iota \in \{0,1,2,3,4\}$ for the vector meson and $\iota \in \{0, T, \bar{T}\}$ in the pseudoscalar case:

$$\Pi^V = \sum_{i=0}^{4} g_i(q^2)\epsilon(Q)\cdot p_i \qquad\qquad \Pi^P = \sum_{i\in\{0,T,\bar{T}\}} g_i(q^2)\epsilon(Q)\cdot p_i \quad . \tag{3.14}$$

The basis tensors are a straightforward extension of the standard basis (2.62) and are given by

$$\begin{aligned}
p_1^\rho =& 2\epsilon^{\rho\alpha\beta\gamma}\eta_\alpha p_\beta Q_\gamma \\
p_2^\rho =& i\left[((p_B+p)\cdot Q)\eta^\rho - (\eta\cdot Q)(p_B+p)^\rho\right] \\
p_3^\rho =& i\left[(\eta\cdot Q)Q^\rho - (\eta\cdot Q)(p_B+p)^\rho \frac{q^2}{Q\cdot(p_B+p)}\right] \\
p_4^\rho =& i\left[(\eta\cdot Q)k^\rho - (\eta\cdot Q)(p_B+p)^\rho \frac{k\cdot Q}{Q\cdot(p_B+p)}\right]
\end{aligned} \tag{3.15}$$

in the vector case and

$$\begin{aligned}
p_T^\rho =& (m_B - m_P)\left[Q^\rho - \frac{q^2}{Q\cdot(p_B+p)}(p_B+p)^\rho\right] \\
p_{\bar{T}}^\rho =& (m_B - m_P)\left[k^\rho - \frac{k\cdot Q}{Q\cdot(p_B+p)}(p_B+p)^\rho\right]
\end{aligned} \tag{3.16}$$

in the pseudoscalar case. The final tensor $p_0^\rho = Q^\rho$ is expected to have coefficient zero due to gauge invariance. Similarly to the kinematics (3.13), this extension is not unique, since the pairs of vectors (p_B, P), (q, Q) and $(p, p+k)$ are not distinguished when the external momenta are on shell ($k = 0$). The choices (3.15) and (3.16) maintain $p_\iota \cdot Q = 0$, since away from $k = 0$ the external photon momentum is Q rather than q. To return to the original basis without k, the matrix elements $G_{1,2,3,T}(q^2)$ are computed from the dispersion representations of $g_{1,2,3,T}(q^2)$ and the functions $g_{4,\bar{T}}(q^2)$ are discarded.

3.2.2 Spectator graphs

The graphs A_1-A_4 (q.v. Figure 3.1) can be straightforwardly evaluated. The light-cone OPE is used to treat the final state meson, and the calculation was performed using FeynCalc [25]

to perform Dirac traces, Passarino–Veltman reduction and basis projection. Following this automated calculation, the functions g_ι are expressed in terms of polynomials of the external momentum squares and eight Passarino–Veltman functions [110], which are:

$$\begin{aligned}
B_a &= B_0(u(p_B^2 - P^2), 0, m_b^2) & B_b &= B_0(p_B^2 - P^2, 0, m_b^2) \\
B_c &= B_0(up_B^2 + \bar{u}q^2, 0, m_b^2) & B_d &= B_0(p_B^2, 0, m_b^2) \\
C_a &= C_0(p_B^2, u(p_B^2 - P^2), \bar{u}P^2 + uq^2, 0, m_b^2, 0) & C_b &= C_0(p_B^2, p_B^2 - P^2, q^2, 0, m_b^2, 0) \\
C_c &= C_0(up_B^2 + \bar{u}q^2, u(p_B^2 - P^2), q^2, m_b^2, 0, m_b^2) & C_d &= C_0(p_B^2, p_B^2 - P^2, q^2, m_b^2, 0, m_b^2) \quad .
\end{aligned} \tag{3.17}$$

Note that the functions in the right-hand column are simply those in the left-hand column at $u = 1$, so dispersion representations will not be given for these separately[3]. To give explicit results, the vector meson amplitudes are broken down into the contribution from longitudinal and transverse polarisations:

$$g_i(q^2) = g_i^{(\perp)} + g_i^{(\parallel)}(q^2) \quad . \tag{3.18}$$

At twist-2 the transverse and longitudinal polarisations are identified directly with the distribution amplitudes $\phi_\perp(u)$ and $\phi_\parallel(u)$. For the perpendicular polarisation the result may be written:

$$g_1^{(\perp)}(q^2) = g_3^{(\perp)}(q^2) = \frac{g_2^{(\perp)}(q^2)}{1 - q^2/P^2} = -\frac{\alpha_s}{8\pi} k_G C_F f_V^\perp m_b^2 \int_0^1 \phi_\perp(u) t_H^{(\perp)}(u) du \quad . \tag{3.19}$$

The relations between $g_{1,2,3}^{(\perp)}$ are not accidental, rather the $g_1^{(\perp)}$–$g_2^{(\perp)}$ relation is a result of the left-handed structure of the $\tilde{\mathcal{O}}_8$ operator inherited from the W boson interaction combined with the leading twist approximation for the vector meson, and the $g_2^{(\perp)}$–$g_3^{(\perp)}$ relation arises because the parity-violating perpendicular polarisation corresponds to a specific linear combination of p_2 and p_3, with the orthogonal combination being the longitudinal polarisation, as discussed in Section 2.9. The integrand kernel $t_H^{(\perp)}$ is given by

$$t_H^{(\perp)}(u) = \frac{Q_q B_a + Q_b B_c + 2(Q_q + Q_b) B_d}{uq^2 + \bar{u}P^2} - 2Q_q C_a - Q_b C_c + \ldots \tag{3.20}$$

where $Q_b = -1/3$ is the b quark charge and $Q_q = +2/3$ or $-1/3$ is the light quark charge which depends on the heavy meson under consideration. The dots represent additional finite terms which do not contribute to the dispersion representation (they disappear under Borel subtraction) and are dependent on the exact treatment of γ_5 in dimensional regularisation owing to the issues touched on in Section 2.4. The longitudinal polarisation will be dealt with

[3] For definiteness the parameter convention used is the same as that used in FeynCalc [25], LoopTools [111] and Denner's review [52].

momentarily. The pseudoscalar function $g_T(q^2)$ is given by

$$g_T^{(\perp)}(q^2) = -\frac{\alpha_s}{8\pi} k_G C_F f_P^{\perp} m_b^2 \int_0^1 \phi_P(u) t_H^{(P)}(u) du \quad ; \tag{3.21}$$

however, in this case the integrand is considerably more complicated and thus the expression for $t_H^P(u)$ is deferred to appendix D.1.

The longitudinally polarised vector meson contribution can be computed from $g_T(q^2)$ using the ultra-relativistic approximation[4]. In the limit of the meson mass going to zero, the longitudinal polarisation vector may be written:

$$\eta = \frac{p}{m_V} + O(m_V) \quad . \tag{3.22}$$

Inserting this into the DA (B.3) yields an expression identical in structure to (B.1) at leading twist-2, aside from the presence of γ_5 in the latter. The $(1+\gamma_5)$ in the $\mathcal{O}_8$ operator can be commuted to the pseudoscalar DA insertion and then the γ_5 is annihilated by $(1+\gamma_5)\gamma_5 = (1+\gamma_5)$. Note that for the operator $\mathcal{O}_8'$ of opposite chirality this relation will include a minus sign. Under the replacement (3.22) the tensor p_3^ρ becomes

$$p_3^\rho \xrightarrow{\eta \to p/m_V} \left(\frac{i(P^2 - q^2)}{2m_V(m_B - m_P)} \right) p_T^\rho \quad . \tag{3.23}$$

The remaining differences between the vector and pseudoscalar DAs can be taken care of by the substitutions $\phi_P(u) \to \phi_\parallel(u)$ and $f_P \to i f_V$. Combining these replacements with (3.23) gives the identity

$$g_3^{(\parallel)}(q^2) = -\frac{f_V}{f_P} \frac{2m_V(m_B - m_P)}{m_B^2 - q^2} \, g_T(q^2)\big|_{\phi_P \to \phi_\parallel} \tag{3.24}$$

$$g_1^{(\parallel)}(q^2) = g_2^{(\parallel)}(q^2) = 0 \quad , \tag{3.25}$$

which is valid up to $O(m_V)$ corrections arising at twist-3. It should be noted that there is a similar relation to (3.23) for the tensor p_2, the reason that the longitudinal polarisation contributes to $g_3(q^2)$ rather than $g_2(q^2)$ is that for a perpendicularly-polarised final-state meson $\eta \cdot Q = 0$ which leads to $p_3 \to 0$, in contrast to the case of p_2 which remains non-zero for perpendicular polarisation vectors. The coefficient g_2 of p_2 is therefore a mixture of perpendicular and longitudinal terms but the coefficient g_3 of p_3 relates to longitudinal terms only, and therefore longitudinal terms computed using the ultra-relativistic approximation belong there.

[4] See Section 2.10.

3.2.3 Dispersion representations of Passarino–Veltman functions

The procedure to construct dispersion representations of Passarino–Veltman functions is in principle rather straightforward; the principal difficulty which may arise is analytic continuation. This procedure will be illustrated in the case of the function B_a (3.17), where it is indeed simple, before proceeding to the rather trickier case of C_a. By definition of B_a:

$$\begin{aligned} B_a \equiv B_0(u(p_B^2 - P^2), 0, m_b^2) \equiv & \frac{(2\pi\mu)^{4-d}}{i\pi^2} \int \frac{d^d k}{(k^2 + i\epsilon)((k + u(p_B^2 - P^2))^2 - m_b^2 + i\epsilon)} \\ = & - \int_0^1 \log \left[\frac{x(m_b^2 - \bar{x} u^2 (p_B^2 - P^2)^2) - i\epsilon}{\mu^2} \right] \quad , \end{aligned} \tag{3.26}$$

where $\bar{x} \equiv 1 - x$. The final form of the expression is taken from [52] fixing the constant $\Delta = 0$ as per the $\overline{\text{MS}}$ scheme, and may be straightforwardly derived from the definition in terms of a loop integral by the standard procedure of Feynman parametrisation to render the integral spherically symmetric, as described in any quantum field theory textbook, e.g. [23].

Construction of the dispersion representation is usually done most straightforwardly via the following two observations: firstly, that the Feynman parameter representation (3.26) does not contain any complex singularities for $\text{Im}\, p_B^2 > 0$, since the imaginary part of the logarithm argument cannot be zero anywhere in the integral region. This generalises to the three-point representation, provided that the imaginary part of all three invariants is positive; however, for the four-point function the Feynman parametrisation is rather more complex and the situation not so clear [88]. Secondly, B_a is real for $p_B^2 \ll 0$, i.e. for real p_B^2 below any thresholds. It follows from these two observations and the Schwarz reflection principle that there are also no complex singularities in the lower half of the complex plane, and thus the entire complex structure of this function consists of a single cut along the real line, as illustrated in Figure 2.3. As B_0 is related to two-point functions this was the only possible outcome since it is the complex structure implied by the Källén-Lehmann spectral representation [89, 90] which exists for any two-point function. In the case of dispersion representations, however, the two observations are more general; n-point correlation functions are generally real when all external momenta are space-like since they are related to correlation functions of a Euclidean field theory by Wick rotation. A dispersion representation valid for space-like external momenta can therefore be constructed straightforwardly. In the case at hand it is:

$$B_0(u(p_B^2 - P^2), 0, m_b^2) - B_0(0, 0, m_b^2) = \frac{p_B^2}{\pi} \int_{\frac{m_b^2}{u} + P^2}^{\infty} \frac{\text{Im}_s\, B_0(u(s - P^2), 0, m_b^2)}{s(s - p_B^2)} ds \quad , \tag{3.27}$$

where a single subtraction has been performed to render the right-hand side finite. The spectral density is given by:

$$\rho_{B_a}(s) = \frac{1}{\pi} \text{Im}_s\, B_0(u(s - P^2), 0, m_b^2) = \left(1 - \frac{m_b^2}{u(s - P^2)}\right) \Theta \left(1 - \frac{m_b^2}{u(s - P^2)}\right) \quad . \tag{3.28}$$

The Borel transform in this case gives:

$$\mathcal{B}_{p_B^2\to M^2}\left[B_0(u(p_B^2-P^2),0,m_b^2)\right]=\frac{1}{\pi}\int_{\frac{m_b^2}{u}+P^2}^{\infty}e^{-s/M^2}\,\mathrm{Im}_s\,B_0(u(s-P^2),0,m_b^2)ds \quad . \tag{3.29}$$

Having constructed a dispersion representation for space-like external momenta by taking the imaginary part, the dispersion representation for time-like external momenta is recovered by analytic continuation in the Lorentz invariants. This is the procedure most commonly used for B physics sum rules, e.g. [75, 105, 106, 112]. All spectral densities (3.17) except for C_a may be derived by this method and the remaining two are:

$$\begin{aligned}\rho_{B_c}=&\left(1-\frac{m_b^2}{us+\bar{u}q^2}\right)\Theta\left(s-\frac{m_b^2-\bar{u}q^2}{u}\right)\\ \rho_{C_c}=&\frac{\log\left(\frac{A-\lambda_1\sqrt{\lambda_3}}{A+\lambda_1\sqrt{\lambda_3}}\right)}{\sqrt{\lambda_3}}\left[\Theta\left(s-\frac{m_b^2-\bar{u}q^2}{u}\right)-\Theta\left(s-\frac{m_b^2}{u}-P^2\right)\right]\\ &+\frac{\log\left(\left(\frac{B-\lambda_2\sqrt{\lambda_3}}{B+\lambda_2\sqrt{\lambda_3}}\right)\left(\frac{A-\lambda_1\sqrt{\lambda_3}}{A+\lambda_1\sqrt{\lambda_3}}\right)\right)}{\sqrt{\lambda_3}}\Theta\left(s-\frac{m_b^2}{u}-P^2\right) \quad ,\end{aligned} \tag{3.30}$$

where

$$\begin{aligned}A\equiv&2m_b^2q^2-u\left(q^2-P^2\right)\left(m_b^2+\bar{u}q^2+us\right)\\ B\equiv&u\left(\left(q^2-P^2\right)\left(m_b^2+u\left(s-P^2\right)\right)-2q^2\left(s-P^2\right)\right)\\ \lambda_1\equiv&m_b^2-us-\bar{u}q^2\\ \lambda_2\equiv&m_b^2-u(s-P^2)\\ \lambda_3\equiv&\lambda\left(us+\bar{u}q^2,u(s-P^2),q^2\right) \quad ,\end{aligned}$$

and $\lambda(x,y,z)=(x-(y+z))^2-4yz$ is the Källén-function. In fact, the function C_c does indeed suffer some of the same difficulties as C_a, but they only occur for q^2 above a high threshold and can be ignored in this analysis.

3.2.4 Dispersion representation of C_a

Before addressing the dispersion representation of C_a specifically, it is worthwhile to analyse its complex singularity structure. For real external momentum invariants, C_a is given by its Feynman parameter representation

$$\begin{aligned}C_a\equiv&\,C_0(p_B^2,\bar{u}P^2+uq^2,u(p_B^2-P^2),m_b^2,0,0)\\ =&\int_0^1dx\int_0^1dy\int_0^1dz\frac{\delta(1-x-y-z)}{z(xp_B^2+yu(p_B^2-P^2)-m_b^2)+xy(\bar{u}P^2+uq^2)+i\epsilon}\\ =&\int_0^1dy'\int_0^1dx\left[(1-y')(xp_B^2+(1-x)y'u(p_B^2-P^2)-m_b^2)+xy'(\bar{u}P^2+uq^2)+i\epsilon\right]^{-1} \quad ,\end{aligned} \tag{3.31}$$

where in the second line a standard substitution $y = (1-x)y'$ has been used to linearise the denominator in x. The procedure for identifying singularities arising in complex integrals is described in [113]. In the case of a Feynman integral it boils down to identifying points where the denominator, henceforth identified as F, is zero, and one of the following holds for each Feynman parameter x_i:

1. Either $x_i = 0$, so that x_i is on the integration boundary
2. or $\frac{\partial F}{\partial x_i} = 0$, so that there is a stationary point at the zero of F.

These conditions are known as the Landau equations[5]. Normal thresholds in p_B^2 can be read off from cuts in the triangle diagram and are given by $p_B^2 = m_b^2$ and $p_B^2 = \frac{m_b^2}{u} + P^2$. These thresholds correspond to the solutions $\frac{\partial F}{\partial x} = 0, y = 0$ and $\frac{\partial F}{\partial y} = 0, x = 0$ of the Landau equations, respectively. A third singularity is at $\bar{u}P^2 + uq^2 = 0$, but that is of no interest here since it does not involve p_B^2. Since these singularities correspond to momentum cuts in a Feynman diagram, they correspond to the Cutkosky rules method of computing the imaginary part of a diagram.

There is an additional solution at $\frac{\partial F}{\partial x} = \frac{\partial F}{\partial y} = 0$ which does not correspond to an identifiable momentum cut in the triangle diagram. This type of singularity is known as an anomalous threshold. This corresponds to all three propagator momenta going on-shell simultaneously in the loop integral, and in the case of C_a this occurs at

$$p_B^2 = s_\pm \equiv \frac{(1+u)m_b^2 + uP^2 \pm \sqrt{(uP^2 - \bar{u}m_b^2)^2 - 4u^2 m_b^2 q^2 - i\epsilon}}{2u} \quad , \tag{3.32}$$

where the $-i\epsilon$ indicates that analytic continuation when the argument of the square root becomes negative is such that $\operatorname{Im} s_+ \leq 0$.

Unfortunately, the Landau conditions only identify the location of potential complex singularities; they do not give an indication on which Riemann sheets they are actually present. In the case of the three-point function, the complex structure was analysed in the framework of axiomatic quantum field theory by Källén and Wightman [114] and shown to be divisible into octants according to the signs of the imaginary parts of the external momenta. The anomalous cuts in this approach are given by [115]

$$(p_B^2 - r)(u(p_B^2 - P^2) - r) + r(\bar{u}P^2 + uq^2) = 0 \quad , \tag{3.33}$$

which reproduces (3.32) after the identification $r = m_b^2$. Construction of integral representations of three-point functions was also considered in [116]. Unfortunately the results there are not suited for constructing sum rules because complex anomalous thresholds are avoided through taking the cut to lie along the negative real axis.

[5] Note that these conditions are written expecting that the δ function is present; in the case of (3.31) this means that $z = 0$ corresponds to $x + y = 1$ which would otherwise also have to be considered.

In the present case however, the simplest way to proceed is rather more straightforward. Since the Feynman parameter representation is correct for $\operatorname{Im} p_B^2 > 0$ and there are therefore no complex singularities in the upper half plane, the contour required for a dispersion representation there lies just above the real line. This therefore suggests that applying the usual dispersion representation construction (3.28) may be useful:

$$\begin{aligned}\frac{1}{\pi}\operatorname{Im} C_a &= -\int_0^1 dy \int_0^1 dx \delta\left((1-y)(uy(p_B^2-P^2)-m_b^2)\right. \\ &\qquad \left. + x(y((1-uy)P^2+uq^2)+(1-y)(1-uy)p_B^2)\right) \\ &= -\int_0^1 dy \frac{\theta(p_B^2 - m_b^2 + \frac{y}{1-y}(\bar{u}P^2+uq^2)) - \theta(uy(p_B^2-P^2)-m_b^2)}{y((1-uy)P^2+uq^2)+(1-y)(1-uy)p_B^2} \quad ,\end{aligned} \tag{3.34}$$

where the imaginary part is applied under the integral using the well known identity

$$\lim_{\epsilon\to 0}\int \frac{f(x)}{x-i\epsilon}dx = \fint \left(i\pi\delta(x)+\frac{1}{x}\right) f(x)dx \quad , \tag{3.35}$$

where $\fint$ denotes a Cauchy principal value integral. To study the integral (3.34), the restrictions imposed by the Heaviside step functions must be analysed. The two constraints lead to

$$p_B^2 - m_b^2 + \frac{y}{1-y}(\bar{u}P^2+uq^2) > 0 \implies \frac{1}{y} < \frac{1}{y_L} = z_L = 1 + \frac{\bar{u}P^2+uq^2}{m_b^2-p_B^2} \tag{3.36}$$

$$uy(p_B^2-P^2)-m_b^2 > 0 \implies \frac{1}{y} < \frac{u(p_B^2-P^2)}{m_b^2} \quad . \tag{3.37}$$

The second of these (3.37) is not satisfied for $p_B^2 < \frac{m_b^2}{u} + P^2$ for any y in the range $0 < y < 1$. It therefore does not lead to any difficulties in the complex structure of C_a, since for $p_B^2 \to -\infty$ it induces no imaginary part and the Schwarz reflection principle applies. The first condition (3.36) is rather more interesting because for $P^2 > 0$ and $q^2 > 0$, values which they will take when put on-shell, $z_L > 1$ for $p_B^2 \to -\infty$ and hence the representation (3.34) implies a cut along the negative real axis as well as the positive one.

The first thing to note in this situation is that the analytic structure in p_B^2 appears to be rather different for $P^2 < 0$ and $q^2 < 0$ than for the physical case $P^2 > 0$ and $q^2 > 0$. This suggests that the traditional approach of starting with space-like external momenta, constructing a dispersion representation and analytically continuing the spectral density function may not be straightforward. Since the Feynman parameter representation already provides an analytic continuation to time-like external momenta for $\operatorname{Im} p_B^2 \geq 0$ it is possible to take an alternative approach: start from the known behaviour of C_a in the upper complex half-plane at physical P^2 and q^2 and analytically continue to the lower complex half-plane in such a way that there is no cut for $p_B^2 \to -\infty$, which is the choice of complex structure that must be made in order to construct a physical dispersion representation.

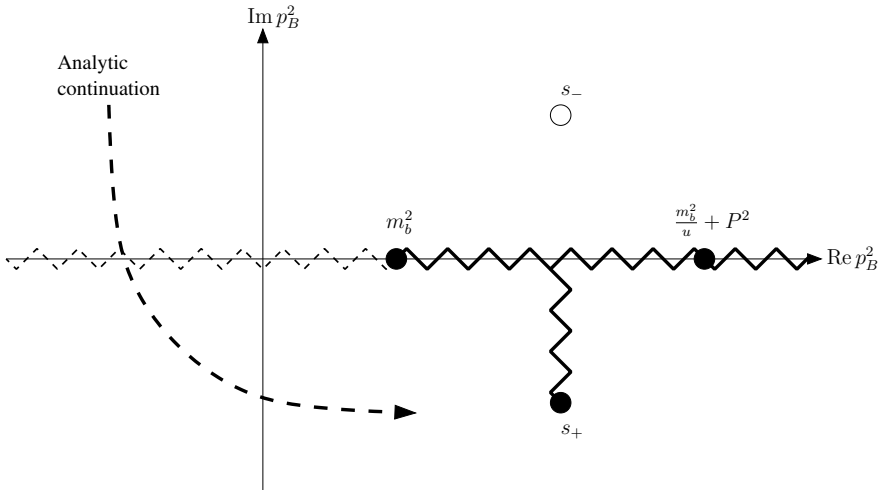

Figure 3.4: Analytic continuation of C_a from the upper half-plane, covered by the Feynman parameter integral representation, to the lower half-plane. The zigzag lines indicate choice of branch cuts. Solid dots represent branch points. The dotted zigzag line represents a discontinuity present in the Feynman parameter integral, which is analytically continued across to produce a dispersion representation. The open circle shows the location of a branch point which is not present on the principle Riemann sheet of the function.

This representation is constructed as follows

$$C_a(p_B^2) = \begin{cases} C_a(p_B^2) & \operatorname{Im} p_B^2 > 0 \\ C_a(p_B^{2*})^* + \delta C_a(p_B^2) & \operatorname{Im} p_B^2 < 0 \end{cases} , \tag{3.38}$$

where $C_a(p_B^2)$ in the upper complex half plane is taken to be defined by the Feynman parameter integral. Since there are no complex singularities in this region a dispersion representation will only need its imaginary part on the real line. For the present calculation, this was worked out directly in terms of logarithms and the result is given in appendix D.2; however, the same result can be obtained from LoopTools [111]. The function δC_a is a stitching function; it corrects for the effects of a non-zero imaginary part along the section of the real axis across which the analytic continuation is done. The benefit of the construction (3.38) is that the correction δC_a is considerably simpler than the full function C_a but carries all of the difficult complex structure; since it is related to the imaginary part of C_a on the real axis, it only contains logarithms rather than the dilogarithms in the full formula for C_a, e.g. [52].

The analytic continuation across the real axis is illustrated in Figure 3.4. For the segment of the real axis to the left of any branch points the branch cut is to be eliminated via the choice of δC_a (3.38), and in order to do this the formulae for C_a must match just below and just above the real axis in this region. It therefore follows that for real $p_B^2 < m_b^2$:

$$\delta C_a(p_B^2) = 2i \operatorname{Im} C_a(p_B^2), \qquad p_B^2 < m_b^2 \quad . \tag{3.39}$$

In this region only the first Θ function appearing in (3.34) contributes and

$$\begin{aligned}\delta C_a(p_B^2) &= -\frac{2\pi i}{u(p_B^2-P^2)}\int_{y_L}^1 \frac{dy}{(y-y_+)(y-y_-)} = -\frac{2\pi i}{p_B^2}\int_1^{z_L}\frac{dz}{(z-z_+)(z-z_-)} \\ &= -\frac{2\pi i}{\sqrt{\lambda}}\left(\log\left(\frac{z_+-z_L}{z_+-1}\right)-\log\left(\frac{z_--z_L}{z_--1}\right)\right) \\ &= \frac{2\pi i}{\sqrt{\lambda}}\left(\log\left(\frac{1-z_+}{1-z_-}\right)-\log\left(\frac{z_+-z_L}{z_--z_L}\right)\right) \quad ,\end{aligned} \tag{3.40}$$

where

$$\lambda = \lambda(p_B^2, \bar{u}P^2+uq^2, u(p_B^2-P^2)) \tag{3.41}$$

$$y_\pm = \frac{(1+u)p_B^2 - P^2 - uq^2 \pm \sqrt{\lambda}}{2u(p_B^2-P^2)} \tag{3.42}$$

$$z_\pm = \frac{(1+u)p_B^2 - P^2 - uq^2 \pm \sqrt{\lambda}}{2p_B^2} \tag{3.43}$$

and $\lambda(x,y,z) \equiv (x-y-z)^2 - 4yz$ is the Källén function, as usual. The integral substitution $z = y^{-1}$ was used in (3.40) to avoid the singularity at $p_B^2 = P^2$. The final step of rearranging logarithms in (3.40) is not guaranteed to preserve the branch structure of the function; however, this step reproduces the correct result on the real axis for $p_B^2 \to -\infty$ and that is all that is required, since the analytic continuation to other regions must be recovered by a more careful analysis, performed below.

It is worth noting immediately that the solutions to $z_\pm = z_L$ are given by $p_B^2 = s_\pm$, and hence a branch point must exist at $p_B^2 = s_+$, because none of the other logarithm branch points coincide with it and thus it cannot be cancelled. There are however no finite solutions to $z_\pm = 1$, so the first logarithm does not introduce any branch points. The branch cuts of C_a may therefore be chosen as shown in Figure 3.4, and the full dispersion relation follows from (3.38)

$$C_a(p_B^2) = C_a^A(p_B^2) + \int_{m_b^2}^\infty \frac{ds}{s-p_B^2}\left(\rho_C(s)+\rho_{\delta C}(s)\right) \quad , \tag{3.44}$$

where

$$\rho_C(s) = \frac{\operatorname{Im} C_a(s)}{\pi} \tag{3.45}$$

$$\rho_{\delta C}(s) = \frac{1}{\sqrt{\lambda(s)}}\left(\log\left(\frac{z_+-z_L}{z_--z_L}\right)-\log\left(\frac{z_+-1}{z_--1}\right)\right)\Bigg|_{p_B^2\to s} \equiv \frac{1}{\sqrt{\lambda(s)}}\left(\log\theta_L - \log\theta_1\right) \tag{3.46}$$

$$C_a^A(p_B^2) = -2\pi i\int_{s_+}^{\operatorname{Re} s_+}\frac{ds}{s-p_B^2}\left[\frac{1}{\sqrt{\lambda}}\Big|_{p_B^2\to s}\right] \tag{3.47}$$

Computation of (3.45) is entirely standard and outlined in appendix D.2. The function $C_a^A(p_B^2)$ gives contribution due to the anomalous threshold, which owing to the choice of branch cuts goes to zero when s_+ is real. The form of $C_a^A(p_B^2)$ follows from (3.46) and the fact that the

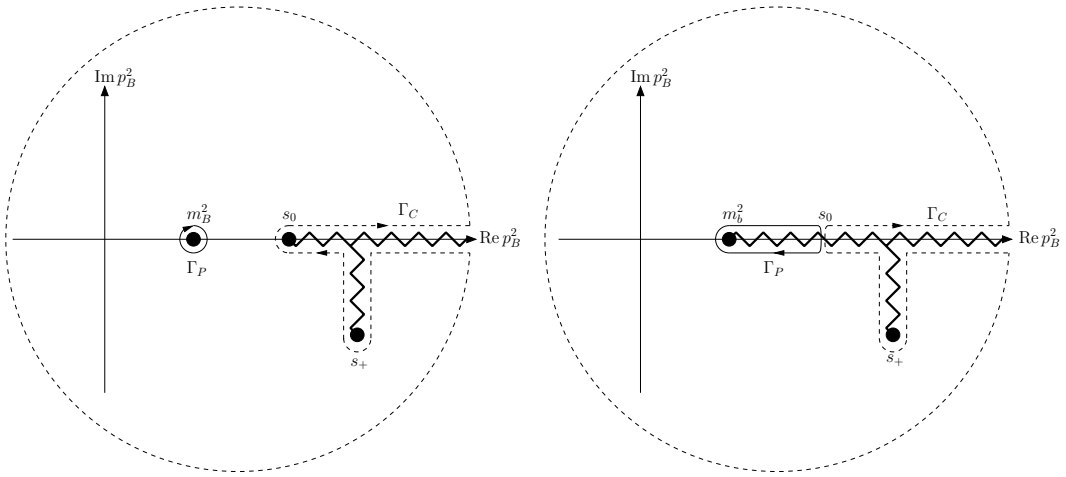

Figure 3.5: Comparison of analytic structure of C_a (3.17) (right) and the expected analytic structure of the matrix element (3.7) in the full theory. The complex branch point s_+ is considered part of the continuum of multi-particle and excited states, identified by Γ_C in both diagrams, and since $\mathrm{Re}\, s_+ > s_0$, the associated branch cut can be safely connected directly to the real line via a vertical cut. The contribution of the B meson state to the perturbative matrix element is given by the contour Γ_P, which by semi-global duality is still expected to approximate the pole residue at $p_B^2 = m_B^2$ in the full theory. Note that the location of the branch point s_+ associated with the anomalous threshold is not expected to be the same in the full theory; however, according to the analysis of Källén & Wightman [114,115] the branch structure is expected to be the same, i.e. there should only be a single branch point in the lower complex half-plane in the full theory.

discontinuity across the branch cut of a logarithm is constant regardless of its location, and equal to $2\pi i$. The appearance of the factor $2\pi i$ can also be viewed as a consequence of the fact that the integrand of (3.47) is the discontinuity of a discontinuity, and hence originates in a dilogarithm rather than a logarithm where the $2\pi i$ would cancel with the factor from Cauchy's formula. The relation between the perturbative analytic structure (3.40) and the analytic structure of the full theory is shown in Figure 3.5.

It now remains to solve the problem of selecting the correct branches of the logarithms appearing in different (3.46) for real s. First, it is useful to define the analytic continuation of the square root of the Källén function λ to the complex plane, given by

$$\sqrt{\lambda(s)} = \bar{u}\sqrt{\lambda_+ - s}\sqrt{\lambda_- - s} \quad , \tag{3.48}$$

where $\lambda_\pm$ are the zeros of λ

$$\lambda_\pm = \frac{\bar{u}P^2 + u(1+u)q^2 \pm 2u\sqrt{q^2(\bar{u}P^2 + uq^2)}}{\bar{u}^2} \quad . \tag{3.49}$$

Note that $\lambda_\pm \geq P^2$, with the equality holding for $P^2 = q^2$, so these zeros are not encountered below $s = m_b^2$. The analytic continuation (3.48) follows from observing that $\sqrt{\lambda} > 0$ for $s < \lambda_-$ implies that $\sqrt{\lambda} < 0$ for $s > \lambda_+$, since far from the roots the function must appear to be linear because it is the square root of a quadratic, so $\sqrt{\lambda(s)} \propto s$ for s going to infinity in any direction.

It can also be seen from this argument that $\text{Im}\sqrt{\lambda(s)} > 0$ in the lower complex half-plane.

The analytic structure for $p_B^2 < m_b^2 < \lambda_-$ can now be understood straightforwardly. It follows from the fact that there are no finite solutions to $z_\pm = 1$ and that $z_- < z_+ < 1$ for $p_B^2 \to 0^+$, that $z_\pm < 1$ for $s < \lambda_-$. However, z_- diverges at $s = 0$ and the argument of the logarithm changes sign. Since there is no branch point below $s = m_b^2$ on the real line it must be the case that $\text{Re}\,\delta C_a(s) = 0$ for $s < m_b^2$ according to (3.39), and therefore the correct result can be obtained by taking the magnitude of both logarithms in (3.46). The arguments to both logarithms in (3.46) can therefore be taken to be real and the logarithms are on the principal branch for $0 < s < m_b^2$ in accordance with the requirement that δC_a is purely imaginary in this region, since this is the easiest place from which to construct the analytic continuation to $s > m_b^2$.

The key to understanding the analytic continuation of the logarithms (3.46) is then to understand how their arguments behave in the complex plane for $\lambda_- < s < \lambda_+$, that it to say when $\lambda(s) < 0$. In this region, the argument to each logarithm is a pure phase since the numerator and denominator of the arguments are complex conjugates of each other. The second logarithm is the simpler of the two so it will be analysed first. Its phase is given for $\lambda(s) < 0$ by

$$\arg\frac{z_+ - 1}{z_- - 1} = -2\arctan\frac{\text{Im}\sqrt{\lambda}}{\bar{u}s + P^2 + uq^2} = -2\arctan\frac{\bar{u}\sqrt{(s-\lambda_-)(\lambda_+ - s)}}{\bar{u}s + P^2 + uq^2} \quad . \tag{3.50}$$

The second equality holds because it is the branch where $\text{Im}\sqrt{\lambda} > 0$ that is being considered[6]. Near $p_B^2 = \lambda_\pm$, the phase is known to be zero. The sign of this expression near $s = \lambda_-$ can be obtained by expanding $s = \lambda_- + \epsilon$:

$$\arg\frac{z_+ - 1}{z_- - 1} = -2\arctan\left(\frac{\bar{u}\sqrt{\epsilon}\sqrt{\lambda_+ - \lambda_-}}{\bar{u}\lambda_- + P^2 + uq^2}\right) \quad . \tag{3.51}$$

Expanding near the other root $s = \lambda_+ - \epsilon$ produces the same expression with $\lambda_- \to \lambda_+$ in the denominator. As the phase cannot go to zero between these points and does not diverge, it can be seen whether the logarithm has switched branches (the argument has circled the origin) by checking the sign of the denominator at either end. Since $\lambda_\pm > P^2$, the phase is positive for all $\lambda(s) < 0$, so it may be concluded that the first logarithm does not change branch and the imaginary part of this logarithm should always be taken to be positive. In order to simplify the

[6]The function δC_a is only defined below the real line and the sign of $\text{Im}\sqrt{\lambda(s - i\epsilon)}$ follows from (3.48)

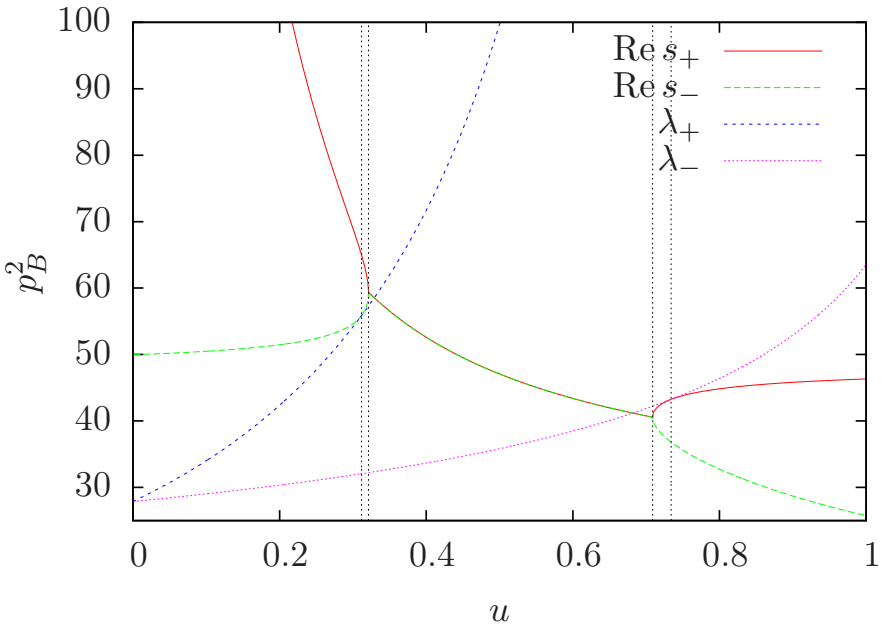

Figure 3.6: Location of the roots of the Källén function $\lambda_\pm$ and the real part of the anomalous threshold $s_\pm$ over the u integration range. $s_\pm$ have the same real part where they are complex. The vertical dotted lines show a tricky region in the integration range where the values of $s_\pm$ and $\lambda_\pm$ do not indicate on which sheet the logarithm arguments should be taken; for example at the left-most dotted line $s_- = \lambda_-$ but in order to achieve the desired analytic continuation all the way to $u = 1$, s_- and λ_- must be taken to orbit each other rather than just to approach and recede, thereby picking up a factor of $2\pi i$. The same thing occurs with s_+ and λ_- at the last dotted line.

notation, two alternative logarithm functions with different branch choices are introduced:

$$\log_+ x = \begin{cases} \log x & \operatorname{Im} x = 0 \\ \log(-x) + i\pi & \operatorname{Im} x \neq 0 \end{cases}$$
$$\log_- x = \log(-x) - i\pi \quad , \tag{3.52}$$

which are the same as the standard logarithm on the real line, but the imaginary parts have known sign, i.e. $\operatorname{Im} \log_+ x \geq 0$ and $\operatorname{Im} \log_- x \leq 0$ on the principal branch of each function. The replacement $\log \theta_1 \to \log_+ \theta_1$ in (3.46) implements the analytic continuation of this logarithm along the entire real line. Further, since it only has an imaginary part when $\sqrt{\lambda}$ is also imaginary, the imaginary part of the result comes entirely from the principal branch of $\operatorname{Im} C_a$ and the second logarithm.

Following the same line of reasoning for the other logarithm, the quantity whose sign gives the sign of the phase of that logarithm near $s = \lambda_\pm$ is

$$r(s) = (1+u-2z_L)s - P^2 - uq^2 = \frac{2m_b^2}{s-m_b^2}\left(\bar{u}P^2 + uq^2\right) - \left[s - u(s-P^2) - (\bar{u}P^2 + uq^2)\right] \tag{3.53}$$

and the notation $r_\pm \equiv r(\lambda_\pm)$ shall be used. It is much simpler to explain the analytic continuation of this logarithm with reference to a diagram of the branch points, which is shown in Figure 3.6. If $\mathrm{sgn}(r_+) = \mathrm{sgn}(r_-)$, then the sign of the imaginary part is taken to be $\mathrm{sgn}(r_-)$ and the analytic continuation is the appropriate logarithm definition in (3.52). Examining (3.53) reveals that $\frac{dr}{ds} < 0$ for $s > m_b^2$ and $P^2, q^2 > 0$, so the only remaining case that is relevant for the dispersion relation at physical external momenta is $r_- > 0$ and $r_+ < 0$; the sign change in the other direction does not arise in this calculation. The logarithms are not expected to produce an imaginary part below the relevant thresholds $\mathrm{Re}\, s_-$ or λ_- and likewise they cannot produce an imaginary part for $s \to \infty$, because then $\mathrm{Im}\, C_a(p_B^2)$ would be logarithmically divergent for any value of p_B^2, and this is not the case. The first logarithm in (3.46) must therefore be on the principal branch for both $s < \min(\lambda_-, \mathrm{Re}\, s_-)$ and $s > \max(\lambda_+, \mathrm{Re}\, s_+)$[7]. It can thus be seen that the branch choice for this logarithm may be discontinuous across $\mathrm{Re}\, s_\pm$ but since this can only introduce a factor of $2\pi i$, that is to say it can only jump between neighbouring Riemann sheets of the logarithm, there are no further complications due to θ_L circling the origin more than once. The only slight catch in writing down the complete analytic continuation on the real line is now that $\lambda_- < \mathrm{Re}\, s_\pm < \lambda_+$ holds nearly but not quite everywhere when $\mathrm{Im}\, s_+ \neq 0$, as shown in Figure 3.6, and the ranges where this fails are easy to miss. Putting all of these constraints together the first logarithm is given, on the real line, for all relevant values of the external parameters, by:

$$\log_L \theta_L = \begin{cases} r_+ > 0 \wedge r_- > 0 & \log_+ \theta_L \\ r_+ < 0 \wedge r_- > 0 & \begin{cases} \lambda < 0 & \begin{cases} s < \mathrm{Re}\, s_+ & \log_+ \theta_L \\ s > \mathrm{Re}\, s_+ & \log_- \theta_L \end{cases} \\ \lambda > 0 & \begin{cases} \theta_L < 0 & \begin{cases} s < \lambda_- & \log_- \theta_L \\ s > \lambda_+ & \log_+ \theta_L \end{cases} \\ \theta_L > 0 & \begin{cases} \mathrm{Re}\, s_+ < s < \lambda_- & \log \theta_L - 2\pi i \\ \lambda_+ < s < \mathrm{Re}\, s_+ & \log \theta_L + 2\pi i \\ \text{otherwise} & \log \theta_L \end{cases} \end{cases} \end{cases} \\ r_+ < 0 \wedge r_- < 0 & \log_- \theta_L \end{cases} \tag{3.54}$$

(3.46) is now replaced by:

$$\rho_{\delta C}(s) = \frac{1}{\sqrt{\lambda(s)}} \left(\log_L \theta_L - \log_+ \theta_1 \right) \quad . \tag{3.55}$$

The correctness of this equation has been verified by comparing the results of computing C_a through (3.44) to the results of LoopTools. This completes the calculation of $G_\iota^{(s)}(q^2)$ (3.10).

[7] The fact that the real part of $s_\pm$ is taken is due to the choice of cut structure in Figure 3.4.

3.2.5 Non-spectator graphs

The non-spectator scattering contribution $G_\iota^{(ns)}(q^2)$, given by the inclusive graphs shown in Figure 3.2, is computed using a local expansion of these graphs in $1/m_c^2$, performed in [104], combined with the form factor calculations of [81, 93]. The result is

$$\begin{aligned} G_i^{(ns)}(q^2) &= \left(-\frac{\alpha_s(m_b)}{4\pi}\right)\left(\frac{Q_b}{-1/3}\right)\left(F_8^{(7)}\,T_i(q^2) + F_8^{(9)}\,H_i(q^2)\right) \qquad i = 1\ldots 3 \\ G_T^{(ns)}(q^2) &= \left(-\frac{\alpha_s(m_b)}{4\pi}\right)\left(\frac{Q_b}{-1/3}\right)\left(F_8^{(7)}\,f_T(q^2) + F_8^{(9)}\,h_T(q^2)\right) \quad , \end{aligned} \tag{3.56}$$

where $T_i(q^2)$, $f_T(q^2)$, H_i and h_+ are defined in (2.69). The functions $F_8^{(7,9)}(q^2)$ are given in [104].

3.3 Comparison with QCD factorisation

The matrix element (3.1) has previously been computed at $q^2 = 0$ using QCDF in [84], or rather its isospin violating part has. This is in fact the most interesting part to compare with this calculation because it is infrared divergent, so the comparison reveals how the LCSR method, which incorporates hard and soft initial-state gluons on equal footing, resolves this divergence.

The specific comparison is of diagrams A_1 and A_2 in Figure 3.1. Since $G_1(0) = G_2(0)$ (3.19) the quantity of interest may be written:

$$G_1^{(s)}(0) = \underbrace{\left[\frac{\alpha_s}{4\pi}\frac{C_F}{N_c}12\pi^2\frac{f_\perp f_B}{m_B^2}\right]}_{\sim m_b^{-5/2}}(Q_q X_\perp + Q_b \bar{X}_\perp) \quad , \tag{3.57}$$

where the large m_b scaling of the bracket is indicated. The quantity $X_\perp$ corresponds to photon emission from the spectator quark line and has the same normalisation as in [84],

$$X_\perp = \int_0^1 \phi_\perp(u) x_\perp(u) du \quad , \tag{3.58}$$

and likewise for $\bar{X}_\perp$ and $\bar{x}_\perp$. The QCDF result for $x_\perp(u)$ is [84]:

$$x_\perp^{\mathrm{QCDF}}(u) = \frac{1+\bar{u}}{3\bar{u}^2} \quad , \tag{3.59}$$

The LCSR result derived in Section 3.2 simplifies considerably at $q^2 = 0$, primarily owing to the absence of problems with the anomalous threshold, but remains rather more complex than the QCDF result

$$x_\perp^{\mathrm{LCSR}}(u) = \int_{m_b^2}^{s_0} ds\, e^{\frac{m_B^2 - s}{M^2}} \rho(s,u) \tag{3.60}$$

and $\bar{x}_\perp^{\rm LCSR}$ has the same relation to $\bar{\rho}$. The integrands are given by:

$$\rho(s,u) = \underbrace{\frac{m_b^2 N_c}{12\pi^2 f_B^2}}_{\sim m_b^3} \left[\frac{\log\left(\frac{\bar{u}s(m_b^2+P^2-s)}{P^2(m_b^2-us)}\right)}{P^2-\bar{u}s} - \frac{s-m_b^2}{\bar{u}sP^2} \right] \tag{3.61}$$

$$\bar{\rho}(s,u) = \frac{m_b^2 N_c}{12\pi^2 f_B^2} \left[\theta(us-m_b^2) \left(\frac{us-m_b^2}{2u^2 sP^2} + \frac{\log\left(\frac{us}{m_b^2}\right)}{2uP^2} \right) - \frac{s-m_b^2}{usP^2} \right] \quad . \tag{3.62}$$

The large m_b scaling of the prefactor arises from $f_B \sim m_b^{-1/2}$ [117]. There are several obvious differences between the QCDF and LCSR results which are to be explained:

1. The integral (3.58) contains an endpoint divergence for $x_\perp(u) \to x_\perp^{\rm QCDF}(u)$, whereas the LCSR result is finite.

2. The LCSR integrand (3.61) contains an imaginary part absent in the QCDF case.

3. Since the LCSR result incorporates soft initial-state radiation and the QCDF result does not, are the two calculations directly comparable?

The answers to all of these questions are closely related. To begin with, it is worthwhile discussing the problem of the endpoint divergence in QCDF and its traditional resolution. Taking the DA to be its asymptotic value,

$$\phi_\perp(u) \to 6\bar{u}u \tag{3.63}$$

the divergent part of the integral (3.58) can be evaluated:

$$X_\perp^{\rm QCDF}(u) = 2\int_0^1 \frac{du}{\bar{u}} - 1 \tag{3.64}$$

Corrections to (3.63) are expressed in terms of a sum of Gegenbauer polynomials; these could in principle soften the endpoint behaviour to $\sim \bar{u}^2$ and thereby remove the endpoint divergence if there is a conspiracy amongst the coefficients, but there is no reason to believe that this is the case. The presence of this infrared divergence can be understood from Figure 3.7 as resulting from a pair of massless propagators going on-shell in the $\bar{u} \to 0$ limit. This also hints at the origin of the problem and its resolution; the gluon propagator in Figure 3.7 (right) carries momentum, which is the difference between the shaded quark propagator and the light quark in the B meson, and this momentum from the initial-state quark is neglected to leading order in $1/m_B$. The infrared divergence is then expected to be softened for $\bar{u} < \Lambda_{\rm QCD}/m_B$ but also implies that a Taylor series in $1/m_B$ cannot be expected to converge. It will later be seen explicitly that this is what occurs in the LCSR calculation, where the $1/m_B$ expansion is not assumed. In view of this problem, it was proposed in [118] for a similar problem in $B \to \pi\pi$

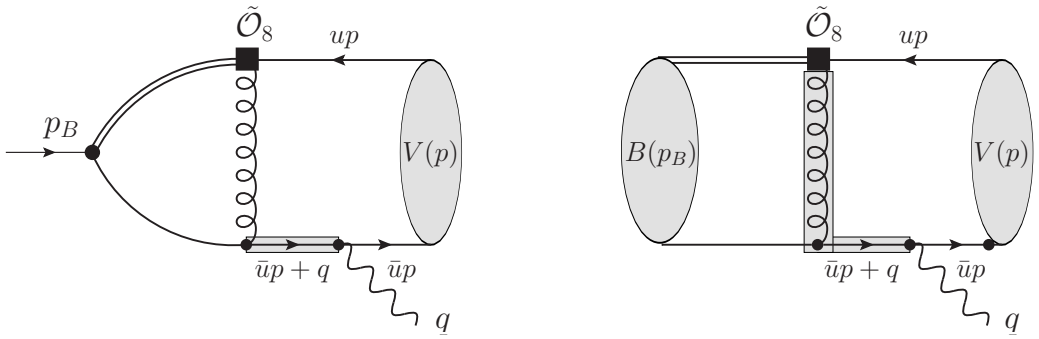

Figure 3.7: Origin of infrared divergences in both LCSR (left) and QCDF (right) calculations. The shaded propagators behave as $\bar{u}^{-1}$ near $\bar{u} \to 0$ at $q^2 = 0$. In the QCDF case two propagators go on shell simultaneously and the resulting $\bar{u}^{-2}$ behaviour is too singular to be cancelled by the asymptotic vector meson DA (3.63). By contrast in the LCSR case the loop cannot produce a singularity worse than $\log \bar{u}$ leading to an overall $(\log \bar{u})/\bar{u}$ behaviour, which is integrable when convoluted with (3.63).

that the divergent propagators be replaced according to $1/(\bar{u}m_B^2) \to 1/((\bar{u}+\epsilon)m_B^2)$, where $\epsilon \sim \Lambda_h/m_B$ parametrises the softening, *and* that a correction term should be added to account for strong phases which might occur in a full calculation of the endpoint behaviour. The exact approach used in [51] is to replace

$$X_\perp^{\text{QCDF}} = \int_0^1 \phi_\perp(u) x_\perp^{\text{QCDF}}(u) du \to (1+\rho e^{i\phi}) \int_0^{1-\Lambda_h/m_B} \phi_\perp(u) x_\perp^{\text{QCDF}}(u) du \quad , \tag{3.65}$$

where ρ, ϕ are real and it is expected that $|\rho| < 1$ [84]. The strong phase arising in the LCSR result has therefore already been anticipated and this difference between the two approaches does not indicate a problem so much as a benefit of the LCSR method that the strong phase can be estimated.

As for the LCSR solution, two points are worth mentioning. First, it is not possible for the diagram of Figure 3.7 (left) to contain a $\bar{u}^{-2}$ singularity since infrared singularities in QCD are at worst logarithmic, e.g. [41]. Combining this with the light-quark propagator it can be seen that the allowed singularities are:

$$x_\perp^{\text{LCSR}} \sim \alpha_\perp \frac{\log \bar{u}}{\bar{u}} + \beta_\perp \log(\bar{u}) + \gamma_\perp \frac{1}{\bar{u}} \quad , \tag{3.66}$$

although as can be seen from (3.61), $\alpha_\perp = 0$. The fact that the leading singularity in the $\bar{u} \to 0$ limit is not present does not have an obvious explanation; it is already apparent from the intermediate result (3.20) that $\alpha_\perp = 0$ and this suggests that it is a result of the simplifying effect of the leading twist vector meson DA[8]. It would therefore appear that $\alpha_\perp = 0$ will not hold in a higher twist calculation.

Second, the interpretation of the LCSR and QCDF calculations is rather different. In

[8] See appendix B

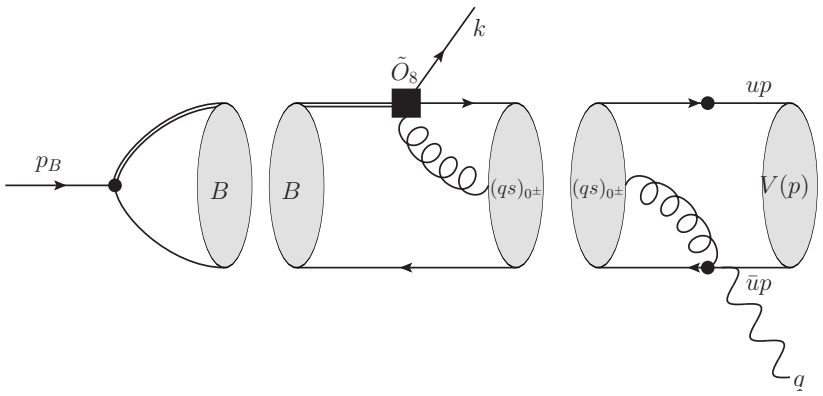

Figure 3.8: Origin of the strong phase in $B \to V\gamma$ through the chromomagnetic operator in the diagram A_1. Other diagrams contain similar strong phases. A strong phase appears because a second cut can be made in addition to the B meson cut required for the sum rule. The use of the momentum insertion k is necessary to achieve this result since it separates B meson cuts that are used to construct the sum rule from other cuts that lead to a strong phase in the amplitude.

the QCDF case, the gluon momentum is fixed by the external DAs, and for $u \sim O(1)$ the gluon is far off shell and therefore said to be hard. The soft gluon contribution is expected to be subleading in $1/m_B$, since it corresponds to an exceptional configuration of the external momentum fraction $\bar{u}$, although as it has already been shown this interpretation fails due to the endpoint singularity. In contrast the LCSR approach integrates over all gluon momentum configurations without any kinematical approximation and therefore large contributions from the soft gluon region can be properly accounted for. Strong phases are allowed in this case because soft gluons can form intermediate three-particle states as shown in Figure 3.8, which in a hadronic picture correspond to excited states in the pseudoscalar $\bar{s}q$ channel. The LCSR calculation therefore appears to include the complete QCDF result since hard gluons are fully accounted for, and the difference between the two arises from LCSR also properly accounting for soft gluons which are neglected in the QCDF scheme.

3.3.1 Heavy quark limit and m_b scaling

Further support for the point of view that the LCSR calculation includes the QCDF result can be obtained by an explicit heavy quark expansion. It was proposed in [117, 119] that the heavy-quark scaling of a correlation function can be recovered from the sum rule using

$$\begin{aligned} m_B &= m_b + \bar{\Lambda} & s_0 &= m_b^2 + 2m_b\omega_0 \\ M^2 &= 2m_b\tau & f_B &= f_B^{(s)} m_b^{-1/2} \end{aligned} \tag{3.67}$$

and taking the large m_b limit. The key statement is that the B meson "binding energy" $\bar{\Lambda} \equiv m_B - m_b$ is independent of the b quark mass. The scaling of s_0 is expected according to $s_0 \sim (m_B + m_\rho)^2$, as argued in Section 2.8, and the Borel parameter scaling is chosen so that the

exponential argument is dimensionless. Explicit use of the f_B scaling will not be made, since f_B only appears in overall proportionality constants and would therefore clutter the notation. If the asymptotic DA $\phi_\perp(u) = 6\bar{u}u$ is used in (3.58), both integrals may be performed exactly. Doing so and performing the large m_b expansion (3.67) gives:

$$X_\perp^{LCSR} = \left[\frac{N_c\omega_0^2}{f_B^2\pi^2}\right]\left\{\frac{2\omega_0}{m_b}\left(\left(\log\left(\frac{m_b}{2\omega_0}\right) - i\pi\right)\langle z^2\rangle - \langle z^2\log z\rangle\right) + O\left(m_b^{-2}\right)\right\} \tag{3.68}$$

$$\bar{X}_\perp^{LCSR} = \left[\frac{N_c\omega_0^2}{f_B^2\pi^2}\right]\left\{\left(\langle z\rangle\left(\frac{2\bar{\Lambda}}{m_b} - 1\right) + \frac{2\omega_0}{m_b}\langle z^2\rangle\right) + O\left(m_b^{-2}\right)\right\} \quad , \tag{3.69}$$

where $\langle f(z)\rangle = \int_0^1 \exp\left(\frac{\bar{\Lambda}-\omega_0 z}{\tau}\right) f(z)dz$. The presence of a $\log m_b$ term in (3.68) means that the Taylor expansion around $m_b \to \infty$ does not exist; the logarithm must be subtracted before the Taylor expansion can be performed.

The scaling of the two expressions (3.68) and (3.69) lead to G_1 scaling of

$$G_1^b(0) \sim m_b^{-3/2} \qquad\qquad G_1^q(0) \sim m_b^{-5/2}(\log m_b + \mathcal{O}(1)) \quad , \tag{3.70}$$

where the superscript indicates the quark from which the photon is emitted. This scaling agrees with [42, 84, 120]. Despite the fact that G_1^b is the leading term, G_1^q is more phenomenologically interesting because it contributes to the isospin asymmetry, since it is proportional to the spectator quark charge, and can lead to measurable CP asymmetries owing to the strong phase.

It is apparent from (3.68) that the real and imaginary parts of $G_1^q(0)$ are of the same order in m_b. This signals the breakdown of the QCDF approximation, since the large imaginary part implies the presence of long distance dynamics which are neither associated to the initial nor final meson states and are therefore non-factorisable. It is also possible to understand the breakdown of QCDF in a more mechanical way by performing the m_b expansion under the s integral (3.60). To start with, it is useful to replace the s integration in (3.60) with an integration over a dimensionless integral z via $s = s_0 + 2m_b\omega_0 z$, that is:

$$x_\perp^{\text{LCSR}}(u) = 2m_b\omega_0\int_0^1 e^{\frac{\bar{\Lambda}-\omega_0 z}{\tau}}\rho(m_b^2 + 2m_b\omega_0 z, u)dz \quad . \tag{3.71}$$

Expanding the density (3.61) in these new variables gives:

$$\begin{aligned}\text{Re}\,\rho =& \frac{2c\omega_0^2 z^2}{m_b}\frac{1+\bar{u}}{\bar{u}^2} \\ \text{Im}\,\rho =& -\frac{cm_b\pi}{u}\Theta\left(\frac{2\omega_0 z}{m_b} - \bar{u}\right) \quad ,\end{aligned} \tag{3.72}$$

where $c \equiv N_c/(12\pi^2 f_B^2 m_b) \sim m_b^0$. The real part recovers the QCDF result (3.59). Although the m_b scaling of the imaginary part appears to be different to the real part here, the narrowness of the integration region owing to the step function compensates for this. In fact, the expressions

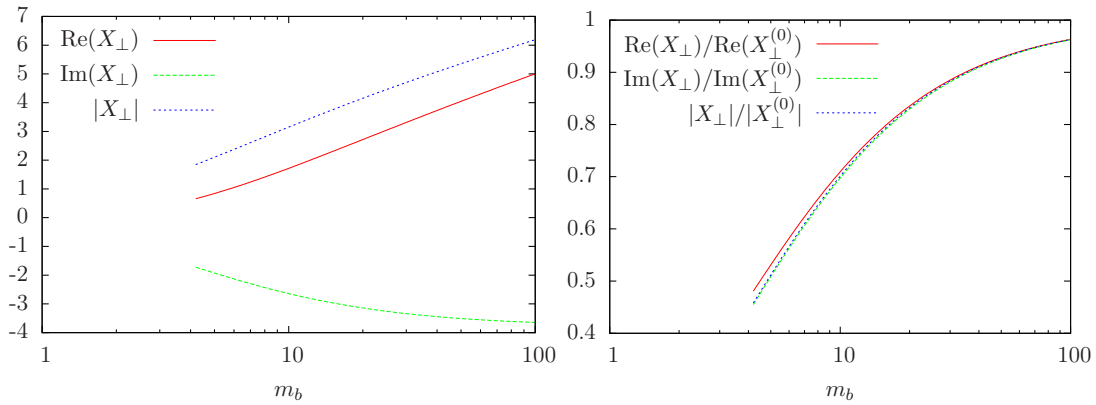

Figure 3.9: (Left) m_b scaling behaviour of $X_\perp$ (3.57) according to LCSR. (Right) Ratio of full LCSR result to the asymptotic expression (3.68). Clearly at the physical value of m_b the large m_b approximation (3.68) is inaccurate; a much larger value of m_b is required to reach the large m_b regime of this quantity. In particular, there are significant cancellations in $\mathrm{Re}\, X_\perp$ at the physical value of m_b and as a result it is smaller than the imaginary part, even though in the $m_b \to \infty$ limit the real part is the larger of the two.

for imaginary and real parts in (3.72) are not really comparable since the operations of large m_b expansion and taking the real and imaginary parts do not commute; taking the large m_b limit on (3.61) and subsequently taking the imaginary part would give $\mathrm{Im}\,\rho = 0$. Likewise, the endpoint singularity arising from the real part (3.72) can be eliminated by splitting the integral into two regions $\bar{u} \sim 1$ and $\bar{u} \sim m_b^{-1}$, and then $\mathrm{Re}\,\rho(\bar{u} \sim m_b^{-1}) \sim m_b$ in accordance with the imaginary part.

Given the difficulties in the $1/m_b$ expansion, it is worth examining whether the approximation (3.68) is a good one, and the comparison between the leading term (3.68) and the full numerical evaluation of $X_\perp^{\mathrm{LCSR}}$ is shown in Figure 3.9. It is apparent from this comparison that considering m_b to be large as in (3.68) does not produce an good approximation at the physical value of m_b.

3.4 G_ι results

In order to get numerical results for $G_\iota^{(s)}(q^2)$ (3.4) from Π^V (3.7):

$$\Pi^V(q^2, p_B^2) = \frac{m_B^2 f_B}{p_B^2 - m_B^2} \langle \gamma^*(q) V(p) | \tilde{\mathcal{O}}_8 | B(p_B) \rangle + \ldots \tag{3.73}$$

The procedure for separating the term of interest from the continuum in Π^V has been described in Section 2.8; however, this in fact leads to an estimate of $[m_B^2 f_B] \langle \gamma^*(q) V(p) | \tilde{\mathcal{O}}_8 | B(p_B) \rangle$. Although f_B is known quite accurately from lattice calculations, in sum rule estimates of matrix elements it has been proposed that the appropriate strategy [121] is to take the sum rule estimate of f_B. This would certainly seem to be a sensible approach since the cuts with B meson quantum numbers in Figure 3.3 can be identified with terms in the f_B sum rule, and

H	s_0	$M^2[G]$	$M^2[f_H]$	m_H	f_H	cond.	value	mass	value
B_s	36(1.5)	9(2)	5.0(5)	5.37	0.162	$\langle\bar{q}q\rangle$	$(-0.24(1))^3$	m_b	4.7(1)
B_q	35(1.5)	9(2)	5.0(5)	5.28	0.142	$\langle\bar{s}s\rangle$	$0.8(1)\,\langle\bar{q}q\rangle$	m_c	1.3(1)
D_s	6.7(7)	6(2)	1.5(2)	1.96	0.185	$\langle g_s\bar{q}Gq\rangle$	$(0.8(1))^2\,\langle\bar{q}q\rangle$	$\bar{m}_s$	0.094(3)
D_q	6.2(7)	6(2)	1.5(2)	1.86	0.156	$\langle g_s\bar{s}Gs\rangle$	$(0.8(1))^2\,\langle\bar{s}s\rangle$		

Table 3.1: Input parameters to sum rules, as well as OPE condensates and quark masses. All quantities are in units of GeV to the appropriate power. The specified values for f_H are the heavy meson decay constants as computed from (3.74) and should not be compared with the actual values since radiative corrections are sizeable. The values $M^2[G]$ and $M^2[f_H]$ are the Borel parameters used in the sum rules for G_ι and f_H respectively; they need not be the same as described below (3.74). The tree-level heavy-quark masses are chosen to satisfy $m_H \simeq m_h + \bar{\Lambda}$ with $\bar{\Lambda} \simeq 0.6\text{GeV}$ approximately. This approach is consistent with previous heavy meson decay calculations, e.g. [42]. The strange quark mass in the $\overline{\text{MS}}$ is given at $\mu_{\overline{\text{MS}}} = 2\,\text{GeV}$. Note that the strange quark mass is neglected in the G_ι sum rule to avoid significant complications in the calculation.

it might be expected that the sensitivity of the final result to the duality approximation would be reduced if the sensitivity to the duality threshold in f_B and Π^V is correlated. The sum rule for f_B is given at $O(\alpha_s^0)$ by [122]:

$$(m_B^2 f_B)^2 = m_b^2 \exp\left(\frac{m_B^2 - m_b^2}{M_{f_B}^2}\right)\left(\frac{3}{8\pi^2}\int_{m_b^2}^{s_0} \exp\left(\frac{m_b^2 - s}{M_{f_B}^2}\right)\frac{(s-m_b^2)^2}{s}ds - m_b\langle\bar{q}q\rangle_\mu - \frac{m_b}{2M_{f_B}^2}\left(1 - \frac{m_b^2}{2M_{f_B}^2}\right)\langle g_s\bar{q}Gq\rangle_\mu\right) \quad . \tag{3.74}$$

Radiative corrections in α_s were excluded because the calculation of Π^V is also at leading order, so subleading terms in the α_s series of the ratio would not be not fully accounted for were a higher order approximation to f_B used. The parameter s_0 should be chosen to be the same in both the f_B and $\mathcal{O}_8$ sum rules, since it is a physical parameter separating perturbative states identified with the B meson from those which are not; clearly this only makes sense because the B meson cuts in both calculations are the same as already discussed. On the other hand, the Borel parameter M^2 may be chosen differently, since the sum rule should in principle be independent of this parameter and deviations from this are indications of semi-global duality violation, although in a practical perturbative calculation the ideal of M^2 independence is replaced by low M^2 sensitivity over a reasonable range, in which both higher dimension OPE condensates and the continuum contribution are effectively suppressed. The necessary numerical inputs for these results are shown in tables 3.1 and 3.2.

The calculation has already been split into terms where the gluon from the $\mathcal{O}_8$ operator connects to the spectator quark and those where it does not (3.10). It is further useful to separate the spectator scattering contribution for the vector meson final state into two parts depending on the polarisation of the final state meson, as for the correlation functions (3.18):

$$G_i^{(s)}(q^2) = G_i^{(\perp)}(q^2) + G_i^{(\parallel)}(q^2) \quad . \tag{3.75}$$

	$f^{\parallel}$[GeV]	$f^{\perp}$[GeV]	$a_2^{\parallel}$	$a_2^{\perp}$	$a_1^{\parallel}$	$a_1^{\perp}$
ρ	0.216(1)(6)	0.160(11)	0.17(7)	0.14(6)		
ω	0.187(2)(10)	0.139(18)	0.15(12)	0.14(12)		
K^*	0.211(7)	0.163(8)	0.16(9)	0.10(8)	0.06(4)	0.04(3)
ϕ	0.235(5)	0.191(6)	0.23(8)	0.14(7)		

Table 3.2: Light vector meson distribution amplitude parameters. Mesons with odd G-parity have vanishing odd Gegenbauer moments. The scale dependent quantities $f^{\perp}$, $a_{1,2}^{\parallel,\perp}$ are evaluated at $\mu = 1\,\text{GeV}$. The computation of these values is described in [103], using experimental values taken from [123], lattice calculations [124, 125] and sum rules from [80, 126–128]. The values for the ω meson are taken to be the same as the ρ with double the uncertainty, since theoretical calculations are unavailable. The decay constants are the same as in [129], subject to updated experimental inputs.

The relations between the correlation functions (3.19) also carry over to the matrix elements $G_i^{(s)}(q^2)$, so

$$G_1^{(\perp)}(q^2) = G_3^{(\perp)}(q^2) = \frac{G_2^{(\perp)}(q^2)}{1 - q^2/m_B^2} \tag{3.76}$$

$$G_1^{(\parallel)}(q^2) = G_2^{(\parallel)}(q^2) = 0 \quad , \tag{3.77}$$

from which it follows that only $G_1^{(\perp)}(q^2)$ and $G_3^{(\parallel)}(q^2)$ need to be specified. Likewise the relation between the longitudinal polarisation of vector mesons and the equivalent pseudoscalar meson (3.24) carries over:

$$G_T(q^2) = -\frac{f_P}{f_V}\frac{m_B^2 - q^2}{2m_V(m_B - m_P)} G_3^{(\parallel)}(q^2)|_{\phi_\parallel \to \phi_P} \quad . \tag{3.78}$$

Results for pseudoscalar decays are therefore qualitatively the same as those for $G_3^{(\parallel)}$ and will not be displayed explicitly. For the sake of completeness the expression for $G_1^{(\perp)}(q^2)$ is

$$\begin{aligned} G_1^{(\perp)}(q^2) = &-\frac{\alpha_s}{8\pi} C_F f_V^{\perp} m_b^2 \frac{1}{m_B^2 f_B} \int_0^1 du\, \phi_\perp(u) \int_{m_b^2}^{s_0} ds \\ &\times e^{\frac{m_B^2 - s}{M^2}} \left[\frac{Q_q \rho_{B_a} + Q_b \rho_{B_c} + 2(Q_q + Q_b)\rho_{B_d}}{uq^2 + \bar{u}P^2} - 2Q_q \rho_{C_a} - Q_b \rho_{C_c} \right] \quad , \end{aligned} \tag{3.79}$$

which follows from (3.19), (3.20) and the standard sum rule procedure. The density functions ρ_i are given in sections 3.2.3 and 3.2.4. The expression for $G_3^{(\parallel)}(q^2)$ is not displayed explicitly owing to the fact that it is exceedingly complex; its derivation, however, is in principle straightforward once the dispersion representation of C_a is known and the resulting polynomials are given in appendix D.1. It has been verified that the expressions in appendix D.1 do not introduce any additional poles in p_B^2 in the expression for $g_3^{(\parallel)}(q^2)$, hence only the cuts arising from the Passarino–Veltman functions need to be accounted for. There are however poles in the individual coefficient functions which are cancelled in the total and some care is required in the numerical integrals in order to get accurate results. Numerical treatment of integrals with

		$\rho[\pi]^+$	$\rho[\pi]^0, \omega$	$\rho[\pi]^-$	$K^*[K]^+$	$K^*[K]^0$	$K^*[K]^-$	$\bar{K}^*[\bar{K}]^0$	ϕ
		$\bar{d}u$	$\bar{u}u \pm \bar{d}d$	$\bar{u}d$	$\bar{s}u$	$\bar{s}d$	$\bar{u}s$	$\bar{d}s$	$\bar{s}s$
B^-	$\bar{u}b$	-	-	$b \to d$	-	-	$b \to s$	-	-
$\bar{B}^0$	$\bar{d}b$	-	$b \to d$	-	-	-	-	$b \to s$	-
$\bar{B}_s$	$\bar{s}b$	-	-	-	-	$b \to d$	-	-	$b \to s$
D^0	$\bar{u}c$	-	$c \to u$	-	-	-	-	-	-
D^+	$\bar{d}c$	$c \to u$	-	-	-	-	-	-	-
D_s	$\bar{s}c$	-	-	-	$c \to u$	-	-	-	-

Table 3.3: Heavy-to-light FCNC transitions into vector and pseudoscalar mesons. Valence quark content of each meson is shown and the main table body indicates the FCNC transition type. The η and η' are not considered. The chromomagnetic transition amplitudes $G_\iota^{(s)}(0)$ are shown in table 3.4 for vector mesons.

local difficulties is something of a standard problem and in this calculation GSL [130], which provides a range of good numerical integration routines, was used.

The list of transitions to which this calculation is applicable is shown in table 3.3. Results for $B \to V\gamma$ type decays are shown in table 3.4. Plots for the key G_i functions are shown in Figure 3.10 for the decay $B \to K^* l^+ l^-$. Tabulated results for these graphs were published in [103]. In spite of some effort, a numerical fit of the graphs in Figure 3.10 with a small number of parameters did not prove effective in contrast to the $\mathcal{O}_7$ case [81], and it appears that in the present case simple interpolation using generic Chebyshev or spline approximation methods is most effective.

The calculation of uncertainties in table 3.4 was done as follows: input parameters are varied according to their uncertainties given in tables 3.1 and 3.2. This leaves three remaining sources of uncertainty: higher-twist and higher-order corrections in α_s, the semi-global duality approximation and renormalisation scale uncertainty, although scale uncertainty and higher-order corrections are related. Violations of the duality approximation are accounted for by variation of the duality threshold s_0, as shown in table 3.1. The effect of neglecting higher twist is assigned an error of 15%. The renormalisation scale uncertainty is accounted for by varying μ around $\mu = \sqrt{\Lambda_H m_b}$ with $\Lambda_H = 0.8(2)\,\text{GeV}$ and rescaling running quantities[9] using their one-loop anomalous dimensions, which are listed in appendix B.5. All of these sources of error are added in quadrature since there is no reason to expect strong correlations.

3.4.1 Qualitative remarks

The previous section only gave explicit results for the spectator scattering parts of the chromomagnetic transition amplitude. A comparison between the spectator and non-spectator scattering amplitudes is presented in table 3.5. This reveals that the non-spectator amplitude is rather the larger of the two; however it is worth noting that only the spectator scattering part contributes to the isospin asymmetry.

[9] Note that the heavy quark mass does not run in this calculation since the PS mass rather than the $\overline{\text{MS}}$ mass has been used.

	$G_1^{(\perp)}(0)\times 10^2$	unc.%		$G_1^{(\perp)}(0)\times 10^2$	unc.%
$B^- \to \rho^-\gamma$	$0.29 - 0.39i$	25%	$D^0 \to \rho^0\gamma$	$-7.0 - 5.0i$	32%
$B^- \to K^{*-}\gamma$	$0.29 - 0.40i$	26%	$D^0 \to \omega\gamma$	$-6.1 - 4.3i$	34%
$\bar{B}^0 \to \rho^0\gamma$	$0.22 + 0.19i$	27%	$D^+ \to \rho^+\gamma$	$-1.9 + 2.5i$	32%
$\bar{B}^0 \to \omega\gamma$	$0.19 + 0.17i$	33%	$D_s^+ \to K^{*+}\gamma$	$-1.8 + 2.1i$	33%
$\bar{B}^0 \to \bar{K}^{*0}\gamma$	$0.20 + 0.20i$	28%			
$\bar{B}_s \to K^{*0}\gamma$	$0.21 + 0.18i$	27%			
$\bar{B}_s \to \phi\gamma$	$0.26 + 0.23i$	26%			

Table 3.4: $G_1^{(s)}(0)$ for $b \to d$, $b \to s$ and $c \to u$ type transitions. This gives the contribution of the diagrams A_{1-4} (see Figure 3.1) to $(B, D) \to V\gamma$ processes. There appear to be four qualitatively distinct cases, depending on whether the initial state is either a B or D meson and whether it is charged or neutral. Charge conjugate transitions follow from multiplication by -1 since every transition is proportional to valence quark charges. The total contribution of the chromomagnetic operator to $B \to V\gamma$ also required the non-spectator amplitude $G_1^{(ns)}$; the two are compared in table 3.5. Pseudoscalar meson decays are not listed since the $B \to P\gamma$ transition is forbidden.

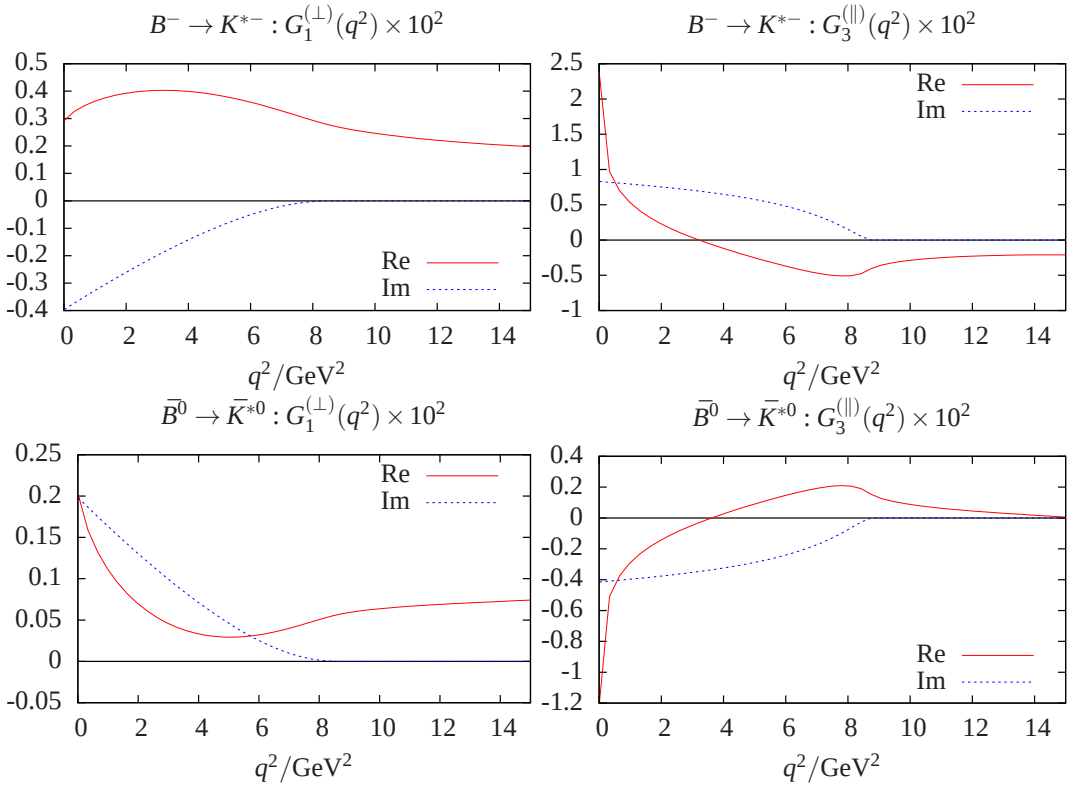

Figure 3.10: Plots of $G_1^{(\perp)}(q^2)$ and $G_3^{(\|)}(q^2)$ for charged and neutral B mesons. The B_s meson will be qualitatively similar to the B^0, and likewise the replacement of the b quark with a charm quark leads to qualitatively similar results after accounting for the smaller q^2 range in that case.

type	$B^- \to \rho^- \gamma$	$\bar{B}^0 \to \rho^0 \gamma$	$D^+ \to \rho^+ \gamma$	$D^0 \to \rho^0 \gamma$
$G_1^{(s)}(0) \times 10^{-2}$	$0.29 - 0.39i$	$0.22 + 0.19i$	$-1.9 + 2.5i$	$-7.0 - 5.0i$
$G_1^{(ns)}(0) \times 10^{-2}$	$0.90 + 1.3i$	$0.90 + 1.3i$	$-8.5 - 12i$	$-8.5 - 12i$
$G_1(0) \times 10^{-2}$	$1.2 + 0.91i$	$1.1 + 1.5i$	$-10 - 9.5i$	$-16 - 17i$
$\left\lvert G_1^{(s)}(0)/G_1^{(ns)}(0) \right\rvert$ [%]	31	18	21	58
$\left\lvert G_1^{(s)}(0)/T_1(0) \right\rvert$ [%]	2	1	4	12
$\lvert G_1(0)/T_1(0) \rvert$ [%]	6	7	20	33

Table 3.5: Comparison of spectator and non-spectator parts of G_ι functions, and the leading form factor T_1 in $B \to V\gamma$. For the $T_1(0)$ form factors the reference values $T_1(0) = 0.27$ [81] for $B \to \rho$ and $T_1(0) = 0.7$ for $D \to \rho$ are used. The ratio of $G_1^{(ns)}$ to $T_1(0)$ can be inferred directly from the method used to compute $G_1^{(ns)}$ described in Section 3.2.5 and is therefore a result of [104].

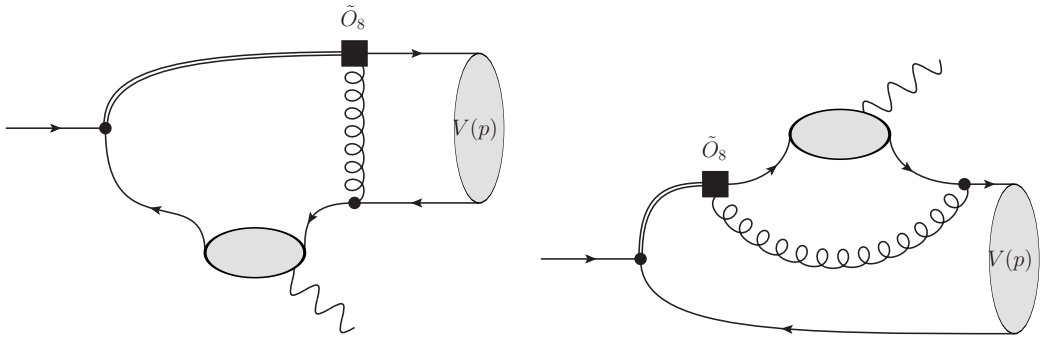

Figure 3.11: Additional contribution from the photon DA at $q^2 = 0$. These diagrams are in fact zero due to Dirac algebra and only the perturbative photon interaction contributes.

A reader familiar with the WA contribution to $B \to V\gamma$ might ask why the contribution of the photon DA has not been raised at all. As will be discussed further in Chapter 5, the photon DA accounts for the susceptibility of the quark condensate to a background photon field and may be viewed as predominantly originating from an intermediate off-shell ρ meson state. The diagrams in Figure 3.11, which are the only two possible arrangements which satisfy kinematical constraints imposed by the DAs, were in fact computed but it transpires that if the meson mass is neglected, as it must be at leading twist, both of these diagrams are zero owing to Dirac algebra. They are, however, non-zero if $q^2 \neq 0$ is allowed; though this does not make sense for an on-shell photon, it is worth mentioning since the vanishing of the photon DA contribution appears to be an accident and this result does not imply that the ρ meson resonance is somehow invisible to $G_i(q^2)$ at leading order.

Since results have been computed for both B and D mesons, the effect of heavy-quark scaling may be re-examined numerically. The electromagnetic form factor $T_1(0)$ scales as $m_b^{-3/2}$ [117] and this carries over to the scaling of $G_1^{(ns)}(0)$, since the $F_{7,8}$ functions used to compute it in Section 3.2.5 clearly scale as m_b^0 [104]. As discussed in Section 3.3.1, the scaling of $G_1^{(ns)}(0)$ can be split into two parts according to the emitting quark charge

$$G_1^{(s)}(0) = Q_h G_1^{h,(s)}(0) + Q_q G_1^{q,(s)}(0) \tag{3.80}$$

and then $G_1^{h,(s)}(0) \sim m_b^{-3/2}$ and $G_1^{q,(s)}(0) \sim m_b^{-5/2}$ up to logarithmic corrections. Photon emission from the heavy-quark line therefore scales as $m_b^{-3/2}$, regardless to which quark line the gluon connects. Numerical investigation of the heavy-quark scaling of $G_1^{(ns)}(0)$ is not within the scope of this investigation, since it is nothing but the scaling of $T_1(0)$. The numerical scaling of the spectator-quark scattering parts may be examined in terms of a pair of ratios using the decomposition (3.80):

$$R_h = \frac{G_1^{b,(\perp)}(0)[B \to \rho\gamma]}{G_1^{c,(\perp)}(0)[D \to \rho\gamma]} = 0.14 \qquad R_l = \frac{G_1^{q,(\perp)}(0)[B \to \rho\gamma]}{G_1^{q,(\perp)}(0)[D \to \rho\gamma]} = 0.05 + 0.04i \quad . \tag{3.81}$$

From the heavy-quark scaling behaviour the expected values of these ratios are

$$|R_h| \approx \alpha_s(\sqrt{m_c\Lambda_H})/\alpha_s(\sqrt{m_b\Lambda_H})(m_c/m_b)^{3/2} = 0.2 \tag{3.82}$$

$$|R_q| \approx \alpha_s(\sqrt{m_c\Lambda_H})/\alpha_s(\sqrt{m_b\Lambda_H})(m_c/m_b)^{5/2} = 0.06 \quad , \tag{3.83}$$

which are really quite close to those in (3.81), in view of the problems with heavy-quark scaling described in Section 3.3.1. It would appear that there is some correlation between the non-leading terms in the heavy-quark mass in the b and charm quark cases, since according to Figure 3.9 the heavy-quark limit is not an especially good approximation in the present case.

Finally the validity of this calculation in q^2 must be discussed. The principle for determining whether this kind of sum rule calculation is valid is that the results cannot be trusted when either full or perturbative QCD predict production of particles. In the case of the $\mathcal{O}_8$ operator, the most problematic region is $0 < q^2 < 1\,\mathrm{GeV}^2$, where the strong ρ meson resonance will appear. The photon case $q^2 = 0$ can however be accounted for correctly, since the influence of non-perturbative contributions may be accounted for using the photon DA, and this procedure will be discussed in the calculation of WA contributions in Section 5.3.6; however, as explained earlier in this section, in the $\mathcal{O}_8$ case it happens that these contributions are zero. There are also resonances due to $\bar{s}b$, $\bar{d}b$ and $\bar{b}b$ vector meson states, i.e. the $B^*_{d,s}$ and the Υ. These heavy states only impose the restriction $q^2 < m_b^2$, so the validity of this calculation covers the vast majority of the physical parameter range.

3.5 Concluding remarks on G_ι

This calculation has resolved a long-standing unknown term in heavy-to-light FCNC decays. The resulting values of the "form factors" G_ι are small and so they are not relevant to the overall branching fractions $(B, D) \to Vll$ or $(B, D) \to V\gamma$; however, they are large enough to contribute significantly to CP and isospin asymmetries as will be seen in chapters 4 and 5. The large strong phase of this amplitude is an important feature for CP asymmetry contribution.

The comparison between the LCSR and QCDF calculations of G_ι is itself rather interesting,

since it reveals that in this instance the large m_b expansion fails due to the endpoint singularity, and the full m_b dependence must be retained in order to regulate this. More sophisticated approaches to factorisation might, however, allow endpoint divergences to be treated consistently. One approach has been put forward in [131] and extended in [132]. The $\mathcal{O}_8$ contribution was calculated using this method in [133]; however, this does not generate the imaginary part.

Perhaps the most interesting feature of this calculation is the unexpected appearance of a complex anomalous threshold in the dispersion relation. Although this is not the conceptual problem it might appear to be since the anomalous threshold can be considered part of the continuum of multi-particle states, it does present some technical difficulty in the calculation. The presence of this anomalous threshold is associated with the introduction of the momentum insertion k which then requires an additional analytic continuation in P^2. This insertion is not usually required at leading order in α_s for $B \to Vll$ processes, because for WA the amplitude can usually be factorised and for the electromagnetic operator the photon momentum plays the same role. As will be shown in Chapter 5, the same difficulty can also arise in WA beyond leading twist, and it would appear that beyond leading order the momentum k will be required in most cases and the anomalous threshold problem should be expected to be generic. A complete next-to-leading order calculation of $B \to Vll$ using LCSR can therefore be expected to involve considerably difficult analytic continuations unless a systematic method is found.

Finally, it should be remarked that an alternative approach to calculating the chromomagnetic form factor was proposed in [134] shortly before the publication of this calculation. In this approach, the B meson external state is treated using a light-cone DA and a sum rule is used for the light meson, although only the soft initial-state gluon contribution is computed, so questions of $1/m_b$ expansion difficulties do not arise. This approach avoids the complications brought about by the k insertion since the parasitic cuts are near m_b^2, which is far above the duality threshold of any light vector meson, and thus the resulting dispersion relations can be expected to be simpler. The problem of endpoint divergences and the $1/m_b$ expansion are likely to be difficult to address properly in this approach, however, since the B meson DA assumes that the $1/m_b$ expansion works.

Chapter 4

CP violation in $D \to V\gamma$ through the chromomagnetic operator

Last year, experimental results from LHCb and CDF indicated a significant direct CP asymmetry in $D^0 \to \pi\pi$ and $D^0 \to KK$ decays [22, 135]. This was something of a surprise because the CP asymmetry in charm decays is expected to be small; it is proportional to the weak phase difference between the current-current and penguin operators, and thus is suppressed by four powers of the Cabibbo angle. The naive expectation is therefore that the CP asymmetry should be of order $\sim 10^{-4}$. The CP asymmetry measured in experiment, however, was [135]

$$\Delta A_{\rm CP} = A_{\rm CP}^{K^+K^-} - A_{\rm CP}^{\pi^+\pi^-} = -0.65(18) \times 10^{-2} \quad , \tag{4.1}$$

where

$$A_{\rm CP}^f \equiv \frac{\Gamma[D^0 \to f] - \Gamma[\bar{D}^0 \to f]}{\Gamma[D^0 \to f] + \Gamma[\bar{D}^0 \to f]} \quad . \tag{4.2}$$

This is at least an order of magnitude higher than expected. Two brief remarks should be made about this measurement: first, in the limit of exact $SU(3)$ flavour symmetry, $A_{\rm CP}^{K^+K^-} = -A_{\rm CP}^{\pi^+\pi^-}$ would hold. Second, both $A_{\rm CP}^{K^+K^-}$ and $A_{\rm CP}^{\pi^+\pi^-}$ should be small separately; the quantity $\Delta A_{\rm CP}$ is preferred because some experimental errors cancel. It is also expected that the pollution from indirect, i.e. time-dependent, CP asymmetries is negligible [22]; thus (4.1) appears to be a true indication of direct, i.e. time-independent, CP asymmetry in D meson decays.

If the value (4.1) is confirmed, the question of why it is so much larger than expectations must be addressed: it could be due to new physics [136–139], or alternatively unexpected strong dynamics [140–143]. Fortunately transitions of the $\Delta I = 3/2$ type, which could lead to sizeable CP violation [144], can be tested with isospin sum rules [145], so the problem is reduced to $\Delta I = 1/2$ operators.

Since this calculation was originally published [94], LHCb have published updated data [146], which along with the updated global average is [147]:

$$\begin{aligned}\Delta A_{CP}|_{2013\ \text{LHCb}} &= (+0.49 \pm .30(\text{stat.}) \pm 0.14(\text{sys.})) \times 10^{-2} \\ \Delta A_{CP}|_{2013\ \text{HFAG}} &= -0.33(12) \times 10^{-2} \quad .\end{aligned} \tag{4.3}$$

This has significantly shifted the world average asymmetry towards zero in comparison to (4.1), and perhaps therefore the SM is set to prevail again. This chapter will continue to use (4.1) as indicative of the magnitude of CP violation in D meson decays, and further comments will be made in the conclusions Section 4.4.

If the CP asymmetry is due to new physics rather than the aforementioned strong dynamics, it turns out that the chromomagnetic operators

$$\mathcal{O}_8 = -\frac{gm_c}{8\pi^2}\bar{u}\sigma^{\mu\nu}G^a_{\mu\nu}\frac{\lambda^a}{2}(1+\gamma_5)c \qquad \mathcal{O}'_8 = -\frac{gm_c}{8\pi^2}\bar{u}\sigma^{\mu\nu}G^a_{\mu\nu}\frac{\lambda^a}{2}(1-\gamma_5)c \tag{4.4}$$

are good candidates, since they do not violate any existing constraints [148]. It should be emphasised that these operators are of the $\Delta I = 1/2$ type and therefore avoid isospin tests. It should also be noted that $C'_8 = (m_u/m_c)C_8$ is negligible in the SM. The reference value for the C_8 Wilson coefficient following, e.g. [149], is taken to be

$$\text{Im}[C_8^{(\prime)NP}] = 0.4 \times 10^{-2} \quad , \tag{4.5}$$

which is two orders of magnitude larger than its value in the SM[1].

The contribution of chromomagnetic operators to CP violation (4.1) can be estimated using QCDF [150] to be

$$\Delta A_{CP}|_{NF} \approx -1.8(\text{Im}\, C_8 - \text{Im}\, C'_8)\sin\delta \quad , \tag{4.6}$$

where δ is the strong phase difference in the $B \to KK$ and $B \to \pi\pi$ systems[2], which is unknown but expected to be $\sim O(1)$, although the sign is not known and hence the sign of $\text{Im}\, C_8$ is not determined. It can be seen that (4.6) is proportional to $\text{Im}\, C_8 - \text{Im}\, C'_8$, because the parity of the D and $\pi\pi/KK$ states implies that these transitions are induced by a parity-violating operator and hence the γ_5 part of the $\mathcal{O}_8^{(\prime)}$ operators, which have opposite signs. The proposed value (4.5) would therefore account for the observed CP violation (4.1), if indeed $\sin\delta \approx 1$.

The unfortunate presence of unknown phases in $D \to \pi\pi$ and $D \to KK$ decays means that it is desirable to study CP violation in other D meson decays which are theoretically more accessible. Another system was therefore chosen in which new physics in the C_8 coefficient would induce sizeable CP violation, $D \to (\rho^0, \omega)\gamma$. This follows previous work which proposed

[1] See Section 4.1.1 for the definition of C_8 used here.

[2] That is to say, the difference between the chromomagnetic amplitude and the leading amplitude which should be approximately equal in both systems assuming $SU(3)$ flavour symmetry.

a scenario for observable CP violation in this channel through new physics in C_7 [149]; the scenario proposed here differs in that the strong (CP-even) phase difference necessary to observe direct CP violation arises in the chromomagnetic matrix element rather than the leading order matrix element, which, it will be argued, in fact has a small strong phase.

4.1 The decay $D \to V\gamma$

The size of contributions of $D \to V\gamma$ decays is very different to those in $B \to V\gamma$ decays, due to the different quark masses and CKM hierarchy involved. The implications of this for theoretical calculations of the $D \to V\gamma$ rate will be discussed in this section. Unfortunately owing to the large renormalisation scale sensitivity and the comparatively small mass of the charm quark relative to the QCD scale and hence poor convergence of the $1/m_c$ expansion, the situation is not at present completely clear. Nonetheless, the argument will be made that the decay $D \to V\gamma$ is dominated by weak annihilation and thus has a small strong phase.

4.1.1 The effective Hamiltonian for $c \to u$ decays

The effective Hamiltonian for $c \to u$ decays is structurally the same as for $b \to s$ decays. Following [148], it is written as:

$$\mathcal{H}^{\text{eff}} = \lambda_d \mathcal{H}_d + \lambda_s \mathcal{H}_d + \lambda_b \mathcal{H}_{\text{peng}} \,, \quad \lambda_D \equiv V_{cD}^* V_{uD} \,, D = d, s, b \quad , \tag{4.7}$$

where

$$\begin{aligned} \mathcal{H}_q =& \frac{G_F}{\sqrt{2}} \sum_{i=1}^{2} C_i^q \mathcal{O}_i^q \,, \qquad q = d, s \\ \mathcal{O}_1^q =& (\bar{u} L_\mu q)(\bar{q} L^\mu c) \,, \qquad \mathcal{O}_2^q = (\bar{u}_\alpha L_\mu q_\beta)(\bar{q}_\beta L^\mu c_\alpha) \\ \lambda_b \mathcal{H}_{\text{peng}} =& \frac{G_F}{\sqrt{2}} \left(C_7 \mathcal{O}_7 + C_7' \mathcal{O}_7' + C_8 \mathcal{O}_8 + C_8' \mathcal{O}_8' + ... \right) \end{aligned} \tag{4.8}$$

and $L_\mu \equiv \gamma_\mu(1 - \gamma_5)$. α and β are colour indices. The CKM factor λ_b has been absorbed into the coefficients $C_{7,8}$, since it cannot be assumed that they are relevant for beyond-SM operators. The dimensionful coupling G_F is retained. The electromagnetic penguin operators are exactly analogous to (4.4)

$$\mathcal{O}_7 = -\frac{e m_c}{8\pi^2} \bar{u} \sigma^{\mu\nu} F_{\mu\nu} (1 + \gamma_5) c \qquad \mathcal{O}_7' = -\frac{e m_c}{8\pi^2} \bar{u} \sigma^{\mu\nu} F_{\mu\nu} (1 - \gamma_5) c \tag{4.9}$$

and have the same chirality structure as the chromomagnetic ones, that is $C_7' = (m_u/m_c) C_7$.

The crucial difference from $b \to s$ decays arises from the fact that the penguin operators $\mathcal{O}_{3-6}$ are only generated in the absence of GIM cancellation in the RG running. In b decays,

the heaviest quark in the up-sector is the top which is above the electroweak scale; thus the penguin operators are generated starting at a very high scale and WCs are expected to be approximately proportional to $\log m_t^2/m_b^2$. In the case of charm decays, this role is played by the bottom quark and thus the relevant logarithm is $\log m_b^2/m_c^2$, so the operators $\mathcal{O}_{3-6}$ thus generated are expected to be small in the SM. Furthermore, the penguin operators $\mathcal{O}_{3-6}$ are proportional to the CKM factor λ_b, which is $O(\lambda^5)$ and thus much smaller than in the B meson case. As a result, the operators $\mathcal{O}_{1,2}$ are expected to dominate D meson decays and the four-quark penguin operators $\mathcal{O}_{3-6}$ in (4.7) have not been included.

The scenario for sizeable observable CP violation will be through transitions induced by the chromomagnetic operator $\mathcal{O}_8$ computed in Chapter 3. The definitions and amplitudes are briefly recapitulated here. The amplitude of the chromomagnetic operator (4.9) is parametrised as

$$\mathcal{A}_i|_8 = \langle V\gamma|\mathcal{H}^{\text{eff}}|_8|D\rangle = \frac{G_F}{\sqrt{2}}\left(\frac{em_c}{2\pi^2}\right)\frac{1}{c_V}\begin{cases}(C_8+C_8')G_1(0) & i=1\\ (C_8-C_8')G_2(0) & i=2\end{cases}, \tag{4.10}$$

where $\mathcal{H}^{\text{eff}}|_8 = \frac{G_F}{\sqrt{2}}(C_8\mathcal{O}_8 + C_8'\mathcal{O}_8')$, cf. (4.8). The factor c_V is inserted to absorb trivial factors due to the $\omega \sim (\bar{u}u+\bar{d}d)/\sqrt{2}, \rho^0 \sim (\bar{u}u-\bar{d}d)/\sqrt{2}$ wave functions, and thus $c_V = \sqrt{2}$ for ρ^0 and ω and $c_V = 1$ in all other cases. This factor will drop out in the CP asymmetry. Eliminating trivial factors, the definition (4.10) combined with (4.8) implies

$$\langle V\gamma|\mathcal{O}_8^{(\prime)}|D\rangle = \left(\frac{em_c}{4\pi^2}\right)\frac{1}{c_V}(G_1(0)P_1 \pm G_2(0)P_2)\,, \tag{4.11}$$

which, as explained in Chapter 3, is designed to be analogous to the definitions of the standard penguin form factors $T_{1,2}(0)$, discussed in Section 2.9. At twist-2 accuracy it was found that $G_1(0) = G_2(0)$, which implies that $\mathcal{O}_8$ and $\mathcal{O}_8'$ generate solely left- and right-handed amplitudes respectively. It can be seen from table 3.5 that $G_1^{D^0\to\rho^0\gamma}(0) \simeq G_1^{D^0\to\omega\gamma}(0)$, $G_1^{D_s^+\to K^{*+}\gamma}(0) \simeq G_1^{D^+\to\rho^+\gamma}(0)$ to an accuracy sufficient for the present purpose, and therefore no distinction will be made between them[3]. The imaginary part, which is the value relevant for the CP asymmetry, is

$$\text{Im}[G_1^{D_0}(0)] \simeq -0.20(8) \qquad \text{Im}[G_1^{D^+}(0)] \simeq -0.10(4)\,, \tag{4.12}$$

where numbers were rounded. The values in (4.12) are sizeable compared to typical estimates $T_1^{D^0}(0) \simeq T_1^{D^+}(0) \simeq 0.7$ of the $\mathcal{O}_7$ operator [149]. The difference between the neutral and charged matrix elements in (4.12) originates from the charges of the valence quarks of the mesons.

[3]The dominant effect of the final state meson is in the decay constants $f_X m_X$ and $f_X^\perp$ for WA and $G_1(0)$ respectively, and thus the correction due to this approximation is expected to be given by $R = r_\rho/r_\omega \approx 1.01$ where $r_X = (f_X^\perp)/(m_X f_X^\parallel)$ in the $\rho-\omega$ case, for instance.

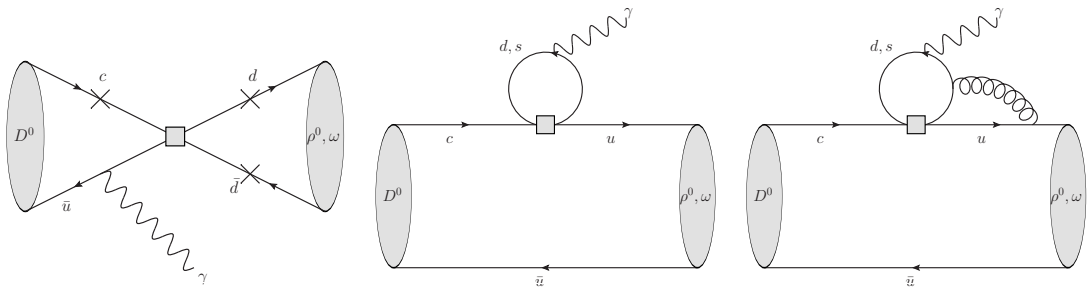

Figure 4.1: The three diagrams whose contributions are expected to be potentially dominant in $D \to V\gamma$ decays. They are WA (left), a factorisable quark loop (middle) and a quark loop with gluon exchange (right). The middle diagram vanishes for an on-shell photon by gauge invariance. The right-hand diagram has a large strong phase, which can be seen from the inclusive calculation in [151]. The question of whether the leading amplitude has a large strong phase or not is then essentially the question of whether the left- or right-hand diagram is the dominant amplitude.

4.1.2 The leading amplitude in $D \to V\gamma$ decays

There are two candidates for the leading amplitude in $D \to V\gamma$ decays: weak annihilation and quark loops, as shown in Figure 4.1. The quark-loop contribution has been calculated in an inclusive approach in [151] and found to dominate all other inclusive contributions; obviously, however, this does not include weak annihilation.

The amplitude will be parametrised as in the B meson case (2.62) as[4]:

$$\begin{aligned}\mathcal{A}[D \to V\gamma] \equiv \langle V\gamma|\mathcal{H}^{\text{eff}}|D\rangle &= \mathcal{A}_1 \frac{P_1}{2} + \mathcal{A}_2 \frac{P_2}{2} \\ &= \mathcal{A}_L \left(\frac{P_1 + P_2}{4}\right) + \mathcal{A}_R \left(\frac{P_1 - P_2}{4}\right) \quad ,\end{aligned} \tag{4.13}$$

where

$$P_1 = 2\epsilon_{\rho\alpha\beta\gamma}\epsilon^\rho \eta^\alpha p^\beta q^\gamma \qquad P_2 = 2i[(p\cdot q)(\eta\cdot\epsilon) - (\eta\cdot q)(p\cdot\epsilon)] \tag{4.14}$$

and $\eta(p)$ and $\epsilon(q)$ stand for the vector meson and photon polarisation tensors. The amplitudes $\mathcal{A}_{L,R}$ will be further parametrised as:

$$\mathcal{A}_{L,R} = l_{L,R} e^{i\delta_{L,R}} e^{i\phi_{L,R}} + g_{L,R} e^{i\Delta_{L,R}} e^{i\Phi_{L,R}} \quad , \tag{4.15}$$

where the terms are separated according to their weak (CP-odd) phases, $\phi_{L,R}$ and $\Phi_{L,R}$. Two weak phases are sufficient to parametrise decays in the SM, since the three relevant CKM coefficients are related by unitarity, and thus one of them can be eliminated in favour of the

[4]The amplitudes $\mathcal{A}_{1,2}$ are often denoted by $\mathcal{A}_{\text{PC,PV}}$ in the literature (up to phases), e.g. [149, 152]. PC and PV stand for parity-conserving and -violating respectively.

other two. In terms of these amplitudes, the partial width for $D \to V\gamma$ is given by:

$$\Gamma[D \to V\gamma] = \frac{1}{32\pi} m_D^3 \left(1 - \frac{m_V^2}{m_D^2}\right)^3 \underbrace{\left(|\mathcal{A}_1|^2 + |\mathcal{A}_2|^2\right)}_{x[V]} \quad , \tag{4.16}$$

where $x[V] = |\mathcal{A}_1|^2 + |\mathcal{A}_2|^2$ has been defined for later convenience.

With these definitions of the amplitude, the CP asymmetry (4.2) may be re-written as

$$A_{CP}[D^0 \to f] = \frac{-2\sum_{i=L,R} l_i g_i \sin(\Delta_i - \delta_i)\sin(\Phi_i - \phi_i)}{\sum_{i=L,R}\left[l_i^2 + g_i^2 + 2 l_i g_i \cos(\Delta_i - \delta_i)\cos(\Phi_i - \phi_i)\right]} \quad , \tag{4.17}$$

which exposes the need for both sizeable CP-odd and CP-even phase differences in order to produce an experimentally measurable CP asymmetry.

Weak annihilation (WA) contribution

The scenario for CP violation will rely on the leading-order strong phase being small. It will be argued that it is reasonable to believe that the WA contribution to $D \to V\gamma$ decay is dominant, and indeed this amplitude has no strong phase at leading order in α_s. The question of the size of the strong phase in subleading corrections will be addressed thereafter.

The contribution of weak annihilation in $\mathcal{A}[D \to V\gamma]$ will be estimated using sum rules computed in [77, 78], and these estimates will be compared to experimentally measured rates. Unfortunately the rate for the process under consideration, $D \to \rho\gamma$, has not yet been measured. The calculation of these matrix elements in B physics including several extensions will be discussed in Chapter 5; however, in the case of SM charm physics, the coefficients of the four-quark penguin operators $\mathcal{O}_{3-6}$ are negligible as described in Section 4.1.1 and thus the additional terms computed for that case are irrelevant.

The measured rates of the $D^0 \to V\gamma$-type are [123]:

$$\mathcal{B}(D^0 \to \bar{K}^{*0}\gamma) = 3.27(34)\cdot 10^{-4} \qquad \mathcal{B}(D^0 \to \phi\gamma) = 2.70(35)\cdot 10^{-5} \quad , \tag{4.18}$$

which are Cabibbo allowed and singly Cabibbo suppressed, respectively. The total amplitude in the $x[V]$ normalisation (4.16) for these decays can therefore be inferred:

$$x[\bar{K}^*]_{\text{ex}} = \ 1.8\cdot 10^{-14}(10\%)\text{GeV}^{-2} \qquad x[\phi]_{\text{ex}} = 2.0\cdot 10^{-15}(10\%)\text{GeV}^{-2} \quad . \tag{4.19}$$

The relation between $\mathcal{A}_{1,2}$ (4.13) and $A_{\text{PC(PV)}}$ of reference [77] for a $D \to V\gamma$ decay is

$$\mathcal{A}_{1(2)}|_{\text{WA},\mathcal{O}(\text{ff}_s^0)} = -\left(\frac{G_F}{\sqrt{2}}\lambda_d a_1\right)\left(\frac{f_V m_V}{c_V}\right) A_{\text{PC(PV)}} \quad , \tag{4.20}$$

where $a_1 = C_1 + C_2/3 \simeq -0.5$ is the colour suppressed WC[5], and the constant c_V is defined below (4.10). The ratio of the LCSR prediction to the experimental value is

$$\frac{x[\bar{K}^*]_{\rm LCSR}}{x[\bar{K}^*]_{\rm ex}} \simeq 0.5 \quad , \tag{4.21}$$

which translates into a factor of $\sim\sqrt{2}$ for the amplitudes. Thus the LCSR prediction accounts for 60% of the experimental result. This result is considered rather good in view of the anticipated uncertainty, which is expected to be largely due to omission of higher order corrections, or equivalently renormalisation scale error, and the use of semi-global quark-hadron duality in the sum rule. Following (4.21), predictions shall be constructed for other $D \to V\gamma$ decay rates by scaling the corresponding LCSR predictions [77] by a factor of two. This entails scaling the amplitude by $\sqrt{2}$, and it is assumed that LCSR accurately predicts the phase, resulting in

$$\mathcal{A}_{1(2)}|_{\rm LD} \simeq 1.4 \times \mathcal{A}_{1(2)}|_{{\rm WA},\mathcal{O}(\mathrm{ff}_s^0)} \quad ; \tag{4.22}$$

then using the notation $l_{1(2)} \equiv \mathcal{A}_{1(2)}|_{\rm LD}$:

$$\begin{aligned}
l_1 &\simeq \frac{-3.7\cdot 10^{-8}}{c_V\, m_D}\left(\frac{a_2}{-0.5}\right) \qquad l_2 \simeq \frac{-2.1\cdot 10^{-8}}{c_V\, m_D}\left(\frac{a_2}{-0.5}\right) \qquad \{D^0 \to (\rho^0,\omega)\} \\
l_1 &\simeq \frac{-13.2\cdot 10^{-9}}{c_V\, m_D}\left(\frac{a_1}{1.0}\right) \qquad l_2 \simeq \frac{-11.8\cdot 10^{-9}}{c_V\, m_D}\left(\frac{a_1}{1.0}\right) \qquad \{D^+_{(d,s)} \to (\rho^+, K^{*+})\} \quad .
\end{aligned} \tag{4.23}$$

Since WA has no strong (CP-even) phase at leading order, $l_{L,R} = l_1 \pm l_2$ in (4.15), and therefore in the left-right basis:

$$\begin{aligned}
l_L &\simeq \frac{-5.8\cdot 10^{-8}}{c_V\, m_D} \qquad l_R \simeq \frac{-1.6\cdot 10^{-8}}{c_V\, m_D} \qquad \{D^0 \to (\rho^0,\omega)\} \\
l_L &\simeq \frac{12.5\cdot 10^{-9}}{c_V\, m_D} \qquad l_R \simeq \frac{0.7\cdot 10^{-9}}{c_V\, m_D} \qquad \{D^+_{(d,s)} \to (\rho^+, K^{*+})\} \quad .
\end{aligned} \tag{4.24}$$

The corresponding estimates for branching ratios are:

$$\begin{aligned}
\mathcal{B}(D^0 \to (\rho^0,\omega)\gamma)|_{(4.22)} &\simeq 0.6\cdot 10^{-5} \\
2\mathcal{B}(D_s^+ \to K^{*+}\gamma) \simeq \mathcal{B}(D^+ \to \rho^+\gamma)|_{(4.22)} &\simeq 1.3\cdot 10^{-6} \quad .
\end{aligned} \tag{4.25}$$

It should be noted at this point that the processes in (4.18) are charged rather than neutral current processes and thus do not have a quark loop contribution since the spectator quark also changes flavour, and therefore would be strongly expected to be WA dominated, which enhances the credibility of the estimates (4.23) as the likely value of the WA amplitude.

To cross-check, the estimated branching fraction $\mathcal{B}(D^0 \to (\rho^0,\omega)\gamma)$ above is compared with

[5]Note that in [77] the colour structures of the operators $\mathcal{O}_{1,2}$ are switched in the effective Hamiltonian, and thus $C_{1,2}$ are switched in the formula for a_1.

the measured rate in $\mathcal{B}(D^0 \to \phi\gamma)_{\text{PDG}}$ (4.18) and it is noted that the former is down by about a factor of four. A factor of two comes from the ρ^0 and ω valence quark contents which imply $c_V^2 = 2$, in contrast to the ϕ for which $c_V^2 = 1$. Another factor 1.2 comes from phase space factors and the $m_V f_V$ prefactor in (4.16). The remaining discrepancy might be partly due to neglecting the strange quark mass; it might be questioned whether $2m_s$, which results from the axial current, is really so small a parameter. A quick order-of-magnitude estimate based on [70] would suggest that such corrections should be on the level of $(f_\phi^\perp/f_\phi)(2m_s/m_\phi) \sim 20\%$[6], which is certainly not negligible. It therefore seems that the estimate (4.25) is plausible and at present this will have to suffice, as it is far below the present experimental upper bound of $2.4 \cdot 10^{-4}$ [123].

Weak annihilation (WA) versus quark loops (QL)

Having estimated the size of the WA contribution, the size of quark loop matrix elements will be estimated next, the leading order contributions to which are illustrated in Figure 4.1. The distinguishing characteristic of the two types of contribution is that in WA the spectator quark also connects to the four-quark operator from $\mathcal{H}^{\text{eff}}$ and is thus a $c\bar{q} \to u\bar{q}$-type transition, whereas in quark loop-type contributions the additional quarks scatter into the final state photon and it is thus a $c \to u\bar{q}q$ transition. The WA contributions have been computed in 1995 for $B \to V\gamma$ and $D \to V\gamma$ in [151] and $B^0 \to (\rho^0, \omega)\gamma$ in [77, 78] at $\mathcal{O}(\alpha_s^0)$, and the QL contribution was computed in [151]. This QL calculation was performed in a $1/m_c$ expansion, whose convergence is rather questionable, but it is expected that it should give a reasonable estimate.

It is argued that the WA amplitude dominates that of QL:

1. *Generic argument:* QL and WA are generated by the same four-quark operator, $\mathcal{O}_{1,2}^{d,s}$ and $\mathcal{O}_{1,2}^{d}$ (4.8) respectively. The QL contribution has two more loops than the WA contribution since the middle diagram in Figure 4.1 is zero due to gauge invariance and thus only diagrams with an additional gluon contribute. From a general point of view it would therefore be expected that WA $\gg$ QL due to these suppressions[7].

2. *Test case in B physics:* The same line of reasoning can be applied to $B \to \rho$ decays to check its validity in that case, which is on a rather more secure theoretical footing. Taking numbers from [129] results in[8] $|\mathcal{A}_{QL}/\mathcal{A}_{WA}|_{B^- \to \rho^-\gamma} \simeq 2 \cdot 10^{-2}$. The QL contribution in this case is taken to come from the diagram where the gluon is radiated into the final-

[6] $m_s(2\,\text{GeV}) = 95\,\text{MeV}$ has been used, and RG running has been applied to 2 GeV of $f_\phi^\perp$ in table 3.2. The RG running itself accounts for a 5% shift. This estimate could easily be out by a factor of two were the calculation done fully since the hard scattering kernel will have an end-point singularity. However, the corresponding FSR terms will have a small strong phase and thus the basis of this argument is not spoiled.

[7] In principle there is a GIM suppression of the QL in addition, though this is not very effective for the matrix elements [151] owing to $m_s \gg m_{u,d}$.

[8] In case the reader is wondering, these numbers do not include CKM matrix coefficients, which lead to a Cabibbo suppression of WA in B physics.

state meson. The QL numbers are of comparable magnitude for both charm and light quarks. The reason that this comparison is done for the charged rather than the neutral channel is that WA in $B^0 \to \rho^0\gamma$ is accidentally small owing to cancellations between the current-current operators $\mathcal{O}_{1,2}$ and the penguin operators $\mathcal{O}_{3-6}$ [129]. Such cancellations cannot be expected in $D^0 \to \rho^0\gamma$ because the coefficients of penguin operators are tiny, as discussed in Section 4.1.1.

3. *The D physics case:* The question is then whether the hierarchy which is indeed present in B physics carries over to D physics. Taking the contribution of QL from [151] and the estimates of [77] for WA, it can be estimated that $|\mathcal{A}_{QL}/\mathcal{A}_{WA}| \simeq 2 \cdot 10^{-2}$, whose closeness to the B meson result is most likely accidental. From another point of view, any differences between the B and D physics cases would be expected to be suppressed by powers of the heavy-quark mass and thus the breakdown of the heavy-quark expansion may be estimated in the charm-quark case. In the heavy-quark limit it is expected that $\mathcal{A}_1 = \mathcal{A}_2$, i.e. $\mathcal{A}_R = 0$, and therefore the breakdown of the heavy-quark expansion can be estimated from the results in [77]. These results indicate that the $1/m_{b,c}$ expansion holds to the level of 70% and 57% in the B and D meson cases respectively, which does not indicate that the $1/m_c$ expansion exhibits sufficiently poor convergence to overcome the difference of two orders of magnitude that is estimated to separate the WA and QL amplitudes.

Thus analysis suggests that WA dominates QL by roughly two orders of magnitude. The opposing viewpoint should be mentioned: an alternative approach to calculating D meson decays has been to model the transitions with hadronic data [152]. In the long-distance contributions calculated there, WA diagrams correspond to pole contributions and QL contributions to the vector meson dominance (VMD) mechanism. In that paper, comparable numbers were found for the pole and VMD terms, which conflicts with the expectation based on the analysis above. There are, however, two deficiencies in this approach: first in the pole part $\mathcal{A}_R = 0$, which contradicts the sum rule calculation [77, 78]. Second, couplings in the VMD approach must be taken from experiment and therefore have unknown phase, and thus this approximation is not able to capture strong cancellations, which would appear to be likely in this case owing to the vanishing of the factorisable QL contribution due to gauge invariance. One of the authors of [152] has made a similar point in [153, 3.1.3].

Strong phases in weak annihilation

It has been argued that the QL contribution, which has a large strong phase, is small compared to WA; however, in order to complete the argument that the overall strong phase of the leading amplitude in $D \to V\gamma$ is small, the strong phase in WA must also be estimated.

At leading order $O(\alpha_s^0)$, the strong phase is zero. This is certainly the case, from the results

in [77, 78], when the light-quark mass is neglected; however, it should also hold for non-zero quark masses because the decay remains factorisable. Details of this factorisation are given in Section 5.3.2, and the argument that the strong phase is zero is essentially that the initial-state radiation matrix element $\langle\gamma|J^{\mu}_{V-A}|B\rangle$ will be far below threshold at the weak current vertex, and the final-state radiation matrix element $\langle\rho\gamma|J^{\mu}_{V-A}|0\rangle$ is well approximated by the light cone OPE, which gives no strong phase at leading order.

Unfortunately the relevant non-factorisable loop corrections to WA, which would contain the strong phase, have not been computed. The size of QCD corrections will therefore be studied in a generic way through the $\mathcal{O}_7$ operator. The corrections due to the chromomagnetic operator $\mathcal{O}_8$ can be viewed as radiative corrections to the leading decay terms and it may be inferred from table 3.5 that they are around the 15% level.

Final remarks

Aside from the question of the suitability of the heavy-quark expansion in D decays, there is also some question over whether the α_s perturbation series converges. In fact, this should not be a problem in $D \to V\gamma$ decays because the D meson mass $m_D = 1.86\,\text{GeV}$ and the photon "mass" $q^2 = 0$ are far from other perturbative and hadronic thresholds[9]. The vacuum polarisation plot, $R(s) \propto \sigma(e^+e^- \to \text{hadrons})$ [123, 154][10], indeed indicates that there are no significant thresholds in either region and in fact the closest threshold is the ω meson pole. Although the electromagnetic current relevant to that cross-section is certainly not the same as the weak current relevant to WA, it should be sufficiently closely related that the non-perturbative effects have similar magnitude. At m_D, the ratio of the leading order partonic cross-section to the measured hadronic cross-section indicates a 15% correction[11] and the three-loop perturbative QCD result is in-between the two. It therefore seems that the non-perturbative corrections in this region should not be expected to be very large.

In view of the discussion above, 25% will be taken as a conservative estimate of the size of radiative corrections. If it is assumed that the real and imaginary part have similar magnitude then the strong phase of WA is taken to be 10°, that is $|\delta_L| \simeq |\delta_R| \simeq 10°$ in (4.15). Of course, a computation of the non-factorisable radiative correction would be preferable to this sort of estimate. In particular, the sign of the strong phase of such a correction is significant, since RG running will mix a beyond-SM correction to C_8^{eff} into C_7^{eff}, and thus the sign of the phase of radiative corrections will determine whether the resulting CP asymmetries cancel or augment each other. This will be discussed in Section 4.3.

[9] The next charmed $J = 0$ meson candidiate listed in PDG [123] is at 2.4 GeV.
[10] Chapter 46, under "Plots of cross sections and related quantities" on pdgLive [123].
[11] $R(s) \approx 2$ at leading order for $m_s \ll \sqrt{s}/2 < m_c$, hadronic data is available from pdgLive [123] under "Data files and plots of cross-sections and related quantities".

4.2 CP violation scenario

A scenario will be proposed where a sizeable CP asymmetry is generated by a large CP-odd imaginary part in the C_8 WC, generated by beyond-SM physics. The amplitudes in (4.15) in this scenario are given by

$$\begin{aligned} l_{L(R)} &= |l_1 \pm l_2|, \quad \delta_{L,R} = \phi_{L,R} = 0 \\ g_{L(R)} e^{i\Delta_{L(R)}} &= \frac{G_F}{\sqrt{2}} \left(\frac{e m_c}{2\pi^2}\right) \frac{1}{c_V} |C_8^{(\prime)}| (2G_1(0)) \\ G_1(0) &= |G_1(0)| e^{i\Delta} \,, \quad C_8 = |C_8| e^{i\Phi_L}, \quad C_8' = |C_8'| e^{i\Phi_R} \,, \end{aligned} \tag{4.26}$$

with $l_{1,2}$ given by (4.23) and $\Delta \equiv \Delta_L = \Delta_R$. The amplitudes $G_1(0)$ and their phases are given in table 3.5; the leading twist result derived there has been used so that $G_1(0) = G_2(0)$, and thus that $\mathcal{O}_8$ and $\mathcal{O}_8'$ solely contribute to the left- and right-handed amplitudes respectively, and that the two have identical strong phases $\Delta_L = \Delta_R$.

Exploiting these simplifications and assuming that $|g_{L,R}| \ll |l_{L,R}|$, the CP asymmetry may be written (4.17) as

$$A_{\rm CP}[D^0 \to V\gamma] \approx \frac{-2}{l_L^2 + l_R^2} \left(g_L l_L \sin(\Delta - \delta_L) \sin(\Phi_L) + g_R l_R \sin(\Delta - \delta_R) \sin(\Phi_R)\right) \quad . \tag{4.27}$$

Since the leading order strong phases $\delta_{L,R}$ are presently unknown, as discussed earlier, they are set to zero, and then the formulae in (4.26) may be used to write a more explicit formula for this scenario:

$$A_{\rm CP}[D^0 \to V\gamma] = \frac{-4}{l_L^2 + l_R^2} \frac{G_F}{\sqrt{2}} \left(\frac{e m_c}{2\pi^2}\right) \frac{\mathrm{Im}[G_1(0)]}{c_V} \left(l_L \,\mathrm{Im}[C_8] + l_R \,\mathrm{Im}[C_8']\right) \quad . \tag{4.28}$$

Numerically, with $m_c = 1.3$GeV and plugging (4.23), (4.5) and the values in table 3.5 into (4.28) the CP asymmetry in the neutral transition may be estimated as

$$\begin{aligned} A_{\rm CP}(D^0 \to (\rho^0, \omega)\gamma) &= \left(-3.84 \mathrm{Im}[C_8^{NP}] - 1.04 \mathrm{Im}[C_8'^{NP}]\right) c_{\mathcal{B}} \\ &= \left(-1.5\% \left(\frac{\mathrm{Im}[C_8^{NP}]}{0.4 \cdot 10^{-2}}\right) - 0.4\% \left(\frac{\mathrm{Im}[C_8'^{NP}]}{0.4 \cdot 10^{-2}}\right)\right) c_{\mathcal{B}} \quad , \end{aligned} \tag{4.29}$$

with an estimated uncertainty of about 45%, which will be discussed below, and where

$$c_{\mathcal{B}} \equiv \left(\frac{0.6 \times 10^{-5}}{\mathcal{B}(D^0 \to (\rho^0, \omega)\gamma)}\right)^{1/2} \tag{4.30}$$

is included so that the branching fraction $\mathcal{B}(D^0 \to (\rho^0, \omega)\gamma)$ may be easily updated when measurements or improved theoretical determinations become available. In going from (4.28) to (4.29) the fact that the imaginary part of $C_8^{\rm SM}$, which is suppressed by four powers of the

Cabibbo angle, is negligible with respect to the value (4.5), has been used.

In the charged case the result is

$$\begin{aligned} A_{\mathrm{CP}}(D^+_{(d,s)} \to (\rho^+, K^{*+})\gamma) &= \left(9.71\mathrm{Im}[C_8^{NP}] + 0.60\mathrm{Im}[C_8'^{NP}]\right) c_{\mathcal{B}} \\ &= \left(3.9\% \left(\frac{\mathrm{Im}[C_8^{NP}]}{0.4 \cdot 10^{-2}}\right) + 0.2\% \left(\frac{\mathrm{Im}[C_8'^{NP}]}{0.4 \cdot 10^{-2}}\right)\right) c_{\mathcal{B}} \,, \end{aligned} \tag{4.31}$$

again with an estimated uncertainty of 45%. The dominance of the $\mathcal{O}_8$ contribution over the $\mathcal{O}_8'$ contribution in both cases is a remnant of heavy-quark symmetry, which indicates that l_R is $1/m_c$ suppressed w.r.t. l_L. In this particular case, a sizeable difference between l_R/l_L in the charged and neutral decays could in principle allow extraction of $\mathrm{Im}\, C_8$ and $\mathrm{Im}\, C_8'$ separately, given sufficient experimental sensitivity.

The significant sources of uncertainty in this calculation are listed below:

- The largest source of uncertainty is in the calculation of $\mathcal{O}_8$ matrix elements, which are estimated to have an error of around 35%; see table 3.5.
- The strong phase of the leading WA contribution $\delta_{L,R}$ was estimated to be on the order of 10° in Section 4.1.2, which leads to a 20% uncertainty.
- The magnitude $l_L^2 + l_R^2$ is not assigned an uncertainty, because it is assumed that it is taken from experiment; however, the ratio l_L/l_R is not determined in this way and has therefore been inferred from the results of [77]. This procedure is assigned an uncertainty of 20%.

Combining these three sources of uncertainty in quadrature leads to an overall uncertainty estimate of 45%. There is no reason to expect that they would be correlated. Uncertainty due to CP violation from $\mathrm{Im}\, C_7$ has not been included, and will be discussed in the next section.

4.3 CP violation through $\mathrm{Im}\, C_7$

In [149], a sizeable value of $\mathrm{Im}\, C_7^{NP}$ was proposed as a possible source of CP violation in the charm system. This effect would however be distinct from the effect in the $D \to \pi\pi$ and $D \to KK$ systems, because it is α_{em} suppressed and therefore expected to be small in hadronic processes. Since the $\mathcal{O}_7$ operator emits the photon in a short-distance process with no strong phase, the strong phase difference necessary for observable CP violation must in this case come from the leading matrix element. According to the arguments of Section 4.1.2, this strong phase is in fact small, on the order of 10°. The ratio of the magnitude of CP violation from C_7 and C_8 can be estimated to be

$$\left|\frac{A_{CP}|_7}{A_{CP}|_8}\right| = \left|\frac{T_1(0)\sin\delta_L}{\mathrm{Im}\, G_1(0)} \times \frac{\mathrm{Im}\, C_7}{\mathrm{Im}\, C_8}\right| \lesssim 0.6 \times \left|\frac{\mathrm{Im}\, C_7}{\mathrm{Im}\, C_8}\right| \quad , \tag{4.32}$$

where values $G_1(0) \approx 0.2$ (4.12), $T_1(0) \approx 0.7$ [149] and $\delta_L \approx 10^\circ$ were used. It is therefore apparent that if $\mathrm{Im}\, C_7$ is comparable to $\mathrm{Im}\, C_8$, they may both give a similar contribution to the CP asymmetry, which could either stack or cancel. However, as explained in Section 4.1.2, the estimate $\delta_L \sim 10^\circ$ is expected to be conservative and thus (4.32) is also likely to be pessimistic. A substantial cancellation between the two cannot however be ruled out without proper calculation of δ_L.

In fact, the beyond-SM contributions from C_7 and C_8 are connected, since RG running mixes C_8 into C_7. As such it was proposed in [149] that this mixing would lead to CP violation in $D \to V\gamma$. As mentioned in the introduction, this calculation depends on a large strong phase in the leading decay amplitude which is expected to be absent according to this analysis, however the mixing of C_7 and C_8 along with (4.32) implies that the combination of these effects should be examined. This case will be illustrated by assuming that the scale of new physics $M_{NP} = 1\,\mathrm{TeV}$ and that only SM degrees of freedom exist below this scale. In that case, the resulting new physics contributions to the WCs at the charm scale [149, (6)-(9)] are

$$\begin{aligned} C_8^{\mathrm{NP}}(m_c) &\approx 0.42 C_8^{\mathrm{NP}}(1\mathrm{TeV}) \\ C_7^{\mathrm{NP}}(m_c) &\approx 0.37 C_7^{\mathrm{NP}}(1\mathrm{TeV}) - 0.26 C_8^{\mathrm{NP}}(1\mathrm{TeV}) \approx 0.37 C_7^{\mathrm{NP}}(1\mathrm{TeV}) - 0.62 C_8^{\mathrm{NP}}(m_c) \end{aligned} \tag{4.33}$$

and hence under the assumption that $C_7^{\mathrm{NP}}(1\,\mathrm{TeV}) \ll C_8^{NP}(1\,\mathrm{TeV})$, also used in [149], $\mathrm{Im}\, C_7(m_c) \approx -0.6\,\mathrm{Im}\, C_8(m_c)$ is obtained. Thus according to (4.32),

$$\left| \frac{A_{CP}|_7}{A_{CP}|_8} \right| \lesssim 0.4 \tag{4.34}$$

is expected under this scenario and hence it is still expected that the $\mathrm{Im}\, C_8$ contribution dominates. It should be noted, however, that if the scale of new physics is sufficiently high this situation could be reversed since $C_7^{\mathrm{NP}}(m_c) \to -8 C_8^{\mathrm{NP}}(m_c)$ as the new physics scale goes to infinity; though this limit is approached rather slowly, and in any case increasing the new physics scale substantially would most likely render the resulting CP asymmetry too small to detect.

4.4 Conclusion

In contrast to B meson decays, theoretical assessment of charm decays is made considerably more difficult by the comparative smallness of m_c and the corresponding increased hadronic uncertainties. Nonetheless the measured size of the CP asymmetry (4.1), should it stand up to future measurements, would seem to indicate the presence of beyond-SM physics due to the fact that it is suppressed by four powers of the Cabibbo angle, although a large enhancement from strong dynamics cannot be ruled out. Owing to the theoretical difficulties in calculating strong decays, the ideas of [149] have been followed.

The advantage of considering the chromomagnetic operator $\mathcal{O}_8$ over the electromagnetic operator $\mathcal{O}_7$ is twofold: first, $\mathcal{O}_8$ is expected to contribute significantly to hadronic as well as radiative decays and thus could potentially explain the current experimental discrepancy with SM expectations through [150]

$$\Delta A_{CP}|_{NF} \approx -1.8(\mathrm{Im}\, C_8 - \mathrm{Im}\, C_8')\sin\delta\,; \tag{4.35}$$

though this can only be taken as an estimate since $\sin\delta$ is unknown. Second, the $\mathcal{O}_8$ operator can provide both the weak and strong phase required to produce an observable CP asymmetry in contrast to $\mathcal{O}_7$, which requires the leading decay amplitude to have a large strong phase, which, as has been argued, it does not.

The prediction corresponding to (4.35) in the $D \to V\gamma$ channel is[12]:

$$\begin{aligned} A_{\mathrm{CP}}(D^0 \to (\rho^0,\omega)\gamma) &= \left(-1.5\% \left(\frac{\mathrm{Im}[C_8^{NP}]}{0.4\cdot 10^{-2}}\right) - 0.4\% \left(\frac{\mathrm{Im}[C_8'^{NP}]}{0.4\cdot 10^{-2}}\right)\right) c_{\mathcal{B}} \\ A_{\mathrm{CP}}(D^+_{(d,s)} \to (\rho^+,K^{*+})\gamma) &= \left(3.9\% \left(\frac{\mathrm{Im}[C_8^{NP}]}{0.4\cdot 10^{-2}}\right) + 0.2\% \left(\frac{\mathrm{Im}[C_8'^{NP}]}{0.4\cdot 10^{-2}}\right)\right) c_{\mathcal{B}} \quad , \end{aligned} \tag{4.36}$$

which has an interesting feature not present in the hadronic decay: because the final state contains two vector particles, it is sensitive to both the parity-conserving and parity-violating parts of the $\mathcal{O}_8^{(\prime)}$ operators and thus potentially the chirality structure of beyond-SM physics is experimentally accessible if the CP asymmetry in both the charged and neutral channel can be measured. This is also partially the result of the smallness of the charm-quark mass; the heavy-quark relation $l_R = O(1/m_{b,c})$ would otherwise be expected to strongly suppress the contribution of the $\mathcal{O}_8'$ operator.

The way forward from here seems rather difficult on both the experimental and theoretical fronts. From the theoretical standpoint, the prediction (4.36) would be vastly improved by a complete calculation of the $O(\alpha_s)$ corrections to WA, specifically the non-factorisable diagrams which are expected to give rise to the strong phase that would determine the contribution of $\mathrm{Im}\, C_7$ to the CP asymmetry. Judging by the calculation of the chromomagnetic form factor in Chapter 3, however, it can be expected that such a calculation using LCSR will be technically difficult since it will almost certainly require dealing with anomalous thresholds at two loops. Another strong motivation for calculation of the $O(\alpha_s)$ corrections is that it would give a much better indication of whether the argument that WA, rather than QL (q.v. Figure 4.1), is indeed the dominant amplitude in radiative D meson decays.

On the experimental side, further LHCb data in the $D \to \pi\pi$ and $D \to KK$ channels is of course desirable, and indeed as remarked in the introduction new data from LHCb [146] rather disappointingly shows no sign of an asymmetry. This is a sizeable shift from their prior result [22] and in comparison to the CDF result [135]; however, since it includes the data of the

[12] See (4.30) for the definition of $c_{\mathcal{B}}$.

earlier analysis, the present experimental situation appears to confirm the SM. An experimental measurement of the $D^0 \to \rho^0\gamma$ and $D^+ \to \rho^+\gamma$ rates would nonetheless be interesting, to see whether the sort of analysis performed in section 4.1.2 is correct and whether charm decays in this channel can be treated perturbatively, although since the estimate (4.25) is two orders of magnitude below the current experimental limits $\mathcal{B}(D^0 \to \rho^0\gamma) \leq 2.4 \times 10^{-4}$ [147], this will have to wait for an LHCb upgrade or future flavour-factory experiment.

Chapter 5

Isospin asymmetry in $B \to (K, K^*, \rho) l^+ l^-$

In this chapter I describe the calculation of the isospin asymmetry in semi-leptonic B decays, as published in [92].

5.1 Introduction

The isospin asymmetry in $B \to K^* l^+ l^-$ was for some time measured by experiment to be negative [155, 156], the opposite sign to the SM prediction. This has not been confirmed by new LHCb data [21], which agrees with the SM prediction; however a large negative deviation from zero, at the level of 4σ when integrated over q^2, appears in the new results for the isospin asymmetry in $B \to K l^+ l^-$, which according to theory is expected to be small. Isospin asymmetries in $B \to K^* \gamma$ and $B \to \rho \gamma$ decays have also been measured and it will be found that these agree with and deviate by 2σ from the SM prediction, respectively.

Since at present measured isospin asymmetries are only marginally in agreement with the SM, it is worthwhile to study the sensitivity of these asymmetries to beyond SM FCNC operators. A complete calculation of the influence of all of these operators will complement constraints from non-leptonic decays on all $\Delta F = 1$ operators. The goal of this calculation is then to compute the contribution of all suitable FCNC operators up to dimension 6 on the isospin asymmetries in all similar processes for which there are presently sufficient statistics, that is $B \to (K, K^*) l^+ l^-$ and $B \to (K^*, \rho) \gamma$ [21, 147], as well as the as-yet unobserved $B \to \rho l^+ l^-$. The extension to the closely related process $B \to \pi l^+ l^-$ is a straightforward matter of replacing certain input parameters but numerical results are not provided here since it appears that experimental data is some way off.

It turns out that isospin violating effects can be divided into two categories: ultraviolet (UV) isospin violation due to four quark operators in the effective Hamiltonian coupling differently to up- and down-type quarks, and infrared (IR) isospin violation which arises from photon emission

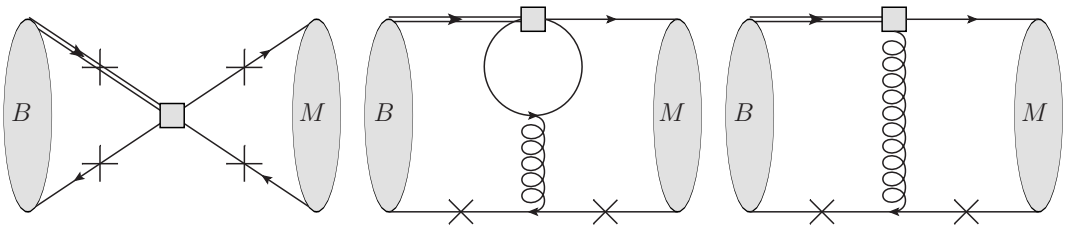

Figure 5.1: Processes contributing to isospin violation in semi-leptonic B decays. The left-hand diagram indicates a weak annihilation (WA) process, the middle diagram a quark loop spectator scattering (QLSS) process and the right-hand diagram indicates isospin violation arising from the chromomagnetic operator $\mathcal{O}_8$. Crosses indicate possible isospin violating photon emission points. Note that in WA emission from the heavy quark line can also violate isospin symmetry, since the four quark operator may couple differently to different flavours of spectator quark.

from the spectator quark since the strength of the electromagnetic interaction depends on the quark flavour. The classes of isospin violating process are included: weak annihilation (WA), quark loop spectator scattering (QLSS) and the $\mathcal{O}_8$ contribution, as shown in Figure 5.1. UV isospin violation only occurs in WA-type diagrams since the four quark operator must connect to the spectator quark line in that case. Isospin violating effects due to differences in the light quark masses and decay constants are below 1% and therefore neglected. Such effects however complicate the calculation of analogous flavour $SU(3)$ asymmetries such as $B_s \to \phi$ vs. $B \to K^*$ since the hadronic differences between B_s and B_0 are too large to be ignored. Although sum rule or lattice calculations of the ratios of meson decay constants could be used, these would have to be very accurate in order to result in useful constraints on Wilson coefficients in the effective Hamiltonian being obtained.

Various aspects of the isospin asymmetry in $B \to (K, K^*)l^+l^-$ decay have been calculated previously. The closely related decay $B \to V\gamma$ has been computed using QCDF in [84] and using a mixture of QCDF and LCSR in [129]. A computation of the isospin asymmetry $B \to K^*\gamma$ in the minimal supersymmetric SM has been reported in [157]. $B \to (K, K^*)l^+l^-$ was computed using QCDF in [51], and a mixed approach was recently employed for $B \to Kl^+l^-$ in [134]. This calculation improves on these works by including the complete basis of dimension six operators for WA and QLSS, the $\mathcal{O}_8$ calculation described in Chapter 3, and the complete set of twist-3 terms for WA. It is therefore a straightforward matter to calculate the isospin asymmetry in a arbitrary model once the Wilson coefficients are known, or conversely to identify which operators may be responsible for any observed deviation, if found, although given the large number of possible operators detailed knowledge of the q^2 spectrum would be necessary to constrain specific operators outside the context of a model.

5.2 Definitions and outline of the calculation

The definition of the effective $b \to s l^+ l^-$ Hamiltonian in the SM is given in Section 2.4 and the decomposition of the $B \to V l^+ l^-$ matrix elements are given in Section 2.9. The extensions of the four quark operator basis will be described in the sections 5.3.1, 5.4.1 and 5.6.1. The isospin asymmetry itself is defined as

$$a_I^{\bar{0}-}(q^2) \equiv \frac{dA_I^{\bar{0}-}}{dq^2} \equiv \frac{c_M^2 d\Gamma[\overline{B}^0 \to \overline{M}^0 l^+ l^-]/dq^2 - d\Gamma[B^- \to M^- l^+ l^-]/dq^2}{c_M^2 d\Gamma[\overline{B}^0 \to \overline{M}^0 l^+ l^-]/dq^2 + d\Gamma[B^- \to M^- l^+ l^-]/dq^2} \tag{5.1}$$

$$\bar{a}_I(q^2) \equiv \frac{1}{2}\left(a_I^{\bar{0}-}(q^2) + a_I^{0+}(q^2)\right) \quad , \tag{5.2}$$

where M stands for a vector or pseudoscalar meson and the second equation defines the CP averaged isospin asymmetry. The experimental definition is of course usually written in terms of the branching fraction and B meson lifetimes. The isospin asymmetry in $B \to V\gamma$ is defined analogously. For the K^* the CP asymmetry is small and thus the result of taking the CP average is primarily improved experimental statistics; however for the K this is essential since in the neutral case it is the K_S^0 which is a CP-eigenstate superposition of the two strangeness eigenstates $|\bar{d}s\rangle$ and $|\bar{s}d\rangle$. By contrast the CP-asymmetry in $B \to \rho$ is sizeable, and this case is discussed in 5.6. The coefficient c_M accounts for cases where the valence quark content of the final state meson does not correspond exactly to the quark pair produced by the short distance decay. This is the case for the neutral ρ meson since $\rho^0 \sim (\bar{u}u - \bar{d}d)/\sqrt{2}$ and thus $c_\rho = \sqrt{2}$, but the remaining cases are simple $c_K = c_{K^*} = 1$. Weak annihilation diagrams can also couple to the $\bar{u}u$ component of the ρ^0 final state however constant the c_ρ is selected with respect to the leading term in the decay arising from $\mathcal{O}_{7,9,10}$ which cannot.

As in previous studies [51, 84], it will be assumed that the isospin asymmetry is small and thus a linear approximation to (5.2) may be used. The leading isospin symmetric term is assumed to arise from the operators $\mathcal{O}_{7,9,10}$ (or rather their effective counterparts). With these approximations, the isospin asymmetry may be written

$$\begin{aligned}
\frac{dA_I^{\bar{0}-}}{dq^2}[B \to K^* l^+ l^-] &= \frac{\sum_i \mathrm{Re}\left[\mathcal{T}_i^{V,0}(q^2)\Delta_i^{d-u}(q^2)\right]}{\sum_i \left[|\mathcal{T}_i^{V,0}(q^2)|^2 + \left|\mathcal{T}_i^{A}(q^2)\right|^2\right]} + O([\Delta_i^{d-u}(q^2)]^2) \\
\frac{dA_I^{\bar{0}-}}{dq^2}[B \to K l^+ l^-] &= \frac{\mathrm{Re}\left[\mathcal{T}_T^{V,0}(q^2)\Delta_T^{d-u}(q^2)\right]}{|\mathcal{T}_T^{V,0}(q^2)|^2 + \left|\mathcal{T}_T^{A}(q^2)\right|^2} + O([\Delta_T^{d-u}(q^2)]^2) \\
a_I^{\bar{0}-}[B \to K^* \gamma] &= \frac{\sum_i \mathrm{Re}\left[\mathcal{T}_i^{V,0}(0)\Delta_i^{d-u}(0)\right]}{\sum_i \left[|\mathcal{T}_i^{V,0}(0)|^2 + \left|\mathcal{T}_i^{A}(0)\right|^2\right]} + O([\Delta_i^{d-u}(0)]^2) \quad ,
\end{aligned} \tag{5.3}$$

where the functions $\mathcal{T}_i^{(V,A)}$ are coefficients of different tensor structures arising in $B \to M l^+ l^-$ decays and are described in Section 2.9. The sums over i may be taken in either the $\{0, +, -\}$

or $\{0, V, A\}$ basis as described there; the only relevant property of these functions here is that the total $B \to V l^+ l^-$ decay rate is proportional to $\sum_{i\in\{0,+,-\}} \sum_{j\in V,A} |\mathcal{T}_i^j(q^2)|^2$. The functions $\mathcal{T}_i^{V,0}$ include only the leading isospin symmetric terms in the decay, namely

$$\begin{aligned} \mathcal{T}_i^{V,0} &= C_9^{\text{eff}}(q^2) H_i(q^2) + C_7^{\text{eff}} T_i(q^2) \\ \mathcal{T}_T^{V,0} &= C_9^{\text{eff}}(q^2) h_T(q^2) + C_7^{\text{eff}} f_T(q^2) \quad , \end{aligned} \tag{5.4}$$

and with this definition the matrix elements for the full decay rate (2.70) are split up as

$$\mathcal{T}_i^V(q^2) = \mathcal{T}_i^{V,0}(q^2) + \mathcal{T}_i^{V,q}(q^2) \qquad \mathcal{T}_i^{V,q}(q^2) = C_8^{\text{eff}} G_i^q(q^2) + W_i^q(q^2) + S_i^q(q^2) \tag{5.5}$$

and the isospin asymmetric part is given by

$$\Delta_i^{d-u}(q^2) = \mathcal{T}_i^{V,d}(q^2) - \mathcal{T}_i^{V,u}(q^2) \quad . \tag{5.6}$$

The functions G_i are the chromomagnetic matrix element described in Chapter 3 and the functions W_i and S_i give the WA and QLSS contributions and will be calculated in sections 5.3 and 5.4 respectively.

As mentioned in the introduction isospin violation owing to quark mass differences and differences in meson decay constants is neglected, which manifests itself here as the assumption that the leading terms $\mathcal{T}_i^0$ are equal in both the charged and neutral decays. The pseudoscalar decay constants differ by roughly 0.5% between the neutral and charged case [158] and thus will turn out to be negligible as compared to the overall uncertainty in this calculation. The mass splitting between the neutral and charged K is somewhat larger at around 1% [123], which occurs because the kaon mass is connected to chiral symmetry breaking[1]. This will not lead to a large isospin asymmetry since both are still very light in comparison to the B meson and the phase space difference between the two would be expected to be on the order of[2] $(m_{K^0}^2 - m_{K^+}^2)/m_B^2 \sim 10^{-4}$, and in any case light meson mass effects shall be neglected entirely in this calculation. The mass splitting between the charged and neutral B mesons is small, $m_{B^0} - m_{B^+} = 0.32(6)\,\text{MeV}$, and this is completely negligible in comparison with every other scale in the problem which are at their smallest on the order of $\Lambda_{\text{QCD}} \sim 300\,\text{MeV}$. It is therefore safe to say that isospin violation arising through quark masses and QCD effects are negligible in comparison to isospin violation from the processes depicted in Figure 5.1, which are to be calculated.

[1] The mass splitting can therefore be estimated from the Gell-Mann–Oakes–Renner relation [102] as $m_{K^0}^2 - m_{K^+}^2 \sim (m_d - m_u)\langle\bar{q}q\rangle / f_K^2$.

[2] It might appear from (2.81) that it should scale linearly rather than quadratically, i.e. as $(m_{K^0} - m_{K^+})/m_B$, however the factor $m_B + m_K$ appearing in that formula is merely due to the standard definition of P_T in (2.62) and is not actually reflected in the rate.

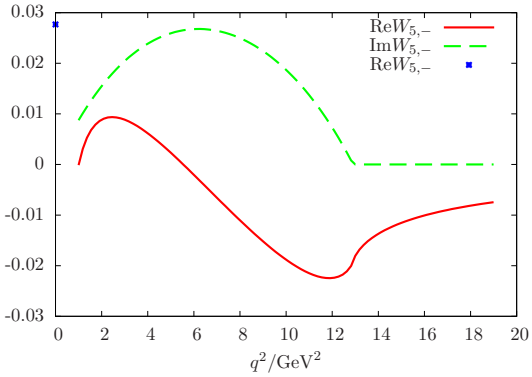

Figure 5.2: Example of a weak annihilation form factor result, specifically contribution of O_5^{WA} and O_6^{WA} to $B \to K^* l^+ l^-$. The definition of the $W^q_{j,\iota}$ is given in (5.18). The region $0\,\mathrm{GeV}^2 < q^2 < 1\,\mathrm{GeV}^2$ is excluded owing to the presence of strong resonances here; note particularly that the point at $q^2 = 0$ (blue dot) does not appear to connect smoothly to the real part (solid red line). The point at $q^2 = 0$ must be calculated using a different method because of this, as described in Section 5.3.6.

5.3 Weak annihilation (WA)

The WA process $B^- \to W^- \to K^{(*)-}$ is described by the "tree-level" operators $\mathcal{O}_{1,2}$ in a process as shown in Figure 5.1 (left). By extension, the same name is also given to diagrams with the same arrangement of quark lines involving $\mathcal{O}_{3-6}$, though they arise from renormalisation group evolution and short distance penguin diagrams.

The WA contribution to $B \to \rho\gamma$ has already been computed in the SM using LCSR in [77, 78]. This contribution was also calculated using QCDF in [120]. This is in principle equivalent to $B \to K^* l^+ l^-$ in the $q^2 = 0$ limit, although, as will be explained in Section 5.3.6, OPE terms must be handled differently in these two cases. The WA contribution to $B \to K^* l^+ l^-$ for general q^2 has been calculated using QCDF in [42, 51]. This calculation extends previous work by using LCSR to calculate WA at general q^2, including all possible dimension 6 four-quark FCNC operators and computing twist-3 corrections from $h_\parallel$ terms in the K^* DA, which contribute to the longitudinal polarisation and were neglected in [42, 51].

As is typical for B meson decays, the range of the validity of the computation is restricted by the presence of resonances, both in the partonic and hadronic pictures. In the case of weak annihilation it is particularly the light ρ and ω resonances which are problematic, so the results of this calculation are not valid in the $0\,\mathrm{GeV}^2 < q^2 < 1\,\mathrm{GeV}^2$ region. This problem manifests as a divergence as $q^2 \to 0$ owing to the $\langle\bar{q}q\rangle$ condensate term. The O_5^{WA} form factor is plotted in 5.2 to illustrate the issue. Note that in this plot charm resonances which would be expected in the $q^2 \sim m^2_{J/\Psi}$ region are absent, owing to the fact that they occur as an order α_s correction to WA. However, the results for the isospin asymmetry remain invalid in this region because other contributions, particularly the C_9^{eff} contribution, are still strongly affected.

5.3.1 Complete WA basis of dimension 6 operators at $O(\alpha_s^0)$

All dimension 6 four-quark operators $\bar{q}\Gamma_1 b\,\bar{s}\Gamma_2 q$ that potentially contribute at $O(\alpha_s^0)$ are included:

$$\begin{aligned}
&O_1^{\mathrm{WA}} \equiv \bar{q}b\,\bar{s}q \qquad && O_2^{\mathrm{WA}} \equiv \bar{q}\gamma_5 b\,\bar{s}q \qquad && O_3^{\mathrm{WA}} \equiv \bar{q}b\,\bar{s}\gamma_5 q \qquad && O_4^{\mathrm{WA}} \equiv \bar{q}\gamma_5 b\,\bar{s}\gamma_5 q \\
&O_5^{\mathrm{WA}} \equiv \bar{q}\gamma_\mu b\,\bar{s}\gamma^\mu q \qquad && O_6^{\mathrm{WA}} \equiv \bar{q}\gamma_\mu\gamma_5 b\,\bar{s}\gamma^\mu q \qquad && O_7^{\mathrm{WA}} \equiv \bar{q}\gamma_\mu b\,\bar{s}\gamma^\mu\gamma_5 q \qquad && O_8^{\mathrm{WA}} \equiv \bar{q}\gamma_\mu\gamma_5 b\,\bar{s}\gamma^\mu\gamma_5 q \\
& && O_9^{\mathrm{WA}} \equiv \bar{q}\sigma_{\mu\nu} b\,\bar{s}\sigma^{\mu\nu} q \qquad && O_{10}^{\mathrm{WA}} \equiv \bar{q}\sigma_{\mu\nu}\gamma_5 b\,\bar{s}\sigma^{\mu\nu} q \qquad ,
\end{aligned} \tag{5.7}$$

parametrised by the effective Hamiltonian:

$$\mathcal{H}^{\mathrm{WA,q}} = -\frac{G_F}{\sqrt{2}}\lambda_t \sum_{i=1}^{10} a_i^q O_i^{\mathrm{WA}} \quad , \tag{5.8}$$

where the q superscript has been suppressed on the operators O_i^{WA}. The operator basis has been organised in terms of scalar and pseudoscalar, vector and axial and tensor currents. Although this is not the optimal fit for weak decays in the SM that have $V-A$ structure, it makes the linear combinations which actually contribute to decays transparent, since the external B, K and K^* mesons are states of definite parity. At higher orders in α_s the size of this basis doubles, since colour octet operators which cannot contribute to factorised decays also appear. In fact, the ρ meson can couple to these octet operators at leading order $O(\alpha_s^0)$ owing to the presence of multiple external d-type quarks in $B^0 \to \rho^0$ decays, which can therefore couple to alternative Fierz arrangements of four-quark operators. The extended effective Hamiltonian required in this case is defined in 5.6.1.

WA coefficients in the SM

In the SM the operators (5.7) obey minimal flavour violation (MFV) [159–163] and furthermore may be expressed in the form $\bar{q}\Gamma P_L b\,\bar{s}P_R\Gamma q$ (2.19). Since WA fixes the quark flavours and couples to just a single colour structure, only two independent combinations of SM WCs appear in each $B \to Mll$ process, which correspond to the scalar-scalar and vector-vector[3] Dirac four quark structures. For a $bq \to sq$ process, with $q = u, d$, the couplings are given by

$$\begin{aligned}
a_1^q &= -a_2^q = a_3^q = -a_4^q = -2\left(\frac{C_5}{N_c} + C_6\right) \\
a_5^q &= -a_6^q = -a_7^q = a_8^q = \left(\frac{C_3}{N_c} + C_4\right) - \delta_{qu}\frac{\lambda_u}{\lambda_t}\left(\frac{C_1}{N_c} + C_2\right) \\
a_9^q &= a_{10}^q = 0 \quad ,
\end{aligned} \tag{5.9}$$

[3] With appropriate left- and right-handed projectors.

where $N_c = 3$ is the number of colours as usual. The vector current couplings a_{5-8} are different for u and d spectator quarks, which follows from the fact that $O_{1,2}$ (2.19) only couple to up-type quarks as a result of the absence of tree-level FCNCs in the SM. As described earlier, the splitting of WCs for different spectator quarks is referred to as UV isospin violation and in this case radiation from all four external quarks (see Figure 5.1, left) contributes to the isospin asymmetry. In $B \to K^{(*)}$ decays the contribution of $\mathcal{O}_{1,2}$ and thus UV isospin violation is suppressed owing to the smallness of λ_u/λ_t. The situation for $B \to \rho$ decays is somewhat more complicated, however, for the CP-averaged case the suppression from $|\cos\alpha_{\text{CKM}}| \ll 1$ plays the same role and the penguin operators $\mathcal{O}_{3-6}$ still dominate the isospin asymmetry. The ρ meson situation will be discussed in more detail in Section 5.6, and the exceptional value of $\cos\alpha_{\text{CKM}}$ will be exploited in Section 5.7.

It must be understood that formulae such as (5.9) are strictly applicable at leading order in α_s. In the present calculation this is all that is required since loop corrections to the WA contribution are not computed; however at higher orders the coefficients will be dependent on the renormalisation scheme, including evanescent operators, e.g. [164]. Both SM and beyond-SM operators would then have to be matched onto this higher order basis, which itself would be a somewhat involved calculation. This may well be unnecessary however: since at this point it must be expected that violations of the SM are small, the most sensible approach to improving the present work would be to complete a higher order calculation of the SM isospin asymmetry to reduce the SM uncertainties. Contributions from beyond SM physics can then be added using leading order results in the generic four-quark basis computed here, since they will be suppressed by new small parameters and thus loop corrections to beyond-SM effects are unlikely to be significant.

5.3.2 Factorisation of WA at leading order $O(\alpha_s^0)$

The WA matrix element with uncontracted photon polarisation tensor $\epsilon(q)_\rho$ reads

$$\begin{aligned}\mathcal{A}^{*\rho}|_{\text{WA}} &= \langle X\gamma^*(\rho)|\bar{q}\Gamma_1 b\,\bar{s}\Gamma_2 q|B\rangle|_{\text{WA}} \\ &= \underbrace{\langle X|\bar{s}\Gamma_2 q|0\rangle\langle\gamma^*(\rho)|\bar{q}\Gamma_1 b|B\rangle}_{\text{initial state radiation (ISR)}} + \underbrace{\langle X\gamma^*(\rho)|\bar{s}\Gamma_2 q|0\rangle\langle 0|\bar{q}\Gamma_1 b|B\rangle}_{\text{final state radiation (FSR)}} + O(\alpha_s) \quad .\end{aligned} \tag{5.10}$$

The two matrix elements shall be referred to as initial state radiation (ISR) and final state radiation (FSR) respectively, as labelled in the equation. ISR terms will be calculated using sum rules as described in Section 2.8. FSR terms will be calculated using the light cone OPE. The Feynman diagrams which were computed are shown in Figure 5.3, although as will be explained below LCSR is only used to approximate the B meson state where necessary. Only one of the two techniques is required in each case because the matrix element which does not emit the photon can always be written in terms of a simple hadronic quantity, i.e. f_B, f_{K^*} or

		Twist	Operator O_n^{WA}									
			1	2	3	4	5	6	7	8	9	10
$B \to K$	Factorisable		✗	✗	✗		✗	✗	✗		✗	✗
	χ-even (ϕ_K)	2								$\mathrm{I,F_c}$		
	χ-odd ($\phi_{P,\sigma}$)	3				I,F						
	Lorentz invariance		✓	✗	✗	✓	✓	✗	✗	✓	✓	✗
$B \to K^*$	Factorisable		✗		✗				✗	✗		
	χ-even ($\phi_\parallel$)	2					I	$\mathrm{I,F_c}$				
	χ-even ($g_\perp^{(v)}, g_\perp^{(a)}$)	3					I	$\mathrm{I,F_c}$				
	χ-odd ($\phi_\perp$)	2		F		F					I	I
	χ-odd ($h_\parallel^{(t)}, h_\parallel^{(s)}$)	3		F								I
	Lorentz invariance		✓	✓	✓	✓	✓	✓	✓	✓	✓	✓

Table 5.1: Operators contributing to WA and which DAs couple to each. The rows marked "Lorentz invariance" indicate which operators are coupled to at all orders in α_s. "Factorisable" indicates which can be coupled to at leading order in α_s, which is considerably more restrictive owing to the fact that the decay can be factored into two separate matrix elements that must obey Lorentz invariance separately. χ-even and χ-odd stand for even and odd chirality, which indicate an odd and even number of gamma matrices respectively. The remaining rows indicate which components of the vector and pseudoscalar meson DAs couple to each operator at leading order α_s^0. This implies that the decays may be factorised, and in these rows I indicates initial state and F final state radiation. F_c indicates that the final state radiation is purely a contact term which can be set to zero in a certain choice of gauge. These terms are therefore accurate to all orders in twist. Note that as far as the twist assignments in this table are concerned, $h_\parallel$ and $g_\perp$ are related to other components of the K^* DA by Wandzura-Wilczek relations [70]. At the present level of approximation where light quark masses and three-particle DAs are neglected this means that $h_\parallel$ and $g_\perp$ may be written in terms of $\phi_\perp$ and $\phi_\parallel$ respectively, and thus the twist-2 and twist-3 contributions are not separately gauge invariant at the $O(m_V)$ level, although the $O(m_V^0)$ part of the twist-2 contribution is gauge invariant.

$f_{K^*}^{\perp}$. Results of this type of calculation are valid away from partonic and hadronic thresholds, which in this case means that the ρ, ω and J/ψ resonance regions must be excluded. The results which will be presented are valid for the range $1\,\mathrm{GeV} < q^2 < 8\,\mathrm{GeV}^2$, although it should be stressed that $8\,\mathrm{GeV}^2$ is just above the perturbative charm pair threshold $\sim 7.8\,\mathrm{GeV}^2$ and thus these results may not be accurate at the very upper end of this range. Results for $B \to V\gamma$ are also included, which are the $q^2 = 0$ limit of the $W_i(q^2)$ functions. In this case the contribution of hadronic ρ and ω resonances is included through the photon DA [77,78,165]. For $q^2 > 1, \mathrm{GeV}^2$, these contributions are replaced by the $\langle \bar{q}q \rangle$ condensate.

5.3.3 Selection rules

As it turns out, the fact that WA matrix elements are factorisable at $O(\alpha_s^0)$ as in (5.10) leads to highly restrictive selection rules on the four quark operators, because parity and Lorentz invariance considerations apply separately to the ISR and FSR terms. These rules are depicted in table 5.1.

However, there is one selection rule which is not dependent on factorisability. For the K meson there is a parity selection rule. Since the K is a pseudoscalar, helicity conservation implies that the final state photon polarisation is longitudinal and thus no final state of even parity can be constructed. Since the B meson also has odd parity, the decay can therefore only be induced by parity conserving operators. To put it another way, only three 4-vectors enter in the final state, and thus it is not possible to create a scalar through use of the Levi–Civita tensor. Since the total number of γ_5 matrices and Levi–Civita tensors appearing in any given term must be even, it follows that the absence of Levi–Civita tensors in the result implies that an even number of γ_5 matrices must appear in the calculation; one from the B meson and one from the K. This immediately eliminates half of the operators in table 5.1, as indicated in the "Lorentz invariance" row of the $B \to K$ transition.

The additional constraints imposed by factorisation, or equivalently truncating at $O(\alpha_s^0)$, occur in two ways. The first, for the scalar- and vector-like current operators $O_{1\ldots8}^{\mathrm{WA}}$ arises in the factored matrix element that does not emit the photon. The second, for the tensor operators $O_{9,10}^{\mathrm{WA}}$, arises due to Lorentz invariance in the final state matrix element.

The $O_{1\ldots8}^{\mathrm{WA}}$ case is a simple parity constraint: neither the K^* or B meson can couple to a vector or scalar current of opposite parity to the particle since three or four vectors are required to construct a Lorentz scalar or vector with opposite parity in four dimensions, and the B and K^* have only one and two respectively. This means that only half of the operators $O_{1\ldots8}^{\mathrm{WA}}$ are coupled to. Note that in the case of the K this rule applies in addition to the global parity selection rule, so in that case only two of the eight operators enter factorisable terms.

The case of the tensor operators $O_{9,10}^{\mathrm{WA}}$ is somewhat different owing to the identity $\epsilon^{\mu\nu\rho\sigma}\sigma_{\rho\sigma} = 2i\sigma^{\mu\nu}\gamma_5$, which means that the presence of one tensor operator parity implies presence of the

	$C_8^{(\prime)}$	WA	Eq.(5.7)	QLSS	Eq.(5.28)	total
K^*	2[1]	12[3]	$a^q_{2,4,5,6,9,10}$	10[3]	all no i=2,f=SU(3)	24[7]
K	1[1]	4[3]	$a^q_{4,8}$	5[3]	idem no $\chi = A$	10[7]

Table 5.2: Summary of operators contributing to isospin in $B \to K^{(*)}ll$. The number of operators that are present in the SM for the respective channel is denoted in square brackets. The QLSS counting in the SM is the number of linearly independent contributions which depends on the number of quark flavours of different mass running in the loop, which in the present approximation is 3. Each of these linear combinations is independent of the coefficients for WA in the SM, so the total number of operators in the final column is simply the sum.

other, subject to global parity considerations. In this case factorisation restricts the K final state from coupling to tensor operators at all since a pseudoscalar meson cannot couple to a local tensor current operator by Lorentz invariance, so whichever factorised matrix element the photon does not couple to is necessarily zero. The K^* however does couple to local tensor currents, so the ISR term is non-zero, even in the case of a longitudinally polarised meson, although that is suppressed by powers of m_{K^*} as described below (5.12).

Combining these selection rules means that the K couples to $8/2/2 + 0 = 2$ four quark operators at this level of approximation, and the K^* couples to $8/2 + 2 = 6$. The situation is depicted in table 5.2, along with the number of operators required for the QLSS and $\mathcal{O}_8$ contributions. The basis for the QLSS contribution is provided later in (5.28), however the only applicable selection rule is the global parity constraint for the K.

The stringent selection rules in the factorisation approximation have important implications when considering which terms in the K and K^* DAs must be included. As can be seen from table 5.1, the O_4^{WA} operator only appears at next-to-leading twist for the K, and similarly the $O_{2,10}^{\mathrm{WA}}$ operators only appear at next-to-leading twist for longitudinally polarised K^* mesons, which are potentially significant in the intermediate q^2 regime where the contribution of longitudinal polarisation is not overwhelmed by the photon pole. This is particularly important for the $O_{2,4}^{\mathrm{WA}}$ operators because these dominate the isospin asymmetry, as will be discussed later, owing to their large Wilson coefficients.

5.3.4 Computation of WA leading order $O(\alpha_s^0)$

The calculation of these matrix elements in (5.10) is somewhat varied, since in almost all cases there are tricks to simplify the process. The very simplest matrix elements appearing in (5.10) are those which do not emit a photon. These are given by

$$\begin{aligned}
\langle 0|\bar{q}\gamma_5 b|B(p_B)\rangle &= -i\frac{f_B m_B^2}{m_b} & \langle 0|\bar{q}\gamma^\mu\gamma_5 b|B(p_B)\rangle &= i f_B p_B^\mu \\
\langle K^*(p,\eta)|\bar{s}\gamma^\mu q|0\rangle &= f_{K^*} m_{K^*}\eta^\mu & \langle K^*(p,\eta)|\bar{s}\sigma^{\mu\nu} q|0\rangle &= i f_{K^*}^\perp(p^\mu\eta^\nu - \eta^\mu p^\nu) \\
\langle K(p)|\bar{s}\gamma_5 q|0\rangle &= -i\mu_K^2 & \langle K(p)|\bar{s}\gamma^\mu\gamma_5 q|0\rangle &= -i f_K p^\mu \quad ,
\end{aligned} \tag{5.11}$$

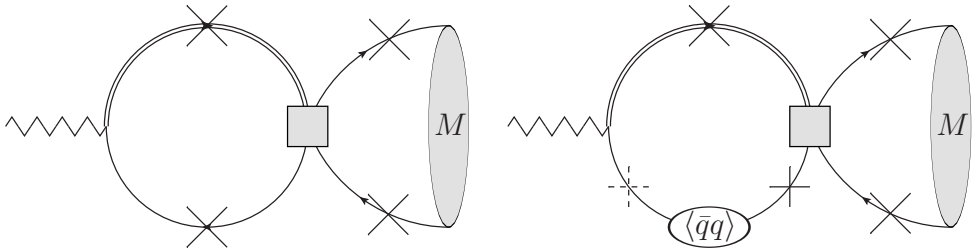

(a) Perturbative photon contributions. (b) OPE quark condensate contribution.

Figure 5.3: Weak annihilation Feynman diagrams for $B \to Ml^+l^-$. The zigzag line is the B-meson current insertion. Crosses mark possible photon insertions, although the contribution from the insertion at the dashed cross is zero.

where $\mu_K^2 = f_K m_K^2/(m_s + m_q)$. All other couplings to local two-particle currents are zero by either angular momentum or parity conservation. In the case of the light mesons these formulae can be recovered from the DAs in appendix B, however these are all order formulae rather than low twist approximations. Note however that use of the formulae (5.11) for the B meson is dependent on the ISR and FSR terms in (5.10) being separately gauge invariant, otherwise contact terms may not cancel between them. In the case of the light mesons this problem is avoided because as already mentioned the DAs reproduce (5.11). The following subsections describe the techniques used to calculate the various different operator contributions. The labels in brackets of the section headings correspond to the operator selection rules shown in table 5.1.

Initial state radiation only (I)

This case occurs for the vector meson final state with the tensor current operators $O_{9,10}^{\mathrm{WA}}$ and the vector operator O_5^{WA}. The operator O_5^{WA} is of course rather more similar to the operators $O_{6,8}^{\mathrm{WA}}$ which also couple to vector currents but in this case the final state contact term must be zero due to parity considerations. Computation of the initial state is straightforward using sum rules as explained in Section 2.8 and the relevant dispersion relations will be given as part of the results in Section 5.3.5. To calculate the initial state sum rule it is most convenient to work at $m_{K^*} = 0$ since this somewhat simplifies the dispersion relations required. As this calculation only includes terms up to $O(m_{K^*})$, it would seem that m_{K^*} could be set to zero immediately since the initial state only depends on the invariant p^2 which is of order $O(m_{K^*}^2)$. However, this only works for transversely polarised K^* mesons; in the longitudinal case the polarisation $\eta \sim 1/m_{K^*}$ and thus $O(m_{K^*}^2)$ corrections in the initial state are lifted to $O(m_{K^*})$.

Fortunately in the longitudinally polarised case this can be avoided by writing the polarisation vector η explicitly in terms of p and $q = p_B - p$. This is similar in concept to the well-known ultra-relativistic approximation discussed in Section 2.10. It is straightforward to

solve for the constraints $\eta^2 = -1$ and $\eta \cdot p = 0$ giving

$$\eta^\mu = \eta_\perp^\mu + 2(\eta \cdot q)\frac{(m_B^2 - m_{K^*}^2 - q^2)p^\mu - 2m_{K^*}^2 q^\mu}{(m_B^2 - m_{K^*}^2 - q^2)^2 - 4m_{K^*}^2 q^2} \quad , \tag{5.12}$$

where $\eta_\perp \cdot q = 0$. At $m_{K^*} = 0$ this reproduces the results of the ultra-relativistic approximation $\eta \to p/m_{K^*}$; however, since the tensor operator requires $p^{[\mu}\eta^{\nu]}$ higher orders are required and the formula (5.12) is exact. Expanding in m_{K^*} the right-hand side of the tensor matrix element in (5.11) may be written:

$$p^\mu \eta^\nu - \eta^\mu p^\nu = (p^\mu \eta_\perp^\nu - \eta_\perp^\mu p^\nu) - \frac{4m_{K^*}^2(\eta \cdot q)}{(m_B^2 - q^2)^2}(p^\mu q^\nu - q^\mu p^\nu) + O(m_{K^*}^4) \tag{5.13}$$

Since the longitudinal polarisation is now explicitly $O(m_{K^*}^2)$ the light meson mass m_{K^*} may be set to zero for the remainder of the calculation, particularly in order to simplify the dispersion relation.

Final state radiation only (F)

This case occurs for the operators $O_{2,4}^{\mathrm{WA}}$ for the K^* final state and is rather straightforward. The initial state matrix element is given by (5.11) and the final state is evaluated using the DAs given in appendix B. A general discussion of calculating with DAs is given in Section 2.7. The only difficulty here is that gauge invariance in the case of O_2^{WA} is non-trivial owing to the presence of two DAs related by equations of motion. The identity

$$u h_\parallel^{(t)}(u) + \frac{u}{2} h_\parallel^{(s)\prime}(u) = 2\int_0^u \left(h_\parallel^{(t)}(v) - \phi_\perp(v)\right) dv \quad , \tag{5.14}$$

which follows from equation (3.21/22) in [70], must be used to show $q \cdot \mathcal{A}^* = 0$.

Initial state radiation plus final state contact term (I,F$_c$)

This case occurs for the operators O_6^{WA} in the vector meson case and O_8^{WA} in the pseudoscalar case. In this case the final state radiation term is purely a contact term in the limit of massless quarks and can be fixed to zero by appropriate choice of gauge. The calculation of this term is detailed in Section 2.7. The initial state term calculation then follows the sum rule procedure as usual. In contrast to the case where both initial and final state radiation are physical, there is no concern over parasitic cuts unlike the (I,F) case discussed below, since the final state contribution is given by (2.43), that is

$$(p+q)_\mu \langle K^* \gamma | \bar{s}\gamma^\mu q | 0 \rangle = e(Q_q - Q_s) f_{K^*} m_{K^*} (\eta \cdot \epsilon) \quad , \tag{5.15}$$

and there are no poles or cuts in this result in the variable $(p+q)^2$.

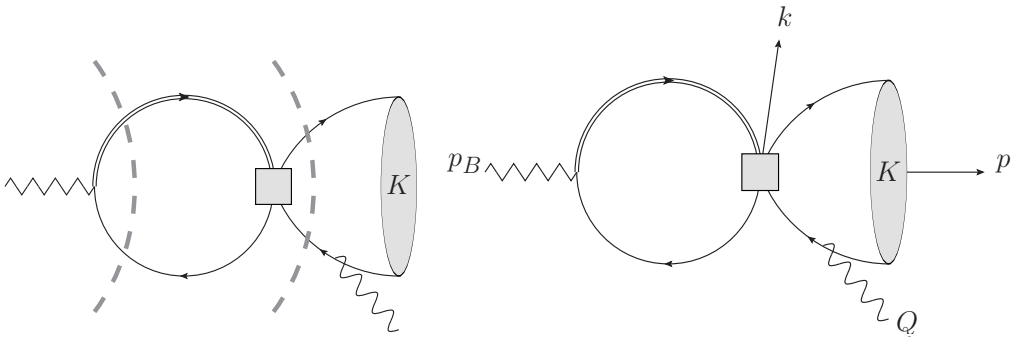

Figure 5.4: The dashed lines in the left-hand figure show cuts with the momentum of the B meson current. The right-most cut however does not have the quantum numbers of the B meson, and so should not be included in the dispersion relation. The solution to this problem is illustrated in the right-hand diagram and essentially consists of lifting the constraint $p_B = p + q$ and allowing momentum to flow into the four quark operator. This solution is described in detail in Section 3.2.1 and subsequent sections.

Both initial and final state radiation (I,F)

This case only occurs for the O_8^{WA} operator at leading order α_s^0, however unfortunately for future higher order calculations of non-factorisable terms, it will be the norm. In this case, the same problem occurs as for the chromomagnetic operator $\mathcal{O}_8$, in that there are cuts with $\bar{q}s$ quantum numbers in the external momentum invariant p_B^2, which clearly should not be counted as part of the perturbative duality approximation to the B meson state. In the case of final state radiation only this problem is avoided because a sum rule need not be used to compute the B meson part of the matrix element; however, in the present case gauge invariance comes into play because the factorised matrix elements in (5.10) are not separately gauge invariant.

This situation really leaves two possible ways forward: either separation of desired cuts with B meson quantum numbers from those without must be managed, or some approximation must be constructed in which it can be argued that gauge invariance violation is small. The latter approach is entirely feasible and in fact closely related to an issue which arises in QCDF calculations, to be discussed in Section 5.4.6; however, the former is more theoretically consistent so that is the approach that shall be taken.

In fact, all the basic results required are those worked out in Section 3.2.1, and the Passarino–Veltman functions which occur in the result are those in Section 3.2.2. There is therefore only one remaining technical point: the sum rule approximation to f_B used in the term

$$\langle K(p)\gamma^*(q,\rho)|\bar{s}\gamma_5 q|0\rangle \langle 0|\bar{q}\gamma_5 b|B(p_B)\rangle = -i\frac{f_B^{\mathrm{wti}} m_B^2}{m_b} \langle K(p)\gamma^*(q,\rho)|\bar{s}\gamma_5 q|0\rangle \tag{5.16}$$

must be chosen carefully. Due to the presence of cancellations between gauge variant terms in ISR and FSR matrix elements, f_B^{wti} must be chosen to be consistent with the way the ISR

terms are calculated. In the present calculation, the correct expression is

$$f_B^{\text{wti}} = \frac{m_b^2}{f_B m_B^4}\left[\frac{3}{8\pi^2}\int_{m_b^2}^{s_0}\exp\left(\frac{m_B^2-s}{M_{\text{WA}}^2}\right)\frac{(s-m_b^2)^2}{s}ds - m_b\langle\bar{q}q\rangle\exp\left(\frac{m_B^2-m_b^2}{M_{\text{WA}}^2}\right)\right] \quad , \tag{5.17}$$

where the Borel parameter M_{WA}^2 must be the same as that used for the ISR term, and f_B is likewise whatever value is taken there. In general therefore f_B and f_B^{wti} will not be equal.

A final point is worth remarking on: again owing to the fact that the ISR and FSR terms are not separately gauge invariant, projection of each term onto the basis (3.16) leads to a $1/q^2$ divergence in the p_T^μ coefficient, which cancels in the sum. Since this is a pseudoscalar decay there is no concern with the presence of a divergence for $q^2 \to 0$ since physically this process does not exist, however it is convenient for numerical purposes to cancel such divergent terms explicitly. It is rather helpful then that in the present case the relevant DA $\phi_K(u)$ (B.1) is restricted to its asymptotic form by equations of motion when three-particle DAs and quark masses are neglected [93], so the resulting integrals are analytic. This rearrangement of terms has been done in the results presented in Section 5.3.5, and must be borne in mind if attempting to reproduce them.

5.3.5 WA results

Due to the choice (5.7) of basis for the four quark operators, it is convenient to present results for the vector meson in the $\{V, A, 0\}$ basis (2.74) since each basis tensor (2.71) then has definite parity. The matrix elements $W_\iota^q(q^2)$, with $\iota \in \{T, V, A, 0\}$, are decomposed as follows:

$$W_\iota^q(q^2) = \sum_{j=1}^{10} a_j^q W_{\iota,j}^q(q^2) \equiv \sum_{j=1}^{10} a_j^q \left[F_{j,\iota}^q(q^2) + I_{j,\iota}^q(q^2)\right] \quad . \tag{5.18}$$

The functions I and F stand for ISR and FSR respectively and are further parametrised as

$$I_{j,\iota}^q(q^2) = \frac{1}{f_B m_B^2}\left(\langle\bar{q}q\rangle\exp\left(\frac{m_B^2-m_b^2}{M_{\text{WA}}^2}\right)V_{j,\iota}^q(q^2) + \int_{m_b^2}^{s_0} ds\,\exp\left(\frac{m_B^2-s}{M_{\text{WA}}^2}\right)\rho_{j,\iota}^q(q^2,s)\right) \quad , \tag{5.19}$$

where $\iota \in \{T, V, A, 0\}$ is common to both the K^* and K cases and

$$F_{j,i}^q(q^2) = f_{K^*}^\perp f_B\left(\frac{m_B}{m_b}\right)^2\int_0^1 f_{j,i}^q(q^2,u)\,du \tag{5.20}$$

$$F_{j,T}^q(q^2) = \mu_K^2 f_B^{\text{wti}}\left(\frac{m_B}{m_b}\right)^2\int_0^1 f_{j,T}^q(q^2,u)\,du \quad , \tag{5.21}$$

where $i \in \{V, A, 0\}$ applies to the K^*-meson case and $F_{j,T}^q$ to the K. The Borel parameter is taken to be $M_{\text{WA}}^2 = 9(2)\text{GeV}$ although as discussed previously the Borel parameter need not be the same for independent terms since the result should only weakly depend on its value within a reasonable range, and when higher twist and/or α_s corrections are included the result may be

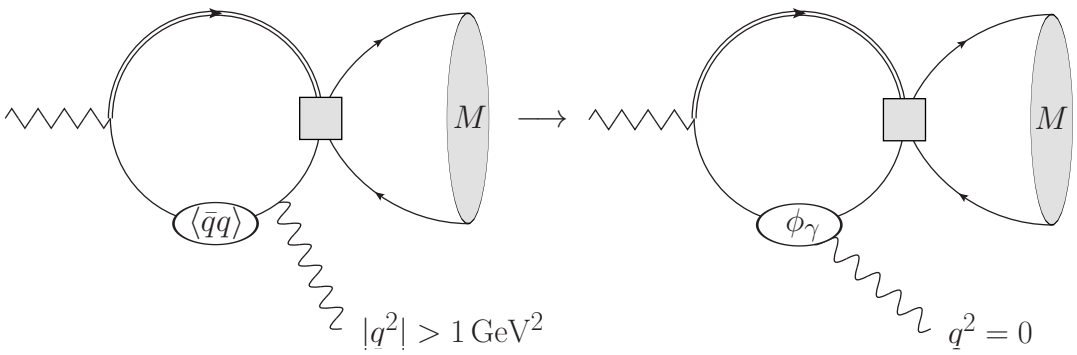

Figure 5.5: Quark condensate contribution to be replaced by the photon DA contribution for $q^2 = 0$ case i.e. $B \to V\gamma$. The important point to realise is that both diagrams are gauge variant and produce, together with the other diagram in Figure 5.3b(right), a fully gauge invariant result.

extremised w.r.t. the Borel parameter. The duality threshold is taken to be $s_0 = 35(1)\text{GeV}^2$ as for the chromomagnetic operator. The quoted uncertainty in the Borel parameter and the duality threshold are the ranges over which they are varied to provide an estimate of the error of the LCSR method; the details of the error estimation method are given in Section 5.5.1. The decay constant f_B^{wti} is fixed by gauge invariance considerations as described above (5.17). The occurrence of f_B in $I^q_{j,\iota}$ is evaluated using the leading order sum rule in the previous Chapter (3.74), and $M^2_{f_B} = 5.0(5)\text{GeV}$ is again used. The occurrence of f_B in $F^q_{j,i}$ is taken from lattice data as $f_B = 191(5)\text{MeV}$ [166,167]. Formulae for DAs of the external light mesons are given in appendix B.1. Formulae for all functions appearing on the RHS of (5.21) are given in appendix E.1.

5.3.6 WA at $q^2 = 0$

The results presented in the previous section cannot be used at $q^2 = 0$. The reason for this is shown in Figure 5.5; there is a term proportional to $Q_q \langle\bar{q}q\rangle / q^2$ in (5.21), e.g. (E.6), when the photon is emitted from the light quark line. Clearly at $q^2 = 0$ this calculation is invalid. This problem arises because for an on shell photon, the quark propagator

$$\langle\gamma(q)|\bar{q}(x)q(0)|0\rangle \tag{5.22}$$

is light cone dominated and a short distance expansion in x fails as described in Section 2.6. Fortunately the solution to this problem is then rather obvious; instead of using a local OPE as may be done for $q^2 > 0$ a non-local OPE on the light cone must instead be employed. Since prior computations of weak annihilation in LCSR were at $q^2 = 0$ [77,78], this technique was already used there. Here, those results are extended to the case of the K final state and the tensor current operators $\text{WA}_{9,10}$. The DA for the quark propagator in an external electromagnetic field is given in appendix B.2.

It must be pointed out in this case that the results given here for the operators $O^{\text{WA}}_{5,6}$ differ

from those in [77] by a small term. The origin of this is the final state contact term discussed in Section 2.7, which is exactly known due to the fact that the required matrix element coincides with a Ward identity. The result for the final state matrix element (5.15) is proportional to $Q_q - Q_s$, so this immediately presents a problem when the graph shown in Figure 5.6 is considered: there is a contact term proportional to $Q_b \langle\bar{q}q\rangle$ in the initial state so therefore there must be a corresponding one proportional to $Q_q \langle\bar{q}q\rangle$, but all $Q_q \langle\bar{q}q\rangle$ terms have been removed to avoid $\langle\bar{q}q\rangle / q^2$ divergences. Of course, this is a gauge dependent statement; however, there seems to be no a priori reason why the gauge of the external electromagnetic field cannot be chosen arbitrarily. The solution to this problem is in fact already incorporated into the expression for the photon DA in (B.10), by realising that, in a covariant gauge $A_\mu = \epsilon_\mu e^{iq\cdot x}$,

$$\langle\gamma(q,\epsilon)|\bar{q}_a(x)\left([x,0]_{\text{EM,QCD}} - [x,0]_{\text{QCD}}\right)q_b(0)|0\rangle = \frac{iQ_q\langle\bar{q}q\rangle}{4N_c}\int_0^1 du\, e^{iuq\cdot x}\epsilon\cdot x\,\delta_{ba} \quad , \tag{5.23}$$

where $([x,0]_{\text{EM,QCD}} - [x,0]_{\text{QCD}})$ is the difference between a Wilson line including and excluding the QED gauge field. The identity (5.23) reflects the fact that the photon DA is usually specified in terms of a operators which are both QED and QCD gauge invariant, but these are not the quantities which typically appear in Feynman diagrams. The right hand side of (5.23) indeed turns out to produce the contact term required when combined with the contact term from the diagram in Figure 5.6, however it is not exactly equal to a contact term. It is the remainder from evaluating (5.23) which is the difference between the result found here and that in [77][4]. The resulting difference between the present result and theirs can be seen in (E.23), although it should be stressed that this term is in fact extremely small and thus the difference between these results and those of [77] are numerically entirely negligible[5].

Results for the $q^2 = 0$ case are given by introducing the function $I^q_{j,i}|_\gamma$, given by

$$I^q_{j,i}|_\gamma = \frac{1}{f_B m_B^2}\left(\langle\bar{q}q\rangle\exp\left(\frac{m_B^2 - m_b^2}{M^2_{\text{WA}}}\right)V^{q,\gamma}_{j,i} + \int_{m_b^2}^{s_0} ds\,\exp\left(\frac{m_B^2 - s}{M^2_{\text{WA}}}\right)\rho^{q,\gamma}_{j,i}(s)\right) \quad , \tag{5.24}$$

which should be used in (5.21) in place of $I^q_{j,i}(q^2)$. The spectral density $\rho^{q,\gamma}_{j,i}(s)$ is defined by re-using the results for $q^2 \neq 0$ and introducing an additional term for the photon DA density,

$$\rho^{q,\gamma}_{j,i}(s) = \rho^q_{j,i}(0,s) + \langle\bar{q}q\rangle\,\widetilde{\rho}^{q,\gamma}_{j,i}(s) \quad . \tag{5.25}$$

The functions $V^{q,\gamma}_{j,i}$ and $\widetilde{\rho}^{q,\gamma}_{j,i}(s)$ are given in appendix E.1.2.

[4] Of course, they calculated at $p^2 > 0$ rather than $p^2 = 0$ as done here, however as noted in Section 2.7 $p^2 = 0$ must be used for non-trivial FSR cases since twist-4 DAs are neglected here, so p^2 is set to zero throughout for consistency and simplicity.

[5] [78] has not been mentioned in this discussion because that paper did not include the tiny $Q_b\langle\bar{q}q\rangle$ contribution so no contact term problem arises.

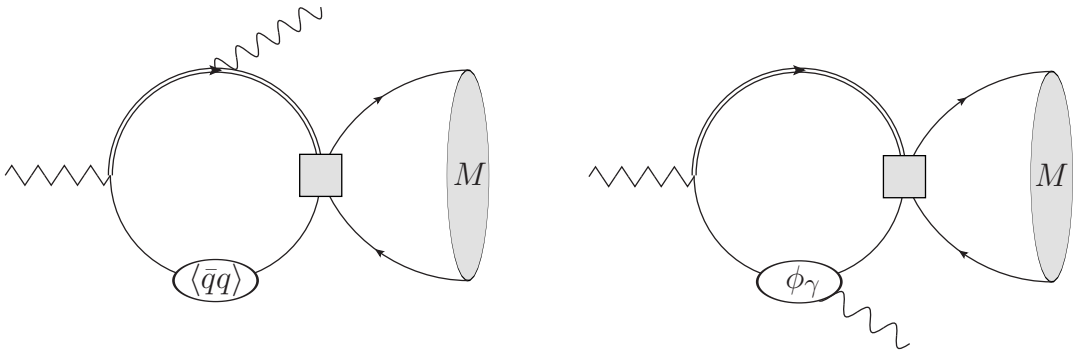

Figure 5.6: The left-hand graph presents a problem at $q^2 = 0$: it is clearly proportional to $Q_b \langle \bar{q}q \rangle$ and there is no reason to exclude it at $q^2 = 0$ since it produces a physical contribution to the decay rate. However, the right-hand graph must then also produce a corresponding contact term proportional to $Q_q \langle \bar{q}q \rangle$ since the contact term from FSR is proportional to $Q_b - Q_q$, but the photon DA expression in [165] contains no such term.

5.4 Quark loop spectator scattering (QLSS)

The QLSS contribution is given by graphs shown in Figure 5.7. This graph is similar to that of the chromomagnetic operator (see Figure 5.1), except that the gluon connecting to the heavy and light quark lines is produced by a perturbative quark loop rather than exclusively short distance effects as in the $\mathcal{O}_8$ case[6]. This means that much of the discussion of Chapter 3 also applies to this diagram, however owing to the presence of the additional loop the computation of this diagram using LCSR would be a significant challenge since anomalous thresholds are to be expected[7]. Such a calculation is beyond the scope of the present work, so QCDF is used which means that only a one-loop calculation must be performed. The computation of QLSS in QCDF has previously been performed in [84] and [51] in the SM for $B \to K^* \gamma$ and $B \to K^* l^+ l^-$, respectively. Here these calculations are extended by including a complete basis of four quark operators contributing to QLSS. It is worth noting immediately that generically this operator basis is completely independent of the operators (5.7) and the extended colour octet basis (5.63) required in the $B \to \rho$ case due to the presence of the additional light s quark, whose mass is taken to be degenerate with that of other two light flavours.

5.4.1 QLSS operator basis

There are ten possible Lorentz structures for four quark operators, as given in equation (5.7). The vector coupling of the gluon restricts this to four possible operators which appear in the QLSS diagram, as well as fixing the colour structure coupling. These relevant operators are

$$Q^{4f}_{1L(R)} \equiv \frac{1}{4} \bar{f} \lambda^a \gamma_\mu f \, \bar{s}_{L(R)} \lambda^a \gamma^\mu b \qquad Q^{4f}_{2L(R)} \equiv \frac{1}{4} \bar{f} \lambda^a \sigma_{\mu\nu} f \, \bar{s}_{L(R)} \lambda^a \sigma^{\mu\nu} b \quad , \tag{5.26}$$

[6] This interpretation is subject to the fact that RG running mixes the two contributions.
[7] See Section 3.2.4 for specific details on this problem.

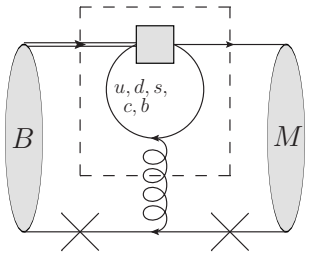

Figure 5.7: Quark loop spectator scattering (QLSS) topology. Crosses denote possible photon insertions which violate isospin symmetry. This parallels the $\mathcal{O}_8$ contribution computed in Chapter 3, but is more complicated owing to the presence of an additional loop. The charm quark gives by far the largest contribution in the SM owing to the large value of $\lambda_c C_2$ in comparison to coefficients of other operators in (2.19). The dashed box indicates a hard subgraph which is computed most straightforwardly without reference to the external hadronic states; this procedure is described in Section 5.4.2.

where $s_L = s\frac{1+\gamma_5}{2}$ and likewise $s_R = s\frac{1-\gamma_5}{2}$ and λ^a are the Gell-Mann matrices. Since in this calculation m_s has been set to zero, the effect of the u, d and s quarks is degenerate and the effects of these three quark can be grouped into a single operator

$$Q^{4SU(3)_F}_{xL(R)} \equiv \left(Q^{4u}_{xL(R)} + Q^{4d}_{xL(R)} + Q^{4s}_{xL(R)}\right) \ , \quad x = 1, 2 \tag{5.27}$$

and the effective Hamiltonian for QLSS may be written

$$\mathcal{H}^{\text{QLSS}} = -\frac{G_F}{\sqrt{2}}\lambda_t \sum_{x,\chi,f} s^f_{x\chi} Q^{4f}_{x\chi} \ , \quad x = 1, 2 \ , \ \ \chi = L, R \ , \ \ f = SU(3)_F, c, b \quad , \tag{5.28}$$

where WCs are denoted $s^f_{x\chi}$. As explained in the introduction to this section, this basis is linearly independent of that which occurs in WA, owing to the fact that WA does not couple to s, c or b quarks.

5.4.2 $b \to sg$ subgraph

The calculation of the $b \to sg$ subgraph, denoted by the dashed box in Figure 5.7, is an entirely standard one loop perturbative procedure. The matrix element needed is

$$a^\mu = \langle sg(r,\mu)|\mathcal{H}^{\text{QLSS}}|b\rangle = \sum_{i=L,R} \left[K^\mu_{1,i} F_{1,i}(r^2) + K^\mu_{2,i} F_{2,i}(r^2)\right] \quad , \tag{5.29}$$

where $K^\mu_{1,2}$ are the only tensor structures allowed by Lorentz covariance and gauge invariance

$$K^\mu_{1,(L,R)} = \frac{r^\mu \not{r} - r^2\gamma^\mu}{r^2} P_{L,R} \qquad\qquad K^\mu_{2,(L,R)} = \frac{r^\mu - \not{r}\gamma^\mu}{r^2} P_{L,R} \tag{5.30}$$

which requires $r \cdot K = 0$. Note that although (5.29) has been written as a matrix element, the result is independent of the external momenta of the b and s quarks due to the structure of the

graph: they have not been assumed on shell even though the QCDF approach to calculating Figure 5.7 implies that they will be, at least to leading order in $1/m_b$. From the effective Hamiltonian (5.28), it clearly follows that the dressing functions F may be parametrised as:

$$F_{x,\chi} = s^{SU(3)}_{x,\chi} H_x(s,0) + s^c_{x,\chi} H_x(s,m_c) + s^b_{x,\chi} H_x(s,b) \quad . \tag{5.31}$$

Dimensional analysis shows that H_2 functions have dimension 1, which necessitates that they are proportional to a particle mass and since the loop fermion mass is the only such quantity appearing in the calculation, it must be the case that $H_x(s,m_f) \sim m_f$. This renders the value of the WCs $s^{SU(3)}_{2L(R)}$ irrelevant since they do not contribute, and therefore reduces the number of effective operators in QLSS from 12 to 10. The functions H_x have simple expressions in terms of standard loop integral functions:

$$H_1(s,m) = -\frac{1}{96\pi^2}\left[9h(s,m)+4\right] \qquad H_2(s,m) = -\frac{m}{4\pi^2} B_0(s,m^2,m^2) \quad , \tag{5.32}$$

where $h(s,m_q)$ is known as the vacuum polarisation owing to its appearance in the one-loop correction to gauge boson propagators and is given in (2.26). The function B_0 is the standard Passarino–Veltman scalar two-point function, which is related to the vacuum polarisation (again, $z \equiv \frac{4m^2}{s}$) function by

$$B_0(s,m^2,m^2) = 2 - \log\frac{m^2}{\mu^2} + 2\frac{\frac{9}{4}h(s,m) + \log\frac{m^2}{\mu^2} - \frac{2}{3} - z}{2+z} \quad . \tag{5.33}$$

Note that these results for H_x are independent of the γ_5 regularisation scheme used owing to the choice of four quark operator basis (5.28), however the projection onto that basis must be done up to $O(D-4)$ order in dimensional regularisation since the B_0 and h functions are $1/(D-4)$ divergent and therefore ultimately expressions for $F_{x,\chi}$ will be scheme dependent. The divergent part is therefore indicated explicitly in (2.26).

5.4.3 Standard Model $b \to sg$ transition

Due to the scheme dependence of the conversion to the QLSS operator basis (5.28), it is most convenient to present the projection of the SM effective Hamiltonian (2.19) onto this basis in terms of the dressing functions $F_{x,\chi}$ (5.31) rather than the WCs $s^f_{x,\chi}$, since these functions are

finite unlike $H_x(s,m)$ (5.32). In the SM this the NDR scheme gives

$$\begin{aligned}
F_{1,L}(s) =& \frac{3}{32\pi^2}\left[h(s,m_c)\left(-\frac{\lambda_c}{\lambda_t}C_2+C_4+C_6\right)+h(s,m_b)(C_3+C_4+C_6)\right.\\
&\left.+h(s,0)\left(-\frac{\lambda_u}{\lambda_t}C_2+C_3+3C_4+3C_6\right)-\frac{8}{27}(C_3-C_5-15C_6)\right]\\
F_{1,R}(s) =& 0\\
F_{2,R}(s) =& \frac{m_b}{8\pi^2}(C_8^{\text{eff}}-C_8)\\
F_{2,L}(s) =& \frac{m_s}{8\pi^2}(C_8^{\text{eff}}-C_8)\to 0+O(m_s) \quad ,
\end{aligned} \tag{5.34}$$

where $F_{1,L}$ was first worked out in [51] although the λ_c dependence has been included explicitly here, which is important in the case of the ρ meson since then $\lambda_c/\lambda_t \approx -1$ does not hold. Finite terms in the results for $F_{1,L}$ and $F_{2,(L,R)}$ are scheme dependent; however the coefficient C_8^{eff} is scheme independent [49, 168] since it is the total contribution to $b\to s\gamma$ with the K_2 tensor structure at one loop. The scheme dependence is illustrated particularly nicely by this case since $C_8^{\text{eff}} = C_8$ in the HV scheme [49] but receives contributions from four quark operators in the NDR scheme (2.23).

As mentioned earlier, the contribution from the charm loop dominates the function $F_{1,L}$ since $|\lambda_c/\lambda_t C_2| \approx 1$, and all other contributions are either suppressed by small WCs C_{3-6}, as can be seen in table 2.1, or small CKM matrix elements λ_u/λ_t in the case of the up quark.

5.4.4 QLSS results

The results of the QLSS calculation will be given here, so that the approximations involved and accuracy of the method may be discussed more effectively in section later in Section 5.4.5. Combining (5.29) with the B and K^* meson DAs the result for the QLSS topology is

$$\begin{aligned}
S_-^q(q^2) =& \sqrt{2}Q_q\frac{C_F}{N_c}\frac{16\pi^3\alpha_s f_B m_B}{m_b}\int_0^1 du\left(F_{1,L}(\bar{u}m_B^2+uq^2)-\frac{1}{m_B}F_{2,R}(\bar{u}m_B^2+uq^2)\right)\\
&\times\left[\frac{f_{K^*}^\perp\phi_\perp(u)}{\bar{u}m_B^2+uq^2}-\frac{f_{K^*}m_{K^*}}{2\lambda_+(q^2)(m_B^2-q^2)}\left(g_\perp^{(v)}(u)-\frac{g_\perp^{(a)'}(u)}{4}\right)\right]\\
&-\frac{F_{2,R}(\bar{u}m_B^2+uq^2)}{m_B}\left[\frac{f_{K^*}^\perp\phi_\perp(u)u(m_B^2-q^2)}{2(\bar{u}m_B^2+uq^2)^2}-\frac{f_{K^*}m_{K^*}}{2\lambda_+(q^2)(m_B^2-q^2)}\frac{g_\perp^{(a)}(u)}{4\bar{u}}\right]
\end{aligned} \tag{5.35}$$

$$S_+^q(q^2) = (L\leftrightarrow R) \tag{5.36}$$

$$\begin{aligned}
d\cdot S_0^{q,V}(q^2) =& -Q_q\frac{C_F}{N_c}\frac{32\pi^3\alpha_s f_B m_B}{m_b}\frac{f_{K^*}m_{K^*}}{\lambda_-(q^2)(m_B^2-q^2)}\int_0^1 du\,\phi_\parallel(u)\\
&\times\left[F_{1,A}(\bar{u}m_B^2+uq^2)+\frac{m_B}{\bar{u}(m_B^2-q^2)}F_{2,A}(\bar{u}m_B^2+uq^2)\right] \quad ,
\end{aligned} \tag{5.37}$$

with $d \equiv -\frac{\sqrt{2}m_B m_V}{\sqrt{q^2}E}$. Likewise for the K meson final state the result is

$$\begin{aligned} S_T^q(q^2) = &- Q_q \frac{C_F}{N_c} \frac{(m_B + m_K) 16\pi^3 \alpha_s f_B f_K}{m_B m_b \lambda_-(q^2)} \int_0^1 du\, \phi_K(u) \\ &\times \left[F_{1,V}(\bar{u} m_B^2 + u q^2) - \frac{m_B}{\bar{u}(m_B^2 - q^2)} F_{2,V}(\bar{u} m_B^2 + u q^2) \right] \quad , \end{aligned} \tag{5.38}$$

where the $F_{1,L}$ terms have previously been worked out in [51,84], although there is a difference of a factor of two in $S_0^{q,V}$ in those two sources. The results here agree with [84] on this point. These results have been expressed in the $\{+,-,0\}$ basis (2.74) because in this case the helicity of the final state meson is directly connected to the helicity of the $b \to sg$ subgraph. Note that unlike in the WA case only include isospin violating terms proportional to Q_q are included here; the isospin-symmetric terms proportional to Q_b were not calculated since UV isospin violation is not possible here. Note that $\lambda_\pm(q^2)$ are momentum-dependent moments of the B meson DA and in no way connected to the Källén function λ; they will be defined shortly below (5.43). In the results for longitudinally polarised K^* and K cases the notation

$$F_{1,V(A)}(s) \equiv F_{1,R}(s) \pm F_{1,L}(s) \tag{5.39}$$

has been used for the sake of brevity. As is normal in this type of calculation Wandzura-Wilczek equations of motion for the K^* have been used to get (5.35).

The appearance of momentum-dependent moments of the B meson DA imply that the $1/m_b$ expansion is not entirely systematic, which will be discussed shortly. To produce the results (5.35) the following two types of term appear

$$X_1 = \int_0^\infty dl_+ \phi_\pm(l_+) H_1(l_+) \tag{5.40}$$

$$X_2 = \int_0^\infty dl_+ \phi_\pm(l_+) \frac{H_2(l_+)}{l_+ - q^2/m_B - i\epsilon} \quad , \tag{5.41}$$

essentially separated by the presence or absence of a pole at $l_+ = q^2/m_B$. $\phi_\pm$ are B meson wave functions to be discussed shortly in Section 5.4.5. Assuming that the functions $H_{1,2}(l_+)$ are smooth on the scale $l_+ \to l_+ \pm \Lambda_{\rm QCD}$ they can be approximated by a constant at the peak of the rest of the integrand

$$X_1 \to \left(\int_0^\infty dl_+ \phi_\pm(l_+) \right) H_1(0) = H_1(0) \tag{5.42}$$

$$X_2 \to \left(\int_0^\infty dl_+ \frac{\phi_\pm(l_+)}{l_+ - q^2/m_B - i\epsilon} \right) H_2(q^2/m_B) \equiv \frac{H_2(q^2/m_B)}{\lambda_\pm(q^2)} \quad , \tag{5.43}$$

which gives the definition of the momentum-dependent moments $\lambda_\pm(q^2)$ in terms of the B meson DA.

Of course, the results for the F_2 contribution in (5.35) suffer the problem that the calculation

in Chapter 3 was done to solve: there is a logarithmic endpoint divergence in the integral arising from the region where $\bar{u} \to 0$. The ways of working around this problem in QCDF are outlined in Section 3.3, however since the LCSR result for the chromomagnetic operator is now available an alternative approach can be adopted. The problematic function $F_{2,i}(r^2)$ is expanded as

$$F_{2,i}(r^2) = [F_{2,i}(0)]_{\text{LCSR}} + \left[F_{2,i}(r^2) - F_{2,i}(0)\right]_{\text{QCDF}} \tag{5.44}$$

and the contribution of each of the terms in square brackets is computed separately using the method specified in the subscript. The endpoint divergence in the QCDF calculation is removed because an additional factor of $\bar{u}$ has been introduced in the appropriate region $F_{2,\pm}(r^2 \to 0)$. As discussed in Section 3.3 the LCSR result includes the contribution of soft gluons from the initial state B meson where the QCDF result does not, so the physical nature of the approximation implied by (5.44) is somewhat unclear. However the removal of the endpoint sensitive term from the QCDF result would appear to largely alleviate any questions over its validity since only the region where $F_{2,i}(r^2) - F_{2,i}(0)$ is sizeable contributes and therefore only far off-shell gluons can possibly appear in the QCDF calculation, and these are well approximated by QCDF.

The final point to be discussed is the absence of the twist-3 corrections to the K result (5.38) in comparison to (5.35) where the twist-3 DAs $g_\perp^{(v,a)}$ appear, which is in contradiction to the previous inclusion of twist-3 K contributions in WA. This difference stems from two issues, one from WA and one from QLSS. On the WA side, the reason that twist-3 K contributions, and also the twist-3 DAs $h_\parallel^{(s,t)}$ in the K^* case, were included, was because the scalar current four quark operators would give no contribution without them. Neither would the tensor current operators in the case of longitudinally polarised K^* mesons. This reasoning does not apply to the QLSS case; all operators are already coupled to at twist-2 accuracy. Therefore the question should really be approached from the other end: why are the twist-3 DAs $g_\perp^{(v,a)}$ included? The reason is that this contribution is expected to have comparable magnitude to the $\phi_\perp$ term, because they are both at the same order in $1/m_b$ power counting. This is because the $\phi_\perp$ term happens to cancel the $1/(l_+ - q^2/m_B)$ pole occurring in the light quark propagator, so it is $1/m_B$ suppressed with respect to a naive diagrammatic power counting. It is therefore necessary to include $g_\perp^{(v,a)}$ since it is of the same order. All other terms appearing in (5.35), (5.37) and (5.38) have their expected $1/m_B$ power, and thus it is not necessary to include either the $\phi_{p,\sigma}$ or $h_\parallel^{(s,t)}$ contributions in the case of the K and K^* respectively.

5.4.5 The B meson DA in QLSS

Since this is the only place in this thesis where the B meson DA is used the calculation of (5.35) will be discussed here briefly. It is most convenient to discuss this calculation using light cone

coordinates in the rest frame of the B meson, with two light like unit vectors $n_\pm$

$$n_+^2 = n_-^2 = 0 \qquad\qquad n_+ \cdot n_- = 2 \quad , \tag{5.45}$$

where an arbitrary vector may be written $x^\mu = \frac{1}{2}(x_+ n_+^\mu + x_- n_-^\mu) + x_\perp^\mu$, although for the most part as this is a two-body decay all perpendicular momenta are zero. In particular for $B \to K^{(*)} l^+ l^-$ the kinematics

$$p_+ = m_B - \frac{q^2}{m_B} \, , \qquad p_- = 0 \, , \qquad q_+ = \frac{q^2}{m_B} \, , \qquad q_- = m_B \, , \tag{5.46}$$

may be chosen. The B meson DA is then given by [118, 169]

$$\begin{aligned}\langle 0|\bar{q}_a(x)[x,z]b_b(0)|B(p_B)\rangle = \frac{-if_B m_B}{4N_c}\int_0^\infty dl_+ e^{-il\cdot x} \\ \times \left[\frac{1+\not{v}}{2}\left\{\phi_+(l_+)\not{n}_+ + \phi_-(l_+)\left(\not{n}_- - l_+\gamma_\perp^\nu \frac{\partial}{\partial l_\perp^\nu}\right)\right\}\gamma_5\right]_{ba}\Bigg|_{l=\frac{l_+ n_+}{2}}\end{aligned} \tag{5.47}$$

where $p_B = m_B v$. The wave functions $\phi_\pm$ and associated formulae are given in appendix B.3.

The first question to address in calculating with the B DA is to ask why it takes the form (5.47) of a light cone propagator in the B meson rest frame; after all there is no a priori reason this should be the case, since one would expect that all of the spatial components of the light quark momentum would have similar magnitude. That it is a light cone propagator arises, much as in the light meson case, from the dynamics of the hard-scattering kernel in the factorised process: it is only sensitive to one component of the light quark momentum [118]. In the present case, only the invariant combination

$$\frac{1}{(q-l)^2} = \frac{1}{q^2 + l^2 - q_+ l_- - q_- l_+} \xrightarrow{q^2 \to 0} \frac{1}{m_B l_+ + l_+ l_-} \approx \frac{1}{m_B l_+} \tag{5.48}$$

is needed and thus to leading order in $1/m_b$ the short distance part of the amplitude is not sensitive to l_-. Clearly however this is subject to corrections from the $q_+ l_-$ term and thus terms at $O(q^2/m_B^2)$ have been neglected, which is somewhat to be expected in this approach since m_b is expected to be the largest scale in the calculation. At $q^2 = 4m_c^2$ this amounts to a potential 30% correction to these results, and thus the full result for the isospin asymmetry computed here cannot be used above the charm resonance region.

The $l_\perp$ derivative in (5.47) is also neglected before performing the bulk of this calculation. This is useful as dealing with derivatives tends to increase the complexity of such calculations by a few times, and there is already a derivative from the K^* DA to be handled. The $l_\perp$ derivative however will introduce a $1/m_b$ suppression in all cases since it will duplicate a denominator, with the exception of the case where the photon is emitted from the light quark originating

from the B meson. In that case the fermion propagator does not lead to a $1/m_b$ suppression straightforwardly; however, in combination with part of the B meson DA the relevant part of the diagram reads

$$l_+\gamma_\perp^\rho \frac{\partial}{\partial l_\perp^\rho}\gamma_5\gamma^\mu S_F(q-l) = il_+\gamma_5\gamma_\perp^\rho\gamma^\mu\left(\frac{\gamma_\perp^\rho}{(q-l)^2} + 2\frac{\not{q}-\not{l}}{(q-l)^4}l_\perp^\rho\right) \quad ,\to O(\Lambda_{\rm QCD}/m_B) \tag{5.49}$$

where $S_F(k) = i(\not{k})^{-1}$ is the massless fermion propagator. That this is $1/m_b$ suppressed can be argued as follows: the second term vanishes by setting $l_\perp = 0$ after taking the derivative. To analyse the first term $\gamma_\perp^\rho\gamma^\mu\gamma_{\perp,\rho}$ is contracted with a polarisation vector ϵ_μ in light-cone coordinates to give

$$l_+\gamma_\perp^\rho \not{\epsilon}\gamma_{\perp,\rho} = -l_+\left[\not{n}_+\epsilon_+ + \not{n}_-\epsilon_-\right] + l_+\underbrace{\gamma_\perp^\rho \not{\epsilon}_\perp\gamma_{\perp,\rho}}_{=0} \quad , \tag{5.50}$$

where the first part must be compared with the other structure coupling to $\phi_-(l_+)$:

$$i\not{n}_-\not{\epsilon}(\not{q}-\not{l}) = \frac{i}{4}\not{n}_-\left[\epsilon_+ q_- + \not{\epsilon}_\perp\not{n}_+(q_+ + l_+)\right] \quad . \tag{5.51}$$

It can therefore be seen that the derivative term is subleading in the ϵ_+ coefficient by $l_+/q_- = O(\Lambda_{\rm QCD}/m_B)$. The coefficient of ϵ_- appearing in (5.50) is not obviously suppressed; however it is necessarily related to the ϵ_+ term by gauge invariance since only a single physical longitudinal polarisation is present, and thus it also must be suppressed.

5.4.6 Gauge invariance in QLSS

The last point leads nicely on to a discussion of gauge invariance in the $1/m_b$ expansion and to some extent approximate gauge invariance generally. The issue of gauge invariance in QLSS away from $q^2 = 0$ is not straightforward since there is potentially a second independent scale in the problem. In principle it would be expected that the sum of the two diagrams emitting a photon from the spectator quark shown in Figure 5.7 is gauge invariant. The computation used in [51][8], which was reproduced for this calculation and extended for non-SM operators, can only be expected to respect gauge invariance at leading order in $1/m_b$. However, the constraint implied by Ward identities will turn out to mix different orders in $1/m_b$ and a careful choice of how to impose this constraint must be made in order not to enhance the inherent violation of gauge invariance by a factor of m_B^2/q^2 and thus have it induce an error in the overall result.

[8] These authors do not discuss the QED gauge invariance.

In full generality, the $B \to K^* l^+ l^-$ decay may be parametrised:

$$\begin{aligned}&\langle K^*(\eta,p)\gamma^*(q,\mu)|\mathcal{H}_{\text{eff}}|B(p+q)\rangle \\ &\quad\equiv U^\mu(q^2) = (\eta\cdot q)p^\mu U_p(q^2) + (\eta\cdot q)q^\mu U_q(q^2) + \eta^\mu(p\cdot q)U_\eta(q^2) + i\epsilon^{\mu\nu\rho\sigma}\eta_\nu p_\rho q_\sigma U_\epsilon(q^2) \quad .\end{aligned} \tag{5.52}$$

The term U_ϵ is of no relevance to the remainder of this discussion as it does not appear in the following Ward identity. Also, the same problem arises for the K meson as can be seen by setting $U_\eta|_K = U_\epsilon|_K = 0$ throughout. The QED Ward identity for this matrix element is

$$0 = q_\mu U^\mu(q^2) = (\eta\cdot q)\left[(p\cdot q)U_p(q^2) + q^2 U_q(q^2) + (p\cdot q)U_\eta(q^2)\right] \quad . \tag{5.53}$$

In principle, provided that gauge invariance is obeyed exactly, any one of the three functions or any linear combination thereof may be eliminated in favour or the remaining two. U_η shall not be considered since it appears on identical footing to U_p in (5.53), so the equations for eliminating the other two functions are:

✗ $$U_q(q^2) \to -\frac{p\cdot q}{q^2}\left[U_p(q^2) + U_\eta(q^2)\right] \tag{5.54}$$

✓ $$U_p(q^2) \to -U_\eta(q^2) - \frac{q^2}{p\cdot q}U_q(q^2) \quad . \tag{5.55}$$

In the $q^2 \to 0$ limit, (5.54) requires that

$$U_p(0) + U_\eta(0) = 0 \quad , \tag{5.56}$$

in order to avoid a $1/q^2$ kinematic singularity in the matrix element (5.52), which would render integral of the differential decay rate (2.80) infinite and is thus clearly unphysical. Since only the leading term in $1/m_b$ has been calculated (5.56) cannot be expected to hold exactly, and this problem is exacerbated by the m_B^2/q^2 enhancement of any error which would be induced by employing (5.54). Computing to higher orders in $1/m_b$ would not really help here since the use of (5.54) will always enhance terms beyond the scope of the calculation. By contrast, applying (5.55) does not introduce any such problems and thus this is the route that should be taken.

The above discussion is best illustrated by an explicit example and for this purpose the simpler pseudoscalar case $B \to K l^+ l^-$ will be used. The matrix element (5.52) is then proportional to:

$$U^\mu \propto \frac{(l_+ m_B - 2q^2)p^\mu + 2(p\cdot q)q^\mu}{l_+ m_B - q^2} = 2\frac{(p\cdot q)q^\mu - q^2 p^\mu}{l_+ m_B - q^2} + \frac{l_+ m_B p^\mu}{l_+ m_B - q^2} \quad . \tag{5.57}$$

The replacement (5.55) then fixes $U_p = -2q^2/(l_+ m_B - q^2)$, which amounts to dropping the second term on the right-hand side. The first term is gauge invariant on its own, and this is the complete result. Note that considering the coefficients of the p^μ and q^μ tensors separately would

have led to the wrong conclusion, since it is the second term rather than the first that contains the largest coefficient of p^μ. It is therefore crucial to use the approach illustrated in (5.54,5.55) to select the appropriate tensor whose coefficient will absorb the non-gauge invariant remainder, which here is p^μ rather than q^μ as would normally be chosen to make the basis orthogonal with the standard tensors (2.62).

Although the preceding discussion is in the context of the $1/m_b$ expansion, the main point stands independent of the particular expansion; if the approximation involved in computing a matrix element necessitates abandonment of strict gauge invariance, the superfluous degree of freedom must be eliminated in such a way that no kinematical singularities are introduced in the region of interest.

5.5 $B \to K^{(*)}$ results

Prior to presenting results for the isospin asymmetry, some small details of the calculation must be discussed. The hadronic inputs are the same as those used in Chapter 3, given in tables 3.1 and 3.2. Error estimates using a method that is perhaps slightly unusual but straightforward from a computational standpoint, which will be describe next.

5.5.1 Error estimation

Error estimates are computed in the following way: the central value of a result is computed using the central values of all inputs. To compute the error, a list of pseudo-random sample points is then generated from the probability distributions of the input parameters, the result computed for each sample point and then the standard deviation estimated from these results fixing the central value as the mean.

The obvious alternative approach is to compute the central value and the derivative w.r.t. each input parameter and then estimate the standard deviation of the result assuming the output distribution has a Gaussian shape. This is not done in the present case for two reasons: first, the input parameter space is quite large, and for large numbers of input parameters it is certainly less computationally intensive to take a Monte Carlo approach when the uncertainty is expected to be dominated by only a few, but it is not known which. The second reason is that a few of the integrals involved are numerically difficult, and they are difficult to compute to an accuracy of much more than one part in 10^3, so it is better to consider finite differences in the input parameters since direct estimates of the derivative are likely to be rather inaccurate.

To be specific, for a function $f(x)$, where x represents all N input parameters and is thus N-dimensional, the variance is estimated as

$$\sigma^2 = \frac{1}{n-1}\sum_{i=1}^{n}(f(x_i) - f(x_c))^2 \,, \tag{5.58}$$

where x_c is the central value of the input parameters and not included in x_i, and n is the number of sample points used to compute an error estimate, excluding the central value x_c. The points x_i are generated from the N-dimensional probability distribution of input parameters; note that x_i is varied for all parameters simultaneously, so *none* of its elements are equal to the central value of any input parameter. In effect, this is a primitive Monte Carlo integration over the input parameter distribution space. All input parameters are assumed to be Gaussian distributed with standard deviation equal to their quoted error, except for the renormalisation scale which will be discussed below. The functions $\mathcal{T}^{(T,\pm,0),0}$ are assigned an error of 20% which arises from the uncertainty in the form factors T_i, $A_{1,3}$, V and $f_{+,T}$ and non form factor corrections. This is imposed at the level of the $\mathcal{T}$ functions so that constraints such as $\mathcal{T}_+ \sim O(1/m_b)$ and $T_3 \sim (1-q^2)T_2$ are maintained. Note that this is not expected to accurately estimate the error in the right-handed form factor T_+, but that contribution is heavily suppressed in any case. A different approach will be taken in Section 6.8.2 where right-handed terms dominate.

To compute the scale uncertainty only 3 points are sampled: μ, $\mu/2$ and 2μ. The renormalisation scale is set to μ to compute the central value of a result. The error is computed as

$$\sigma_\mu^2 = \frac{1}{2n-1}\sum_{i=1}^{n}\left[\left(f\left(\frac{\mu}{2}\right) - f(\mu)\right)^2 + \left(f(2\mu) - f(\mu)\right)^2\right], \tag{5.59}$$

although in practice this is implemented by generating $2n$ pseudo-random numbers y_i in $[-1,1]$ and selecting $\mu/2$ or 2μ depending on whether $y > 0$. This may then be incorporated into the same procedure as sampling all other input parameters. The central renormalisation scale is taken to be $\mu = m_b = 4.7\text{GeV}$ for all processes except QLSS and $\mathcal{O}_8$, which are taken to be renormalised at $\mu' = \sqrt{\Lambda_H \mu}$, where $\Lambda_H = 0.5(2)\text{GeV}$ as in Chapter 3.

5.5.2 q^2 dependence and validity

In this section the validity of the LCSR approach in q^2 is discussed, as well as the underlying reasons for the shape of the graphs in Figure 5.8, which will also apply to beyond SM contributions to the asymmetry.

Physical spectrum and approximation ranges

The physical range of the decay spectrum is $4m_l^2 < q^2 < (m_B - m_K^{(*)})^2 = 22.9(19.3)\text{GeV}^2$. This calculation of the isospin asymmetry has employed two methods of calculation, LCSR and QCDF. The LCSR results in principle should be valid over nearly the whole q^2 spectrum provided that $m_B^2 - q^2 \gg m_B\Lambda_{\text{QCD}}$, excluding regions within $1-2\text{GeV}^2$ of partonic or hadronic resonances. However, the QCDF results are not so widely applicable, as they are limited by the assumption, already discussed, that $q^2 \ll m_B^2$ and terms of order q^2/m_B^2 have been neglected, as discussed in Section 5.4.5.

Considering the combination of these restrictions, the perturbative charm pair production threshold provides a convenient upper cutoff for the validity of these results. Results are therefore presented for the region $1\text{GeV}^2 < q^2 < 8\text{GeV}^2$, bounded on the lower end by the ρ meson resonance region and on the upper end by the J/Ψ meson resonance. In this region $q^2/m_B^2 < 0.3$ so the violation of the QCDF approximations is not expected to be too large.

It should be mentioned that it is possible to extend the LCSR calculation to include the effects of resonances by replacing the sum rule calculation with a narrow resonance approximation in the duality region of the meson. The details of this approach are given in Section 6.2.2; however, this method presents some difficulties in particular in the presence of anomalous thresholds, so it has not been attempted in the present case.

Isospin asymmetry in $B \to K^* ll$ decreases for high q^2

The q^2 spectrum of the isospin asymmetry turns out to be primarily dominated by the q^2 behaviour of the leading isospin-symmetric terms in the decay rather than the small isospin violating terms. The leading term in the decay rate is controlled by two factors:

a) $C_{9,10}$ are large in comparison with the other WC (q.v. table 2.1), partially as a result of a $1/\sin\theta_W^2 \simeq 4$ enhancement, where θ_W is the Glashow–Weinberg angle.

b) The leading terms in the $B \to Mll$ decay rate may be written as:

$$\begin{aligned} \mathcal{T}_T \sim &\quad [C_{9,10}^{\text{eff}}\mathcal{O}(1) + C_7^{\text{eff}}\mathcal{O}(1)] \\ \mathcal{T}_0 \sim &\sqrt{q^2}[C_{9,10}^{\text{eff}}\mathcal{O}(1) + C_7^{\text{eff}}\mathcal{O}(1)] \,, \\ \mathcal{T}_\pm \sim &\quad [C_{9,10}^{\text{eff}}\mathcal{O}(q^2/m_B^2) + C_7^{\text{eff}}\mathcal{O}(1)] \quad . \end{aligned} \tag{5.60}$$

This behaviour can be inferred from (2.69), (2.70), and (2.74). The underlying reason for this is that the semi-leptonic operators $\mathcal{O}_{9,10}$ do not generate the lepton pair via an intermediate photon but rather represent the contribution of the Z boson and loop corrections, and thus are not $1/q^2$ enhanced as $q^2 \to 0$.

It therefore follows that at low q^2 in $B \to K^* ll$ isospin violating terms only compete against C_7^{eff}, but at high q^2 they must compete with the much larger $C_{9,10}$ and hence the asymmetry decreases for large q^2. In $B \to Kll$ no such argument applies as in $\mathcal{T}_T$ C_7^{eff} and $C_{9,10}$ are on equal footing; however, the asymmetry is expected to be small over the whole q^2 range as a result.

High $q^2 \geq m_B(m_B - m_B\Lambda_{\text{QCD}})$ region

As mentioned above, the methods employed for this calculation are not valid for the low recoil regime, that is where $m_B^2 - q^2 \sim m_B\Lambda_{\text{QCD}}$. Nonetheless it can be expected that the isospin asymmetry will be small in this region, which can be seen from two separate arguments:

- Form factor contributions in the high q^2 region: in this region the $C_{7,9,10}$ form factors are expected to be enhanced by the presence of the nearby B_s^* resonance at $q^2 = m^2_{B_s^*}$, which can be seen from the plots and form factor parametrisations in [81]. No such enhancement is present in the isospin violating terms, except for UV isospin violating effects at $O(\alpha_s)$ in WA which are of course α_s and CKM suppressed. It is therefore expected that the isospin asymmetry in the high q^2 regime is suppressed in comparison to the intermediate regime by resonant contributions to the $C_{7,9,10}$ form factors, and doubly suppressed in comparison to the low q^2 region where isospin violating terms are enhanced by ρ, ω resonances and the proximity of the photon pole.

- Low recoil OPE: some time ago an OPE in q^2 and m_b^2 was proposed [170] for the low recoil region and implemented phenomenologically in [171]. It has also been recently reinvestigated in [172]. Obviously the low recoil region entails a different power counting in $1/m_b$ since q^2 is then a comparable large scale. In this language the leading isospin symmetry decay contributions come as dimension three matrix elements and isospin violating terms originate from higher dimensional operators (dimension 6 for WA and dimension 5 for QLSS and $\mathcal{O}_8$) and are therefore naturally small.

5.5.3 Isospin asymmetry in the Standard Model

The results of the calculation of the $B \to K^{(*)} l^+ l^-$ in the SM are shown in Figure 5.8, including a breakdown into the contributions of different operators. Tabulated data are given in appendix E.3. In both cases the isospin asymmetry for $q^2 > 1\,\text{GeV}^2$ is very small, below 1%. These results are similar to previous determinations of the isospin asymmetry [51, 134] in this range, which is a non-trivial result since this calculation has employed a mostly LCSR-based approach in contrast to the QCDF dominated approaches used previously[9]. The result for $B \to K^* l^+ l^-$ is consistent with the experimental average in the $[2.0, 4.3]\text{GeV}^2$ bin according to the Heavy Flavour Averaging Group (HFAG) [147]; however, the present experimental uncertainty in this bin is rather large. By contrast the $B \to K l^+ l^-$ asymmetry in this bin is currently $-0.42^{+0.20}_{-0.22}$ and thus the SM prediction is two standard deviations away from the experimental value[10]. Further experimental data in this channel are therefore eagerly anticipated. Finally, the comparison between this calculation of $B \to K^* \gamma$ and the HFAG world average is

$$\bar{a}_I(K^*\gamma)_{\text{HFAG}} = 5.2(2.6)\% \qquad \bar{a}_I(K^*\gamma)_{\text{LZ}} = 4.9(2.6)\% \tag{5.61}$$

and the two are in surprisingly good agreement. This value is also close to values previously found by [51, 84, 129]. It would therefore appear that at present the $B \to K^*(\gamma, l^+ l^-)$ channels

[9] [134] computed some terms using K^* sum rules with the B meson DA

[10] Although HFAG citation [147] is dated 2012, these data are taken from the June 2013 update on their website http://www.slac.stanford.edu/xorg/hfag/index.html.

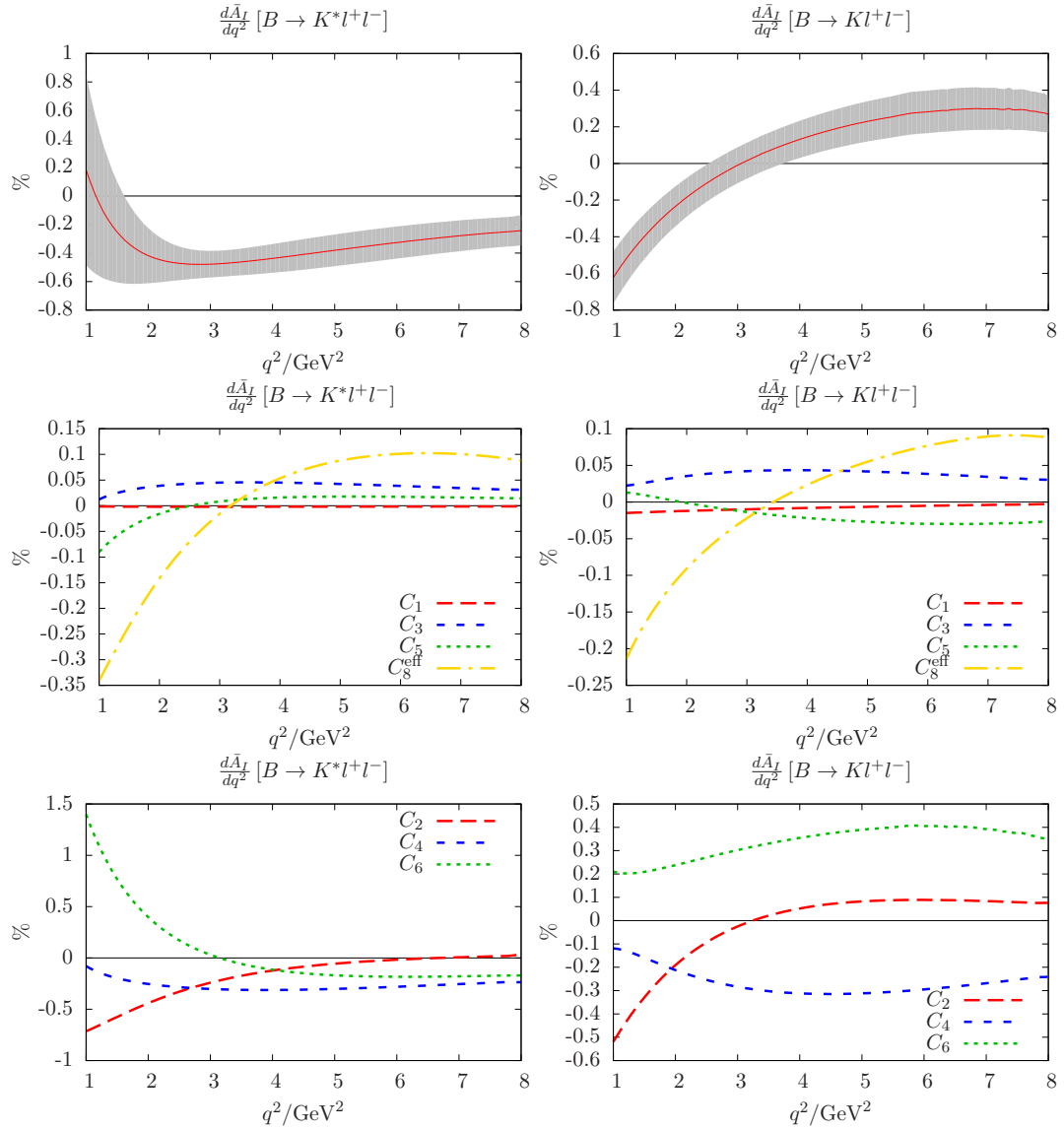

Figure 5.8: Isospin asymmetry results for $B \to K^{(*)} ll$ with grey error bands. Graphs in the left-hand column correspond to the $B \to K^*$ asymmetry and those in the right-hand column to the $B \to K$ asymmetry. The top row of graphs shows the total predicted isospin asymmetry in the SM. The middle and bottom rows show breakdowns into the contributions of seven separate short distance operators. The bottom graphs contain the larger contributions. The dominance of $C_6 + C_5/3$ has been found previously [84]. See Section 5.5.1 for details of the calculation of the grey error band.

$b \to s(d)$		WA		QLSS		$\mathcal{O}_8$	
Operator	WC	CKM	M.E.	CKM	M.E.	CKM	M.E.
$\mathcal{O}_{1,2}$	tree	$\lambda_u \sim \lambda^4(\lambda^3)$	tree	$\lambda_c \sim \lambda^2(\lambda^3)$	loop	-	-
$\mathcal{O}_{3-6}$	penguin	$\lambda_t \sim \lambda^2(\lambda^3)$	tree	$\lambda_t \sim \lambda^2(\lambda^3)$	loop	-	-
$\mathcal{O}_8$	penguin	-	-	-	-	$\lambda_t \sim \lambda^2(\lambda^3)$	loop
$\mathcal{O}_7$	penguin	not isospin sensitive & dominates rate in low q^2 region					
$\mathcal{O}_{9,10}$	penguin	not isospin sensitive & dominates rate in high q^2 region					

Table 5.3: Factors influencing the size of various operators contributing to the decays $B \to K^{(*)}l^+l^-$ in the SM. *WC* gives the type of the leading UV diagram which generates the given operator(s). *CKM* gives the magnitude of the CKM matrix coefficients appearing in the effective Hamiltonian (2.19) in terms of the Wolfenstein parameter $\lambda \simeq 0.22$. The alternative value in brackets applies to the $b \to d$ rather than the $b \to s$ transition, although there the CKM phases also play a significant role in the $B \to \rho$ decay, as discussed in Section 5.6.3. *M.E.* indicates whether the matrix element is loop suppressed. Note that the $\mathcal{O}_8$ contribution is considered to be loop suppressed in comparison to the WA terms, due to the $1/16\pi^2$ factor appearing in the operator definition (2.19); in any case it is clear from (5.34) that it is on the same level as QLSS. The last two rows of the table describe the contributions of the $\mathcal{O}_{7,9,10}$ operators which dominate the decay rate and therefore set the scale of the asymmetry. This is discussed in more detail in Section 5.5.2.

show no signs of non-SM physics.

The factors affecting the size of contributions of each operator to the isospin asymmetry are given in table 5.3, which also summarises the q^2 behaviour discussed in Section 5.5.2. It can be seen from the plots in Figure 5.8 that the dominant contribution to the $B \to K^*l^+l^-$ isospin asymmetry comes from the $\mathcal{O}_6$ operator followed by the $\mathcal{O}_2$ operator. This can be further analysed according to table E.2 to see that for $q^2 > 1\,\text{GeV}^2$ the C_6 contribution comes primarily from WA and the C_2 contribution from QLSS. Their relatively close magnitude indicates that the loop suppression in QLSS is similar to the suppression of C_6 arising from the fact that it is generated entirely by penguin diagrams in the UV. The contribution of the $\mathcal{O}_2$ operator through WA is negligible owing to its heavy CKM suppression. The situation for $B \to K^*\gamma$ is rather different because WA is strongly enhanced by the nearby ρ resonance here as described in Section 5.3.6. This effect is absent at the present level of approximation in the QLSS calculation[11]. Therefore $B \to K^*\gamma$ is strongly C_6 dominated, as has been found previously [84].

For $B \to Kl^+l^-$ the contributions of $\mathcal{O}_{2,4,6}$ are comparable, which is a result of the WA and QLSS contributions for $\mathcal{O}_{4,6}$ and $\mathcal{O}_2$ respectively, and again the $\mathcal{O}_8$ contribution is small. This is broadly similar to the $B \to K^*$ result at $q^2 > 4\text{GeV}^2$; the differences in the detail will be the result of the absence of transverse polarisations and the difference in the structure of twist-3 terms as discussed in Section 2.10. Recent LHCb results for $B \to Kl^+l^-$ [21] indicate a large deviation from zero at the level of 4σ when integrated over q^2 and even at 2σ in the $[2.0, 4.3]\,\text{GeV}^2$ bin, where the theoretical calculation is most trustworthy. Since the prediction of the isospin asymmetry (Figure 5.8) is at the 1% level and the world average measured asymmetry is 40% [147] in this bin, this channel could potentially be a strong signal of beyond

[11] The fermion traces that would be required to compute this contribution in LCSR have been evaluated and they are zero, as occurred in the $\mathcal{O}_8$ case, so this is not an artefact but genuine α_s suppression.

SM physics if improved experimental measurements have a similar magnitude. Of course, in that case it would be necessary to scrutinise the theoretical calculation again; however, it is hard to believe that the result could be out by an order of magnitude. This issue will be discussed again briefly in Section 5.8.

5.6 $B \to \rho$ isospin asymmetry

$B \to \rho$ decays differ from $B \to K^*$ decays in two important ways: first, the CKM hierarchy for the effective Hamiltonian is different, and second the neutral ρ meson is a mixture of two valence quark states $\rho^0 \sim (\bar{u}u - \bar{d}d)$ as explained below (5.2).

In fact, it transpires that the first point is not important in the CP-averaged isospin asymmetry. As will be discussed further in Section 5.6.3, the CP-averaged asymmetry is sensitive to the real part of the CKM coefficient, given by

$$\mathrm{Re}\,\frac{\lambda_u^{bd}}{\lambda_t^{bd}} = -\left|\frac{\lambda_u^{bd}}{\lambda_t^{bd}}\right| \cos\alpha_{\mathrm{CKM}} \tag{5.62}$$

where $\lambda_i^{bd} = V_{id}^* V_{ib}$. The present PDG value gives $\cos\alpha_{\mathrm{CKM}} = 0.02(7)$ [123] and hence the contribution of C_2 to the asymmetry is suppressed by an amount comparable to the λ^2 suppression in the $B \to K^*$ case. This occurrence will be exploited to create a stringent test of the SM in Section 5.7.

The isospin asymmetry in $B \to \pi l^+ l^-$ will not be computed here. The extension of the results for $B \to K l^+ l^-$ in the previous section is straightforward; however, at present $B^+ \to \pi^+ l^+ l^-$ has only recently been observed at LHCb [173] and the neutral mode remains unseen. An experimental determination of the isospin asymmetry in this channel therefore seems some way off. The ρ–ω asymmetry might also be considered as in [129] except that in this case there is a substantial asymmetry due to QCD effects; by comparison the asymmetry due to electromagnetic effects is small and will only be relevant when a more precise theoretical determination of the leading form factor is available.

5.6.1 Extending the effective Hamiltonian for $B^0 \to \rho^0 l^+ l^-$

Since the neutral ρ meson is a mixture of valence quark states $(\bar{u}u - \bar{d}d)/\sqrt{2}$, alternative arrangements of the four quark operators in the WA diagrams are possible either coupling to the $\bar{u}u$ state (absent in the K^* case) or swapping the d quark connections owing to the presence of more than one d quark line in the diagram. To recover the factorised form (5.10) the four quark operator can be rearranged by a Fierz transform of the Dirac structure, and a similar operation on the colour matrices. This transform mixes the colour singlet and octet operators and therefore introduces the octet operators which do not couple to the K^* into the ρ^0 channel.

Accordingly colour-octet operators are defined analogously to the singlet operators (5.7) as

$$O_i^{\mathrm{WA}} = \bar{q}\Gamma_1 b\,\bar{s}\Gamma_2 q \implies O_i^{\mathrm{WA},8} = \frac{1}{4}\bar{q}\lambda^a\Gamma_1 b\,\bar{s}\lambda^a\Gamma_2 q \quad , \tag{5.63}$$

so that for example $O_1^{\mathrm{WA},8} = \frac{1}{4}\bar{q}\lambda^a b\,\bar{s}\lambda^a q$, and the effective Hamiltonian is modified (5.8) to be:

$$\mathcal{H}^{\mathrm{WA},q} = -\frac{G_F}{\sqrt{2}}\lambda_t \sum_{i=i}^{10}\left[a_i^q O_i^{\mathrm{WA}} + a_i^{8q} O_i^{\mathrm{WA},8}\right] \quad . \tag{5.64}$$

In spite of the introduction of these new operators, the number of linearly independent WCs contributing to WA cannot in fact have increased since the situation presented in table 5.1 is entirely due to Lorentz invariance constraints on the factorised matrix elements. There are therefore again only six linearly independent contributions and the contribution of $B^0 \to \rho^0 l^+ l^-$ to the isospin asymmetry will be presented in terms of a set of effective coefficients $\tilde{a}_i^d$, which couple to the same Feynman graphs as in the $B^0 \to K^{*0}$ case. Results for the $B \to \rho$ asymmetry will therefore be presented in terms of

$$\rho^{\pm} \leftrightarrow a_i^u \qquad\qquad \rho^0 \leftrightarrow \tilde{a}_i^d \tag{5.65}$$

where the effective coefficients $\tilde{a}_i^d$ are linear combinations of a_i^d and $a_i^{8u,d}$.

The formulae for the charged coefficients a_i^u in terms of SM WCs are the same as for the K^* and are given in (5.9). The effective neutral coefficients $\tilde{a}_i^d$ in the SM are given by:

$$\begin{aligned}
\tilde{a}_2^d &= \tilde{a}_4^d = 2\left(\frac{C_5}{N_c} + C_6\right) \\
\tilde{a}_5^d &= -\tilde{a}_6^d = \left(\frac{C_3}{N_c} + C_4\right) + \frac{\lambda_u}{\lambda_t}\left(C_1 + \frac{C_2}{N_c}\right) \\
\tilde{a}_9^d &= \tilde{a}_{10}^d = 0 \quad .
\end{aligned} \tag{5.66}$$

Formulae for the colour octet coefficients a_i^{8q} in the SM and the effective coefficients $\tilde{a}_i^d$ in the general case are given in appendix E.2, and the SM formulae given in (5.66) may be derived from those and (5.9). An important aspect of (5.66) is that the coefficients of the QCD penguin operators $C_{3\ldots6}$ are the same as in the $B \to K^*$ case (5.9), which will be important in Section 5.7, and is due to the left-handed structure of the SM operators.

5.6.2 Isospin asymmetry $B \to \rho l^+ l^-$ in the Standard Model

Results for the $B \to \rho l^+ l^-$ isospin asymmetry are shown in Figure 5.9. Again, tabulated data are provided in appendix E.3. The general discussion of q^2 behaviour in Section 5.5.2 still applies in this case.

Inconveniently, the experimental measurement of the isospin asymmetry in the $B \to \rho$ case

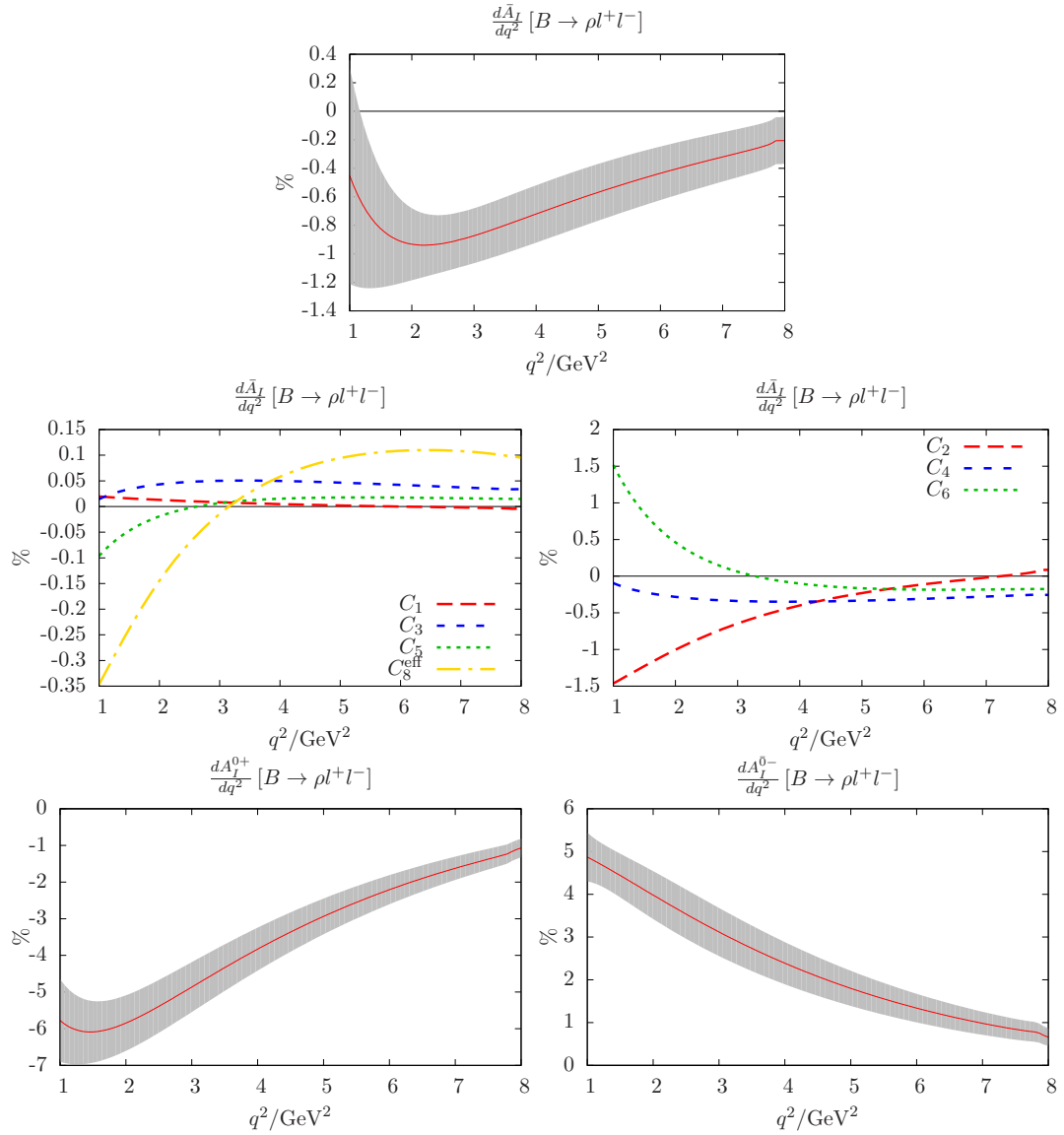

Figure 5.9: The CP-averaged isospin asymmetry for $B \to \rho l^+ l^-$ with grey error bands is shown in the top row. The middle row shows the contributions of different SM operators to the CP-averaged isospin asymmetry in $B \to \rho l^+ l^-$. The right hand graph shows the larger contributions. Note that unlike at $q^2 = 0$ the C_2 contribution is comparable to the C_6 contribution here; this is due to a small weak phase arising from C_9^{eff} alleviating the $\cos\alpha_{\mathrm{CKM}}$ suppression slightly. See Section 5.5.1 for details of the calculation of the grey error band. The bottom row shows the isospin asymmetry for individual CP modes of $B \to \rho l l$; $b \to d$ and $\bar{b} \to \bar{d}$-type. The isospin asymmetry differs greatly between CP conjugate modes since the separate modes depend on the combination of strong and weak phases both of which are sizeable. This effect is explained in detail in 5.6.3.

is calculated differently from the $B \to K^*$ case, as [174]

$$\Delta(\rho\gamma) = \frac{\tau_{B^0}}{2\tau_{B^+}} \frac{\mathcal{B}(B^+ \to \rho^+\gamma)}{\mathcal{B}(B^0 \to \rho^0\gamma)} - 1 = \frac{-2\bar{a}_I(\rho\gamma)}{1+\bar{a}_I(\rho\gamma)} \overset{a_I(\rho\gamma)\ll 1}{\approx} -2\bar{a}_I(\rho\gamma) \tag{5.67}$$

$$\bar{a}_I(\rho\gamma) = -\frac{\Delta(\rho\gamma)}{2+\Delta(\rho\gamma)} \quad , \tag{5.68}$$

where the CP-averaged asymmetry has been used. In this normalisation, the present result compares with the measured value as [147]

$$\Delta(\rho\gamma)_{\rm HFAG} = -46(17)\% \,, \qquad \Delta(\rho\gamma)_{\rm LZ} = -10(6)\% \,. \tag{5.69}$$

Δ is quoted as a percentage following convention, even though $\Delta(\rho\gamma) = 1$ has no particular significance. For completeness the result of this calculation for the CP-averaged isospin asymmetry in $B \to \rho\gamma$ in using the K^* type normalisation is

$$\bar{a}_I(\rho\gamma)_{\rm HFAG} = 30^{+16}_{-13}\% \,, \qquad \bar{a}_I(\rho\gamma)_{\rm LZ} = 5.2(2.8)\% \,, \tag{5.70}$$

where (5.69) and (5.67) have been used to produce the "HFAG" value. This result is comparable to that obtained in [129][12] and somewhat larger than that in [175], principally due to a different choice of $\alpha_{\rm CKM}$.

The result (5.69) is marginally consistent with the current experimental status. Using table 12 of [129], with a linear extrapolation, $|V_{\rm td}/V_{\rm ts}|$ can be extracted from $R_\rho = \mathcal{B}(B \to \rho\gamma)/\mathcal{B}(B \to K^*\gamma)$. Given that the asymmetry (5.70) is rather large, this calculation is performed separately in the charged and neutral channels to give

$$\left|\frac{V_{\rm td}}{V_{\rm ts}}\right|_{R_{\rho^0}} = 0.229(25) \qquad \left|\frac{V_{\rm td}}{V_{\rm ts}}\right|_{R_{\rho^+}} = 0.165(25) \qquad \left|\frac{V_{\rm td}}{V_{\rm ts}}\right|_{\rm PDG} = 0.211(7) \quad , \tag{5.71}$$

where the current value from PDG [123] is quoted for comparison. The values used for the $B \to \rho$ and $B \to K^*$ branching fractions are given in (5.80). The results in (5.71) rather indicate that it is the $B^+ \to \rho^+$ rate which appears to be causing the majority of the discrepancy from the prediction (5.69).

5.6.3 The effect of CP averaging in ρ meson decays

The results presented in the previous subsection are all based on CP-averaged branching fractions. To examine the effect of CP averaging on the isospin asymmetry, it is useful to begin by

[12] Note that [129] uses the opposite sign convention for $\Delta(\rho\gamma)$. The sign convention used in (5.69) matches that used by Belle [174] and HFAG.

parametrising a term in a matrix element as

$$M = |M| e^{i\delta_{\text{strong}}} e^{i\phi_{\text{weak}}} \qquad \bar{M} = |M| e^{i\delta_{\text{strong}}} e^{-i\phi_{\text{weak}}} \quad , \tag{5.72}$$

which allows the CP-conjugate term $\bar{M}$ to be written explicitly. In the context of computing the isospin asymmetry in $B \to \rho\gamma$, $\mathcal{T}_{\pm}^{0}(0)\Delta_{\pm}^{d-u}(0)$ is needed. Since $\mathcal{T}_{\pm}^{0}(0)$ is real, it follows from (5.3) that

$$\begin{aligned} &\text{no } CP\text{-average:} \quad a_I^{\bar{0}-}[B \to \rho\gamma] \propto \mathcal{T}_{-}(0)\,\text{Re}\left[\mathcal{T}_{-}^{V,d}(0) - \mathcal{T}_{-}^{V,u}(0)\right] \\ &CP\text{-average:} \quad \bar{a}_I[B \to \rho\gamma] \propto \mathcal{T}_{-}(0)\,\text{Re}\left[\mathcal{T}_{-}^{V,d}(0) - \mathcal{T}_{-}^{V,u}(0) + \bar{\mathcal{T}}_{-}^{V,d}(0) - \bar{\mathcal{T}}_{-}^{V,u}(0)\right] \quad , \end{aligned} \tag{5.73}$$

where again $\bar{\mathcal{T}}$ denotes a CP conjugate. The isospin violating part $\mathcal{T}_i^{V,q}$ is the sum of a number of terms, however it is clear from (5.72) and (5.73) that the effect of CP averaging is schematically:

$$\begin{aligned} &\text{no } CP\text{-average:} \quad a_I^{\bar{0}-}[B \to \rho\gamma] \sim \text{Re}[e^{i\delta_{\text{strong}}} e^{i\phi_{\text{weak}}}] \\ &CP\text{-average:} \quad \bar{a}_I[B \to \rho\gamma] \sim \text{Re}[e^{i\delta_{\text{strong}}}]\,\text{Re}[e^{i\phi_{\text{weak}}}] \quad . \end{aligned} \tag{5.74}$$

The situation away from $q^2 = 0$ is essentially the same, although the leading term can also have small weak and strong phases there from $C_9^{\text{eff}}(q^2)$ so in that case the phases δ_{strong} and ϕ_{weak} are relative. It is obvious from (5.74) that the CP averaged result will be significantly different to the CP eigenstate results if both the strong and weak phases are large.

The question then is when there are both large strong and weak phases present. The weak phase is not q^2 dependent, so will be discussed first. For the K^*, $\lambda_c^{bs}/\lambda_t^{bs}$ is real up to λ^3 in the Wolfenstein parametrisation (2.8), and the contribution of terms proportional to λ_u is small, so the weak phase is essentially zero. By contrast, the contribution of the $\mathcal{O}_2$ operator to the ρ meson decay is dependent on weak phase $\arg \lambda_u^{bd}/\lambda_t^{bd} = \alpha_{\text{CKM}}$ and therefore in the CP average this term is suppressed by $\cos\alpha_{\text{CKM}} = 0.02(7)$ [123].

The question of strong phases then arises. Since strong phases in the leading isospin symmetric term are small, the important question is the size of the strong phase in the isospin violating terms. The contribution of the $\mathcal{O}_8$ operator to the isospin asymmetry is rather small, so will be ignored here; only the QLSS and WA terms will be considered. Away from $q^2 = 0$ it can be seen from Figure 5.2 that weak annihilation in vector current operators has a large phase, but no phase at $q^2 = 0$. All other WA operators give no strong phase at $q^2 = 0$, and have a strong phase away from $q^2 = 0$ when they have an ISR term as given in table 5.1. QLSS terms generically have a non-zero strong phase, however they are small compared to WA at $q^2 = 0$. It is therefore concluded that the generic case is that large strong phases are present

away from $q^2 = 0$, within the range of validity of this calculation results, but absent at $q^2 = 0$, and it is expected that as a result the ρ meson isospin asymmetry will be strongly affected by CP averaging but the K^* asymmetry will not. The isospin asymmetry for $B \to \rho$ in the two different CP channels is shown in the bottom row of Figure 5.9 and confirms this analysis.

The result that the $K^{(*)}$ isospin asymmetry is CP independent is entirely in the context of the SM. It would therefore be interesting in a future experiment to measure the CP modes separately as a difference between the two results would be a strong indication of beyond-SM physics. Unfortunately as described in the introduction, this is impossible for the K system since experimentally the K^0_S is measured in this case which implies CP averaging.

5.7 $B \to (K^*, \rho)$ isospin asymmetry splitting as an SM null test

Following on from the previous section, the smallness of $\cos\alpha_{\rm CKM}$ can be exploted to construct an observable with extremely small theoretical uncertainty, although the present experimental uncertainty will be somewhat larger.

The prediction that will be made is essentially that the isospin asymmetry for $B \to K^*\gamma$ and $B \to \rho\gamma$ should be similar, once differences in the leading form factors and hadronic parameters are accounted for. The reduction in theoretical uncertainty arises because the dominant source of uncertainty in the $B \to (K^*, \rho)\gamma$ isospin asymmetry comes from the scale dependence of Wilson coefficients, since the leading term is proportional to C_6 which is small but mixes with the large coefficient C_2 under renormalisation group running. This scale dependence can be cancelled by constructing an appropriate ratio, namely

$$\delta_{a_I} \equiv 1 - \frac{\bar{a}_I(\rho\gamma)}{\bar{a}_I(K^*\gamma)} R_{\rho K^*} = 1 + \frac{\Delta(\rho\gamma)}{(2+\Delta(\rho\gamma))\bar{a}_I(K^*\gamma)} R_{\rho K^*} \quad , \tag{5.75}$$

where

$$R_{\rho K^*} \equiv \sqrt{\frac{\bar{\Gamma}(B \to \rho\gamma)}{\bar{\Gamma}(B \to K^*\gamma)}} \left|\frac{V_{ts}}{V_{td}}\right| \tag{5.76}$$

and where a barred partial width $\bar{\Gamma}$ implies a CP-average, and omission of charges implies an isospin average[13]. The dominant contributions to the right-hand side of (5.75) are:

$$\bar{a}_I(V\gamma) \approx \frac{C_6 + C_5/3}{C_7^{\rm eff}} \frac{f_V^\perp F^{\rm WA}(0)}{T_1^V(0)} + \ldots \quad \bar{\Gamma}(B \to V\gamma) \approx \frac{3\alpha C_F}{8\pi} \left|\lambda_t C_7^{\rm eff}\right|^2 |T_1^V(0)|^2 \quad , \tag{5.77}$$

where the dots stand for $C_{3,4}$-contributions, which lead to small corrections to δ_{a_I} because K^* and ρ cases are very similar; quark mass corrections, and $B^0 \to \rho^0$ diagrams at $O(\alpha_s^2)$, where the different structure of the ρ^0 matters even for small $\cos\alpha_{\rm CKM}$. The function $F^{\rm WA}(0)$ is essentially the contribution of the functions $F^q_{j,(2,4)}(q^2)$ defined in (5.24) to the isospin asymmetry, with

[13] For the ρ-meson this implies $\bar{\Gamma}(B \to \rho\gamma) = \frac{1}{2}\bar{\Gamma}(B^+ \to \rho^+\gamma) + \bar{\Gamma}(B^0 \to \rho^0\gamma)$ due to $\rho^0 \sim (\bar{u}u - \bar{d}d)/\sqrt{2}$ as discussed previously.

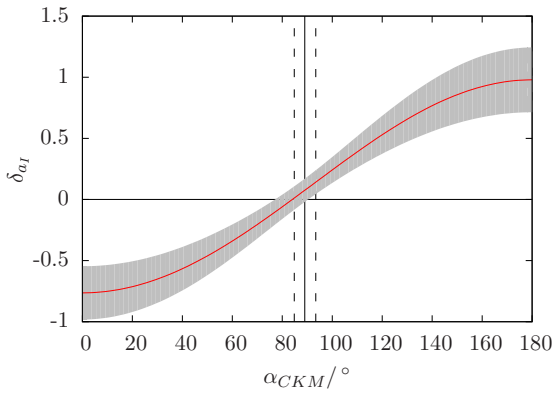

Figure 5.10: Plot of the effective ρ to K^* isospin asymmetry difference δ_{a_I} (5.75) as a function of the CKM matrix angle $\alpha_{\rm CKM}$. Vertical lines indicate the current experimental value of $\alpha_{\rm CKM}$ [123] and its uncertainty. At the present small value of $\cos\alpha_{\rm CKM}$, δ_{a_I} is well determined theoretically.

the meson decay constant $f^\perp$ explicitly factored out. As can be seen from the full results in (E.1), this function then only depends on the final state meson through higher twist Gegenbauer moments. Since $F^{\rm WA}(0)$ is approximately independent of the final state, it follows from (5.75) and (5.77) that

$$\delta_{a_I} = 1 - \frac{f_\rho^\perp}{f_{K^*}^\perp} + \text{small corrections} \quad , \tag{5.78}$$

where the corrections are expected to be much smaller than 1, and thus the leading source of uncertainty, scale dependence of $C_6 + C_5/3$, has dropped out. It is also convenient for this construction that[14] $f_\rho^\perp/f_{K^*}^\perp = 0.98(8)$ and thus it is expected that $\delta_{a_I} \approx 0$. The factor $R_{\rho K^*}$ is included to eliminate the dependence on form factors T_1^V since there is no reason to leave factors which may be so easily accounted for in (5.78).

The full calculation of δ_{a_I} is a straightforward extension of the calculation of the isospin asymmetry, except that in this particular case the linearising approximation used to reach (5.3) is avoided in favour of the definition (5.2). Quadratic corrections to the isospin asymmetry are included in this case because the cancellation of uncertainty raises the $\lambda_u^2 C_2$ WA in the $B \to \rho$ transition above the level of error in the calculation and thus the $\cos\alpha_{\rm CKM}$ suppression is not quite as effective as it appears in the linear approximation.

In terms of experimentally measured quantities (5.2) is given by

$$\delta_{a_I} = 1 - \left|\frac{V_{ts}}{V_{td}}\right| \frac{2\frac{\tau_{B^+}}{\tau_{B^0}}\mathcal{B}(B^0 \to \rho^0\gamma) - \mathcal{B}(B^+ \to \rho^+\gamma)}{\frac{\tau_{B^+}}{\tau_{B^0}}\mathcal{B}(B^0 \to K^{*0}\gamma) - \mathcal{B}(B^+ \to K^{*+}\gamma)} \sqrt{\frac{\frac{\tau_{B^+}}{\tau_{B^0}}\mathcal{B}(B^0 \to K^{*0}\gamma) + \mathcal{B}(B^+ \to K^{*+}\gamma)}{2\frac{\tau_{B^+}}{\tau_{B^0}}\mathcal{B}(B^0 \to \rho^0\gamma) + \mathcal{B}(B^+ \to \rho^+\gamma)}} \quad . \tag{5.79}$$

[14] See table 3.2.

The values [123]

$$\begin{aligned} \frac{\tau_{B^+}}{\tau_{B^0}} &= 1.079(7) & \left|\frac{V_{\rm td}}{V_{\rm ts}}\right| &= 0.211(7) \\ \mathcal{B}(B^+ \to \rho^+\gamma) &= 9.8(2.5) \times 10^{-7} & \mathcal{B}(B^0 \to \rho^0\gamma) &= 8.6(1.5) \times 10^{-7} \\ \mathcal{B}(B^+ \to K^{*+}\gamma) &= 4.21(18) \times 10^{-5} & \mathcal{B}(B^0 \to K^{*0}\gamma) &= 4.33(15) \times 10^{-5} \end{aligned} \tag{5.80}$$

are used and errors combined in quadrature to estimate error. The prediction therefore compares with the experimental result as

$$[\delta_{a_I}]_{\rm exp} = -4.0(3.5) \qquad [\delta_{a_I}]_{\rm LZ} = 0.10(11) \tag{5.81}$$

and it can be seen that the theoretical uncertainty is indeed small[15] at 11% compared to roughly 50% uncertainties in determining the isospin asymmetry in (5.61) and (5.70). Given the sensitivity of this observable to $\alpha_{\rm CKM}$ it has also been plotted as a function of that variable in Figure 5.10. Improved measurements of the inputs to (5.79) might therefore provide a signal of beyond-SM physics in certain cases. It should be noted that the ratios $|V_{ts}/V_{td}|$ and τ_{B^+}/τ_{B^0} are already experimentally sufficiently well determined and contribute a negligible amount to the experimental uncertainty in (5.81). The uncertainty in this result arises mainly from the ratio of the isospin conjugate branching fractions; in fact, although the current experimental value of the $B \to \rho$ isospin asymmetry has a larger asymmetry than the K^* case, the size of the errors in percentage terms is similar and thus improved determination of all branching fractions in (5.80) is necessary to reduce substantially the uncertainty in (5.81).

It is clear that the structure of the SM is responsible for the smallness of δ_{a_I} (5.75). In general the quantity δ_{a_I} is thus highly sensitive to certain kinds of new physics which act differently on the $B \to \rho$ and $B \to K^*$ decays. Some examples are:

- *Non-MFV isospin violation*: if the ratios between WCs for $b \to s$ and $b \to d$ transitions are not $\lambda_t^{bs}/\lambda_t^{bd}$.
- *UV isospin violation*: if four quark operators of the type (5.7) with different WCs for $u-$ and $d-$ type quarks are present, because the $K^{*,0}$ and ρ^0 valence quark states are not a simple matter of an $s \to d$ replacement.
- *Colour octet operators*: as with the previous point, non-SM structure of colour octet operators may give significant contribution to the $B \to \rho^0$ decay; see appendix E.2 for formulae.

Some examples to illustrate the sensitivity of this measurement to beyond SM physics are provided in table 5.4.

[15] It should be compared to 1 according to (5.78).

x	$a_1^d \to a_1^d + x$	$a_8^d \to a_8^d + x$
-0.3	1.16(15)	1.71(20)
-0.2	0.82(11)	1.21(13)
-0.1	0.47(9)	0.67(9)
0.1	−0.29(14)	−0.51(15)
0.2	−0.68(18)	−1.14(21)
0.3	−1.08(23)	−1.78(28)

Table 5.4: Examples of the effect of introducing non-SM operators on the value δ_{a_I}. All a_i^q are fixed to their SM values and then one is altered by the specified amount as specified in at the top of the table. The resulting variation of δ_{a_I} can be large and is primarily the result of the ρ^0 coupling to a different combination of a_i as discussed in Section 5.6.1, and these are therefore examples of UV isospin violation. The uncertainties quoted in this table do not include uncertainty from varying the renormalisation scale: this would require a computation of the scale dependence of the extended effective Hamiltonian (5.64) and is thus beyond the scope of this work. The renormalisation scale is taken to be the usual central value, $\mu = 4.7\text{GeV}$.

5.8 Isospin asymmetries beyond the Standard Model

In this section the problem of applying this calculation to identifying any beyond-SM contributions to $B \to (K^*, \rho)$ isospin asymmetries will be approached. Before discussing the application of the results in sections 5.3 and 5.4, the other possible source of potential deviation from the SM prediction should be mentioned: a sizeable deviation in the rate from the SM expectation. The possible beyond-SM isospin symmetric operators that could affect the rate are the right-handed $\mathcal{O}'_{7,9,10}$; however, they are already quite constrained [100, 176, 177].

An important question is therefore what present constraints there are on four quark operators? The contributions of the operators defined in (5.8) and (5.28) have been plotted to the $B \to (K, K^*, \rho) l^+ l^-$ asymmetries in figures 5.11 and 5.12. Given that the present experimental uncertainty in $B \to K^* l^+ l^-$ is rather large and $B \to \rho l^+ l^-$ has not been observed, no attempt is made to constrain the four-quark operators in these channels pending future, more accurate, measurements. Two sources of constraints on four-quark operators are identified:

- $B \to \rho/K^*\gamma$ *isospin asymmetries.* Bounds are derived on the four quark operators in the following way: the discrepancy in the WC of each operator that would be required to saturate the experimental uncertainty at the 2σ level, for values given in (5.61) and (5.70), is computed. The results of this procedure are given in tables 5.5 and 5.6. Note that these constraints are calculated by varying only a single operator at a time from its SM value, which of course cannot be expected to be a realistic scenario. Nonetheless this would generically be expected to provide approximately correct constraints unless there are strong cancellations between the contributions of beyond-SM operators. As can be seen from figures 5.11 and 5.12, such a cancellation would not hold for the entire q^2 range in $B \to (K^*, \rho) l^+ l^-$, so if the electromagnetic decay does not produce results there is still hope for the semi-leptonic channel.

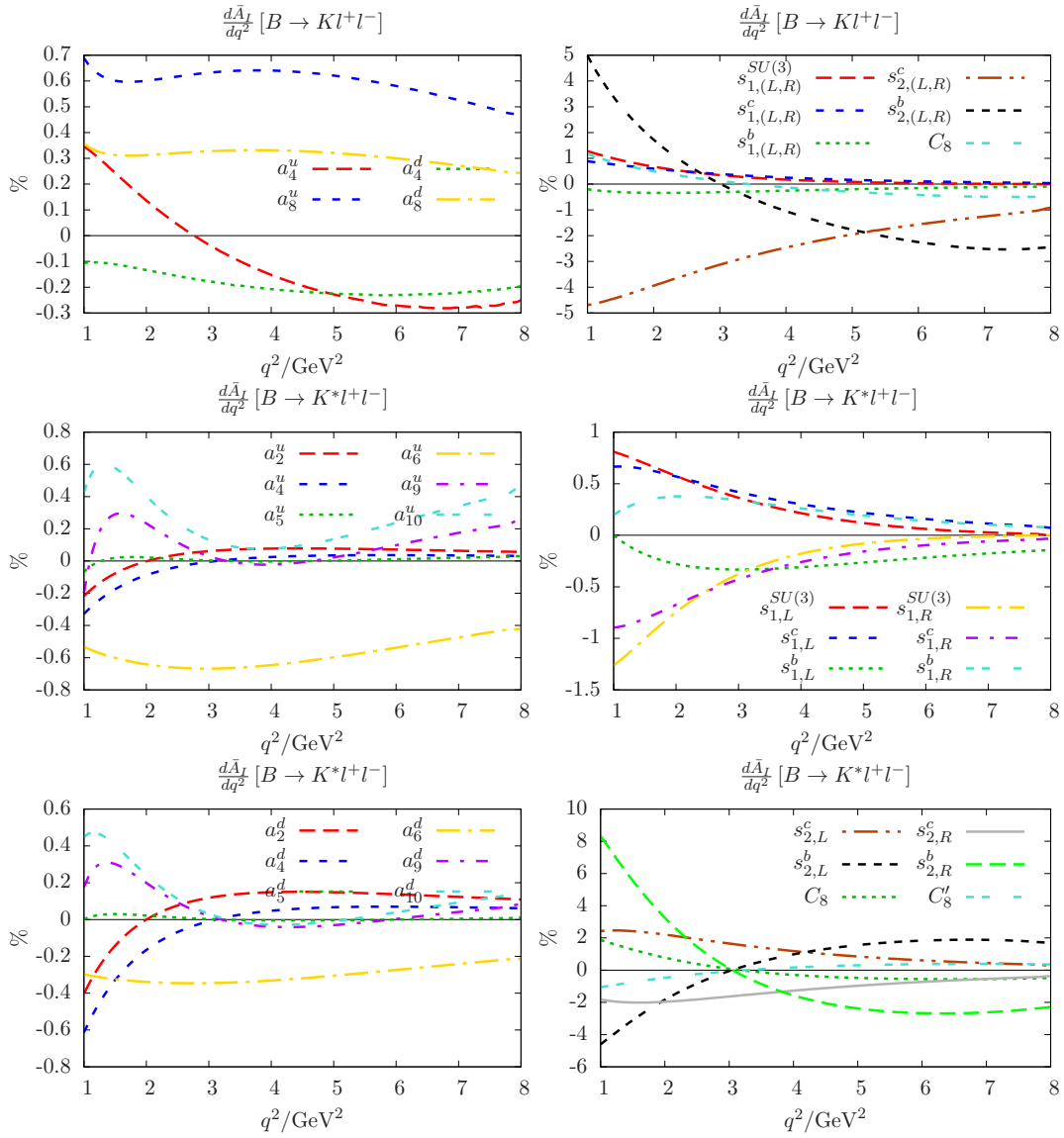

Figure 5.11: Breakdown of contributions of WA (a_i), QLSS ($s^f_{x,\chi}$) and $\mathcal{O}_8^{(\prime)}$ to the isospin asymmetry $B \to K^{(*)}ll$ in the linear approximation (5.3). Contributions have been split as detailed in table 5.3 into different graphs in order to make them more readable. Note that $a_i^q = 0.1$ and $s^f_{x,\chi} = 1$ are used to produce these figures, as in the tables.

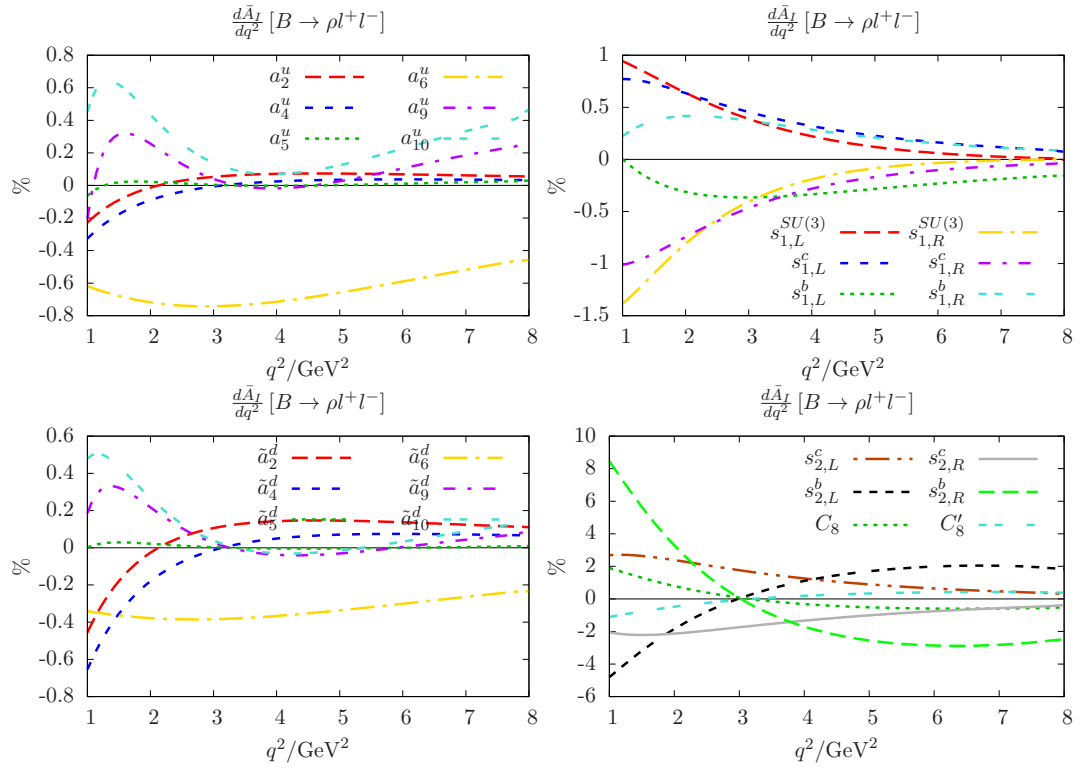

Figure 5.12: Breakdown of contributions of WA (a_i), QLSS ($s^f_{x,\chi}$) and $\mathcal{O}_8^{(\prime)}$ to the isospin asymmetry $B \to \rho ll$ in the linear approximation (5.3). Contributions have been split as detailed in table 5.3 into different graphs in order to make them more readable. Note that $a_i^u = 0.1$, $\tilde{a}_i^d = 0.1$ and $s^f_{x,\chi} = 1$ are used to produce these figures, as in the tables.

$B \to K^*\gamma$	Min.	SM	Max.		Min.	SM	Max.
a_2^u	-0.39	-0.068	0.25	a_2^d	-0.24	-0.068	0.11
a_4^u	-0.38	-0.068	0.25	a_4^d	-0.24	-0.068	0.10
a_5^u	-0.41	-0.021	0.37	a_5^d	-0.67	-0.028	0.61
a_6^u	-0.62	0.021	0.57	a_6^d	-1.0	0.028	1.0
a_9^u	-0.049	0	0.049	a_9^d	-0.080	0	0.080
a_{10}^u	-0.048	0	0.048	a_{10}^d	-0.080	0	0.080

Table 5.5: Constraints on WCs a_i^q (5.8) from $B \to K^*\gamma$ at 2σ, assuming no accidental cancellations occur, along with SM values. $0 < \bar{a}_I(K^*\gamma) < 10\%$ is assumed, and constraints derived from table E.2, assuming that only a single coefficient a_i^q deviates from its SM value. SM values are calculated from (5.9) and table 2.1. All constraints are for the real part of these coefficients; the imaginary part is not constrained by the isospin asymmetry unless it is extremely large and the linear approximation (5.3) is invalidated.

- *Non-leptonic decays.* Four quark operators give significant contribution to non-leptonic decays where the electromagnetic and chromomagnetic operators occur at subleading orders in the gauge couplings. A deviation from SM values of these operators would therefore be expected to give a more significant contribution to those processes than semi-leptonic decays. However, it is much more difficult to predict these processes from a theoretical standpoint since the relative strong phases of different contributions suffer significant uncertainties, e.g. [118]. The MFV structure of the SM can be constrained from studies of these decays [178–180] which fit CKM matrix angles but cannot distinguish Lorentz and colour structure of different operators at all. Constraints on four quark electric penguin operators have however been obtained in [181, 182][16]. It would appear from those papers that beyond-SM contributions to four quark operators are at most $O(1)$ corrections to their SM values. A global fit of all experimental data might be able to provide better constraints on the WC than are currently available, but this is beyond the scope of this work.

It should be noted that constraints from isospin asymmetries are essentially complementary to those from direct CP asymmetries, since isospin asymmetries are sensitive to corrections to the real parts of WCs, whereas direct CP asymmetries are sensitive to the imaginary parts, or rather CP-odd phases.

Finally the current experimental state of $B \to Kl^+l^-$ must be evaluated in view of the above discussion. The SM results in Figure 5.8 imply that for beyond-SM corrections in one operator to account for isospin asymmetry at the 50% level would require a WC an order of magnitude larger than its SM value. The above discussion of the effects of four quark operators in non-leptonic decays seems to imply that this scenario is rather unlikely.

[16] Note that in this calculation, the contribution of these operators can be easily included since the effective WCs coupling to u and d-type quarks have been separated.

$B \to \rho\gamma$	SM	Bound		SM	Bound
a_2^u	-0.068	-4.1	$\tilde{a}_2^d$	-0.068	-2.1
a_4^u	-0.068	-4.0	$\tilde{a}_4^d$	-0.068	-2.0
a_5^u	-0.021	4.9	$\tilde{a}_5^d$	-0.028	8.1
a_6^u	0.021	-7.6	$\tilde{a}_6^d$	0.028	-13
a_9^u	0	0.56	$\tilde{a}_9^d$	0	0.94
a_{10}^u	0	0.56	$\tilde{a}_{10}^d$	0	0.93

Table 5.6: Constraints on operators a_i^q from $B \to \rho\gamma$ at 2σ, assuming no accidental cancellations occur, along with SM values. $6\% < \bar{a}_I(\rho\gamma) < 67\%$ is assumed, and constraints derived as described below table 5.5. Again note that only the real part is listed, as this is what enters the CP-averaged isospin asymmetry. Since the calculated SM value is the lower bound of this range (within uncertainties), the SM value of the coefficient and the other bound are quoted; the true value is expected to lie in this range.

5.9 Conclusions

The isospin asymmetry in the SM in radiative and semi-leptonic $B \to K^*$, $B \to \rho$ and $B \to K$ decays has been discussed. At present the result for $B \to K^*$ is in excellent agreement with experiment [147], in spite of its rather sizeable uncertainty:

$$\bar{a}_I(K^*\gamma)_{\text{HFAG}} = 5.2(2.6)\% \qquad \bar{a}_I(K^*\gamma)_{\text{LZ}} = 4.9(2.6)\% \quad . \tag{5.82}$$

The situation in $B \to \rho$ and $B \to K$ is far less clear. There is a 2σ discrepancy between the SM expectation and experiment:

$$\bar{a}_I(\rho\gamma)_{\text{HFAG}} = 30^{+16}_{-13}\% \qquad \bar{a}_I(\rho\gamma)_{\text{LZ}} = 5.2(2.8)\% \quad ; \tag{5.83}$$

however, it appears that the charged decay $B^+ \to \rho^+\gamma$ is principally responsible for the large measured isospin asymmetry, and it will not be at all surprising if the measurement in that channel shifts somewhat. In particular, the normalised difference between the $B \to K^*\gamma$ and $B \to \rho\gamma$ isospin asymmetry introduced in Section 5.7 seems strongly to indicate that a large difference between the two is inconsistent with the current measurements of the CKM matrix and the absence of beyond-SM physics.

The measurement of $B \to Kl^+l^-$ is also significantly larger than the prediction: the asymmetry is expected to be on the 1%-level, and the present measurement $-0.42^{+0.20}_{-0.22}$ [147] in the $[2.0, 4.3]\text{GeV}^2$ range is 2σ away from that. This result is difficult to reconcile with SM expectations: it would appear that for the isospin asymmetry to be so large, an order-of-magnitude enhancement in one or more of the WCs is required, and in spite of the difficulties in calculating hadronic decays it would be expected that order-of-magnitude enhancements would be noticeable since the theoretical uncertainties are not generally quite so extreme, e.g. [183]. It should be remarked that there is no generic expectation that the $B \to Kl^+l^-$ asymmetry should be similar to the $B \to K^*l^+l^-$: if new physics generates sizeable right-handed current

operators they will couple differently, and even in the SM the different structure of the K and longitudinally polarised K^* beyond leading twist leads to moderate differences. It appears to be very difficult to accommodate an isospin asymmetry in $B \to K l^+ l^-$ and the 50% level in the SM at all. In view of this it seems sensible to reserve judgement until further experimental results.

Aside from the the present discrepancy with experiment, the principal problem in this computation is the lack of a calculation of the non-factorisable loop corrections in WA, since this should be the dominant $O(\alpha_s)$ contribution as it potentially couples to large colour unsuppressed WCs. This should reduce the uncertainty in the theoretical result substantially by reducing the dominant renormalisation scale uncertainty. Such a calculation is expected to be technically difficult owing to the likely presence of anomalous thresholds.

Chapter 6

Long-distance charm loops in $B \to V l^+ l^-$

In the SM, it has been known for a long time that radiative B meson decays produce predominantly left-handed photons and that the amplitude for right-handed decays is $1/m_b$ suppressed [97]. For the short-distance electromagnetic penguin amplitude the $1/m_b$ suppression can be seen from the structure of the effective Hamiltonian, which after restoration of the light-quark mass term neglected in (2.19) gives [184]

$$\mathcal{H}_{\text{eff}}|_7 = \frac{G_F \lambda_t}{\sqrt{2}} \frac{e}{8\pi^2} \bar{s}\sigma \cdot F(m_b(1+\gamma_5) + m_s(1-\gamma_5))b \quad . \tag{6.1}$$

The $\mathcal{O}_7$ operator therefore couples to left- and right-handed quark currents in the ratio m_s/m_b and since it can be shown from Lorentz invariance considerations, e.g. [75], that the parity-conserving and -violating form factors are equal at $q^2 = 0$, the partonic prediction carries over to the hadronic level.

The form factor contribution from $\mathcal{O}_7'$ is however not necessarily the leading right-handed amplitude in $B \to V\gamma$, since it is at the same order in $1/m_b$ power counting as possible long-distance corrections. It was argued in [185] using an inclusive approach, that there are potentially much larger corrections arising from the $\mathcal{O}_2$ operator when a charm-quark loop emits a soft gluon into the final-state vector meson, which could give a right-handed amplitude on the order of 10% of the left-handed one. In [129, 186], however, the same contribution was computed using a $1/m_c$ expansion, which gave an effect only on the 1% level. In this chapter, the relevant charm-loop contribution will be calculated in a fully exclusive LCSR approach, so that the question of the magnitude of right-handed photon production in the SM can finally be settled. This calculation will be contrasted with the previous estimates and it shall be argued that neither the inclusive nor the $1/m_c$ expansion approach was correct; however, the results of the $1/m_c$ calculation were in fact at the right order of magnitude.

For the process $B \to V\gamma$ it was shown [187] that the time-dependent CP asymmetry is

sensitive to the interference of the left- and right-handed amplitudes. More recently, the full set of angular observables in $B \to K^* l^+ l^-$ have been considered [98] and optimised quantities, minimising the sensitivity to form factors and thus to theoretical uncertainties, have been proposed [99, 100]. One in particular, P_1, is sensitive to the interference between the left- and right-handed amplitudes and hence this calculation is also relevant there. Updated predictions in light of these results will therefore be provided for both of these observables in Section 6.8.

The contents of this chapter are to be published in [95].

6.1 Matrix element

The function $L_i(q^2)$ which gives the contribution of a quark loop radiating a soft gluon into the final-state meson in $B \to V l^+ l^-$ decay shall be computed. The definition of this function in the context of B meson form factors is given in Section 2.9. The functions $L_i(q^2)$ are further broken into contributions due to different quark flavours, which gives

$$L_i(q^2) = -C_2 Q_u \sum_{q=u,c} \frac{\lambda_q}{\lambda_t} L_{q,i}(q^2) + (C_4 - C_6) \sum_{\substack{q=u,c,\\ d,s,b}} Q_q L_{q,i}(q^2) + C_3 Q_s L_{s,i}(q^2) \quad , \tag{6.2}$$

after the effective Hamiltonian (2.19) is taken into account[1]. The hierarchy of the coefficients is given by $C_2 \sim 1$ and $|C_{3,4,6}| \ll 1$, and $|\lambda_c/\lambda_t| \sim 1$, $|\lambda_u/\lambda_t| \sim \lambda^2$. By far the largest contribution is therefore given by the charm quark, since it is neither suppressed by a small WC nor the Cabibbo angle. Taking the case of the charm current, these functions correspond to the matrix element

$$\sum_{i=V,A,0} P_i^\mu L_{c,i}(q^2) = \frac{4\pi^2}{m_b} i \int d^4x e^{iq\cdot x} \langle V(p)|\mathcal{T}\{\bar{c}\gamma^\mu c(x)\, 2\tilde{Q}_1^c(0)\}|B(p_B)\rangle \quad , \tag{6.3}$$

where the operator $\widetilde{Q}_1^c$ is defined as

$$\widetilde{Q}_1^c = \left(\bar{c}\frac{\lambda_a}{2}c\right)_{V-A} \left(\bar{s}\frac{\lambda_a}{2}b\right)_{V-A} \quad , \tag{6.4}$$

which in terms of operators in the effective Hamiltonian (2.19) gives $N_c Q_2^c = Q_1^c + 2N_c \widetilde{Q}_1^c$, that is $\widetilde{Q}_c^1$ is the colour-traceless part. The functions $L_{c,i}(q^2)$ are further broken down into three contributions

$$L_{c,i}(q^2) = L_{c,i}^{gV}(q^2) + L_{c,i}^{gB}(q^2) + L_{c,i}^{R}(q^2) \quad , \tag{6.5}$$

[1] The small term arising from $\mathcal{O}_3$ with a different Lorentz structure has been neglected since the much larger charm bubble term is the primary concern of this calculation. Furthermore, for $b \to d\gamma$ transitions the photon DA does not give a contribution, since the resulting light-quark loop with the vector weak current has an odd number of Dirac matrices, and therefore this contribution is either suppressed by a small WC or light-quark mass in contrast to the case of WA.

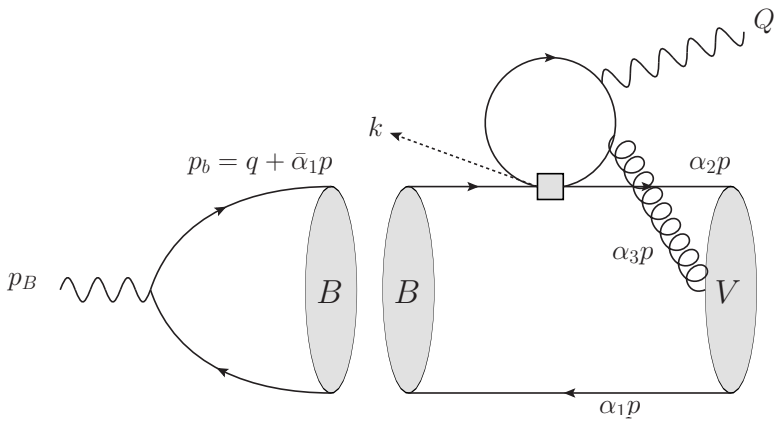

Figure 6.1: Sum rule matrix element and kinematics assignments for soft gluon charm loop process.

according to the nature of the radiated gluon, that is whether it is a soft gluon in the final-state vector meson, a soft gluon in the initial-state heavy meson or any other gluon, respectively[2]. The projection tensors P_i^μ are given in (2.71). The functions $L_{q,i}^{gV}(q^2)$ have already been worked out in [129] for massless quarks. This chapter will focus on the calculation of soft gluons radiated into the final state $L_{c,i}^{gV}(q^2)$, since this contribution generates a large strong (CP-even) phase. The function $L_{c,i}^{gB}(q^2)$ will also be discussed briefly in Section 6.4. Calculation of the hard gluon contribution $L_{c,i}^{R}(q^2)$ would involve a two-loop sum rule and since it has been found to be factorisable [42] and should not be expected to lead to a large right-handed amplitude, the calculation of $L_{c,i}^{R}(q^2)$ will not be attempted.

6.2 Sum rule calculation

The functions $L_{c,i}^{gV}(q^2)$ will be computed using a sum rule approach. The general method was discussed in Section 2.8. The correlation function used to calculate the matrix elements (6.3) is:

$$\mathcal{C}^\rho(p,q,k) = \left(\frac{4\pi^2}{m_b}\right)\left(\frac{1}{f_B m_B^2}\right) i^2 \int d^4x d^4y e^{iQ\cdot x} e^{-ip_B\cdot y} \langle V(p)|\mathcal{T}\{\bar{c}\gamma^\rho c(x) 2\widetilde{Q}_1(0) J_B(y)\}|0\rangle \quad . \tag{6.6}$$

As in Chapter 3, the issue of parasitic cuts arises and cuts with the correct quantum numbers for a B meson must be separated from other parasitic cuts. The solution used here is the same as in Section 3.2.1, and a spurious momentum k at the weak operator vertex is introduced following [106]. The introduced momenta are

$$p_B = p + q \qquad P = p_B - k \qquad Q = q - k \tag{6.7}$$

[2]The exact nature of this division rather depends on the method of calculation used, since the separation between hard and soft gluons will usually depend on a factorisation scale.

Invariant	Hadron	J^P	Flavour	Comments
Q^2	J/ψ	1^-	$\bar{c}c$	Charmonium resonances
p_B^2	B_q	0^-	$\bar{q}b$	B meson states
q^2	B_s	$1^\pm$	$\bar{s}b$	Would be charmonium parasite $q^2 \xrightarrow{k\to 0} Q^2$
P^2	multi-hadron	$0^\pm$	$\bar{c}c\bar{s}q$	Would be B meson parasite $P^2 \xrightarrow{k\to 0} p_B^2$

Table 6.1: Interpretation of external momentum cuts in terms of quark and hadron states.

and the corresponding cuts are listed in table 6.1. The resulting Feynman diagram and momentum assignments are shown in Figure 6.1. Unlike in the calculation of Chapter 3, anomalous thresholds do not occur here. Problems are largely avoided because in this instance the diagram cleanly separates into two pieces according to

$$p_B = p + q \qquad\qquad P = p + Q \quad , \tag{6.8}$$

where the charm loop does not contain p_B or q and the remainder of the diagram does not contain P or Q, and hence the invariant $(p-k)^2$, which cannot be set on-shell $(p-k)^2 \to m_{K^*}^2$ simultaneously with $k^2 \to 0$, does not appear in any denominators.

The correlation function $\mathcal{C}$ is decomposed into scalar components, using an extension of the decomposition in Section 2.9, to include the additional momentum k, as in Chapter 3:

$$\mathcal{C}^\rho = \mathcal{C}_V P_V^\rho + \mathcal{C}_A P_A^\rho + \mathcal{C}_0 P_0^\rho + \mathcal{C}_k P_k^\rho \quad . \tag{6.9}$$

The additional tensor introduced to accommodate the spurious momentum k is given by

$$P_k^\rho = k^\rho + \frac{Q^2 - q^2}{p_B^2 - m_{K^*}^2 - q^2} p^\rho \qquad q \cdot P_k = 0 \qquad \eta \cdot k = \eta \cdot P_k = 0 \quad ,$$

where the selection of p^ρ rather than q^ρ to make the tensor gauge invariant is due to the discussion in Section 5.4.6, and differs from the choice in Chapter 3. Using the three-particle distribution amplitudes in appendix B.1.1 and the quark propagator in B.4, the diagram in Figure 6.1 can be evaluated to

$$\begin{aligned}
\mathcal{C}_V &= -\left(\frac{f_V m_b m_V}{f_B m_B^2}\right) \int_{(x,v,\underline{\alpha})} d\mu_5 \frac{xv\,(P^2 - Q^2)}{(l^2 - m_x^2)(p_b^2 - m_b^2)} \mathcal{V}(\underline{\alpha}) \quad , \\
\mathcal{C}_A &= -\left(\frac{f_V m_b m_V}{f_B m_B^2}\right) \int_{(x,v,\underline{\alpha})} d\mu_5 \frac{xv\,(P^2 - Q^2)}{(p_b^2 - m_b^2)(l^2 - m_x^2)} \mathcal{A}(\underline{\alpha}) \quad , \\
\mathcal{C}_0 &= -\left(\frac{f_V^\perp m_b m_V}{f_B m_B^2}\right) \sqrt{\frac{q^2}{2m_b^2}} \int_{(x,v,\underline{\alpha})} d\mu_5 \frac{x(\bar{v}(p_B^2 - q^2) + \frac{1}{2}v(p_B^2 - q^2 - P^2 + Q^2))}{(p_b^2 - m_b^2)(l^2 - m_x^2)} \mathcal{T}(\underline{\alpha}) \quad ,
\end{aligned} \tag{6.10}$$

where $\bar{x} \equiv (1-x)$ and $m_x^2 \equiv m_c^2/(x\bar{x})$ is a convenient combination of the mass of the charm quark and the Feynman integration parameter x. The five-parameter integration measure $d\mu_5$

is defined as

$$\int_{(x,v,\underline{\alpha})} d\mu_5 = \int_0^1 dx \int_0^1 dv \int_0^1 d\alpha_1 d\alpha_2 d\alpha_3 \delta(1-\alpha_1-\alpha_2-\alpha_3) \quad . \tag{6.11}$$

The momenta in the denominators are $l \equiv Q + v\alpha_3 p$ and $p_b \equiv q + \bar{\alpha}_2 p$ and therefore the required invariant momentum squares are:

$$\begin{aligned} l^2 &= v\alpha_3 P^2 + \overline{v\alpha_3} Q^2 + \alpha_3 \overline{v\alpha_3} m_{K^*}^2 \quad , \\ p_b^2 &= \alpha_2 q^2 + \bar{\alpha}_2 p_B^2 + \alpha_2 \bar{\alpha}_2 m_{K^*}^2 \quad , \end{aligned} \tag{6.12}$$

where $\overline{v\alpha_3} \equiv 1 - v\alpha_3$. The result for $\mathcal{C}_0$ has been confirmed to reproduce [106, eq. 27] when the quark mass is set to zero, which is as expected since it is the $\mathcal{T}(\underline{\alpha})$ DA which structurally resembles the three-particle pion DA. All of the results in (6.10) have been computed using a light cone approximation to the quark propagator in a one gluon background, which is given in appendix B.4. This has been checked to be the same as the result using the full quark propagator in a one gluon background, also given in appendix B.4, although the equivalence of the two results is non-trivial since they are only equal under the five-parameter integration and not otherwise. It can be seen immediately from (6.10) that all three amplitudes have the same cut structure, and from (6.12) that as promised the cuts have separated the invariant pairs P^2, Q^2 and p_B^2, q^2.

In order to extract the contribution of the B meson state to the components (6.10), each function must be rewritten in terms of a dispersion relation in the momentum p_B^2 using Cauchy's integral theorem

$$\mathcal{C}_i(q^2, Q^2, p_B^2, P^2) = \frac{1}{\pi} \int_{m_b^2}^{\infty} \frac{ds}{s - p_B^2} \operatorname{Im}_s \mathcal{C}_i(q^2, Q^2, s, P^2) \quad , \tag{6.13}$$

and then a Borel transformation recovers the sum rule estimate for the B meson matrix element:

$$L_{c,i}^{gV,k}(q^2, Q^2, P^2) = \frac{1}{\pi} \int_{m_b^2}^{s_0^B} ds e^{(m_B^2 - s)/M^2} \operatorname{Im}_s \mathcal{C}_i(q^2, Q^2, s, P^2) \quad . \tag{6.14}$$

The superscript k indicates the presence of the additional momentum k in this function. Unlike the sum rule calculations in chapters 3 and 5, the relation between the function $L_{c,i}^{gV,k}(q^2, Q^2, P^2)$ is not yet apparent because q^2 and Q^2 are not set equal. The reason for this is that a second dispersion relation in the variable Q^2 will be considered to account for the presence of the J/ψ resonance, and this procedure, along with the relation to the matrix elements (6.3), will be discussed in Section 6.2.2.

In contrast to other calculations in this thesis, in this case a great deal of progress can be made analytically, and in fact only two of the five integrals need to be done numerically. The procedure for reducing (6.14) to a simpler form will be outlined, since it is significantly simpler

if the integrals are done in the right order.

To begin with all momentum squares will be considered to be space-like so that integrals can be performed without having to consider the complex structure, which will allow the complex branch cuts to be identified straightforwardly rather than having to resort to Landau equations[3]. Using the explicit form of the DAs given in appendix B.1.1, the α_1, α_2 and v integrals can be performed to give

$$\begin{aligned}\mathcal{C}_i = \int_0^1 \int_0^1 \frac{d\alpha_3 dx\, x}{(P^2-Q^2)(p_B^2-q^2)^3} \Big\{ &((\log[m_b^2 - p_B^2] - \log[m_b^2 - \alpha_3 p_B^2 - \bar{\alpha}_3 q^2])P_{i,1} + P_{i,2}) \\ &\times \left(\log[m_x^2 - Q^2] - \log[m_x^2 - \alpha_3 P^2 - \bar{\alpha}_3 Q^2]P_{i,3} + P_{i,4}\right) \Big\} P_{i,5} \quad ,\end{aligned} \tag{6.15}$$

where $P_{i,n}$ are polynomials in the integration variables, mass and external momentum squares. They are given in appendix F.1 for the leading-twist component of the three-particle DAs to allow the results of this calculation to be checked; the full expressions are much larger but present no additional technical difficulties. The pole at $p_B^2 = q^2$ has zero residue and therefore the discontinuity is entirely due to the logarithms in p_B^2, so the dispersion representation for $\mathcal{C}_i$ in p_B^2 is

$$\begin{aligned}\mathcal{C}_i^k = -\int_{m_b^2}^{\infty} \frac{ds}{s-p_B^2} \int_0^1 dx\, x \int_0^{\alpha_3^*} \frac{d\alpha_3\, P_{i,1}P_{i,5}}{(P^2-Q^2)(s-q^2)^3} \\ \times \Big((\log[m_x^2 - Q^2] - \log[m_x^2 - \alpha_3 P^2 - \bar{\alpha}_3 Q^2])P_{i,3} + P_{i,4}\Big) \quad ,\end{aligned} \tag{6.16}$$

with

$$\alpha_3^* \equiv \frac{m_b^2 - q^2}{s - q^2} \quad . \tag{6.17}$$

The α_3 integral may now be performed analytically and the imaginary part on the right-hand side of (6.14) is then

$$\begin{aligned}\frac{1}{\pi}\,\mathrm{Im}_s\, \mathcal{C}_i^k(q^2, s, P^2)_{s>m_b^2} = \int_0^1 \frac{dx\, x}{(P^2-Q^2)^3(s-q^2)^3} \times \\ (\log[m_x^2 - Q^2] - \log[m_x^2 - \alpha_3^* P^2 - \overline{\alpha_3^*} Q^2])R_{i,6} + R_{i,7})R_{i,8} \quad ,\end{aligned} \tag{6.18}$$

where $R_{i,n}$ are polynomials in momentum squares, masses and x and are again given in appendix F.1 for the leading-twist three-particle DAs. This represents the final form which can be reached through simple analytic integration and thus the momentum invariant P^2 may now be set on-shell, which according to table 6.1 entails the analytic continuation $P^2 \to m_B^2$. As mentioned previously, the analytic continuation in q^2 and Q^2 is complicated by the presence of the charmonium resonances and the procedure used to deal with these will be given in Section 6.2.2.

[3] See Section 3.2.4.

6.2.1 Large m_c cross-check

The calculation of (6.18) has already been calculated in the large m_c limit using LCSR in [129, 186] at $q^2 = 0$. The result from that paper converted into the normalisation (6.3) is

$$L_{c,A}^{gV}(0)|_{\text{[186]}} = -\frac{5}{4}\frac{f_{K^*}m_{K^*}}{m_c^2 m_b m_B^2 f_B}\zeta_{3K^*}^{\parallel}\int_{m_b^2}^{s_0^B} ds\, e^{(m_B^2-s)/M^2}\left(\frac{m_b^2}{s}\right)^5 (s-m_b^2) \quad . \tag{6.19}$$

By comparison, the result (6.18) combined with (6.14) gives

$$L_{c,A}^{gV,k}(0) \xrightarrow{m_c\to\infty} -\frac{5}{4}\frac{f_{K^*}m_{K^*}}{m_c^2 m_b m_B^2 f_B}\zeta_{3K^*}^{\parallel}\int_{m_b^2}^{s_0^B} ds\, e^{(m_B^2-s)/M^2}\left(\frac{m_b^2}{s}\right)^5 (s-m_b^2)\left(\frac{P^2}{s}\right) \quad , \tag{6.20}$$

which is identical except for a factor P^2/s. In fact, this factor cannot appear in the result of [186], since in that case the use of the $1/m_c$ expansion obviates the need for the additional momentum k; rather, the photon momentum plays the role of eliminating parasitic cuts as in the case of the electromagnetic form factors coupling to $\mathcal{O}_7$. Since that calculation would therefore be expected to be equivalent to this one at $k = 0$, P and p_B are not distinguished thus $P^2 \to p_B^2$, or rather $P^2 \to s$ under the dispersion integral, and thus the expressions (6.19) and (6.20) are indeed equivalent. It is worth mentioning that, as will be discussed in Section 6.5, the $1/m_c$ expansion is not actually convergent at the physical value of m_c, and in addition the $1/m_c$ and $1/m_b$ expansions interfere here, so that the the large m_c and m_b scaling in (6.19) is correct for the case $m_c \gg m_b \to \infty$ but not $m_b \gg m_c \to \infty$.

6.2.2 Perturbative calculation near the J/ψ resonance

The treatment of the two momenta appearing in the correlation function $\mathcal{C}^\rho$ (6.13), corresponding to the external photon momentum, q^2 and Q^2, must now be addressed. The variable q^2 can be set directly to the desired physical value, however Q^2 cannot as can be seen from table 6.1 which implies the presence of a perturbative multi-particle threshold at $Q^2 = 4m_c^2$. Therefore setting Q^2 to the physical value of the external momentum is incorrect because perturbative QCD is not applicable near partonic or hadronic thresholds. The solution to this problem is to construct a sum rule for J/ψ production using the correlation function $\mathcal{C}^\rho$. The Q^2 range attributed to J/ψ production is then subtracted from the dispersion representation of $\mathcal{C}^\rho$ and replaced by a simple pole which is the expected structure in the hadronic picture, with the residue of that pole given by the sum rule for J/ψ production. This method has previously been used in [188, 189].

The dispersion relation satisfied by $L_{c,i}^{gV,k}$ in Q^2 is

$$L_{c,i}^{gV,k}(Q^2,q^2) = L_{c,i}^{gV,k}(0,q^2) + \frac{Q^2}{\pi}\int_{\text{cut}}\frac{dt\ \text{Im}_t\, L_{c,i}^{gV}(t,q^2)}{t(t-Q^2-i0)} \quad , \tag{6.21}$$

where one subtraction has been used so that the resulting integral is not divergent, and other momentum squares have been omitted from function parameters for brevity.

In order to sensibly associate the complex cut on the right-hand side of (6.21) with charmonium production it must be the case that the cut begins at $Q^2 = 4m_c^2$ in perturbation theory. This is not in fact what happens, as can be seen from (6.18): the second logarithm $\log[m_x^2 - \alpha_3^* P^2 - \overline{\alpha_3^*} Q^2]$ has a threshold even for space-like Q^2 due to the presence of $P^2 = m_B^2$. In this calculation the complex branch cut of this second logarithm is not considered to contribute to charmonium production but rather the strong phase of the overall matrix element. This picture is correct in the small q^2 region where $\overline{\alpha_3^*} = O(\Lambda_{\text{QCD}}/m_b)$ and the second logarithm is approximately independent of Q^2. The situation at high q^2 is reversed; at $q^2 \to m_b^2$, the maximum possibly accessible through sum rules, $\alpha_3^* = 0$ and the two logarithms in (6.18), cancel. In the low recoil region it therefore does not make sense to treat the two logarithms differently. In this calculation, the dispersion relation (6.21) shall only be applied to the first logarithm which is clearly associated with the charmonium spectrum. Justification of this approach is deferred until the result is obtained in (6.25) which will shed more light on the situation.

Applying the usual semi-global quark hadron duality approach to (6.21), the dispersion integral is split into two regions separated at an effective continuum threshold $s_0^{J/\psi}$, and the region between the perturbative threshold at $4m_c^2$ and this duality threshold is attributed to the charmonium resonances. The resulting formula for $L_{c,i}^{gV}$ with the perturbative threshold region replaced is

$$L_{c,i}^{gV,k}(Q^2, q^2) = L_{c,i}^{gV,k}(0, q^2) + Q^2 \sum_{V=J/\psi,\Psi',\ldots} \frac{r_i^V(q^2)}{m_V^2(m_V^2 - Q^2)} + \frac{Q^2}{\pi} \int_{s_0^V} \frac{dt\ \text{Im}_t\, L_{c,i}^{gV,k}(t, q^2)}{t(t - Q^2)} \quad , \tag{6.22}$$

where the sum runs over all low-lying $\bar{c}c$ vector mesons. Although there are two narrow low-lying resonances, the J/ψ and the $\psi(2S)$, only a single resonance at the J/ψ mass will be used in this calculation since it will transpire that the result is not valid above the J/ψ mass, and using only a single pole avoids any question of how to partition the duality region contribution between them. The residues $r_i^{J/\psi}$ in (6.22) is the amplitude for J/ψ meson production and can therefore be calculated using standard sum rule methods leading to

$$r_i^{J/\psi}(q^2) = \frac{1}{\pi} \int_{4m_c^2}^{s_0^{J/\psi}} dt\ \text{Im}_t\, L_{c,i}^{gV,k}(t, q^2) e^{(m_{J/\psi}^2 - t)/M_{J/\psi}^2} \quad . \tag{6.23}$$

Inserting this result into (6.22) and neglecting other charmonium resonances gives

$$\begin{aligned} L_{c,i}^{gV,k\prime}(Q^2, q^2) = L_{c,i}^{gV,k}(0, q^2) &+ \frac{Q^2}{\pi} \int_{4m_c^2}^{s_0^{J/\psi}} \frac{dt\ \text{Im}_t\, L_{c,i}^{gV,k}(t, q^2)}{m_{J/\psi}^2(m_{J/\psi}^2 - Q^2)} e^{(m_{J/\psi}^2 - t)/M_{J/\psi}^2} \\ &+ \frac{Q^2}{\pi} \int_{s_0^{J/\psi}} \frac{dt\ \text{Im}_t\, L_{c,i}^{gV,k}(t, q^2)}{t(t - Q^2)} \quad , \end{aligned} \tag{6.24}$$

where the prime denotes that the resonance subtraction procedure has been performed. The expression (6.24) is however rather inconvenient for numerical computation and it proves advantageous to combine it with (6.21) to produce

$$L_{c,i}^{gV,k\prime}(Q^2,q^2) = L_{c,i}^{gV,k}(Q^2,q^2) + \frac{Q^2}{\pi}\int_{4m_c^2}^{s_0^{J/\psi}} dt\,\mathrm{Im}_t\, L_{c,i}^{gV,k}(t,q^2)\left[\frac{e^{\frac{m_{J/\psi}^2-t}{M_{J/\psi}^2}}}{m_{J/\psi}^2(m_{J/\psi}^2-Q^2)} - \frac{1}{t(t-Q^2)}\right] , \tag{6.25}$$

in which the t integrals are now over a finite range. Integration contours for each term may also be taken off the real line into the lower complex half plane $\mathrm{Im}\, t < 0$ when Q^2 lies inside the integration region, to avoid numerically tricky integrations which contain simple poles. The final result is then given by setting the external momenta to their on-shell values according to table 6.1, that is $P^2 \to m_B^2$ and q^2 to the external photon momentum, so that all external momenta are correct for the physical matrix element (6.3) subject to the the standard semi-global duality approximation described in Section 2.8. Q^2 is set to the same value as q^2, and then the final result for $L_{c,i}^{gV}$ is

$$L_{c,i}^{gV}(q^2) = L_{c,i}^{gV,k\prime}(q^2,q^2,m_B^2) \quad . \tag{6.26}$$

It is apparent that (6.24) and thus (6.25) cannot be valid for all Q^2. The final term describes the contribution due to the density-of-states of a multi-particle continuum, and it would therefore be expected that $\mathrm{Im}_t\, L_{c,i}^{gV,k}(s_0^{J/\psi},q^2) = 0$, because the phase space volume is zero at the multi-particle threshold. However, since the lightest states in the perturbative and hadronic spectra have different masses, the perturbative density-of-states is non-zero at the duality threshold. This problem manifests itself as a logarithmic divergence for $Q^2 \to s_0^{J/\psi}$. Unfortunately there is little that can be done to repair this deficiency; although it should be the case that for sufficiently large Q^2 local duality becomes a good approximation, it can be seen from the famous R function plot in [123, 154][4] that there are resonances in the charm threshold region up to around $\sqrt{s} \approx 4.6\,\mathrm{GeV}$, which is far too close to the perturbative b-quark mass for there to be a significant window between the charm pair region and the kinematical upper bound of the $B \to V$ process. It should be stressed that this problem is specific to the matrix element under consideration; it is still expected that form factors calculated using LCSR should *in general* be valid up to $m_B^2 - q^2 \sim O(m_B\Lambda_{\mathrm{QCD}})$ but the presence of a significant charm threshold prevents this. Fortunately this low-recoil region is accessible via other means, either the low-recoil OPE [171] or lattice simulations[5], although these approaches are only suitable for local operator form factors and do not include long-distance effects. The justification for only considering the cut due to the first logarithm in (6.18) as contributing to the charmonium

[4] Figure 46.7, available separately under "Plot of cross sections and related quantities" on the website.

[5] Although lattice usually simulates the high q^2 region of these decays, to date results for the K^* meson are not yet available owing to the fact that it is unstable [190].

	$L^{gV}_{c,V}(0)\times 10^3$	$L^{gV}_{c,A}(0)\times 10^3$
$B\to K^*$	$-(0.23\pm0.37)-(2.17\pm1.23)i$	$-(0.73\pm1.89)-(3.97\pm1.61)i$
$B\to \rho$	$(0.01\pm0.33)-(2.79\pm1.20)i$	$-(0.85\pm1.78)-(3.78\pm1.28)i$
$B_s\to K^*$	$(0.26\pm0.14)-(1.88\pm0.91)i$	$-(0.62\pm1.73)-(2.62\pm0.73)i$
$B_s\to \phi$	$(0.04\pm0.26)-(2.23\pm0.98)i$	$-(0.04\pm1.46)-(4.09\pm1.45)i$
	$L^{gV}_{c,-}(0)\times 10^3$	$L^{gV}_{c,+}(0)\times 10^3$
$B\to K^*$	$-(0.68\pm1.58)-(4.34\pm2.01)i$	$(0.35\pm1.10)+(1.27\pm0.29)i$
$B\to \rho$	$-(0.60\pm1.44)-(4.64\pm1.75)i$	$(0.61\pm1.09)+(0.70\pm0.20)i$
$B_s\to K^*$	$-(0.25\pm1.21)-(3.18\pm1.15)i$	$(0.62\pm1.25)+(0.52\pm0.23)i$
$B_s\to \phi$	$(0.00\pm1.18)-(4.47\pm1.72)i$	$(0.05\pm0.90)+(1.32\pm0.34)i$

Table 6.2: Results for $L^{gV}_{c,i}$ at $q^2=0$ for various different final-state mesons. The top half of the table gives results in the parity basis, and the bottom half in the helicity basis.

resonances and treating the second perturbatively, is that at low q^2 this is justified by the smallness of $\overline{\alpha}^*_3$, and the high q^2 region is inaccessible in any case as $m_b^2/4m_c^2$ is not sufficiently large to reach the region where charm production can be treated perturbatively.

This is, however, not entirely the end of the matter of treating contributions from vector meson resonances. Although the charm-quark loop is the dominant one in $b\to s$ decays due to the hierarchy of CKM and WCs, there is also the case of $b\to d$ decays to consider, as well as the subleading contributions in $b\to s$. It is therefore necessary to consider the case of light-quark loops, where the relevant mesons are the ρ, ω and ϕ. Examining the R function plot [123, 154] in the low momentum region reveals that perturbation theory appears to be a good approximation above 1.3GeV or so. Considering that the s-quark loop and therefore the ϕ meson are likely to be the dominant source of deviation from the perturbative prediction in the $1.0-1.3$GeV range and that the s-quark loop is suppressed by a small WC in both $b\to d$ and $b\to s$ transitions, taking the local duality result (6.18) for light-quarks in the region $q^2>1\,\text{GeV}^2$ seems reasonable. It will turn out that the uncertainties in this result are large in any case, and thus difficulties caused by the ρ, ω and ϕ mesons are unlikely to be the dominant source of error. At $q^2=0$ the light-quark contribution is treated using the resonance modelling approach described in this section following [129].

6.3 Results

Plots of the functions $L^{gV}_{c,i}$ are shown in Figure 6.2 for $B\to K^*$ transitions, and values at $q^2=0$ for various final-state mesons are given in table 6.2. Two features of these results are interesting:

- The strong phase is large, even at $q^2=0$. This is a result of the cut in P^2 of the multi-particle $\bar{c}c\bar{q}s$ state, and the situation remains the same up to $q^2\sim 4m_c^2$. Near $q^2=4m_c^2$, the J/ψ intermediate state dominates the matrix element which approaches a simple pole due to the construction in Section 6.2.2), and as discussed in that section, these results

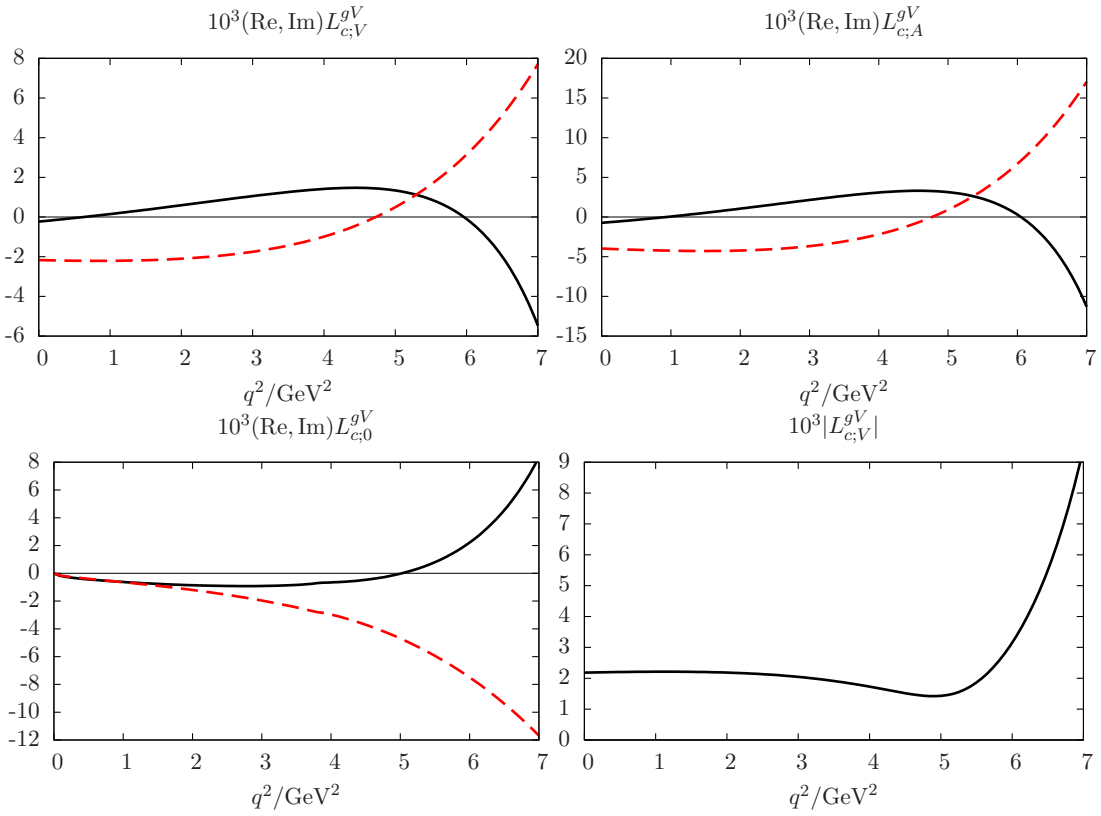

Figure 6.2: Plots of the real and imaginary parts of $L^{gV}_{c,i}$ for $i \in \{V, A, 0\}$, and the magnitude of $L^{gV}_{c,V}$ for $B \to K^*$ transitions. The solid black line is the real part, and the dashed red line the imaginary part. It is clear from these plots that the large m_c expansion fails, since in the $m_c \to \infty$ limit the matrix element should have no strong phase at $q^2 = 0$.

are not reliable beyond this point.

- The left-handed amplitude is large compared to the right-handed one. Although this is the normal situation in $B \to V$ decays at leading order in $1/m_b$, there is no reason to expect that it should be the case here since the parity conserving and violating amplitudes, whose sum and difference is the left- and right-handed amplitudes, are not related, arising from the conformal expansion parameters of the $\mathcal{V}$ and $\mathcal{A}$ DAs respectively. This is even further emphasised by the fact that G-parity constraints on the expansion parameters mean that the dominant contribution to the parity conserving and violating amplitudes arise at different orders in the twist expansion. A fuller discussion of the structure of these results and their helicity structure is deferred to Section 6.6, where they are contrasted with those of [185].

On a technical level, this calculation appears to be significantly more complicated than the calculations done for $B \to \pi\pi$ in [106] and for $B \to J/\psi K$ in [191]. The reason for this is that those papers were treating the case of purely hadronic final states and thus only needed to compute the term analogous to the r_i^V term in (6.22) but not the continuum term which contributes to the production of photons and lepton pairs. This allowed them to use a $1/m_b$ expansion since the dispersion variable analogous to t is then restricted to $t < s_0^{J/\psi} \ll m_b^2$, which is not true in the radiative and semi-leptonic cases[6].

6.4 Initial state soft gluon contribution

In this section the contribution of charm loops coupling to a soft gluon from the initial-state B meson will be discussed, although a conclusive result will not be provided, for reasons to be explained. As will be argued in Section 6.5, the largest momentum invariant arising in the charm loop for a soft initial state gluon is $O(m_b\Lambda_{\rm QCD})$ rather than $O(m_b^2)$. Because of this the charm-pair production threshold is not expected to be crossed and the leading term in the $1/m_c$ expansion should provide a reasonable approximation.

Since this estimate will employ the $1/m_c$ expansion, emission of the photon via the charm loop is a local process, and the calculation will be further simplified by setting $q^2 = 0$, since only qualitative features of the result will be of interest. The effective local $\bar{s}bg\gamma$ operator induced by $\mathcal{O}_2$ in the large m_c limit was worked out in [192] and is

$$i\epsilon^{*\mu} \int d^4x e^{iqx}\, \mathcal{T}\{[\bar{c}(x)\gamma_\mu c(x)]Q_2^c(0)\} = 2c_F q_F + \dots \tag{6.27}$$

[6] It might seem from (6.25) that in fact only the range $4m_c^2 < t < s_0^{J/\psi}$ is used; however, the term $L_{c,i}^{gV}(Q^2, q^2)$ there contains a $\log[m_x^2 - Q^2]$ term from (6.18) which cannot be $1/m_b$ expanded since it is independent of m_b.

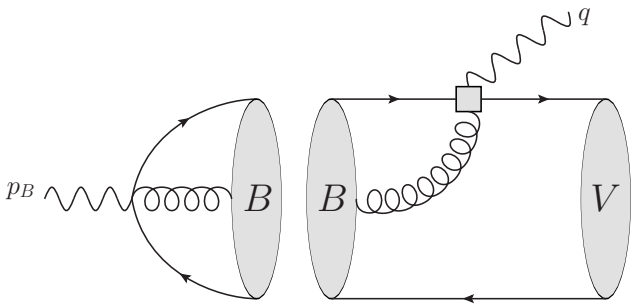

Figure 6.3: Sum rule diagram for initial-state soft gluon contribution $L^{gB}_{c,i}(0)$. The use of the three-particle current J_{3B} means that cuts select only the three-particle B meson state, thus giving the contribution of initial state soft gluons.

where

$$q_F = (D^\rho F^{\alpha\beta})[\bar{s}\gamma_\rho(1-\gamma_5)g\widetilde{G}^a_{\alpha\beta}\frac{\lambda^a}{2}b] \,, \qquad c_F = -\frac{1}{48\pi^2 m_c^2} \quad . \tag{6.28}$$

From (6.3) and (6.27), the relation of this operator to the desired form factor $L^{gB}_{c,i}$ is found to be

$$\frac{-1}{12m_c^2 m_b}\langle \bar{K}^*|q_F|\bar{B}\rangle = \epsilon_\mu(P_V^\mu L^{gB}_{c,V} + P_A^\mu L^{gB}_{c,A}) \quad . \tag{6.29}$$

A suitable correlation function for the extraction of the these form factors is

$$C(p_B,q) = i\int d^4x e^{-ip_B\cdot x}\,\langle \bar{K}^*|T q_F(0)\, J_{3B}(x)|0\rangle \quad , \tag{6.30}$$

where the interpolating current J_{3B}, defined by

$$J_{3B} = \bar{b}g\,G\cdot\sigma\gamma_5 q \qquad \langle \bar{B}|J_{3B}|0\rangle = 2if_B m_B(\lambda_E^2+\lambda_H^2) \quad , \tag{6.31}$$

is used to select the three-particle component of the B meson. The normalisation of the current J_{3B} was introduced in [193]. The Feynman diagram for the sum rule implied by (6.30) is depicted in Figure 6.3. Following the usual sum rule procedure, the correlation function $C(p_B,q)$ is matched to a hadronic representation

$$C(p_B,q) = [2if_B m_B(\lambda_E^2+\lambda_H^2)]\frac{\langle \bar{K}^*|q_F|\bar{B}\rangle}{m_B^2-p_B^2} + \ldots \tag{6.32}$$

where the dots stand for higher resonances and states. The evaluation of the correlation function (6.30) in QCD is standard, except that it turns out that twist-3 terms in the K^* DA must be included since the twist-2 terms give no contribution. The K^* DA is given to the necessary order in appendix B.1[7]. It is also noteworthy that the gluon correlator required $\langle G^a_{\mu\nu}(x)G^b_{\alpha\beta}(y)\rangle$ is the same in any gauge in which global colour symmetry is unbroken, and hence the use of

[7]Since only perpendicular polarisations are of interest at $q^2=0$, the twist-3 term $h_\parallel^{(s,t)}$ may be ignored.

the Fock-Schwinger gauge in deriving (6.27) and (6.28) does not entail any complications here. The resulting sum rule for $L^{gB}_{c,(V,A)}(0)$ is

$$L^{gB}_{c,V}(0) = L^{gB}_{c,A}(0) = -\frac{\alpha_s f_{K^*} m_{K^*}}{144\pi m_c^2 f_B m_B(\lambda_E^2+\lambda_H^2)} \int_{m_b^2}^{s_0^{LE}} ds\, e^{\frac{m_B^2-s}{M^2}} \int_{m_b^2/s}^1 du \frac{\left(us-m_b^2\right)^2}{us} g_\perp^{(a)}(u) \quad . \tag{6.33}$$

Inserting numerical values from table 3.2 along with $\alpha_s(\mu_h) = 0.35$ gives

$$L^{gB}_{c,V}(0) = L^{gB}_{c,A}(0) = -0.15 \times 10^{-3} \left(\frac{0.4\text{GeV}^2}{\lambda_E^2+\lambda_H^2}\right) \quad . \tag{6.34}$$

This value is considerably smaller than $L^{gB}_{c,V} = -3.6 \times 10^{-2}$ given in [194][8]. In fact, this sum rule is problematic because it is highly sensitive to the duality threshold s_0^{LE}, or to put it another way, the Borel transform is ineffective in suppressing the continuum contribution. It should further be remarked that the existing determinations of $\lambda_E^2+\lambda_H^2$ are also rather problematic since the value $\lambda_E^2+\lambda_H^2|_{\text{GN}} = 0.29(13)\,\text{GeV}^2$ [193] is dominated by the highest dimension condensates considered and the value $\lambda_E^2+\lambda_H^2|_{\text{KMO}} = 0.48\,\text{GeV}^2$ [195] is dependent on the choice of B meson model wave functions. Since the parameters λ_E^2 and λ_H^2 appear in the numerator rather than the denominator of the B DA calculation, a significant shift in their values could bring the estimate (6.34) and the B DA value $L^{gB}_{c,V} = -3.6 \times 10^{-2}$ [194] much closer.

To try and bring some clarity to this situation, the computation of $\lambda_E^2+\lambda_H^2$ using a diagonal sum rule for $\langle J_{3B}(x) J_{3B}(0)\rangle$ was attempted, and the resulting formula is

$$(\lambda_E^2+\lambda_H^2)^2 = \frac{\alpha_s C_F N_c}{160\pi^3 f_B^2 m_B^2} \int_{m_b^2}^{s_0^{LE}} ds e^{\frac{m_B^2-s}{M_{LE}^2}} \left(\frac{m_b^8}{4s} + \frac{11m_b^6}{3} - 3m_b^4 s - m_b^2 s^2 + \frac{s^3}{12} + \left(2m_b^6 + 3m_b^4 s\right)\log\left(\frac{s}{m_b^2}\right)\right) \quad . \tag{6.35}$$

However, this suffers from the same problem as (6.33); the continuum contribution is far too large to make the result trustworthy[9] and it is highly sensitive to the duality threshold s_0. $\lambda_E^2+\lambda_H^2 = 0.4\,\text{GeV}^2$, the average of the two previous determinations [193, 195], is therefore taken here as an indicative value, but only a lattice determination will definitively resolve this question.

Ultimately, this estimate of the initial-state radiation contribution, as well as the B DA computation [194], both lead to the same qualitative features: $L^{gB}_{c,V} = L^{gB}_{c,A}$ and $\text{Im}\, L^{gB}_{c,V} = 0$. The initial-state contribution therefore does not contribute to either CP asymmetries or the breaking of the heavy-quark symmetry relation $\mathcal{T}_V = \mathcal{T}_A$, although the result in [194] is significant because it gives a sizeable correction to the decay rate at intermediate q^2.

[8] Note that the comparison in that paper between the results in equations (6.3) and (6.4) is questionable, since soft gluon emission into the initial and final state hadrons is not physically comparable.

[9] Note that the contribution of $\langle\bar{q}q\rangle$ was included in this calculation but it turns out to be zero, which only raises further questions as to the validity of this sum rule.

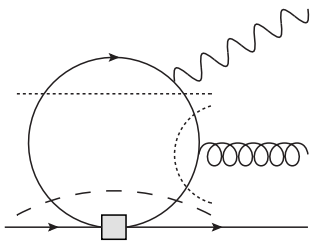

Figure 6.4: The inclusive $b \to sg\gamma$ graph, the external kinematics of which determine the convergence (or otherwise) of the $1/m_c$ expansion. The dashed and dotted lines indicate cuts which can give rise to complex branch cuts; the dotted lines are considered below threshold because the soft gluon is expected to be almost on-shell and the photon is assumed to be below the $q^2 = 4m_c^2$ threshold where the $1/m_c$ expansion must break down. Only the momentum flowing through the weak vertex is therefore relevant.

6.5 The $1/m_c$ expansion in soft gluon effects

In this chapter, the contribution to $B \to Vl^+l^-$ decay of a charm loop with soft gluon emitted into the final-state meson has been computed, and a large imaginary part or the resulting amplitude found. Previous calculations of this term have used the $1/m_c$ expansion to rewrite it in terms of an effective local operator and then proceeded to compute $\langle V|\mathcal{O}|B\rangle$ [186]. This operator product expansion procedure of course produces no imaginary part since the charm pair production threshold is implicitly not crossed. The $1/m_c$ expansion was however employed in Section 6.4 for the initial-state soft gluon contribution examined there, and thus the details of convergence merit further examination.

The $b \to sg\gamma$ sub-graph relevant to the convergence of the $1/m_c$ expansion in processes considered in this chapter is shown in Figure 6.4. For simplicity the photon shall be taken to be on-shell, so that the assumption that the gluon is soft then means that there is only a single non-zero momentum invariant in the problem. It is then expected that the convergence or otherwise of the $1/m_c$ expansion will be determined by whether that momentum invariant, which will be labelled l^2 in accordance with (6.10), ever reaches the charm pair production threshold, $l^2 \geq 4m_c^2$.

For the case of soft gluon emission into the final-state meson computed in Section 6.2, it can be seen from (6.10) that the relevant loop integral at $Q^2 = q^2 = 0$ is

$$\int_0^1 dx \int_0^1 dv \frac{\bar{x}x^2v}{\bar{x}xv\alpha_3 P^2 - m_c^2} = \frac{1}{4\alpha_3 P^2}\left[1 - \frac{\arcsin\sqrt{z}}{\sqrt{z(1-z)}}\right] = -\frac{1}{4m_c^2}\sum_{n=0}^{\infty}\frac{4^n((n+1)!)^2}{(2n+3)!}z^n \quad , \tag{6.36}$$

where $z \equiv \frac{\alpha_3 P^2}{4m_c^2}$. The series coefficients can be seen to scale as $n^{-1/2}$ by Stirling's approximation, and thus the radius of convergence is $|z|< 1$ as expected from considering the cuts. Since the range of α_3 is $0 < \alpha_3 < 1$, it follows that $P^2 = m_B^2 > 4m_c^2$ and therefore the pair production threshold is crossed for soft gluon emission into the K^* meson.

The next case to be addressed is that of a soft gluon in the initial state, that is to say the three-particle component of the B meson state. The $1/m_c$ expansion has already been assumed to converge for this case in Section 6.4, and this assumption is consistent with the results of [195], which do not have a strong phase. It is not in fact possible in an LCSR approach to separate the soft gluon term cleanly from that of a hard gluon connecting to either of the quark lines forming the B meson in the proper two-loop calculation of this term. Nonetheless a straightforward kinematical argument can be made that the $1/m_c$ expansion converges for soft initial-state gluons. The soft gluon momentum is taken in the B meson rest frame to be given by

$$p_{gB} = (\Lambda, -\Lambda, 0, 0) \qquad Q = \left(\frac{m_B}{2}, \frac{m_B}{2}, 0, 0\right) \quad , \tag{6.37}$$

where the photon momentum, again at $Q^2 = 0$, is included to make the relative directions clear. The gluon momentum has been chosen to lie along the opposite light-cone direction to that of the photon, which is in accordance with the construction of the light-cone B meson DA neglecting the direction to which the short-distance amplitude is not sensitive. The series expansion parameter in this case is

$$z_{gB} = \frac{(p_{gB} - Q)^2}{4m_c^2} \xrightarrow{\Lambda \ll m_B} \frac{m_B \Lambda}{4m_c^2} \approx \frac{\Lambda}{1.3\,\text{GeV}} \quad , \tag{6.38}$$

which implies that the series converges, since it is expected that $\Lambda < m_B - m_b < 1.3\,\text{GeV}$. The use of the local operator in Section 6.4 is therefore justified.

There is one remaining puzzle to address: why the numerical results in table 6.2 are the same order of magnitude as those computed previously using the $1/m_c$ expansion in [129, 186], which give $|L_{c;1}^{gV}| \sim 10^{-3}$. The asymptotic behaviour of (6.36) in both limits is given by

$$\int_0^1 dx \int_0^1 dv \frac{\bar{x}x^2 v}{\bar{x}xv\alpha_3 P^2 - m_c^2} = \begin{cases} \dfrac{1}{4\alpha_3 P^2} & P^2 \to \infty \\ -\dfrac{1}{24m_c^2} & P^2 \to 0 \end{cases} \tag{6.39}$$

and thus in a sense the fact that the magnitude of the result in [129, 186] is comparable to this result is a coincidence arising from the fact that $6m_c^2$ and m_B^2 are not of vastly differing magnitudes. This point of view is however overstating the case; were m_B many orders of magnitude larger than m_c, the $1/m_c$ expansion would not have been employed in the first place since it could not have been expected to converge. The similarity in magnitude between these results and the local operator approximation is therefore not unexpected, although the degree of similarity is surprising.

6.6 Comparison with the inclusive approach

The predictions of the exclusive LCSR calculation given in table 6.2 are very different to those calculated in [185]: the present approach gives a contribution to the amplitude at the level of 1% of the leading electromagnetic form factor term, whereas [185] predicted that an effect on the 10% level could be expected. The question of why the two differ by an order of magnitude must therefore be addressed.

The most obvious potential source of discrepancy between the two results is their scaling in the large m_b and m_c limits. The prediction of [185] is that

$$\left.\frac{L_{c,1}^{gV}(0)}{C_7^{\rm eff}T_1(0)}\right|_{[185]} \sim \frac{C_2}{C_7^{\rm eff}}\frac{\Lambda_{\rm QCD}}{m_b} \quad . \tag{6.40}$$

To contrast this with the results of Section 6.2, it can be seen from (6.20) and (6.39) that the large m_b scaling found here is

$$L_{c,1}^{gV}(0) \sim \zeta_{3K^*}^{\parallel}\frac{\Lambda_{\rm QCD}^4}{f_B m_b^3} \quad , \tag{6.41}$$

which in combination with $T_1(0) \sim (f_B m_B^2)^{-1}$ [97] entails

$$\left.\frac{L_{c,1}^{gV}(0)}{C_7^{\rm eff}T_1(0)}\right|_{\rm LZ} \sim \zeta_{3K^*}^{\parallel}\frac{C_2}{C_7^{\rm eff}}\frac{\Lambda_{\rm QCD}}{m_b} \tag{6.42}$$

and therefore the two results are not fundamentally different as far as their asymptotic behaviour is concerned.

The key difference between the two estimates therefore appears to be the use of a fully exclusive approach in the present calculation, which gives an additional dimensionless factor of $\zeta_{3K^*}^{\parallel}$ in (6.42) not present in (6.40). The value $\zeta_{3K^*}^{\parallel} = 0.023$ was found in [127], and the smallness of this coefficient, along with the smallness of other coefficients in the three-particle K^* DAs, would certainly account for the smallness of the present results.

The calculation in Section 6.2 also finds that the amplitude for right-handed photon production is significantly smaller than the left-handed amplitude, which does not have an apparent origin in the $1/m_b$ expansion as is usually the case for $B \to V\gamma$ decays, since the formulae for $\mathcal{C}_V$ and $\mathcal{C}_A$ in (6.10) have the same structure. In fact, were the three-particle DAs restricted to the leading collinear twist form only, the approximate G-parity of the K^* meson would have led to $\mathcal{C}_V \approx 0$ and thus reproduced the result of the inclusive calculation [185], that the left- and right-handed amplitudes are equal.

The conclusion that must be drawn is that the results presented here are not directly responsible for the discrepancy between the inclusive predictions of [185] and the present exclusive calculation. Rather, the smallness of the exclusive prediction and its helicity structure reflect the underlying three-particle DA parameters. It would therefore appear that the amplitude for

a gluon and two quarks to hadronise into a light vector meson is significantly smaller than would be expected on dimensional grounds, and in fact the authors of [185] attempted to estimate this effect using Ali-Greub shape function models [196] which reduced ratio (6.40) from 10% to 3%, much closer to the value from the exclusive calculation.

6.7 Right handed amplitudes in the SM

Although the results of Section 6.2 found that even in this soft charm loop contribution the right-handed amplitude is smaller than the left-handed one, the suppression is mild compared to the usual $1/m_b$ suppression which appears in the $C_{7,9}$ form factor contributions and WA terms. The non-factorisable charm loop is therefore expected to give a significant contribution to right-handed amplitudes in $B \to V\gamma$ and $B \to Vl^+l^-$ as predicted in the introduction.

To give an indication of the relative magnitude of different right-handed amplitudes in the SM, the right-handed amplitudes from factorisable operators $C_{7,9}$ and non-factorisable $\mathcal{O}_2$ are plotted in Figure 6.5. The much smaller right-handed WA contribution is also shown for comparison. It appears that the short-distance form factor term proportional to m_s is dominant at large recoil and the non-factorisable charm loop calculated in this chapter is several times smaller. The results computed here are therefore not expected to alter predictions for all observables sensitive to final state helicities significantly, although they will give the dominant contribution to time-dependent CP in some cases since the weak phases of the $\mathcal{O}_2$ and $\mathcal{O}_7$ operators are different. They are however significant insofar as the uncertainty of right-handed amplitudes is reduced very substantially in comparison with the [185], and time-dependent CP asymmetries corresponding to a right-handed amplitude much above the 1% level would indeed appear to be a signal for new physics.

6.8 Observable effects

There are two presently measured quantities sensitive to the helicity of the photon in radiative and semi-leptonic B meson decays, the time-dependent CP asymmetry in $B \to V\gamma$ and the angular observables P_1 and S_3 in $B \to Vl^+l^-$. Updated predictions in light of the present calculation are therefore presented.

6.8.1 Time dependent CP asymmetries

It was pointed out in [187] that the time dependent CP asymmetry in $B \to V\gamma$ is produced by interference of left- and right-handed photon polarisations. Following the notation of [197] the

[10] This estimate is constructed rather naively by multiplying $C_7 T_1(0) \approx 0.1$ by values in table E.2 and m_s/m_b; however, according to the equation in [75], the strange quark mass enters as an m_s/m_{K^*} correction in the twist-3 $h_\parallel$ DAs, which are expected to be m_{K^*}/m_b suppressed w.r.t. the leading amplitude by comparing (E.2) to (E.3).

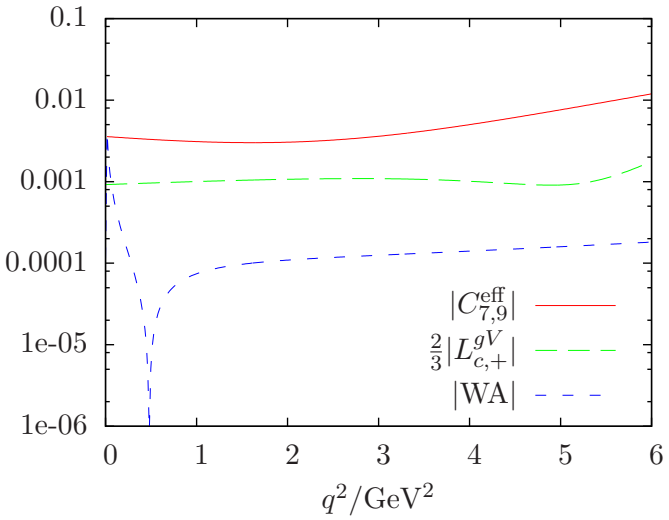

Figure 6.5: Magnitude of contributions to right-handed lepton pair production in $B \to K^* l^+ l^-$ in the SM. The three types of contribution are factorisable form factor contributions labelled $C_{7,9}^{\mathrm{eff}}$, weak annihilation labelled WA, and long-distance charm loops (where the approximation $|C_2\lambda_c/\lambda_t| \to 1$ has been taken for simplicity). The form factor contributions in this case are taken from fits in [190], due to their good small q^2 behaviour. Since the published fits of the form factors [81, 190, 194] are all done in the parity basis, the small right-handed contribution from the form factors cannot be reliably extracted, although in fact for $q^2 \lesssim 5\,\mathrm{GeV}^2$ the form factor contribution is dominated by the short-distance right-handed amplitude proportional to m_s in the C_7 WC and therefore it is expected that the result is reasonably accurate in this region. It can be seen from this plot that the right-handed component of WA is negligible in the SM, although terms proportional to m_s arising from the operators $\mathcal{O}_{3-6}$ were neglected, which would be expected to give a contribution on the 10^{-5} level[10]. The contribution of long-distance charm loops computed in this chapter therefore appears to be a significant correction to the leading amplitude at large recoil, at the 25% level.

	$\lvert q/p\rvert$	Φ_q
B_d^0	0.9997(13)	$2\arg(-V_{td}^* V_{tb}) \equiv 2\beta = 43°$
B_s^0	1.0086(28)	$2\arg(-V_{ts}^* V_{tb}) \approx -2\lambda^2\eta = -2.0°$

Table 6.3: Neutral B meson mixing parameters relevant to this calculation. $|q/p|$ is taken from the HFAG 2013 update [147]. Note that the angle Φ_q here is the complex phase of q/p which is denoted ϕ_q in [197] but is different from ϕ_q used in B-$\bar{B}$ mixing studies [198], which have a related angle $\phi_M \approx \pi - \Phi_q$, which is the complex phase of the off-diagonal entry in the B meson mass matrix. The leading order SM result for this angle is used, and the required numerical values for CKM parameters are taken from [123].

CP asymmetry may be written as

$$\begin{aligned}\mathcal{A}_{\mathrm{CP}}[B_q \to V\gamma](t) &\equiv \frac{\Gamma[\bar{B}_q \to V\gamma](t) - \Gamma[B_q \to \bar{V}\gamma](t)}{\Gamma[\bar{B}_q \to V\gamma](t) - \Gamma[B_q \to \bar{V}\gamma](t)} \\ &= \frac{S\sin(\Delta m_s t) - C\cos(\Delta m_s t)}{\cosh(\frac{1}{2}\Delta\Gamma_s t) - H\sinh(\frac{1}{2}\Delta\Gamma_s t)} \quad ,\end{aligned} \tag{6.43}$$

where the signs are chosen such that $\Delta m_s = m_H - m_L$ and $\Delta\Gamma_s = \Gamma_L - \Gamma_H$, with L corresponding to the lighter and H to the heavier of the CP conjugate B mesons, are both positive in the SM. The parameters S, C and H are given by [187, 197]

$$\begin{aligned} C &= N\left[|\mathcal{T}_-|^2+|\mathcal{T}_+|^2-|\overline{\mathcal{T}}_-|^2-|\overline{\mathcal{T}}_+|^2\right] & S &= 2N\,\mathrm{Im}\left[\tfrac{q}{p}\left(\overline{\mathcal{T}}_-\mathcal{T}_-^* + \overline{\mathcal{T}}_+\mathcal{T}_+^*\right)\right] \\ N &= \left[|\mathcal{T}_-|^2+|\mathcal{T}_+|^2+|\overline{\mathcal{T}}_-|^2+|\overline{\mathcal{T}}_+|^2\right]^{-1} & H &= 2N\,\mathrm{Re}\left[\tfrac{q}{p}\left(\overline{\mathcal{T}}_-\mathcal{T}_-^* + \overline{\mathcal{T}}_+\mathcal{T}_+^*\right)\right] \quad , \end{aligned} \tag{6.44}$$

where N is a normalisation constant and the notation of Section 2.9 has been slightly extended so that $\overline{\mathcal{T}}_i$ is the CP conjugate amplitude corresponding to $\mathcal{T}_i$. $q/p = |q/p|\exp(i\Phi_q)$ is the ratio of B meson mixing parameters which are given in table 6.3.

If the left- and right-handed amplitudes are parametrised as

$$\mathcal{T}_- = A_L e^{i\phi_L} \qquad\qquad \mathcal{T}_+ = A_R e^{i\phi_R} \quad , \tag{6.45}$$

where $\phi_{L,R}$ is the CP-odd weak phase and the strong phase is retained in $A_{L,R}$, then the CP conjugate amplitudes are

$$\overline{\mathcal{T}}_+ = \xi A_L e^{-i\phi_L} \qquad\qquad \overline{\mathcal{T}}_- = \xi A_R e^{-i\phi_R} \quad , \tag{6.46}$$

where ξ is the CP eigenvalue of the final state. $\xi = 1$ for ρ, ω and ϕ and for the K^* it depends on the daughter state: it is $\xi = 1$ for the $K_S\pi^0$ state and $\xi = -1$ for the $K_L\pi^0$ state [197]. The

$B \to V\gamma$	$B^0 \to K^*\gamma$	$B^0 \to (\rho,\omega)\gamma$	$B_s \to \phi\gamma$	$B_s \to \bar{K}^*\gamma$
Type	$b \to s$	$b \to d$	$b \to s$	$b \to d$
$S[B \to V\gamma]_{\rm LZ}$	$1.2 \pm 0.9\%$	$-1.2 \pm 0.8\%$	$0.01 \pm 0.03\%$	$-0.3 \pm 0.5\%$
$H[B \to V\gamma]_{\rm LZ}$	$(1.2 \pm 1.0\%)$	$(-0.9 \pm 1.4\%)$	$1.6 \pm 1.1\%$	$-1.7 \pm 2.1\%$
$S[B \to V\gamma]_{\mathcal{O}_7}$	$1.7 \pm 0.4\%$	0%	0%	0%
$H[B \to V\gamma]_{\mathcal{O}_7}$	$(1.8 \pm 0.3\%)$	(0%)	$2.5 \pm 0.5\%$	0%
$S[B \to V\gamma]_{\rm HFAG}$	$-0.16(22)$	$-0.83(65)(18)$		

Table 6.4: Predictions for the CP violation parameters S and H in $B \to V\gamma$ type decays. The top section shows the prediction along with the associated uncertainty. $\xi = 1$ has been taken for all final states in (6.46); in the K^* case it depends on the daughter state as described below (6.46). Results for H in brackets are given for purposes of comparison but are not expected to be experimentally measurable since the width difference of B_d mesons is too small [197]. The middle section leading order results from the $\mathcal{O}_7$ operator only, for comparison purposes. The quoted uncertainty for these values arises from scale variation of the strange quark mass only. In the last line, the present experimental average from HFAG [147] is included, which is consistent with the theoretical result, although the uncertainty must be substantially reduced before a truly meaningful comparison is possible.

CP asymmetry parameters S and H may then be written

$$\begin{aligned} \begin{Bmatrix} S \\ H \end{Bmatrix} &= 2\xi \frac{\mathrm{Re}[A_L^* A_R]}{|A_L|^2+|A_R|^2} \begin{Bmatrix} \sin \\ \cos \end{Bmatrix} (\Phi_q - \phi_L - \phi_R) \\ &\xrightarrow{A_R \ll A_L} 2\xi\, \mathrm{Re}\left[\frac{A_R}{A_L}\right] \begin{Bmatrix} \sin \\ \cos \end{Bmatrix} (\Phi_q - \phi_L - \phi_R) \quad , \end{aligned} \tag{6.47}$$

where the approximation $|q/p| = 1$ has been used, which holds to good accuracy as can be seen from table 6.3. It is then apparent that a measurement of S or H is an indirect measurement of the right-handed amplitude.

The results of this calculation are given in table 6.4, along with the short-distance penguin contribution for comparison. In no case does the result including the $\mathcal{O}_2$ contribution differ from the short-distance value by more than 1.5σ. This is due to two factors: first, the $\mathcal{O}_2$ contribution is smaller than previously expected at only the 1% level and second, the uncertainties in table 6.2 are large. The result which stands out in table 6.4 is for $S[B_s \to \phi\gamma]$, which is both much smaller and more precisely determined than all the others. This is a result of (6.47) and the hierarchy of CKM coefficients in $b \to s$ decays. The factor $\sin(\Phi_q - \phi_L - \phi_R)$ is zero if the spectator quark in the B meson has the same flavour as the b quark decay product, which results in the weak phase of the $\bar{B}$-B oscillation being the same as the weak phase of the $B \to V\gamma$ transition. For the $B \to \rho\gamma$ decay this suppression, along with the independent m_d/m_b suppression, is lifted by the $\mathcal{O}_2$ operator which has a different weak phase but for $B_s \to \phi\gamma$ it survives since $|\lambda_u| \ll |\lambda_t|$ and hence the difference between the weak phases is small.

6.8.2 The P_1 and S_3 angular observables

In recent years, the full angular structure of $B \to V l^+ l^-$ decays have been studied [98], and optimized observables with reduced form factor uncertainty proposed [99] and improved [100]. One of these angular observables, P_1, originally introduced as $A_T^{(2)}$ in [199], is sensitive to interference between the left- and right-handed amplitudes. In the normalisation conventions introduced in Section 2.9, P_1 is given by[11]

$$P_1 \equiv A_T^{(2)} = \frac{|\mathcal{T}_V^V|^2+|\mathcal{T}_V^A|^2-|\mathcal{T}_A^V|^2-|\mathcal{T}_A^A|^2}{|\mathcal{T}_V^V|^2+|\mathcal{T}_V^A|^2+|\mathcal{T}_A^V|^2+|\mathcal{T}_A^A|^2} \quad , \tag{6.48}$$

where lepton masses have been neglected. P_1 is closely related to another observable S_3 [98], which has a stronger dependence on form factors than P_1 and is thus less theoretically clean but at present has smaller experimental errors [200], so predictions for S_3 will also be provided. In the $\mathcal{T}$ convention, it is given by

$$S_3 = \frac{1}{2}\frac{|\mathcal{T}_V^V|^2+|\mathcal{T}_V^A|^2-|\mathcal{T}_A^V|^2-|\mathcal{T}_A^A|^2}{|\mathcal{T}_V^V|^2+|\mathcal{T}_V^A|^2+|\mathcal{T}_A^V|^2+|\mathcal{T}_A^A|^2+|\mathcal{T}_0^V|^2+|\mathcal{T}_0^A|^2} \quad , \tag{6.49}$$

where again lepton masses have been set to zero.

Since the $\mathcal{T}$ amplitudes used in this thesis differ from the $A_{\perp,\parallel,0}^{V,A}$ used to define the P_1 and S_3 by a q^2 dependent normalisation factor, in addition to a linear change of basis, averaging over a q^2 bin must be performed with an appropriate weight according to

$$\begin{aligned}\langle P_1 \rangle &= \frac{\left\langle |\mathcal{T}_V^V|^2+|\mathcal{T}_V^A|^2-|\mathcal{T}_A^V|^2-|\mathcal{T}_A^A|^2 \right\rangle_\Gamma}{\left\langle |\mathcal{T}_V^V|^2+|\mathcal{T}_V^A|^2+|\mathcal{T}_A^V|^2+|\mathcal{T}_A^A|^2 \right\rangle_\Gamma} \\ \langle S_3 \rangle &= \frac{1}{2}\frac{\left\langle |\mathcal{T}_V^V|^2+|\mathcal{T}_V^A|^2-|\mathcal{T}_A^V|^2-|\mathcal{T}_A^A|^2 \right\rangle_\Gamma}{\left\langle |\mathcal{T}_V^V|^2+|\mathcal{T}_V^A|^2+|\mathcal{T}_A^V|^2+|\mathcal{T}_A^A|^2+|\mathcal{T}_0^V|^2+|\mathcal{T}_0^A|^2 \right\rangle_\Gamma} \quad ,\end{aligned} \tag{6.50}$$

where the weighted average $\left\langle f(q^2) \right\rangle_\Gamma$ is defined as

$$\left\langle f(q^2) \right\rangle_\Gamma \equiv \int f(q^2) \left[\frac{\lambda(m_B^2, m_{K^*}^2, q^2)^{3/2}}{q^2} \right] dq^2 \quad . \tag{6.51}$$

This brings amplitudes $|\mathcal{T}_i|^2$ into the same q^2 normalisation convention as the I_i angular coefficients[12] defined in [98] up to an overall constant which cancels in both (6.48) and (6.49).

The results of these calculations are presented in tables 6.5 and 6.6. Plots of the full q^2 dependence are shown for the $[1, 6]\,\text{GeV}^2$ range in Figure 6.6. The form factors used in these calculations are those described in [190] because they appear to give better small q^2 behaviour, that is to say, the right-handed component at $q^2 = 0$ is smaller than in other available form factor fits [81, 194]. The uncertainties in the tables and plots are calculated using the method

[11] The upper index denotes the parity of the operator producing the lepton pair, and the lower index the vector meson polarisation

[12] Also frequently known as J_i, e.g. [99, 100]

	Prediction		LHCb [200]	
Bin/GeV^2	P_1	S_3	P_1	S_3
$[1,6]$	$-0.037(47)$	$-0.006(7)$	$0.15^{+0.39+0.03}_{-0.41-0.03}$	$0.03^{+0.07+0.01}_{-0.07-0.01}$
$[2,4.3]$	$-0.027(48)$	$-0.003(7)$	$-0.29^{+0.65+0.02}_{-0.46-0.03}$	$-0.04^{+0.10+0.01}_{-0.06-0.01}$
$[4.3,6]$	$-0.069(73)$	$-0.013(11)$		

Table 6.5: P_1 and S_3 angular observables integrated over standard q^2 bins in the recoil range accessible to this calculation. The $[4.3,6]\,\mathrm{GeV}^2$ bin is included for comparison with [100]. The present level of experimental uncertainty indicates no deviation from the SM, and indeed the theoretical prediction is essentially zero in view of those uncertainties. See text for details of the uncertainties.

Bin/GeV^2	P_1	S_3
$[1,2]$	$0.011(51)$	$0.002(9)$
$[2,3]$	$-0.010(49)$	$-0.001(6)$
$[3,4]$	$-0.035(50)$	$-0.004(7)$
$[4,5]$	$-0.056(62)$	$-0.010(8)$
$[5,6]$	$-0.074(78)$	$-0.014(12)$

Table 6.6: Theoretical predictions for P_1 and S_3 in $1\,\mathrm{GeV}^2$ bins. See text for a discussion of the uncertainties.

described in Section 5.5.1 but in this case there is an additional problem due to extracting the right-handed form factor from fits given in a parity basis. To allow for this, the right-handed form factor is assigned an uncertainty of 2.5% of the magnitude of the left-handed form factor, which is given as the maximum fit error in [81]. Although a different method of fitting is used in [190] than in [81] the former does not discuss the precision of the fit, but since it uses the latter as input it seems reasonable to assume the precision of both fits is similar. Unfortunately m_s/m_b is also at the percent level, so this assumption makes the uncertainty in the right-handed short-distance amplitude large, and since the results of Section 6.3 indicate that the $\mathcal{O}_2$ contribution is in fact sub-leading, the overall uncertainty in P_1 and S_3 is dominated by this fit precision error. These uncertainties are similar to those quoted in [100] as a result of $\Lambda_{\mathrm{QCD}}/m_b$ corrections. It should be possible to reduce them by an order of magnitude if form factors can be calculated and fitted for the right-handed amplitude separately.

6.9 Conclusions

LCSR has been used to compute the contribution of charm loops emitting a soft gluon to the $B \to K^* l^+ l^-$ decay amplitude at large recoil. The contributions of charm loops exchanging gluons with the B and K^* valence quarks are significant because they are not suppressed by small WC, the Cabibbo angle, or gauge invariance at $q^2 = 0$, as is the factorisable charm bubble. They therefore represent a potentially significant contribution to the overall branching fraction. The contribution of hard gluons has been worked out in an inclusive approach in [104] and that of soft initial-state gluons in [194], so that the present calculation means that the set of next-to-leading charm bubble diagrams is now in principle complete.

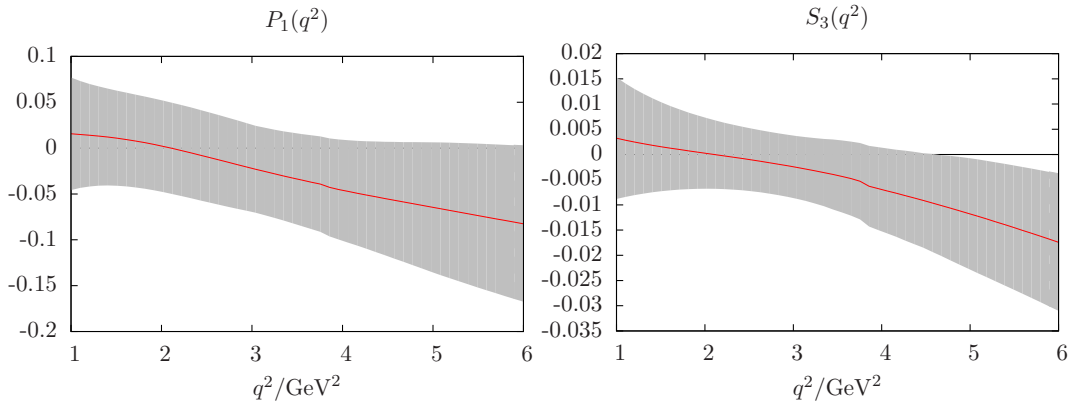

Figure 6.6: Plot of P_1 and S_3 estimate including $\mathcal{O}_2$ soft gluon effects. See text for a discussion of the error bands.

It transpires that in fact the amplitude for a soft gluon to be radiated into the final-state meson is small and is thus not relevant to the overall branching fraction. It is nonetheless important since it was previously claimed [185] that it could give the dominant contribution to the right-handed decay amplitude in $B \to V\gamma$. This has been found not to be the case, although it still represents a sizeable correction to the short distance right handed amplitude from the electromagnetic operator $\mathcal{O}_7$. The principal result of this calculation is therefore not so much an accurate calculation of the non-factorisable charm bubble term, since the uncertainties in table 6.2 are substantial compared to the overall result, but the finding that it does not represent a significant enhancement to the short-distance term, as can be seen in Figure 6.5.

The contribution of the $\mathcal{O}_2$ operator with a soft gluon from the initial-state B meson has been discussed in Section 6.4. Although the attempt there to produce a result quantitatively comparable to that computed using QCDF in [194] failed due to instability of the sum rules constructed, the same qualitative features were found, including that this contribution does not give a contribution to the right-handed amplitude. It also appears that the present state of knowledge of the three-particle B meson DA is unsatisfactory as the available sum rules for $\lambda_E^2 + \lambda_H^2$, both as originally developed in [193] and an alternate sum rule given in Section 6.4, are not numerically stable. This does not mean that large corrections are expected since there is no reason to believe that the value $\lambda_E^2 + \lambda_H^2 = 0.48\,\mathrm{GeV}^2$, derived from equations of motion in [195], is substantially incorrect; however, it is dependent on the B meson wave-function model chosen and therefore $O(1)$ corrections are to be expected.

Finally, the new result for the non-factorisable $\mathcal{O}_2$ diagram has been applied to produce updated predictions of CP asymmetries in various $B \to V\gamma$ decays and the P_1 and S_3 angular coefficients in $B \to K^* l^+ l^-$. At present, experimental errors in these channels are rather large in comparison to the theoretical uncertainty, and the theoretical prediction is for a small effect in all cases. The prediction of the angular coefficients P_1 and S_3 is obstructed somewhat, due to the lack of an accurate fit of the right-handed component of $B \to V$ form factors over the whole

q^2 range. Computing the right-handed form factor is beyond the scope of this chapter but it would appear possible to extend [81] to give the required result, and this would be expected to reduce the error in the right-handed $B \to V l^+ l^-$ amplitude by around an order of magnitude when combined with the results calculated in this chapter, which provide a similar improvement over the previous inclusive estimate [185] of the non-factorisable charm loop effect.

Chapter 7

Conclusions

In this thesis, calculations of several new contributions to the closely-related semi-leptonic and radiative B meson decays have been presented. Although these decays are rare, they play a crucial role in testing the decays of the b quark because non-perturbative QCD effects are under good theoretical control, and factorisation and sum rules give predictions with good accuracy. Despite the fact that they represent only a small class of possible B meson decays, the processes $B \to X\gamma$ and $B \to Xl^+l^-$ offer many observables such as asymmetries and angular coefficients, which can provide independent constraints on the short-distance physics of b quark decays. Progress in the search for physics beyond the SM in the B sector therefore depends both on improved measurements of these many different quantities and better theoretical understanding of the contributions of effective operators to each of them. The variety of observables means that each can be sensitive to different operators and different quark-level processes induced by those operators.

The calculation of the chromomagnetic matrix element in Chapter 3 means that the leading amplitudes for each of the ten operators contributing to semi-leptonic B decays are now known. That this contribution was not computed previously was due to a breakdown of QCDF due to the presence of a power-like infrared divergence in one Feynman diagram. The LCSR method was used to overcome this difficulty, but a new difficulty was encountered not previously seen in B meson sum rules, that of anomalous thresholds. Whilst these do not lead to any theoretical problems in the LCSR method, they do make the required analytic continuation more complicated than is usually the case. Unfortunately such difficulties are to be expected in future multi-loop sum rule calculations, and indeed they were encountered again in the calculation of a certain higher twist WA diagram in Chapter 5.

Although the chromomagnetic operator gives a small contribution to the overall branching fraction and is also not a major contributor to the isospin asymmetry computed in Chapter 5, this development means that should deviations from SM predictions be found it would be

possible to assess whether new contributions to the C_8 WC are responsible. In light of data showing unexpectedly large CP violation in hadronic D decays and the fact that an enhanced C_8 WC could be responsible [150], Chapter 4 put forward an argument that should the future measurement of the CP asymmetry in $D \to V\gamma$ also be above expectations in the SM, new contributions to C_8 must be considered a strong possibility, since it is not as well constrained as four-quark operators by the overall branching fraction, and the associated chromomagnetic matrix element has a large strong phase necessary to produce observable direct CP violation when the dominant amplitude is real. Unfortunately, recent data from LHCb on the direct CP asymmetries in D decays did not confirm the earlier measurements and there is now much less reason to expect new physics to be found through measuring the CP asymmetry of $D \to V\gamma$ decays. Nonetheless, the points in Chapter 4 remain valid; both the analysis of the leading amplitude in radiative D meson decays and the argument that the chromomagnetic matrix element is the most promising candidate should sizeable CP asymmetries eventually be found, once the decay $D \to V\gamma$ is measured with sufficient accuracy.

The analysis of the isospin asymmetry in $B \to V$ decays in Chapter 5 extends prior results in two orthogonal directions: first, the LCSR method is used for the calculation of WA in $B \to Vl^+l^-$ decays and previous results using QCDF are confirmed, and second, the WA and QLSS processes are extended to a general basis of four-quark operators to facilitate beyond-SM analyses in this channel. The isospin asymmetry in $B \to P$ decays was also considered, which included calculation of a new term at sub-leading twist which turns out to give a large contribution in the SM but violates the oft-made assumption that the pseudoscalar-meson decay amplitude is equivalent to the longitudinal amplitude for vector-meson decay. The best-measured isospin asymmetry, that in $B \to K^*\gamma$, was found to be in good agreement with SM expectations; however, the decays $B \to \rho\gamma$ and $B \to Kl^+l^-$ were not. In the case of the ρ meson it was argued that a large splitting between the CP-averaged $B \to \rho\gamma$ and $B \to K^*\gamma$ isospin asymmetries cannot be accommodated in the SM, given that the large WA contribution separating the two amplitudes is suppressed by an order of magnitude in the CP-average by CKM factors. In the absence of a combined fit of $b \to d$ decays it is not possible to attribute this discrepancy to a specific cause, but it does appear to be the neutral rather than the charged decay which is presently at odds with the SM prediction. The situation for the $B \to K$ is rather different, firstly because the measured isospin asymmetry is very large and secondly because the SM prediction is much smaller than the case of vector final states since the rate is dominated by the $\mathcal{O}_{9,10}$ operators rather than $\mathcal{O}_7$, which has a much smaller WC but is enhanced, along with the isospin-violating WA terms, by the photon pole in $B \to V\gamma$ decays. An isospin asymmetry on the 40% level in $B \to Kl^+l^-$ decays would therefore imply an enhancement of an order-of-magnitude in one of the operators contributing to isospin violation, and such a large deviation from SM expectations would be expected to show up in other channels. It was however pointed out that by a careful choice of the Lorentz structure of an effective operator it can be made to

contribute to only the vector or pseudoscalar case.

Chapter 6 is centred on the calculation of radiative and semi-leptonic B meson decays through a charm-quark loop induced by the $\mathcal{O}_2$ operator, where a soft gluon is emitted into the final-state meson. This contribution has been a significant source of uncertainty in certain observables for some years since the amplitudes to emit left- and right-handed photons have comparable magnitudes, and it had been thought that it could dominate the right-handed rate. The main contribution of the improved calculation presented here is that in spite of the fact that its uncertainty is large in comparison to its own magnitude, it reduces the overall uncertainty in the right-handed decay rate substantially, because it has been shown not to be the dominant term. Unfortunately, since up until now published fits of the $B \to V$ form factors have not used the left-right polarisation basis, estimating the right-handed matrix element accurately is not straightforward. A computation of the right-handed form factor amplitude should be possible, although LCSR must be used since QCDF cannot be easily extended to power-suppressed corrections, and would represent the next step in reducing the theoretical uncertainty in the relevant angular observables P_1 and S_3. The computation of time-dependent CP asymmetries fortunately avoids such problems because the form factors are known to preserve the short-distance helicity structure exactly for the on-shell photon, and therefore predictions of these quantities with percent-level accuracy are possible.

The way forward from these results is mainly a case of waiting for further experimental data, since the majority of theoretical predictions given in this thesis are already ahead of experimental precision. There are exceptions in the isospin asymmetry of $B \to \rho\gamma$ and $B \to Kl^+l^-$ where there is a significant tension between the current measurements and theoretical expectations, but given past experience, such as in the case of the CP asymmetry in hadronic charm decays discussed in Chapter 4 where new data has shifted the world average result significantly, it would seem sensible not to draw firm conclusions at this stage. Nonetheless there remain open theoretical challenges in this area: sub-leading power corrections and α_s corrections are not well-known in all cases, and a calculation of the QLSS terms and non-factorisable WA using LCSR would reduce the theoretical uncertainty in the isospin asymmetry and right-handed amplitudes significantly, although it is expected that this would be obstructed by anomalous thresholds. The QLSS diagram in particular is of interest because an LCSR calculation of that topology would also include the soft initial-state gluon contribution through the $\mathcal{O}_2$ operator, discussed in Chapter 6, which has been claimed to give a significant correction to the overall branching fraction [194]. That statement however was dependent on B meson wave-function models and confirmation through an alternative approach would be significant. Similarly, an update of LCSR form factor estimates in the helicity rather than the parity basis would reduce the large uncertainties in the P_1 angular observable.

Appendix A

Definitions

As explained in Section 2.1, the convention used in this thesis for the Levi-Civita tensor is different from that used in FeynCalc [25] by default. The choice of convention implies the sign of the trace

$$\mathrm{Tr}\{\gamma^\mu\gamma^\nu\gamma^\rho\gamma^\sigma\gamma_5\} = 4i\epsilon^{\mu\nu\rho\sigma} \ , \tag{A.1}$$

and fortunately this is configurable in FeynCalc using the code

```
Tr[GA[a,b,c,d,5]]
SetOptions[Tr, LeviCivitaSign -> 1];
SetOptions[DiracTrace, LeviCivitaSign -> 1];
Tr[GA[a,b,c,d,5]]
```

which should print

$-4i\epsilon^{abcd}$

$4i\epsilon^{abcd}$

to indicate that the convention has been changed.

Appendix B

Distribution amplitudes

In this appendix the distribution amplitudes used throughout this thesis are collected.

For further references see the classic review [82], the LCSR review [105] and the thorough paper on higher twist DA [70].

B.1 Light meson DA

The 2-particle DA for the pseudoscalar at twist-2 (ϕ_K) and -3 ($\phi_{p,\sigma}$) (e.g. [201]) is given by

$$\begin{aligned}\langle K(p)\,|\,\bar{s}(x)_a[x,z]q(z)_b\,|\,0\rangle = \int_0^1 du e^{i(up\cdot x+\bar{u}p\cdot z)}\Bigg[i\frac{f_K}{4N_c}[\not{p}\gamma_5]_{ba}\phi_K(u) \\ -i\frac{\mu_K^2}{4N_c}[\gamma_5]_{ba}\phi_p(u) - i\frac{\mu_K^2}{24N_c}p_\mu(x-z)_\nu[\sigma^{\mu\nu}\gamma_5]_{ba}\phi_\sigma(u)\Bigg] + \text{higher twist}\,,\end{aligned} \tag{B.1}$$

where a, b are Dirac indices, $\bar{u} \equiv 1-u$, $\mu_K^2 \equiv f_K m_K^2/(m_s+m_q)$ and the $[x,z]$ represents a QCD Wilson line to make the matrix element gauge invariant. The asymptotic forms of the DA functions are

$$\phi_K(u) = \phi_\sigma(u) = 6\bar{u}u \qquad\qquad \phi_p(u) = 1 \quad . \tag{B.2}$$

From the appendix of [93] it is seen that upon neglecting quark masses and three-particle DAs, equations of motion constrain $\phi_{p,\sigma}(u)$ to their asymptotic forms. $\phi_K(u)$ is expanded in Gegenbauer moments as usual.

The 2-particle DA for the vector meson at twist-2 ($\phi_{\parallel,\perp}$) and -3 ($g_\perp^{(v,a)}$) (e.g. [81]) is

$$\begin{aligned}\langle K^*(p,\eta)\,|\,\bar{s}(x)_a[x,z]q(z)_b\,|\,0\rangle = \int_0^1 du\, e^{i(up\cdot x+\bar{u}p\cdot z)}\Bigg\{\frac{f_{K^*}^\perp}{4N_c}\Bigg[(\not{\eta}\not{p})_{ba}\phi_\perp(u)\\ -\frac{i}{2}(1)_{ba}(\eta\cdot(x-z))m_{K^*}^2 h_\parallel^{(s)}(u) - i(\sigma_{\mu\nu})_{ba}p^\mu(x-z)^\nu\frac{\eta\cdot(x-z)}{(p\cdot(x-z))^2}m_{K^*}^2 h_\parallel^{(t)}(u)\Bigg]\\ +\frac{m_{K^*}f_{K^*}}{4N_c}\Bigg[(\not{p})_{ba}\frac{\eta\cdot(x-z)}{p\cdot(x-z)}\phi_\parallel(u) + \left(\not{\eta}-\not{p}\frac{\eta\cdot(x-z)}{p\cdot(x-z)}\right)_{ba} g_\perp^{(v)}(u)\\ +\frac{1}{4}\epsilon_{\mu\nu\rho\sigma}\eta^\nu p^\rho(x-z)^\sigma\,(\gamma^\mu\gamma_5)_{ba}\,g_\perp^{(a)}(u)\Bigg]\Bigg\} + \text{higher twist}\,.\end{aligned} \tag{B.3}$$

The asymptotic DAs are

$$\begin{aligned}\phi_\perp(u) = \phi_\parallel(u) = g_\perp^{(a)}(u) = h_\parallel^{(s)}(u) = 6\bar{u}u\\ g_\perp^{(v)}(u) = \frac{3}{4}\left(1+(u-\bar{u})^2\right) \qquad\qquad h_\parallel^{(t)}(u) = 3(u-\bar{u})^2\,.\end{aligned} \tag{B.4}$$

In fact, these functions overparametrise the K^* state and are related by QCD equations of motion [70], the use of which in calculating B meson weak annihilation is described in Section 5.3.2.

B.1.1 Three particle distribution amplitudes

The leading twist-3 distribution amplitudes for vector mesons are [127]

$$\langle 0|\bar{q}_2(z)g\widetilde{G}_{\mu\nu}(vz)\gamma_\alpha\gamma_5 q_1(-z)|V(p,\eta)\rangle = -f_V m_V T^3_{\alpha\mu\nu}\mathcal{A}(v,pz) + O(m_V^3) \tag{B.5}$$

$$\langle 0|\bar{q}_2(z)gG_{\mu\nu}(vz)\gamma_\alpha q_1(-z)|V(p,\eta)\rangle = +if_V m_V T^3_{\alpha\mu\nu}\mathcal{V}(v,pz) + O(m_V^3) \tag{B.6}$$

$$\langle 0|\bar{q}_2(z)gG_{\mu\nu}(vz)\sigma_{\alpha\beta} q_1(-z)|V(p,\eta)\rangle = \frac{1}{2}f_V^\perp m_V^2\frac{\eta\cdot z}{p\cdot z}T^4_{\alpha\beta\mu\nu}\mathcal{T}(v,pz) + O(m_V^3)\quad, \tag{B.7}$$

where $\widetilde{G}_{\mu\nu} = {}^1\!/_2\epsilon_{\mu\nu\alpha\beta}G^{\alpha\beta}$ and the $T^{3,4}$ tensors are given by

$$\begin{aligned}T^3_{\alpha\mu\nu} &= p_\alpha[p_\mu\eta^{(\lambda)}_{\perp\nu} - p_\nu\eta^{(\lambda)}_{\perp\mu}]\\ T^4_{\alpha\beta\mu\nu} &= p_\alpha p_\mu g^\perp_{\beta\nu} - p_\beta p_\mu g^\perp_{\alpha\nu} - p_\alpha p_\nu g^\perp_{\beta\mu} + p_\beta p_\nu g^\perp_{\alpha\mu}\quad.\end{aligned}$$

At $m_{K^*}^2 = 0$ identical results are produced with the replacements $\eta_\perp \to \eta$ and $g^\perp \to g$. The distribution amplitudes are parametrised as

$$[\mathcal{A},\mathcal{V},\mathcal{T}](v,pz) = \int_0^1 d\alpha_1\int_0^1 d\alpha_2\int_0^1 d\alpha_3\delta(1-\alpha_1-\alpha_2-\alpha_3)e^{-ipz(\alpha_2-\alpha_1+v\alpha_3)}[\mathcal{A},\mathcal{V},\mathcal{T}](\underline{\alpha})\quad,$$

and the conformal expansion of the DA reads

$$\begin{aligned}
\mathcal{A}(\underline{\alpha}) &\equiv \tilde{\phi}^{\parallel}_{3;V} = 360\alpha_1\alpha_2\alpha_3^2(\zeta^{\parallel}_{3;V} + \tilde{\lambda}^{\parallel}_{3;V}(\alpha_1-\alpha_2) + \tilde{\omega}^{\parallel}_{3;V}\frac{1}{2}(7\alpha_3-3) + \dots) \\
\mathcal{V}(\underline{\alpha}) &\equiv \phi^{\parallel}_{3;V} = 360\alpha_1\alpha_2\alpha_3^2(\kappa^{\parallel}_{3;V} + \omega^{\parallel}_{3;V}(\alpha_1-\alpha_2) + \lambda^{\parallel}_{3;V}\frac{1}{2}(7\alpha_3-3) + \dots) \\
\mathcal{T}(\underline{\alpha}) &\equiv \phi^{\perp}_{3;V} = 360\alpha_1\alpha_2\alpha_3^2(\kappa^{\perp}_{3;V} + \omega^{\perp}_{3;V}(\alpha_1-\alpha_2) + \lambda^{\perp}_{3;V}\frac{1}{2}(7\alpha_3-3) + \dots) \quad .
\end{aligned} \tag{B.8}$$

The notation with $\phi^{\parallel}$ has been used in the recent literature [127, 186] to make the notation more systematic. The values used in thesis for the K^* are [127, table 1]

$$\begin{aligned}
\zeta^{\parallel}_{3K^*} &= 0.023(8) & \tilde{\lambda}^{\parallel}_{3K^*} &= 0.035(15) & \tilde{\omega}^{\parallel}_{3K^*} &= -0.07(3) \\
\kappa^{\parallel}_{3K^*} &= 0.000(1) & \omega^{\parallel}_{3K^*} &= 0.10(04) & \lambda^{\parallel}_{3K^*} &= -0.008(4) \\
\kappa^{\perp}_{3K^*} &= 0.003(3) & \omega^{\perp}_{3K^*} &= 0.3(1) & \lambda^{\perp}_{3K^*} &= -0.025(20) \quad ,
\end{aligned} \tag{B.9}$$

at $\mu = 1\,\text{GeV}$. The parameters κ and λ are zero for the vector mesons which have definite G-parity such as the ρ. Here these parameters are small since G-parity breaking is small but non-zero in the K^*.

B.2 Photon DA

The leading twist 2 photon DA [165] is:

$$\begin{aligned}
\langle\gamma(q,\epsilon)|\bar{q}_a(x)[x,z]q_b(z)|0\rangle &= ie\int_0^1 d^4y\epsilon_\mu e^{iq\cdot y}\,\langle 0|T\bar{q}_a(x)[x,z]q_b(z)j^\mu_{\text{em}}(y)|0\rangle \\
&= \frac{iQ_q\,\langle\bar{q}q\rangle}{4N_c}\int_0^1 du e^{i(uq\cdot x+\bar{u}q\cdot z)}(\phi_\gamma(u)\sigma^{\alpha\beta}\epsilon_\alpha q_\beta + (x-z)\cdot\epsilon)_{ba} + \text{higher twist}\,.
\end{aligned} \tag{B.10}$$

The first and second term on the last line correspond to the left-hand side of equation [165] and second term on the right-hand side of the same equation. The reason (B.10) is not gauge invariant is that $[x,z]$ does not contain the QED Wilson line as in the expansion of the external field to first order. The use of a polarisation vector ϵ_μ implies the use of the Lorentz gauge $A_\mu \to \epsilon_\mu e^{iq\cdot x}$ where $\epsilon\cdot q = 0$. It is however possible to check gauge invariance of results computed using this formula by the replacement

$$\epsilon_\mu \to \epsilon_\mu - \frac{n\cdot\epsilon}{n\cdot q}q_\mu \tag{B.11}$$

which allows axial gauges to be accessed. Note that the perturbative photon contribution must be included in addition to the photon DA since it is a separate term in the OPE. The asymptotic photon DA is given by

$$\phi_\gamma(u) = 6\chi\bar{u}u \quad , \tag{B.12}$$

where χ is the magnetic susceptibility of the quark condensate, calculated to be $\chi = -3.15(10)\text{GeV}^{-2}$ at $\mu = 1\text{GeV}$ in [165] (the sign is adjusted to the convention of the covariant derivative (2.1)).

B.3 B-meson DA

The leading order two particle B meson DA and its associated definitions are given in Section 5.4.5. Here the complete definition is given along with the wave functions $\phi_\pm$ commonly used, which are the model functions defined in [193]

$$\phi_+(\omega) = \frac{\omega}{\omega_0^2} e^{-\omega/\omega_0} \qquad \phi_-(\omega) = \frac{1}{\omega_0} e^{-\omega/\omega_0} \quad , \tag{B.13}$$

with $\omega_0 = 2\Lambda_{\text{HQET}}/3 \simeq 0.4\text{GeV}$. Note that these two functions are related by Wandzura-Wilczek type equations of motion [118]. The moment functions appearing in (5.35) are

$$\lambda_\pm^{-1}(q^2) = \int_0^\infty dl_+ \frac{\phi_\pm(\omega)}{l_+ - q^2/m_B - i\epsilon} \tag{B.14}$$

and they may owing to the choice of wave function (B.13) be integrated analytically

$$\lambda_+^{-1}(q^2) = \frac{1}{\omega_0}\left[1 + ye^{-y}(i\pi - \text{Ei}(y))\right] \ , \qquad \lambda_-^{-1}(q^2) = \frac{e^{-y}}{\omega_0}(i\pi - \text{Ei}(y)) \ , \tag{B.15}$$

where $y = q^2/\omega_0 m_B$ and the function Ei is the exponential integral.

B.4 Fermion propagator on the light-cone in a background field

The massive propagator in a gluonic background field on the light-cone can be obtained in the Fock-Schwinger gauge $x \cdot A = 0$ using the heat kernel method presented in the appendix of [76]. The propagator is expanded in powers of x^2

$$\begin{aligned} \langle 0|Tc(x)\bar{c}(0)|0\rangle_A &= i\int \tfrac{d^4k}{(2\pi)^4} e^{-ik\cdot x} S_c(k) \\ S_c(k) &= S_c^{(0)}(k) + S_c^{(2)}(k) + \dots \quad , \end{aligned} \tag{B.16}$$

where only the first correction $S_c^{(2)}$ is needed:

$$\begin{aligned} S_c^{(0)} &= \frac{\not{k} + m_c}{k^2 - m_c^2} \ , \\ S_c^{(2)} &= -\frac{g}{2}\int_0^1 dv \left(v\sigma\cdot G(vx)\frac{\not{k} + m_c}{(k^2 - m_c^2)^2} + \bar{v}\frac{\not{k} + m_c}{(k^2 - m_c^2)^2}\sigma\cdot G(vx)\right) . \end{aligned} \tag{B.17}$$

The computation of Chapter 6 can also be performed using the perturbative propagator without a light cone expansion, derived using the Fock-Schwinger gauge relation $A_\mu(x) = \int_0^1 vx^\rho G_{\rho\mu}(vx)dv$:

$$S_c^{(2)} = i\int d^4y \int_0^1 vdv\, gG_{\mu\nu}(vy) \int \frac{d^4l}{(2\pi)^4} e^{iy.(k-l)} \frac{\not{k} + m_c}{k^2 - m_c^2}\gamma^\mu \frac{\not{l} + m_c}{l^2 - m_c^2}\gamma^\nu \frac{\not{l} + m_c}{l^2 - m_c^2} \tag{B.18}$$

This has been confirmed to give the same results as those in Chapter 6 computed using the light cone expansion of the quark propagator.

B.5 Anomalous dimensions

Here the one-loop anomalous dimensions relevant to DA parameters and local OPE condensates used in this thesis are collected. The convention for the one-loop anomalous dimensions is chosen such that

$$c(q^2) = c(\mu^2)\left(\frac{\alpha_s(q^2)}{\alpha_s(\mu^2)}\right)^{-\gamma_c/2\beta_0} \quad , \tag{B.19}$$

where $\beta_0 = (11N_c - 2N_f)/3$ is the leading term in the QCD beta function as usual. Some authors define this equation with the exponent as $\pm\gamma_c/\beta_0$ instead, e.g. [70].

Anomalous dimensions for local operators, as well as associated coefficients specifically the quark mass and meson tensor decay constants such as $f_{K^*}^\perp$, are

$$\begin{aligned}
\gamma_{\bar{q}q} &= -\gamma_m = 6C_F && \text{e.g. [202]} \\
\gamma_{\bar{q}\sigma^{\mu\nu}q} &= \gamma_{f^\perp} = -2C_F && [203] \\
\gamma_{g_s\bar{q}Gq} &= C_F && [204],
\end{aligned} \tag{B.20}$$

where of course $C_F = 4/3$. The vector current, and thus the meson decay constants $f_{K^{(*)}}$, have no anomalous dimension. By construction, the anomalous dimension of the magnetic susceptibility appearing in the photon DA is given by, e.g. [77]:

$$\gamma_\chi \equiv \gamma_{\bar{q}\sigma^{\mu\nu}q} - \gamma_{\bar{q}q} = -8C_F \quad . \tag{B.21}$$

Anomalous dimensions for Gegenbauer coefficients appearing in the pseudoscalar and vector meson DAs are:

$$\begin{aligned}
\gamma_n^\perp &= -8C_F\left(\psi(n+1) + \gamma_E - \frac{3}{4} + \frac{1}{n+1}\right) && [70, (3.57)] \\
\gamma_n^\parallel = \gamma_n &= -8C_F\left(\psi(n+2) + \gamma_E - \frac{3}{4} - \frac{1}{2(n+1)(n+2)}\right) && [70, (4.49)], [201, (3.6)],
\end{aligned}$$

where n indicates it is associated with the n^{th} coefficient, ψ is the digamma function and γ_E is the Euler–Mascheroni constant as usual. $\gamma_n^{\perp,\parallel}$ are anomalous dimensions for the vector meson

DAs $\phi_{\perp,\parallel}(u)$ and γ_n is for the pseudoscalar DA $\phi_K(u)$. Note that these anomalous dimensions are for combinations like $f_{K*}^{\perp} a_n^{\perp}$, not the Gegenbauer moments themselves.

$\gamma_n^{\parallel} = \gamma_n$ is a consequence of both being the anomalous dimension of the same light cone operator, cf. Section 2.10. The appearance of a special function in a one loop anomalous dimension is explained by [83]

$$\psi(n) + \gamma_E = \sum_{k=1}^{n-1} \frac{1}{k} \tag{B.22}$$

and thus $\gamma_0^{\perp} = \gamma_{\bar{q}\sigma^{\mu\nu}q}$ and $\gamma_0^{\parallel} = \gamma_{\bar{q}\gamma^{\mu}q} = 0$ reduce to the local operator results.

Anomalous dimensions for the three-particle DAs are more complex due to mixing between the $\mathcal{A}$ and $\mathcal{V}$ expansion parameters beyond leading twist and therefore they are not listed here. They are available from [127] but it should be noted that a different convention for the anomalous dimensions is employed there: the exponent used in equations analogous to (B.19) is γ/β_0 and therefore the anomalous dimensions listed there must be scaled by a factor of -2 so that they can be used in (B.19).

Appendix C

Dyson-Schwinger equations (DSEs)

DSEs [58–60] were briefly mentioned in the main text, and so a brief discussion of their derivation is included here. In Minkowski space DSEs generally take the form

$$\left\langle \Psi \middle| \mathcal{T}\{\frac{\delta F[\phi]}{\delta\phi_i(x)} + iF[\phi]\frac{\delta S[\phi]}{\delta\phi_i(x)}\} \middle| \Phi \right\rangle = 0 \tag{C.1}$$

where $F[\phi]$ is an arbitrary polynomial of the field operators $\phi_i(x)$, and $S[\phi]$ is the classical action. Ψ and Φ are arbitrary external states. The equation (C.1) follows straightforwardly for $\Psi = \Phi = 0$ from the path integral representation of correlation functions, since

$$\begin{aligned}\left\langle 0 \middle| \mathcal{T}\{\frac{\delta F[\phi]}{\delta\phi_i(x)} + iF[\phi]\frac{\delta S[\phi]}{\delta\phi_i(x)}\} \middle| 0 \right\rangle &\propto \int \mathcal{D}\phi \left(\frac{\delta F[\phi]}{\delta\phi_i(x)} + iF[\phi]\frac{\delta S[\phi]}{\delta\phi_i(x)}\right)\exp(iS[\phi]) \\ &= \int \mathcal{D}\phi \ \frac{\delta}{\delta\phi_i(x)} F[\phi]\exp(iS[\phi]) = 0\end{aligned} \tag{C.2}$$

where $\int \mathcal{D}\phi$ denotes a path integral. This derivation of course assumes that the integral of a total derivative is zero, which is indeed the case when boundary terms vanish, as is generally assumed. It is however not always the case; DSEs for ghosts in Yang-Mills theory must be derived via a different method [205] in order to be non-perturbatively valid owing to the Gribov problem [206]. That this equation also holds for transitions between arbitrary states follows from the fact that external states may be represented by boundary conditions on space-like surfaces [59], and therefore the equation holds provided that such surfaces are well separated from the point x.

In DSE based calculations the usual next step is to define the connected generating functional W through

$$Z[J] = e^{W[J]} = \int \mathcal{D}\phi \ \exp\left(iS[\phi] + \int d^dx J(x)\phi(x)\right) \tag{C.3}$$

and then define the one-particle irreducible generating functional Γ as the Legendre transform of $W[J]$. These functionals are more useful than the partition function $Z[J]$ in most cases

because they reveal considerable internal structure of correlation functions, they are not as general as $Z[J]$ and (C.1), which because they apply to transitions between arbitrary states may be considered equations between time ordered products of operators. The definition $W[J] = \log Z[J]$ can only be applied to transitions between overlapping states, i.e. usually forward scattering problems, since for non-overlapping states $Z[0] = 0$. This breakdown is hardly surprising since the resulting DSEs on the connected generating functional W are non-linear and the utility DSEs requires that different derivatives of W commute with each other which is guaranteed by only considering expectation values rather than operators.

Appendix D

Additional chromomagnetic operator material

D.1 $t_H^{(P)}(u)$ formula

$$t_H^{(P)}(u) = \sum_{i\in\{a,b,c,d\}} \left[b_i^P B_i + c_i^P C_i\right] \tag{D.1}$$

$$\begin{aligned}
b_a^P =& \frac{1}{2}(u-1)^{-1} m_b^{-1} P^2 (q^2)^{-1} ((u-1)P^2 - uq^2)^{-1} (u(P^2-q^2)^2 + 4(P^2-p_B^2)q^2)^{-2} \\
& ((P^2-p_B^2)^2 + 2u(p_B^2+q^2)(P^2-p_B^2) + u^2(p_B^2-q^2)^2)^{-1} (m_b^2(u^2(Q_b(P^2-q^2) \\
& (-14q^2(P^2)^2 + (P^2)^3 + (8p_B^2-5q^2)q^2P^2 + 2p_B^2(q^2)^2) - Q_q(4(16p_B^2-13P^2)q^2 \\
& (P^2)^2 + (P^2)^4 + 6(3P^2-4p_B^2)(11P^2-12p_B^2)(q^2)^2 + 4(40p_B^2-53P^2)(q^2)^3 + 33 \\
& (q^2)^4))(P^2-p_B^2)^2 - 2uq^2((Q_b+4Q_q)(P^2)^2 - (Q_b+56Q_q)q^2P^2 + 4Q_qq^2(16p_B^2+5 \\
& q^2))(P^2-p_B^2)^3 - 16Q_q(q^2)^2(P^2-p_B^2)^4 + 5u^6(Q_b-Q_q)(p_B^2-q^2)^2(P^2-q^2)^4 + u^5 \\
& (P^2-q^2)^2(-2(8(Q_b-Q_q)(p_B^2)^2 + (9Q_b-7Q_q)q^2p_B^2 + (13Q_b-3Q_q)(q^2)^2) \\
& (P^2)^2 + 2(5Q_b(p_B^2+q^2) - Q_q(5p_B^2+q^2))(P^2)^3 + q^2((41Q_b-72Q_q)(p_B^2)^2 + 2(41 \\
& Q_q-6Q_b)q^2p_B^2 + (31Q_b-46Q_q)(q^2)^2)P^2 + 2Q_qq^2(-32q^2(p_B^2)^2 + 20(p_B^2)^3 + 17(q^2)^2 \\
& p_B^2 + (q^2)^3) - Q_bq^2(-17q^2(p_B^2)^2 + 14(p_B^2)^3 + 22(q^2)^2p_B^2 + (q^2)^3)) + u^3 \\
& (p_B^2-P^2)(2Q_q((72(p_B^2)^2 - 104P^2p_B^2 + 33(P^2)^2)q^2(P^2)^2 + (4p_B^2-3P^2) \\
& (P^2)^4 + 2(-176P^2(p_B^2)^2 + 64(p_B^2)^3 + 152(P^2)^2p_B^2 - 47(P^2)^3)(q^2)^2 + 2(12 \\
& (p_B^2)^2 - 60P^2p_B^2 + 61(P^2)^2)(q^2)^3 + (44p_B^2-63P^2)(q^2)^4 + 5(q^2)^5) + Q_b \\
& (P^2-q^2)(q^2(69p_B^2+50q^2)(P^2)^2 - (8p_B^2+29q^2)(P^2)^3 + 6(P^2)^4 + q^2(-36
\end{aligned}$$

$$(p_B^2)^2 - 62q^2p_B^2 + 3(q^2)^2)P^2 + p_B^2(10p_B^2 - 3q^2)(q^2)^2)) + u^4(q^2((201Q_b - 556$$
$$Q_q)q^2(p_B^2)^2 + 8(5Q_b - 16Q_q)(p_B^2)^3 + 2(113Q_b + 2Q_q)(q^2)^2p_B^2 + (64Q_b - 171Q_q)$$
$$(q^2)^3)(P^2)^2 + q^2(4Q_q(70(p_B^2)^2 + 71q^2p_B^2 + 30(q^2)^2) - Q_b(129(p_B^2)^2 + 222q^2$$
$$p_B^2 + 133(q^2)^2))(P^2)^3 + (18(Q_b - Q_q)(p_B^2)^2 + 58(2Q_b - 3Q_q)q^2p_B^2 + (97Q_b - 79Q_q)$$
$$(q^2)^2)(P^2)^4 + (22(Q_q - Q_b)p_B^2 + 4(7Q_q - 8Q_b)q^2)(P^2)^5 + 5(Q_b - Q_q)$$
$$(P^2)^6 + (q^2)^2(2Q_q(-68q^2(p_B^2)^2 + 208(p_B^2)^3 + 103(q^2)^2p_B^2 + 14(q^2)^3) - Q_b$$
$$(129q^2(p_B^2)^2 + 66(p_B^2)^3 + 98(q^2)^2p_B^2 + (q^2)^3))P^2 + (q^2)^2(13Q_b$$
$$(p_B^2)^2q^2(2p_B^2 + 3q^2) - Q_q(50(p_B^2)^2(q^2)^2 + 22p_B^2(q^2)^3 + (q^2)^4 - 32(p_B^2)^3$$
$$q^2 + 80(p_B^2)^4))))u^{-1} + (P^2 - p_B^2)((p_B^2 - P^2)(Q_b(q^2(24(p_B^2)^2 + 67q^2$$
$$p_B^2 + (q^2)^2)(P^2)^2 - q^2(25p_B^2 + 17q^2)(P^2)^3 - (p_B^2 - 13q^2)$$
$$(P^2)^4 + (P^2)^5 + (q^2)^2(-50(p_B^2)^2 - 35q^2p_B^2 + 54(q^2)^2)P^2 - 2p_B^2(q^2)^3(p_B^2 + 15$$
$$q^2)) - Q_q(P^2 - p_B^2)(-2(48(p_B^2)^2 - 80P^2p_B^2 + 29(P^2)^2)(q^2)^2 + 4(27P^2 - 8p_B^2)$$
$$(q^2)^3 + 33(q^2)^4 + 12(P^2)^3q^2 + (P^2)^4))u^2 + (2Q_q(P^2 - p_B^2)((-24(p_B^2)^2 + 40$$
$$P^2p_B^2 - 15(P^2)^2)q^2(P^2)^2 + (P^2)^5 + 2(80P^2(p_B^2)^2 - 32(p_B^2)^3 - 68(P^2)^2p_B^2 + 29$$
$$(P^2)^3)(q^2)^2 - 2(4(p_B^2)^2 - 44P^2p_B^2 + 59(P^2)^2)(q^2)^3 + (69P^2 - 56p_B^2)$$
$$(q^2)^4 + 5(q^2)^5) + Q_b(-q^2(285q^2(p_B^2)^2 + 60(p_B^2)^3 + 214(q^2)^2p_B^2 + 9(q^2)^3)$$
$$(P^2)^2 + q^2(123(p_B^2)^2 + 250q^2p_B^2 + 69(q^2)^2)(P^2)^3 - q^2(92p_B^2 + 71q^2)(P^2)^4 + (2$$
$$p_B^2 + 23q^2)(P^2)^5 - 2(P^2)^6 + (q^2)^2(159q^2(p_B^2)^2 + 130(p_B^2)^3 + 90(q^2)^2p_B^2 - 30$$
$$(q^2)^3)P^2 + p_B^2(q^2)^3(-50(p_B^2)^2 - 57q^2p_B^2 + 24(q^2)^2)))u^3 + (q^2((201Q_b - 292$$
$$Q_q)q^2(p_B^2)^2 + 8(7Q_b - 8Q_q)(p_B^2)^3 + 2(101Q_b - 58Q_q)(q^2)^2p_B^2 + (74Q_b - 221Q_q)$$
$$(q^2)^3)(P^2)^2 + q^2((136Q_q - 111Q_b)(p_B^2)^2 + 2(98Q_q - 93Q_b)q^2p_B^2 + 5(40Q_q - 23Q_b)$$
$$(q^2)^2)(P^2)^3 + (6(Q_b - Q_q)(p_B^2)^2 + 10(8Q_b - 9Q_q)q^2p_B^2 + (67Q_b - 97Q_q)$$
$$(q^2)^2)(P^2)^4 + 2(5(Q_q - Q_b)p_B^2 - 8Q_bq^2 + 10Q_qq^2)(P^2)^5 + 3(Q_b - Q_q)$$
$$(P^2)^6 - (q^2)^2((87Q_b + 88Q_q)q^2(p_B^2)^2 + 2(57Q_b - 112Q_q)(p_B^2)^3 + 2(61Q_b - 121Q_q)$$
$$(q^2)^2p_B^2 + (7Q_b - 52Q_q)(q^2)^3)P^2 + (q^2)^2(-(9Q_b + 38Q_q)(p_B^2)^2(q^2)^2 + 2$$
$$(18Q_b - 25Q_q)p_B^2(q^2)^3 + (Q_q - 6Q_b)(q^2)^4 + (58Q_b + 32Q_q)(p_B^2)^3q^2 - 48Q_q$$
$$(p_B^2)^4))u^4 + (P^2 - q^2)^2(-2(4(Q_b - Q_q)(p_B^2)^2 + (7Q_b - 5Q_q)q^2p_B^2 + (7Q_b - 9$$
$$Q_q)(q^2)^2)(P^2)^2 + 6(Q_b - Q_q)(p_B^2 + q^2)(P^2)^3 + q^2((33Q_b - 40Q_q)$$
$$(p_B^2)^2 + (46Q_q - 24Q_b)q^2p_B^2 + 3(9Q_b - 14Q_q)(q^2)^2)P^2 + q^2((29Q_b - 40Q_q)q^2$$
$$(p_B^2)^2 + 6(4Q_q - 3Q_b)(p_B^2)^3 + 22(Q_q - Q_b)(q^2)^2p_B^2 - (Q_b - 6Q_q)(q^2)^3))$$
$$u^5 + 3(Q_b - Q_q)(p_B^2 - q^2)^2(P^2 - q^2)^4u^6 - 2(P^2 - p_B^2)^2q^2(Q_b((p_B^2 - q^2)(P^2)^2 + 2$$
$$(P^2)^3 + 7q^2(p_B^2 + 3q^2)P^2 - 6p_B^2(q^2)^2) - 4Q_q(P^2 - p_B^2)((P^2)^2 + 2q^2P^2 + 5$$

$$(q^2)^2))u - 4(P^2 - p_B^2)^3(4Q_q p_B^2 + 3Q_b P^2 - 4Q_q P^2)(q^2)^2)) \tag{D.2}$$

$$b_b^P = -2(u-1)^{-1}m_b^{-1}P^2(q^2)^{-1}(Q_b - Q_q)(q^2(q^2 - 4p_B^2) + 2P^2q^2 + (P^2)^2)^{-1}(m_b^2$$
$$(P^2 - q^2) + (P^2 + q^2)(P^2 - p_B^2)) \tag{D.3}$$

$$b_c^P = \frac{1}{2}(u-1)^{-1}u^{-1}m_b^{-1}Q_b P^2(p_B^2 - q^2)^{-1}((u-1)q^2 - uP^2)^{-1}(up_B^2 - uq^2 + q^2)^{-1}(u(P^2 - q^2)^2 + 4$$
$$(P^2 - p_B^2)q^2)^{-2}(((P^2)^3((3-7u)u(p_B^2)^2 + 2(u(17u-28)+5)q^2p_B^2 - 3(u-1)(9u-14)(q^2)^2)$$
$$u^2 + (P^2)^4(-5up_B^2 + p_B^2 + 5(u-1)q^2)u^3 + (P^2)^2(2(13u-5)(p_B^2)^3u^2 + (-57u^2 + 75u - 14)$$
$$(p_B^2)^2q^2u + 2(u(3u(u+4) - 28) + 7)p_B^2(q^2)^2 +$$
$$(u-1)(u(25u-88)+78)(q^2)^3)u + P^2q^2(-2(u(26u-61)+11)$$
$$(p_B^2)^3u^2 + (5u(3u-4)(9u-19) - 46)(p_B^2)^2q^2u -$$
$$2((u-1)u(u(47u-164)+114)+2)p_B^2(q^2)^2 + (u-1)(u(u(11u-52)+50) - 4)$$
$$(q^2)^3) + q^2(-2u(7u-2)(q^2)^4(u-1)^2 + (u(u(59u-12) - 38) + 4)$$
$$p_B^2(q^2)^3(u-1) + (4 - u(u(u(71u+93) - 294) + 138))$$
$$(p_B^2)^2(q^2)^2 + 16(1-5u)u^2(p_B^2)^4 + 2u(u(13u(u+8) - 115) + 14)(p_B^2)^3q^2))m_b^2 + u(up_B^2 - u$$
$$q^2 + q^2)((-p_B^2(10(p_B^2)^2 - 9P^2p_B^2 + (P^2)^2)(P^2)^2 - (-225P^2(p_B^2)^2 + 124$$
$$(p_B^2)^3 + 78(P^2)^2p_B^2 + 51(P^2)^3)(q^2)^2 + (63(p_B^2)^2 - 152P^2p_B^2 + 121(P^2)^2)$$
$$(q^2)^3 + (13p_B^2 - 31P^2)(q^2)^4 + 4(q^2)^5 + (2p_B^2 + P^2)(-41P^2(p_B^2)^2 + 24(p_B^2)^3 + 16$$
$$(P^2)^2p_B^2 + 5(P^2)^3)q^2)u^2 + (p_B^2 - q^2)(P^2 - q^2)^2(-6(p_B^2)^2 + 3P^2p_B^2 + 9q^2p_B^2 + 5$$
$$(P^2)^2 + 2(q^2)^2 - 13P^2q^2)u^3 + 2q^2(3(2(p_B^2)^2 + 5q^2p_B^2 - 23(q^2)^2)(P^2)^2 + 2$$
$$(p_B^2 + 7q^2)(P^2)^3 + (-66q^2(p_B^2)^2 - 17(p_B^2)^3 + 123(q^2)^2p_B^2 + 8(q^2)^3)P^2 - 60$$
$$(p_B^2)^2(q^2)^2 - 4p_B^2(q^2)^3 + 8(p_B^2)^4 - (q^2)^4 + 41(p_B^2)^3q^2)u - 2(P^2 - p_B^2)$$
$$(q^2)^2(8(p_B^2)^2 - 7P^2p_B^2 + 23q^2p_B^2 + (q^2)^2 - 25P^2q^2))) \tag{D.4}$$

$$b_d^P = 2m_b^{-1}(P^2Q_q((P^2)^2 - p_B^2q^2)^{-1}(q^2(q^2 - 4p_B^2) + 2P^2q^2 + (P^2)^2)^{-1}(2u(P^2 - p_B^2)$$
$$(p_B^2 + q^2) + (P^2 - p_B^2)^2 + u^2(p_B^2 - q^2)^2)^{-1}(m_b^2(u(p_B^2 - q^2)^2(q^2(p_B^2 + P^2) + P^2$$
$$(P^2 - 3p_B^2)) + (P^2 - p_B^2)^2(P^2(3p_B^2 + q^2) + q^2(q^2 - 5p_B^2))) + p_B^2(p_B^2 - P^2)(u(3$$
$$P^2 + q^2)(p_B^2 - q^2)^2 - (P^2 - q^2)(P^2 - p_B^2)(-3p_B^2 + 2P^2 + q^2))) + Q_b(m_b^2 - p_B^2)$$
$$(p_B^2 - P^2)(p_B^2 - q^2)^{-1}((u-1)q^2 - uP^2)^{-1} + P^2Q_q(p_B^2 - m_b^2)(p_B^2 - P^2)(-uP^2 + P^2 + uq^2)^{-1}$$
$$(p_B^2q^2 - (P^2)^2)^{-1} - (u-1)^{-1}Q_b(p_B^2 - q^2)^{-1}(q^2(q^2 - 4p_B^2) + 2P^2q^2 + (P^2)^2)^{-1}$$
$$(m_b^2(P^2(p_B^2 + q^2) + p_B^2(q^2 - 4p_B^2) + (P^2)^2) - p_B^2(P^2 - p_B^2)(4p_B^2 + P^2 - q^2))) \tag{D.5}$$

$$c_a^P = -4(u-1)^{-1}um_b^{-1}P^2Q_q(2u(P^2 - p_B^2)(p_B^2 + q^2) + (P^2 - p_B^2)^2 + u^2(p_B^2 - q^2)^2)^{-1}(m_b^2$$
$$(-(u+1)p_B^2 + P^2 + uq^2) + m_b^4 + up_B^2(p_B^2 - P^2)) \tag{D.6}$$

$$c_b^P = 4(u-1)^{-1}m_b^{-1}P^2Q_q(q^2(q^2 - 4p_B^2) + 2P^2q^2 + (P^2)^2)^{-1}(m_b^2(-2p_B^2 + P^2 + q^2) + m_b^4 + p_B^2$$
$$(p_B^2 - P^2)) \tag{D.7}$$

$$
\begin{aligned}
c_c^P =&(u-1)^{-1}u^{-1}m_b^{-1}Q_bP^2(4q^2(P^2-p_B^2)+u(P^2-q^2)^2)^{-2}(2m_b^4(u(q^2(9p_B^2+q^2)-11P^2\\
&q^2+(P^2)^2)+q^2(P^2-p_B^2)-3u^2(P^2-q^2)^2)+2(u-1)um_b^2(u(P^2-q^2)^2(-3p_B^2+2P^2+q^2)+q^2\\
&(P^2-p_B^2)(-6p_B^2+5P^2+q^2))+u(P^2-p_B^2)(u(P^2)^2((2u^2+u-3)q^2-2u(u+1)p_B^2)-2P^2q^2\\
&(u((5-2u)u+1)p_B^2+(u(2(u-3)u+1)+3)q^2)+\\
&q^2(-2(u(u(u+8)-4)-3)p_B^2q^2+2u(7u+1)(p_B^2)^2+u(2u^2+u-3)\\
&(q^2)^2))) \qquad \text{(D.8)}\\
c_d^P =&4(u-1)^{-1}m_b^{-1}Q_bP^2(q^2(q^2-4p_B^2)+2P^2q^2+(P^2)^2)^{-1}(m_b^4+p_B^2(P^2-p_B^2)) \qquad \text{(D.9)}
\end{aligned}
$$

D.2 C_0 imaginary part with up to two massive propagators

In order to make use of the formula (3.44) an equation for $\operatorname{Im} C_0$ on the principal branch is required. This is straightforward to derive from its Feynman parameter integral and is presented here. The integral representation is given by

$$
\begin{aligned}
&C_0(p_1^2,p_2^2,p_3^2,m_0^2,0,m_2^2)\\
&\quad=\int_0^1 dx\int_0^{1-x} dy\left[(1-x-y)(xp_1^2+yp_3^2-m_0^2)+xyp_2^2-ym_2^2+i\epsilon\right]^{-1}\\
&\quad=\int_0^1 dx\int_0^1 dy\left[(1-y)(xp_1^2+(1-x)yp_3^2-m_0^2)+xyp_2^2-ym_2^2+i\epsilon\right]^{-1} \qquad \text{(D.10)}
\end{aligned}
$$

where setting one mass to zero allows a change of integration variables which considerably simplifies the problem. The imaginary part is recovered from the well-known relation (3.35)

$$
\begin{aligned}
&\operatorname{Im} C_0(p_1^2,p_2^2,p_3^2,m_0^2,0,m_2^2)\\
&\quad=-\pi\int_0^1 dx\int_0^1 dy\delta\left((1-y)(xp_1^2+(1-x)yp_3^2-m_0^2)+xyp_2^2-ym_2^2\right)\\
&\quad=-\pi\int_0^1 dy\frac{\Theta(\bar{y}(p_1^2-m_0^2)+y(p_2^2-m_2^2))-\Theta(\bar{y}(yp_3^2-m_0^2)-ym_2^2)}{\bar{y}(p_1^2-yp_3^2)+yp_2^2} \qquad \text{(D.11)}
\end{aligned}
$$

The regions where the step functions are non-zero are given by the inequalities

$$y(p_2^2-p_1^2+m_0^2-m_2^2)+p_1^2-m_0^2>0 \qquad \text{(D.12)}$$

$$-y^2p_3^2+y(p_3^2+m_0^2-m_2^2)-m_0^2>0 \qquad \text{(D.13)}$$

The two step functions can be treated entirely separately and it is a straightforward matter in computer code to intersect the constraints (D.12) and (D.13) with the range $[0,1]$ to reduce

(D.11) to a pair of integrals of the form

$$\int_{y_1}^{y_2} \frac{dy}{\bar{y}(p_1^2 - yp_3^2) + yp_2^2} = \frac{1}{\sqrt{\lambda(p_1^2, p_2^2, p_3^3)}} \log\left[\frac{(y_2 - y_-)(y_1 - y_+)}{(y_1 - y_-)(y_2 - y_+)}\right] \tag{D.14}$$

$y_\pm$ are given by the roots of $\bar{y}(p_1^2 - yp_3^2) + yp_2^2 = 0$, explicitly:

$$y_\pm = \frac{p_1^2 + p_3^2 - p_2^2 \pm \sqrt{\lambda(p_1^2, p_2^2, p_3^2)}}{2p_3^2} \tag{D.15}$$

Note that the square root of the Källén function obeys $\sqrt{\lambda(p_1^2, p_2^2, p_3^2)} = p_3^2(y_+ - y_-)$ and provided that this constraint is maintained exchanging y_+ with y_- does not alter the value of (D.14), so there is no possible issue with the branch choice of the square root.

The case $p_3^2 = 0$ requires special treatment. First, note that the second inequality becomes $\bar{y}m_0^2 + ym_2^2 < 0$ and this cannot be satisfied for real masses. The first inequality is unaffected. Then the integral (D.14) is replaced by

$$\int_{y_1}^{y_2} \frac{dy}{\bar{y}p_1^2 + yp_2^2} = \frac{1}{p_2^2 - p_1^2} \log\left(\frac{y_2 + y_S}{y_1 + y_S}\right) \tag{D.16}$$

where $y_S = \frac{p_1^2}{p_2^2 - p_1^2}$.

The entire computation of (D.11) therefore only requires calculating a few square roots and logarithms. The results of this method have been compared to the output of LoopTools [111] and found to be the same; the benefit of not using LoopTools is that computing only the imaginary part is considerably computationally cheaper and thus the complicated two dimensional integrals implied by appendix D.1 take much less time.

Appendix E

Additional isospin asymmetry material

E.1 Weak annihilation formulae

Functions defined on the right-hand side of (5.21) are listed here. Any function not listed is zero, and which functions are zero can be inferred from table 5.1 plus the additional consideration that each operator will either couple to the V or $A, 0$ basis tensors according to its parity. The functions ρ_{C_b} an ρ_{C_d} are the dispersion representations of the Passarino–Veltman functions C_b and C_d in (3.17) and are therefore given by (3.45) and (3.30) respectively, given that:

$$\rho_{C_b} = \rho_{C_a}|_{u=1} \qquad \rho_{C_d} = \rho_{C_c}|_{u=1} \quad . \tag{E.1}$$

The functions in (5.21) which apply at $|q^2| > 1\text{GeV}^2$ are given in subSection E.1.1, and the functions in (5.24) which apply at $q^2 = 0$ are given in subSection E.1.2.

E.1.1 WA formulae $|q^2| > 1\text{GeV}^2$

Defining, as before, $d \equiv -\frac{\sqrt{2} m_B m_V}{\sqrt{q^2} E}$, the formulae for WA are:

$$f^q_{2,A}(q^2, u) = 2\pi^2 \phi_\perp(u) \left(\frac{Q_q}{(u-1)m_B^2 - uq^2} - \frac{Q_b}{um_B^2 - uq^2 + q^2} \right) \tag{E.2}$$

$$d \cdot f^q_{2,0}(q^2, u) = \frac{32\pi^2 m_{K^*}^2 m_B^2}{(m_B^2 - q^2)^2} h_\parallel^{(s)'}(u) \left[\frac{\bar{u} Q_b}{um_B^2 + \bar{u} q^2} - \frac{u Q_q}{\bar{u} m_B^2 + uq^2} \right] \tag{E.3}$$

$$f^q_{4,V}(q^2, u) = -2\pi^2 \phi_\perp(u) \left(\frac{Q_b}{um_B^2 - uq^2 + q^2} + \frac{Q_q}{-um_B^2 + m_B^2 + uq^2} \right) \tag{E.4}$$

$$\rho^q_{5,V}(q^2,s) = \frac{3}{2} m_b f_{K^*} m_{K^*} \left(s\left(s-q^2\right)^3\right)^{-1} \left(\left(m_b^2-s\right)\left(Q_b-Q_q\right)\left(s^2-\left(q^2\right)^2\right) - sQ_b\left(2m_b^2q^2-sq^2+s^2\right)\log\left(\frac{sm_b^2}{m_b^2q^2-sq^2+s^2}\right) + sQ_qq^2\left(2m_b^2+q^2-s\right)\log\left(\frac{s\left(m_b^2+q^2-s\right)}{m_b^2q^2}\right)\right) \tag{E.5}$$

$$V^q_{5,V}(q^2) = \frac{2\pi^2 f_{K^*} m_{K^*}\left(m_b^2Q_q - Q_bq^2\right)}{m_b^2q^2} \tag{E.6}$$

$$\rho^q_{6,A}(q^2,s) = \frac{3}{2} m_b f_{K^*} m_{K^*} \left(s^2\left(s-q^2\right)^3\left(q^2-m_B^2\right)\right)^{-1} \left(\left(m_b^2-s\right)\left(s-q^2\right)\left(m_b^2\left(Q_b-Q_q\right)\left(-sq^2+\left(q^2\right)^2+2s^2\right) - s\left(s-q^2\right)\left(s\left(Q_b-Q_q\right)-2Q_bq^2\right)\right) + s^2Q_qq^2\left(-2m_b^2\left(s-q^2\right)+2m_b^4+\left(s-q^2\right)^2\right)\log\left(\frac{s\left(m_b^2+q^2-s\right)}{m_b^2q^2}\right) + s^2Q_b\left(-2sm_b^2\left(s-q^2\right)-2m_b^4q^2+s\left(s-q^2\right)^2\right)\log\left(\frac{sm_b^2}{m_b^2q^2-sq^2+s^2}\right)\right) \tag{E.7}$$

$$V^q_{6,A}(q^2) = -\frac{2\pi^2 f_{K^*} m_{K^*}\left(-m_b^2q^2\left(Q_b-3Q_q\right)+m_b^4Q_q+Q_b\left(q^2\right)^2\right)}{m_b^2q^2\left(m_B^2-q^2\right)} \tag{E.8}$$

$$d\cdot\rho^q_{6,0}(q^2,s) = 3m_bm_B^2 f_{K^*} m_{K^*}\left(s^2\left(s-q^2\right)^3\left(m_B^2-q^2\right)\right)^{-1}\left(2s^2m_b^4Q_b\log\left(\frac{sm_b^2}{m_b^2q^2-sq^2+s^2}\right) - 2s^2m_b^2Q_q\left(m_b^2+q^2-s\right)\log\left(\frac{s\left(m_b^2+q^2-s\right)}{m_b^2q^2}\right) + \left(m_b^2-s\right)\left(Q_b-Q_q\right)\left(s-q^2\right)\left(m_b^2\left(q^2-3s\right)+s\left(s-q^2\right)\right)\right) \tag{E.9}$$

$$d\cdot V^q_{6,0}(q^2) = \frac{8\pi^2m_B^2f_{K^*}m_{K^*}Q_q}{q^2\left(m_B^2-q^2\right)} \tag{E.10}$$

$$\rho^q_{9,V}(q^2,s) = \frac{3}{2}\left(s\left(s-q^2\right)^3\right)^{-1} f^\perp_{K^*}\left(-2sm_b^4Q_bq^2\log\left(\frac{sm_b^2}{m_b^2q^2-sq^2+s^2}\right) + \left(m_b^2-s\right)\left(s-q^2\right)\left(m_b^2\left(Q_b-Q_q\right)\left(q^2+s\right)-s\left(Q_b+Q_q\right)\left(s-q^2\right)\right) + 2sm_b^4Q_qq^2\log\left(\frac{s\left(m_b^2+q^2-s\right)}{m_b^2q^2}\right)\right) \tag{E.11}$$

$$V^q_{9,V}(q^2) = \frac{4\pi^2 f^\perp_{K^*}\left(m_b^2Q_q-Q_bq^2\right)}{m_bq^2} \tag{E.12}$$

$$\rho_{10,A}^{q}(q^2,s) = -\frac{3}{2} f_{K^*}^{\perp} \left(s\left(s-q^2\right)^2\left(q^2-m_B^2\right)\right)^{-1} \left(-2sm_b^4 Q_b q^2 \log\left(\frac{sm_b^2}{m_b^2 q^2 - sq^2 + s^2}\right)\right.$$
$$+ \left(m_b^2 - s\right)\left(s-q^2\right)\left(m_b^2\left(Q_b - Q_q\right)\left(q^2+s\right) - s\left(Q_b+Q_q\right)\left(s-q^2\right)\right)$$
$$\left. + 2sm_b^4 Q_q q^2 \log\left(\frac{s\left(m_b^2+q^2-s\right)}{m_b^2 q^2}\right)\right) \tag{E.13}$$

$$V_{10,A}^{q}(q^2) = \frac{4\pi^2\left(m_b^2-q^2\right) f_{K^*}^{\perp}\left(m_b^2 Q_q - Q_b q^2\right)}{m_b q^2\left(m_B^2-q^2\right)} \tag{E.14}$$

$$d\cdot\rho_{10,0}^{q}(q^2,s) = -12m_B^2 m_{K^*}^2 f_{K^*}^{\perp}\left(\left(q^2-s\right)^2\left(m_B^2-q^2\right)^3\right)^{-1}\left(m_b^2 Q_b\left(m_b^2\left(q^2+s\right)\right.\right.$$
$$\left. + 2s\left(s-q^2\right)\right)\log\left(\frac{sm_b^2}{m_b^2 q^2 - sq^2 + s^2}\right)$$
$$- \left(m_b^2-s\right)\left(s-q^2\right)\left(2m_b^2\left(Q_b-Q_q\right) + \left(Q_b+Q_q\right)\left(s-q^2\right)\right)$$
$$\left. + m_b^2 Q_q\left(q^2+s\right)\left(m_b^2+q^2-s\right)\left(-\log\left(\frac{s\left(m_b^2+q^2-s\right)}{m_b^2 q^2}\right)\right)\right) \tag{E.15}$$

$$d\cdot V_{10,0}^{q}(q^2) = \frac{16\pi^2 m_B^2 m_{K^*}^2\left(m_b^2-q^2\right) f_{K^*}^{\perp}\left(m_b^2 Q_q - Q_b q^2\right)}{m_b q^2\left(q^2-m_B^2\right)^3} \tag{E.16}$$

$$\rho_{4,T}^{q}(q^2,s) = -\frac{3}{2}\mu_K^2\left(m_B\right.$$
$$\left. + m_K\right)\left(sm_B^2\left(2m_B^2 q^2 + m_B^4 - 4sq^2 + \left(q^2\right)^2\right)\right)^{-1}\left(2sQ_b m_B^2\left(m_b^4 + s\left(m_B^2 - s\right)\right)\rho_{C_d}(s)\right.$$
$$+ 2sm_B^2 Q_q \rho_{C_b}(s)\left(m_b^2\left(m_B^2+q^2-2s\right) + m_b^4 + s\left(s-m_B^2\right)\right)$$
$$\left. + \left(m_b^2-s\right)\left(Q_b-Q_q\right)\left(m_b^2\left(m_B^2+q^2-4s\right) + s\left(-3m_B^2-q^2+4s\right)\right)\right) \tag{E.17}$$

$$V_{4,T}^{q}(q^2) = -\frac{4\pi^2 m_b \mu_K^2 Q_q\left(m_B+m_K\right)}{m_B^2 q^2} \tag{E.18}$$

$$f_{4,T}^{q}(q^2,u) = \frac{2\pi^2}{m_B^2}(m_B+m_K)\left[\phi_P(u)\left(\frac{\bar{u}Q_b}{um_B^2+\bar{u}q^2} - \frac{uQ_q}{\bar{u}m_B^2+uq^2}\right)\right.$$
$$\left. + \frac{\phi_\sigma(u)}{6}\left(Q_b\frac{u(1+2\bar{u})m_B^2 + 2\bar{u}^2q^2}{u(um_B^2+\bar{u}q^2)^2} - Q_q\frac{\bar{u}(1+2u)m_B^2+2u^2q^2}{\bar{u}(\bar{u}m_B^2+uq^2)^2}\right)\right] \tag{E.19}$$

$$\rho_{8,T}^{q}(q^2,s) = \frac{3}{2}m_b f_K\left(m_B+m_K\right)\left(s^2\left(s-q^2\right)^3\right)^{-1}\left(2s^2 m_b^4 Q_b \log\left(\frac{sm_b^2}{m_b^2 q^2 - sq^2 + s^2}\right)\right.$$
$$- 2s^2 m_b^2 Q_q\left(m_b^2+q^2-s\right)\log\left(\frac{s\left(m_b^2+q^2-s\right)}{m_b^2 q^2}\right)$$
$$\left. + \left(m_b^2-s\right)\left(Q_b-Q_q\right)\left(s-q^2\right)\left(m_b^2\left(q^2-3s\right) + s\left(s-q^2\right)\right)\right) \tag{E.20}$$

$$V_{8,T}^{q}(q^2) = \frac{4\pi^2 f_K Q_q\left(m_B+m_K\right)}{q^2} \tag{E.21}$$

E.1.2 WA formulae $q^2 = 0$

$$\widetilde{\rho}^{q,\gamma}_{5,V}(s) = \frac{2\pi^2 f_{K^*} m_{K^*} Q_q \phi_\gamma\left(\frac{m_b^2}{s}\right)}{s} \qquad V^{q,\gamma}_{5,V} = -\frac{2\pi^2 Q_b f_{K^*} m_{K^*}}{m_b^2} \tag{E.22}$$

$$\widetilde{\rho}^{q,\gamma}_{6,A}(s) = -\frac{2\pi^2 f_{K^*} m_{K^*} Q_q\left(s\phi_\gamma\left(\frac{m_b^2}{s}\right) - 2\right)}{s m_B^2} \qquad V^{q,\gamma}_{6,A} = \frac{2\pi^2 f_{K^*} m_{K^*}\left(Q_b - 2Q_q\right)}{m_B^2} \tag{E.23}$$

$$\widetilde{\rho}^{q,\gamma}_{9,V}(s) = \frac{4\pi^2 m_b Q_q f^\perp_{K^*} \phi_\gamma\left(\frac{m_b^2}{s}\right)}{s} \qquad V^{q,\gamma}_{9,V} = -\frac{4\pi^2 Q_b f^\perp_{K^*}}{m_b} \tag{E.24}$$

$$\widetilde{\rho}^{q,\gamma}_{10,A}(s) = \frac{4\pi^2 m_b Q_q f^\perp_{K^*} \phi_\gamma\left(\frac{m_b^2}{s}\right)}{m_B^2} \qquad V^{q,\gamma}_{10,A} = -\frac{4\pi^2 m_b Q_b f^\perp_{K^*}}{m_B^2} \tag{E.25}$$

E.2 Wilson coefficients in $B^0 \to \rho^0$ decay

Here the formulae for $\tilde{a}_i^d$ omitted from Section 5.6.1 are collected.

$$\begin{aligned}\tilde{a}_2^d =& a_2^d + \frac{1}{6}(-a_2^u - a_3^u + 4a_6^u - 4a_7^u + 3a_{10}^u) + \frac{2}{9}(-a_2^{8u} - a_3^{8u} + 4a_6^{8u} - 4a_7^{8u} + 3a_{10}^{8u}) \\ &+ \frac{1}{12}(-a_2^d - a_3^d + 4a_6^d - 4a_7^d + 3a_{10}^d) + \frac{1}{9}(-a_2^{8d} - a_3^{8d} + 4a_6^{8d} - 4a_7^{8d} + 3a_{10}^{8d})\end{aligned} \tag{E.26}$$

$$\begin{aligned}\tilde{a}_4^d =& a_4^d + \frac{1}{6}(-a_1^u - a_4^u + 4a_5^u - 4a_8^u + 3a_9^u) + \frac{2}{9}(-a_1^{8u} - a_4^{8u} + 4a_5^{8u} - 4a_8^{8u} + 3a_9^{8u}) \\ &+ \frac{1}{12}(-a_1^d - a_4^d + 4a_5^d - 4a_8^d + 3a_9^d) + \frac{1}{9}(-a_1^{8d} - a_4^{8d} + 4a_5^{8d} - 4a_8^{8d} + 3a_9^{8d})\end{aligned} \tag{E.27}$$

$$\begin{aligned}\tilde{a}_5^d =& a_5^d + \frac{1}{12}\left(2(a_5^d - a_5^u) + 2(a_8^d - a_8^u) + (a_4^d - a_4^u) - (a_1^d - a_1^u)\right) \\ &+ \frac{1}{9}\left(2(a_5^{8d} - a_5^{8u}) + 2(a_8^{8d} - a_8^{8u}) + (a_4^{8d} - a_4^{8u}) - (a_1^{8d} - a_1^{8u})\right)\end{aligned} \tag{E.28}$$

$$\begin{aligned}\tilde{a}_6^d =& a_6^d + \frac{1}{12}\left(2(a_6^d - a_6^u) + 2(a_7^d - a_7^u) + (a_2^d - a_2^u) - (a_3^d - a_3^u)\right) \\ &+ \frac{1}{9}\left(2(a_6^{8d} - a_6^{8u}) + 2(a_7^{8d} - a_7^{8u}) + (a_2^{8d} - a_2^{8u}) - (a_3^{8d} - a_3^{8u})\right)\end{aligned} \tag{E.29}$$

$$\tilde{a}_9^d = a_9^d + \frac{1}{6}(a_9^d - a_9^u) + \frac{1}{12}((a_1^d - a_1^u) + (a_4^d - a_4^u)) + \frac{1}{9}((a_1^{8d} - a_1^{8u}) + (a_4^{8d} - a_4^{8u})) \tag{E.30}$$

$$\tilde{a}_{10}^d = a_{10}^d + \frac{1}{6}(a_{10}^d - a_{10}^u) + \frac{1}{12}((a_2^d - a_2^u) + (a_3^d - a_3^u)) + \frac{1}{9}((a_2^{8d} - a_2^{8u}) + (a_3^{8d} - a_3^{8u})) \tag{E.31}$$

	q^2/GeV^2							
$B \to Kll$	1	2	3	4	5	6	7	8
$a_4^u = 0.1$	0.35%	0.14%	-0.03%	-0.15%	-0.23%	-0.27%	-0.28%	-0.25%
a_8^u	0.68%	0.60%	0.63%	0.64%	0.62%	0.58%	0.53%	0.47%
a_4^d	-0.10%	-0.13%	-0.18%	-0.21%	-0.22%	-0.23%	-0.22%	-0.20%
a_8^d	0.35%	0.31%	0.33%	0.33%	0.32%	0.30%	0.27%	0.24%
$s_{1(R,L)}^{SU(3)} = 1$	1.28%	0.68%	0.35%	0.18%	0.08%	0.04%	0.01%	-0.01%
$s_{1(R,L)}^c$	0.88%	0.60%	0.39%	0.25%	0.16%	0.11%	0.07%	0.04%
$s_{1(R,L)}^b$	-0.20%	-0.34%	-0.31%	-0.25%	-0.20%	-0.15%	-0.12%	-0.09%
$s_{2(R,L)}^c$	-4.68%	-3.94%	-3.13%	-2.46%	-1.96%	-1.57%	-1.25%	-0.91%
$s_{2(R,L)}^b$	5.03%	1.75%	0.03%	-1.04%	-1.76%	-2.25%	-2.51%	-2.44%
C_1	-0.00%	-0.00%	-0.00%	-0.00%	-0.00%	-0.00%	-0.00%	-0.00%
C_2	-0.84%	-0.45%	-0.22%	-0.10%	-0.03%	0.01%	0.03%	0.04%
C_3	0.02%	0.04%	0.04%	0.04%	0.04%	0.04%	0.03%	0.03%
C_4	-0.11%	-0.21%	-0.28%	-0.31%	-0.31%	-0.29%	-0.27%	-0.24%
C_5	0.01%	-0.00%	-0.01%	-0.02%	-0.03%	-0.03%	-0.03%	-0.03%
C_6	0.20%	0.23%	0.30%	0.35%	0.39%	0.41%	0.39%	0.34%
C_8^{eff}	-0.22%	-0.09%	-0.02%	0.02%	0.05%	0.08%	0.09%	0.09%
SM total	-0.93%	-0.48%	-0.20%	-0.01%	0.12%	0.20%	0.24%	0.24%

Table E.1: Breakdown of contributions to $B \to Kll$ isospin asymmetry in SM operator coefficients C_i, and in a generalised basis of four quark WA operators with coefficients a_i and QLSS contributions with coefficients $s_{x\chi}^q$. $a_i^q = 0.1$ and $s_{x,\chi}^q = 1$ was used to produce these values.

The coefficients for colour octet operators in the SM are:

$$\begin{aligned} a_1^{8q} &= -a_2^{8q} = a_3^{8q} = -a_4^{8q} = -4C_5 \\ a_5^{8q} &= -a_6^{8q} = -a_7^{8q} = a_8^{8q} = 2C_3 - 2\delta_{qu}\frac{\lambda_u}{\lambda_t}C_1 \\ a_9^{8q} &= a_{10}^{8q} = 0 \end{aligned} \tag{E.32}$$

E.3 Tabulated isospin asymmetry results in the SM and beyond SM operator breakdown

The data tables here correspond to the graphs in figures 5.8, 5.9, 5.11 and 5.12. Results for the K are given in table E.1, the K^* in table E.2 and the ρ in table E.3. Data for $B \to (K^*, \rho)\gamma$ are also provided, denoted by $q^2 = 0$ in tables E.2 and E.3.

	q^2/GeV^2								
$B \to K^* ll$	0	1	2	3	4	5	6	7	8
$a_2^u = 0.1$	-1.55%	-0.22%	-0.00%	0.06%	0.08%	0.08%	0.07%	0.06%	0.06%
a_4^u	-1.58%	-0.33%	-0.09%	-0.00%	0.02%	0.03%	0.04%	0.03%	0.03%
a_5^u	1.29%	-0.07%	0.02%	0.00%	-0.00%	0.00%	0.01%	0.02%	0.03%
a_6^u	-0.84%	-0.53%	-0.64%	-0.67%	-0.65%	-0.60%	-0.54%	-0.47%	-0.42%
a_9^u	10.3%	-0.20%	0.23%	0.03%	-0.02%	0.02%	0.10%	0.17%	0.26%
a_{10}^u	10.5%	0.43%	0.40%	0.13%	0.08%	0.14%	0.24%	0.34%	0.47%
$a_2^d = 0.1$	-2.85%	-0.40%	-0.00%	0.12%	0.15%	0.15%	0.14%	0.12%	0.11%
a_4^d	-2.91%	-0.61%	-0.17%	-0.01%	0.05%	0.07%	0.07%	0.07%	0.06%
a_5^d	0.78%	0.00%	0.02%	0.00%	-0.00%	-0.00%	-0.00%	0.00%	0.01%
a_6^d	-0.50%	-0.30%	-0.34%	-0.35%	-0.33%	-0.31%	-0.27%	-0.24%	-0.21%
a_9^d	6.23%	0.18%	0.20%	0.02%	-0.04%	-0.03%	0.00%	0.04%	0.08%
a_{10}^d	6.29%	0.45%	0.24%	0.03%	-0.03%	-0.01%	0.04%	0.09%	0.16%
$s_{1R}^{SU(3)} = 1$	0.00%	-1.26%	-0.75%	-0.38%	-0.18%	-0.08%	-0.03%	-0.01%	0.00%
s_{1R}^c	0.00%	-0.90%	-0.67%	-0.43%	-0.26%	-0.16%	-0.10%	-0.06%	-0.03%
s_{1R}^b	0.01%	0.20%	0.38%	0.34%	0.26%	0.19%	0.14%	0.10%	0.08%
$s_{1L}^{SU(3)}$	-0.28%	0.81%	0.58%	0.36%	0.21%	0.12%	0.06%	0.03%	-0.00%
s_{1L}^c	-0.40%	0.67%	0.57%	0.42%	0.30%	0.22%	0.16%	0.11%	0.07%
s_{1L}^b	0.95%	-0.00%	-0.28%	-0.33%	-0.31%	-0.26%	-0.22%	-0.18%	-0.14%
s_{2R}^c	1.59%	-1.82%	-1.96%	-1.64%	-1.27%	-0.97%	-0.73%	-0.54%	-0.36%
s_{2R}^b	5.03%	8.33%	3.25%	0.12%	-1.56%	-2.38%	-2.67%	-2.62%	-2.28%
s_{2L}^c	0.02%	2.43%	2.21%	1.66%	1.19%	0.85%	0.61%	0.44%	0.29%
s_{2L}^b	0.05%	-4.60%	-1.84%	-0.05%	0.98%	1.56%	1.83%	1.88%	1.69%
C_1	-0.01%	-0.00%	-0.00%	-0.00%	-0.00%	-0.00%	-0.00%	-0.00%	-0.00%
C_2	0.11%	-0.71%	-0.44%	-0.24%	-0.12%	-0.06%	-0.02%	0.01%	0.03%
C_3	0.09%	0.01%	0.04%	0.04%	0.05%	0.04%	0.04%	0.03%	0.03%
C_4	-0.98%	-0.08%	-0.25%	-0.30%	-0.31%	-0.30%	-0.28%	-0.26%	-0.24%
C_5	-0.51%	-0.09%	-0.02%	0.01%	0.02%	0.02%	0.02%	0.02%	0.01%
C_6	6.41%	1.40%	0.40%	0.03%	-0.11%	-0.17%	-0.18%	-0.18%	-0.17%
C_8^{eff}	-0.19%	-0.34%	-0.14%	-0.02%	0.05%	0.09%	0.10%	0.10%	0.09%
SM total	4.92%	0.18%	-0.42%	-0.48%	-0.44%	-0.38%	-0.33%	-0.28%	-0.24%

Table E.2: Breakdown of contributions to $B \to K^* ll$ isospin asymmetry in SM operator coefficients C_i, and in a generalised basis of four quark WA operators with coefficients a_i and QLSS contributions with coefficients $s^q_{x\chi}$. $a^q_i = 0.1$ and $s^q_{x,\chi} = 1$ was used to produce these values. The $q^2 = 0$ value corresponds to the process $B \to K^* \gamma$ and is computed slightly differently to $B \to K^* ll$ as described in Section 5.3.6. The value for s^f_{1R} and s^f_{2L} are zero at $q^2 = 0$ as a consequence of $h_+(0) = 0$ in this approximation.

	q^2/GeV^2								
$B \to \rho ll$	0	1	2	3	4	5	6	7	8
$a_2^u = 0.1$	-1.55%	-0.23%	-0.01%	0.05%	0.07%	0.07%	0.07%	0.06%	0.06%
a_4^u	-1.59%	-0.33%	-0.09%	-0.01%	0.02%	0.04%	0.04%	0.04%	0.03%
a_5^u	1.25%	-0.06%	0.02%	0.00%	-0.00%	0.00%	0.01%	0.02%	0.03%
a_6^u	-0.81%	-0.62%	-0.72%	-0.74%	-0.71%	-0.66%	-0.59%	-0.52%	-0.46%
a_9^u	11.0%	-0.20%	0.26%	0.04%	-0.02%	0.03%	0.11%	0.19%	0.28%
a_{10}^u	11.1%	0.45%	0.43%	0.14%	0.07%	0.12%	0.23%	0.33%	0.47%
$\tilde{a}_2^d = 0.1$	-3.10%	-0.46%	-0.03%	0.11%	0.14%	0.15%	0.14%	0.12%	0.11%
$\tilde{a}_4^d$	-3.17%	-0.65%	-0.18%	-0.01%	0.05%	0.07%	0.07%	0.07%	0.07%
$\tilde{a}_5^d$	0.76%	0.00%	0.02%	0.00%	-0.00%	-0.00%	-0.00%	0.00%	0.01%
$\tilde{a}_6^d$	-0.48%	-0.34%	-0.38%	-0.38%	-0.37%	-0.34%	-0.30%	-0.26%	-0.23%
$\tilde{a}_9^d$	6.62%	0.19%	0.22%	0.03%	-0.04%	-0.03%	0.00%	0.04%	0.09%
$\tilde{a}_{10}^d$	6.68%	0.48%	0.27%	0.04%	-0.03%	-0.01%	0.03%	0.09%	0.16%
$s_{1R}^{SU(3)} = 1$	0.00%	-1.39%	-0.81%	-0.41%	-0.19%	-0.08%	-0.03%	-0.01%	0.00%
s_{1R}^c	0.00%	-1.01%	-0.74%	-0.47%	-0.28%	-0.17%	-0.10%	-0.06%	-0.03%
s_{1R}^b	0.01%	0.22%	0.42%	0.37%	0.29%	0.21%	0.15%	0.11%	0.08%
$s_{1L}^{SU(3)}$	-0.40%	0.94%	0.64%	0.39%	0.22%	0.12%	0.06%	0.03%	-0.00%
s_{1L}^c	-0.44%	0.77%	0.64%	0.45%	0.32%	0.23%	0.16%	0.12%	0.07%
s_{1L}^b	1.12%	0.00%	-0.31%	-0.36%	-0.33%	-0.28%	-0.23%	-0.19%	-0.15%
s_{2R}^c	1.76%	-2.05%	-2.13%	-1.74%	-1.34%	-1.01%	-0.76%	-0.57%	-0.38%
s_{2R}^b	4.02%	8.46%	3.29%	0.06%	-1.70%	-2.55%	-2.86%	-2.82%	-2.47%
s_{2L}^c	0.02%	2.69%	2.38%	1.76%	1.26%	0.89%	0.64%	0.46%	0.30%
s_{2L}^b	0.05%	-4.81%	-1.85%	0.03%	1.11%	1.70%	1.99%	2.04%	1.83%
C_1	0.01%	0.02%	0.01%	0.01%	0.00%	0.00%	-0.00%	-0.00%	-0.00%
C_2	0.01%	-1.46%	-1.00%	-0.65%	-0.40%	-0.23%	-0.11%	-0.02%	0.09%
C_3	0.08%	0.01%	0.04%	0.05%	0.05%	0.05%	0.04%	0.04%	0.03%
C_4	-0.93%	-0.09%	-0.28%	-0.34%	-0.35%	-0.33%	-0.31%	-0.28%	-0.26%
C_5	-0.54%	-0.10%	-0.02%	0.01%	0.02%	0.02%	0.02%	0.02%	0.01%
C_6	6.74%	1.51%	0.46%	0.06%	-0.10%	-0.16%	-0.18%	-0.18%	-0.18%
C_8^{eff}	-0.14%	-0.35%	-0.14%	-0.01%	0.06%	0.09%	0.11%	0.11%	0.09%
SM total	5.22%	-0.45%	-0.93%	-0.87%	-0.72%	-0.57%	-0.43%	-0.32%	-0.21%

Table E.3: Breakdown of contributions to $B \to \rho ll$ isospin asymmetry in SM operator coefficients C_i, and in a generalised basis of four quark WA operators with coefficients a_i and QLSS contributions with coefficients $s^q_{x\chi}$. $a_i^u = 0.1$, $\tilde{a}_i^d = 0.1$ and $s^q_{x,\chi} = 1$ was used to produce these values. The modified four-quark coefficients $\tilde{a}_i$ are explained in Section 5.6. The $q^2 = 0$ value corresponds to the process $B \to \rho\gamma$ and is computed slightly differently to $B \to \rho ll$ as described in Section 5.3.6. The value for s^f_{1R} and s^f_{2L} are zero at $q^2 = 0$ as a consequence of $h_+(0) = 0$ in this approximation.

Appendix F

Additional charm loop material

F.1 Explicit results

Here the polynomials are listed which where omitted from Section 6.2 for the sake of brevity. As can be seen from (6.10) and (B.1.1) the expressions for $P_{V,n}$ and $P_{A,n}$ have the same structure, as do $R_{V,n}$ and $R_{A,n}$. Expressions for $P_{A,n}$ and $R_{A,n}$ are therefore omitted. The expressions here are for the leading terms in the relevant DAs:

$$\mathcal{V}(\underline{\alpha}) = 360\alpha_1\alpha_2\alpha_3^2\kappa_{3;V}^{\parallel} \qquad \mathcal{T}(\underline{\alpha}) = 360\alpha_1\alpha_2\alpha_3^2\kappa_{3;V}^{\perp} \tag{F.1}$$

The expressions for the full DAs still retain the structure outlined in Section 6.2, but are significantly longer so are not included here.

$$\begin{aligned}
P_{V,1} = P_{A,1} = P_{0,1} =& 2(m_b^2 - p_B^2)(m_b^2 - \alpha_3 p_B^2 - \bar{\alpha}_3 q^2)\\
P_{V,2} = P_{A,2} = P_{0,2} =& \bar{\alpha}_3(p_B^2 - q^2)((m_b^2 - p_B^2) + (m_b^2 - \alpha_3 p_B^2 - \bar{\alpha}_3 q^2))\\
P_{V,3} = P_{A,3} =& Q^2 - m_x^2\\
P_{0,3} =& -\alpha_3(p_B^2 - q^2)(P^2 - Q^2) + \frac{1}{2}(m_x^2 - Q^2)(P^2 + p_B^2 - Q^2 - q^2)\\
P_{V,4} = P_{A,4} =& \alpha_3(P^2 - Q^2)\\
P_{0,4} =& -\frac{1}{2}\alpha_3(P^2 - Q^2)(P^2 + p_B^2 - Q^2 - q^2)\\
P_{V,5} =& \frac{1}{2} \times \frac{f_V m_b m_V}{f_B m_B^2} 360\kappa_{3K^*}^{\parallel}\\
P_{A,5} =& \frac{1}{2} \times \frac{f_V m_b m_V}{f_B m_B^2} 360\zeta_{3K^*}^{\parallel}\\
P_{0,5} =& \frac{1}{2} \times \frac{f_V^{\perp} m_b m_V}{f_B m_B^2} \sqrt{\frac{q^2}{2m_b^2}} \frac{360\kappa_{3K^*}^{\perp}}{(P^2 - Q^2)}
\end{aligned} \tag{F.2}$$

$$
\begin{aligned}
R_{V,6} = R_{A,6} =& -6(Q^2-m_x^2)(m_x^2-\bar{\alpha}_3^* Q^2-\alpha_3^* P^2)((-2+\alpha_3^*)P^2q^2+2m_b^2(P^2-Q^2)+q^2Q^2- \\
& \alpha_3^* q^2Q^2-\alpha_3^* P^2 s+Q^2 s+\alpha_3^* Q^2 s+q^2 m_x^2-s m_x^2) \\
R_{0,6} =& (m_b^2-p_B^2)(m_b^2(P^2-Q^2)+m_x^2(q^2-p_B^2)+p_B^2Q^2-P^2q^2)^2(2m_b^2(P^2-Q^2)+ \\
& m_x^2(p_B^2-3P^2-q^2+3Q^2)-p_B^2Q^2-2P^2q^2+3P^2Q^2+3q^2Q^2-3(Q^2)^2) \\
R_{V,7} = R_{A,7} =& \alpha_3^*(P^2-Q^2)(4(\alpha_3^*)^2(P^2-Q^2)^2(q^2-s)-3\alpha_3^*(P^2-Q^2)(-2m_b^2P^2+2P^2q^2+ \\
& 2m_b^2Q^2-3q^2Q^2+Q^2s+q^2m_x^2-sm_x^2)+6(Q^2-m_x^2)(-2P^2q^2+2m_b^2(P^2-Q^2)+ \\
& q^2Q^2+Q^2s+q^2m_x^2-sm_x^2)) \\
R_{0,7} =& \frac{1}{6}(p_B^2-q^2)^{-1}(P^2-Q^2)(m_b^2-p_B^2)(m_b^2-q^2)(-m_b^2(P^2-Q^2)(3m_x^2(p_B^2-q^2)(p_B^2+ \\
& 9P^2-q^2-9Q^2)+Q^2(q^2(3P^2-26p_B^2)-3p_B^2(p_B^2+9P^2)+29(q^2)^2)+4P^2q^2(8p_B^2+ \\
& 3P^2-8q^2)+3(Q^2)^2(9p_B^2-5q^2))+2m_b^4(P^2-Q^2)^2(8p_B^2+3P^2-8q^2-3Q^2)+ \\
& 6(m_x^2)^2(p_B^2-q^2)^2(-p_B^2+3P^2+q^2-3Q^2)+3m_x^2(p_B^2-q^2)(Q^2((4p_B^2-5q^2) \\
& (p_B^2-q^2)-6P^2(2p_B^2+q^2))+P^2q^2(p_B^2+9P^2-q^2)-3(Q^2)^2(q^2-4p_B^2))+ \\
& (Q^2)^2(-2(q^2)^2(4p_B^2+9P^2)+3p_B^2q^2(7p_B^2+6P^2)+6(p_B^2)^2(3P^2-p_B^2)-7(q^2)^3)+ \\
& P^2q^2Q^2(9P^2(q^2-3p_B^2)-(p_B^2-q^2)(3p_B^2+29q^2))+2(P^2)^2(q^2)^2(8p_B^2+3P^2-8q^2)+ \\
& 3(Q^2)^3(3p_B^2q^2-6(p_B^2)^2+(q^2)^2)) \\
R_{V,8} =& \frac{1}{12}(s-m_b^2)\times\frac{f_V m_b m_V}{f_B m_B^2}360\kappa_{3K^*}^{\parallel} \\
R_{A,8} =& \frac{1}{12}(s-m_b^2)\times\frac{f_V m_b m_V}{f_B m_B^2}360\zeta_{3K^*}^{\parallel} \\
R_{0,8} =& \frac{1}{12}\times\frac{f_K^{\perp} m_b m_K}{f_B m_B^2}\sqrt{\frac{q^2}{2m_b^2}}\frac{360\kappa_{3K^*}^{\perp}}{(P^2-Q^2)(s-q^2)}
\end{aligned}
\tag{F.3}
$$

Glossary

ADM Anomalous dimension matrix.

BPHZ Bogoliubov–Parasiuk–Hepp–Zimmermann.

CKM Cabibbo–Kobayashi–Maskawa.

DA Distribution amplitude. Describes the probability of finding a set of partons with a given momentum inside a hadron. See Section 2.7.

DSE Dyson–Schwinger equation. An exact equation of motion for a quantum field theory. See appendix C.

FCNC flavour-changing neutral current.

FSR final state radiation.

GIM Glashow–Iliopoulos–Maiani.

HFAG Heavy Flavour Averaging Group [147].

HV 't Hooft–Veltman regularisation scheme in which $\gamma_5 = i\gamma_0\gamma_1\gamma_2\gamma_3$.

IR infrared.

ISR initial state radiation.

LCSR Light cone sum rule, see Section 2.8.

LHC Large Hadron Collider.

LSZ Lehmann–Symanzik–Zimmermann; formula relating S-matrix elements to vacuum correlation functions [71].

MFV Minimal flavour violation: a class of beyond SM flavour models in which flavour transitions are still controlled by the CKM matrix. See references in Section 5.3.1.

NDR Naive dimensional regularisation, in which γ_5 is treated as anticommuting.

OPE Operator product expansion. See Section 2.5.

QCD quantum chromodynamics.

QCDF QCD factorisation; throughout this thesis used to denote a method for computing heavy to light B meson decays where both the B and final state mesons are treated using a light cone expansion.

QL quark loops.

QLSS quark loop spectator scattering.

RG renormalisation group.

SM The standard model of particle physics, see Section 2.2.

UV ultraviolet.

VEV vacuum expectation value.

WA weak annihilation.

WC Wilson coefficient.

Bibliography

[1] S. Glashow, "Partial Symmetries of Weak Interactions," *Nucl.Phys.* **22** (1961) 579–588.

[2] S. Weinberg, "A Model of Leptons," *Phys.Rev.Lett.* **19** (1967) 1264–1266.

[3] A. Salam, "Weak and Electromagnetic Interactions," *Conf.Proc.* **C680519** (1968) 367–377.

[4] F. Englert and R. Brout, "Broken Symmetry and the Mass of Gauge Vector Mesons," *Phys.Rev.Lett.* **13** (1964) 321–323.

[5] P. W. Higgs, "Broken Symmetries and the Masses of Gauge Bosons," *Phys.Rev.Lett.* **13** (1964) 508–509.

[6] M. Gell-Mann, "A Schematic Model of Baryons and Mesons," *Phys.Lett.* **8** (1964) 214–215.

[7] G. Guralnik, C. Hagen, and T. Kibble, "Global Conservation Laws and Massless Particles," *Phys.Rev.Lett.* **13** (1964) 585–587.

[8] D. Gross and F. Wilczek, "Ultraviolet Behavior of Nonabelian Gauge Theories," *Phys.Rev.Lett.* **30** (1973) 1343–1346.

[9] H. D. Politzer, "Reliable Perturbative Results for Strong Interactions?," *Phys.Rev.Lett.* **30** (1973) 1346–1349.

[10] **ATLAS Collaboration** Collaboration, G. Aad *et al.*, "Observation of a new particle in the search for the Standard Model Higgs boson with the ATLAS detector at the LHC," *Phys.Lett.* **B716** (2012) 1–29, arXiv:1207.7214 [hep-ex].

[11] **CMS Collaboration** Collaboration, S. Chatrchyan *et al.*, "Observation of a new boson at a mass of 125 GeV with the CMS experiment at the LHC," *Phys.Lett.* **B716** (2012) 30–61, arXiv:1207.7235 [hep-ex].

[12] **Super-Kamiokande Collaboration** Collaboration, Y. Fukuda *et al.*, "Evidence for oscillation of atmospheric neutrinos," *Phys.Rev.Lett.* **81** (1998) 1562–1567, arXiv:hep-ex/9807003 [hep-ex].

[13] **SNO Collaboration** Collaboration, Q. Ahmad *et al.*, "Direct evidence for neutrino flavor transformation from neutral current interactions in the Sudbury Neutrino Observatory," *Phys.Rev.Lett.* **89** (2002) 011301, arXiv:nucl-ex/0204008 [nucl-ex].

[14] **ALEPH Collaboration, DELPHI Collaboration, L3 Collaboration, OPAL Collaboration, SLD Collaboration, LEP Electroweak Working Group, SLD Electroweak Group, SLD Heavy Flavour Group** Collaboration, S. Schael *et al.*, "Precision electroweak measurements on the Z resonance," *Phys.Rept.* **427** (2006) 257–454, arXiv:hep-ex/0509008 [hep-ex].

[15] H. Fritzsch and Z.-z. Xing, "Mass and flavor mixing schemes of quarks and leptons," *Prog.Part.Nucl.Phys.* **45** (2000) 1–81, arXiv:hep-ph/9912358 [hep-ph].

[16] M. Gavela, P. Hernandez, J. Orloff, O. Pene, and C. Quimbay, "Standard model CP violation and baryon asymmetry. Part 2: Finite temperature," *Nucl.Phys.* **B430** (1994) 382–426, arXiv:hep-ph/9406289 [hep-ph].

[17] P. Huet and E. Sather, "Electroweak baryogenesis and standard model CP violation," *Phys.Rev.* **D51** (1995) 379–394, arXiv:hep-ph/9404302 [hep-ph].

[18] **DELPHI Collaboration** Collaboration, P. Abreu *et al.*, "A Precision measurement of the average lifetime of B hadrons," *Z.Phys.* **C63** (1994) 3–16.

[19] **ALEPH Collaboration** Collaboration, D. Buskulic *et al.*, "Measurement of the B_s^0 lifetime," *Phys.Lett.* **B322** (1994) 275–286.

[20] **LHCb Collaboration** Collaboration, B. Adeva *et al.*, "Roadmap for selected key measurements of LHCb," arXiv:0912.4179 [hep-ex].

[21] **LHCb Collaboration** Collaboration, R. Aaij *et al.*, "Measurement of the isospin asymmetry in $B \to K^{(*)}\mu^+\mu^-$ decays," *JHEP* **1207** (2012) 133, arXiv:1205.3422 [hep-ex].

[22] **LHCb Collaboration** Collaboration, R. Aaij *et al.*, "Evidence for CP violation in time-integrated $D^0 \to h^-h^+$ decay rates," *Phys.Rev.Lett.* **108** (2012) 111602, arXiv:1112.0938 [hep-ex].

[23] M. E. Peskin and D. V. Schroeder, *An Introduction to quantum field theory*. Westview Press, 1995.

[24] J. D. Bjorken and S. D. Drell, "Relativistic quantum fields,".

[25] R. Mertig, M. Bohm, and A. Denner, "FEYN CALC: Computer algebraic calculation of Feynman amplitudes," *Comput.Phys.Commun.* **64** (1991) 345–359.

[26] W. H. Press, S. A. Teukolsky, W. T. Vetterling, and B. P. Flannery, *Numerical Recipes 3rd Edition: The Art of Scientific Computing*. Cambridge University Press, 3 ed., 2007.

[27] N. Cabibbo, "Unitary Symmetry and Leptonic Decays," *Phys.Rev.Lett.* **10** (1963) 531–533.

[28] M. Kobayashi and T. Maskawa, "CP Violation in the Renormalizable Theory of Weak Interaction," *Prog.Theor.Phys.* **49** (1973) 652–657.

[29] S. Glashow, J. Iliopoulos, and L. Maiani, "Weak Interactions with Lepton-Hadron Symmetry," *Phys.Rev.* **D2** (1970) 1285–1292.

[30] L.-L. Chau and W.-Y. Keung, "Comments on the Parametrization of the Kobayashi-Maskawa Matrix," *Phys.Rev.Lett.* **53** (1984) 1802.

[31] L. Wolfenstein, "Parametrization of the Kobayashi-Maskawa Matrix," *Phys.Rev.Lett.* **51** (1983) 1945.

[32] A. J. Buras, M. E. Lautenbacher, and G. Ostermaier, "Waiting for the top quark mass, $K^+ \to \pi^+ \nu\bar{\nu}$, B_s^0-$\bar{B}_s^0$ mixing and CP asymmetries in B decays," *Phys.Rev.* **D50** (1994) 3433–3446, arXiv:hep-ph/9403384 [hep-ph].

[33] N. Bogoliubov and O. a. Parasiuk, "On the Multiplication of the causal function in the quantum theory of fields," *Acta Math.* **97** (1957) 227–266.

[34] K. Hepp, "Proof of the Bogolyubov-Parasiuk theorem on renormalization," *Commun.Math.Phys.* **2** no. 1, (1966) 301–326.

[35] W. Zimmermann, "Convergence of Bogolyubov's method of renormalization in momentum space," *Commun.Math.Phys.* **15** no. 3, (1969) 208–234.

[36] G. 't Hooft and M. Veltman, "Regularization and Renormalization of Gauge Fields," *Nucl.Phys.* **B44** (1972) 189–213.

[37] S. L. Adler, "Axial vector vertex in spinor electrodynamics," *Phys.Rev.* **177** (1969) 2426–2438.

[38] J. Bell and R. Jackiw, "A PCAC puzzle: $\pi^0 \to \gamma\gamma$ in the σ model," *Nuovo Cim.* **A60** (1969) 47–61.

[39] S. L. Adler, J. C. Collins, and A. Duncan, "Energy-Momentum-Tensor Trace Anomaly in Spin 1/2 Quantum Electrodynamics," *Phys.Rev.* **D15** (1977) 1712.

[40] J. C. Collins, A. Duncan, and S. D. Joglekar, "Trace and Dilatation Anomalies in Gauge Theories," *Phys.Rev.* **D16** (1977) 438–449.

[41] T. Muta, *Foundations of quantum chromodynamics: An Introduction to perturbative methods in gauge theories*, vol. 5 of *World scientific lecture notes in physics*. World Scientific, 1987.

[42] M. Beneke, T. Feldmann, and D. Seidel, "Systematic approach to exclusive $B \to V l^+ l^-, V\gamma$ decays," *Nucl.Phys.* **B612** (2001) 25–58, arXiv:hep-ph/0106067 [hep-ph].

[43] A. Pich, "Effective field theory: Course," arXiv:hep-ph/9806303 [hep-ph].

[44] G. Buchalla, A. J. Buras, and M. E. Lautenbacher, "Weak decays beyond leading logarithms," *Rev.Mod.Phys.* **68** (1996) 1125–1144, arXiv:hep-ph/9512380 [hep-ph].

[45] K. G. Chetyrkin, M. Misiak, and M. Munz, "Weak radiative B meson decay beyond leading logarithms," *Phys.Lett.* **B400** (1997) 206–219, arXiv:hep-ph/9612313 [hep-ph].

[46] P. Breitenlohner and D. Maison, "Dimensional Renormalization and the Action Principle," *Commun.Math.Phys.* **52** (1977) 11–38.

[47] M. S. Chanowitz, M. Furman, and I. Hinchliffe, "The Axial Current in Dimensional Regularization," *Nucl.Phys.* **B159** (1979) 225.

[48] M. Misiak, "The $b \to s e^+ e^-$ and $b \to s\gamma$ decays with next-to-leading logarithmic QCD corrections," *Nucl.Phys.* **B393** (1993) 23–45.

[49] M. Ciuchini, E. Franco, G. Martinelli, L. Reina, and L. Silvestrini, "Scheme independence of the effective Hamiltonian for $b \to s\gamma$ and $b \to sg$ decays," *Phys.Lett.* **B316** (1993) 127–136, arXiv:hep-ph/9307364 [hep-ph].

[50] B. Grinstein, M. J. Savage, and M. B. Wise, "$B \to X(s) e^+ e^-$ in the Six Quark Model," *Nucl.Phys.* **B319** (1989) 271–290.

[51] T. Feldmann and J. Matias, "Forward backward and isospin asymmetry for $B \to K^* l^+ l^-$ decay in the standard model and in supersymmetry," *JHEP* **0301** (2003) 074, arXiv:hep-ph/0212158 [hep-ph].

[52] A. Denner, "Techniques for calculation of electroweak radiative corrections at the one loop level and results for W physics at LEP-200," *Fortsch.Phys.* **41** (1993) 307–420, arXiv:0709.1075 [hep-ph].

[53] M. Czakon, U. Haisch, and M. Misiak, "Four-Loop Anomalous Dimensions for Radiative Flavour-Changing Decays," *JHEP* **0703** (2007) 008, arXiv:hep-ph/0612329 [hep-ph].

[54] C. Bobeth, M. Misiak, and J. Urban, "Photonic penguins at two loops and m_t dependence of $BR[B \to X_s l^+ l^-]$," *Nucl.Phys.* **B574** (2000) 291–330, arXiv:hep-ph/9910220 [hep-ph].

[55] M. Misiak and M. Steinhauser, "Three loop matching of the dipole operators for $b \to s\gamma$ and $b \to sg$," *Nucl.Phys.* **B683** (2004) 277–305, arXiv:hep-ph/0401041 [hep-ph].

[56] K. Wilson and W. Zimmermann, "Operator product expansions and composite field operators in the general framework of quantum field theory," *Commun.Math.Phys.* **24** (1972) 87–106.

[57] K. Chetyrkin, F. Tkachov, and S. Gorishnii, "Operator product expansion in the minimal subtraction scheme," *Phys.Lett.* **B119** (1982) 407–411.

[58] F. Dyson, "The S matrix in quantum electrodynamics," *Phys.Rev.* **75** (1949) 1736–1755.

[59] J. S. Schwinger, "On the Green's functions of quantized fields. 1.," *Proc.Nat.Acad.Sci.* **37** (1951) 452–455.

[60] J. S. Schwinger, "On the Green's functions of quantized fields. 2.," *Proc.Nat.Acad.Sci.* **37** (1951) 455–459.

[61] G. Wick, "The Evaluation of the Collision Matrix," *Phys.Rev.* **80** (1950) 268–272.

[62] W. Zimmermann, "Local operator products and renormalization in quantum field theory," in *Lectures on Elementary Particles and Quantum Field Theory*, S. Deser, M. Grisaru, and Hugh, eds., vol. 1. MIT Press, 1970.

[63] R. Gastmans and R. Meuldermans, "Dimensional regularization of the infrared problem," *Nucl.Phys.* **B63** (1973) 277–284.

[64] K. Chetyrkin, "Infrared R*-operation and operator product expansion in the minimal subtraction scheme," *Phys.Lett.* **B126** no. 5, (1983) 371–375.

[65] K. Chetyrkin and V. A. Smirnov, "R*-Operator corrected," *Phys.Lett.* **B144** (1984) 419–424.

[66] T. Kinoshita, "Mass singularities of Feynman amplitudes," *J.Math.Phys.* **3** (1962) 650–677.

[67] T. Lee and M. Nauenberg, "Degenerate Systems and Mass Singularities," *Phys.Rev.* **133** (1964) B1549–B1562.

[68] J. C. Collins, D. E. Soper, and G. F. Sterman, "Factorization of Hard Processes in QCD," *Adv.Ser.Direct.High Energy Phys.* **5** (1988) 1–91, arXiv:hep-ph/0409313 [hep-ph].

[69] C. W. Bernard, A. Duncan, J. LoSecco, and S. Weinberg, "Exact Spectral Function Sum Rules," *Phys.Rev.* **D12** (1975) 792.

[70] P. Ball, V. M. Braun, Y. Koike, and K. Tanaka, "Higher twist distribution amplitudes of vector mesons in QCD: Formalism and twist - three distributions," *Nucl.Phys.* **B529** (1998) 323–382, arXiv:hep-ph/9802299 [hep-ph].

[71] H. Lehmann, K. Symanzik, and W. Zimmermann, "On the formulation of quantized field theories," *Nuovo Cim.* **1** (1955) 205–225.

[72] V. M. Braun, A. Khodjamirian, and M. Maul, "Pion form-factor in QCD at intermediate momentum transfers," *Phys.Rev.* **D61** (2000) 073004, arXiv:hep-ph/9907495 [hep-ph].

[73] V. Braun, G. Korchemsky, and D. Müller, "The Uses of conformal symmetry in QCD," *Prog.Part.Nucl.Phys.* **51** (2003) 311–398, arXiv:hep-ph/0306057 [hep-ph].

[74] D. J. Gross and S. Treiman, "Light cone structure of current commutators in the gluon quark model," *Phys.Rev.* **D4** (1971) 1059–1072.

[75] P. Ball and V. M. Braun, "Exclusive semileptonic and rare B meson decays in QCD," *Phys.Rev.* **D58** (1998) 094016, arXiv:hep-ph/9805422 [hep-ph].

[76] I. Balitsky and V. M. Braun, "Evolution Equations for QCD String Operators," *Nucl.Phys.* **B311** (1989) 541–584.

[77] A. Khodjamirian, G. Stoll, and D. Wyler, "Calculation of long distance effects in exclusive weak radiative decays of B meson," *Phys.Lett.* **B358** (1995) 129–138, arXiv:hep-ph/9506242 [hep-ph].

[78] A. Ali and V. M. Braun, "Estimates of the weak annihilation contributions to the decays $B \to \rho + \gamma$ and $B \to \omega + \gamma$," *Phys.Lett.* **B359** (1995) 223–235, arXiv:hep-ph/9506248 [hep-ph].

[79] A. Khodjamirian and D. Wyler, "Counting contact terms in $B \to V\gamma$ decays," arXiv:hep-ph/0111249 [hep-ph].

[80] P. Ball and V. M. Braun, "The Rho meson light cone distribution amplitudes of leading twist revisited," *Phys.Rev.* **D54** (1996) 2182–2193, arXiv:hep-ph/9602323 [hep-ph].

[81] P. Ball and R. Zwicky, "$B_{d,s} \to \rho, \omega, K^*, \phi$ decay form-factors from light-cone sum rules revisited," *Phys.Rev.* **D71** (2005) 014029, arXiv:hep-ph/0412079 [hep-ph].

[82] V. Chernyak and A. Zhitnitsky, "Asymptotic Behavior of Exclusive Processes in QCD," *Phys.Rept.* **112** (1984) 173.

[83] M. Abramowitz and I. Stegun, eds., *Handbook of Mathematical Functions with Formulas, Graphs, and Mathematical Tables*. Dover Publications, 1964.

[84] A. L. Kagan and M. Neubert, "Isospin breaking in $B \to K^*\gamma$ decays," *Phys.Lett.* **B539** (2002) 227–234, arXiv:hep-ph/0110078 [hep-ph].

[85] P. Ball, V. Braun, and A. Lenz, "Twist-4 distribution amplitudes of the K^* and ϕ mesons in QCD," *JHEP* **0708** (2007) 090, arXiv:0707.1201 [hep-ph].

[86] M. A. Shifman, A. Vainshtein, and V. I. Zakharov, "QCD and Resonance Physics. Sum Rules," *Nucl.Phys.* **B147** (1979) 385–447.

[87] M. A. Shifman, A. Vainshtein, and V. I. Zakharov, "QCD and Resonance Physics: Applications," *Nucl.Phys.* **B147** (1979) 448–518.

[88] G. 't Hooft and M. Veltman, "Scalar One Loop Integrals," *Nucl.Phys.* **B153** (1979) 365–401.

[89] G. Källén, "On the definition of the Renormalization Constants in Quantum Electrodynamics," *Helv.Phys.Acta* **25** (1952) 417.

[90] H. Lehmann, "On the Properties of propagation functions and renormalization contants of quantized fields," *Nuovo Cim.* **11** (1954) 342–357.

[91] R. Cutkosky, "Singularities and discontinuities of Feynman amplitudes," *J.Math.Phys.* **1** (1960) 429–433.

[92] J. Lyon and R. Zwicky, "Isospin asymmetries in $B \to (K^*, \rho)\gamma/l^+l^-$ and $B \to Kl^+l^-$ in and beyond the Standard Model," arXiv:1305.4797 [hep-ph].

[93] P. Ball and R. Zwicky, "New results on $B \to \pi, K, \eta$ decay formfactors from light-cone sum rules," *Phys.Rev.* **D71** (2005) 014015, arXiv:hep-ph/0406232 [hep-ph].

[94] J. Lyon and R. Zwicky, "Anomalously large $\mathcal{O}_8$ and long-distance chirality from $A_{\rm CP}[D^0 \to (\rho^0, \omega)\gamma](t)$," arXiv:1210.6546 [hep-ph].

[95] J. Lyon and R. Zwicky, "Long distance charm loops in $B \to Vl^+l^-$ and $B \to V\gamma$,". In preparation.

[96] N. Isgur and M. B. Wise, "Relationship between form factors in Semileptonic $\bar{B}$ and D decays and exclusive rare $\bar{B}$-meson decays," *Phys.Rev.* **D42** (1990) 2388–2391.

[97] J. Charles, A. Le Yaouanc, L. Oliver, O. Pene, and J. Raynal, "Heavy to light form-factors in the heavy mass to large energy limit of QCD," *Phys.Rev.* **D60** (1999) 014001, arXiv:hep-ph/9812358 [hep-ph].

[98] W. Altmannshofer, P. Ball, A. Bharucha, A. J. Buras, D. M. Straub, and others "Symmetries and Asymmetries of $B \to K^* \mu^+ \mu^-$ Decays in the Standard Model and Beyond," *JHEP* **0901** (2009) 019, arXiv:0811.1214 [hep-ph].

[99] J. Matias, F. Mescia, M. Ramon, and J. Virto, "Complete Anatomy of $\bar{B}_d \to \bar{K}^{*0}(\to K\pi) l^+ l^-$ and its angular distribution," *JHEP* **1204** (2012) 104, arXiv:1202.4266 [hep-ph].

[100] S. Descotes-Genon, J. Matias, M. Ramon, and J. Virto, "Implications from clean observables for the binned analysis of $B \to K^* \mu^+ \mu^-$ at large recoil," *JHEP* **1301** (2013) 048, arXiv:1207.2753 [hep-ph].

[101] A. Ali, V. M. Braun, and H. Simma, "Exclusive radiative B decays in the light cone QCD sum rule approach," *Z.Phys.* **C63** (1994) 437–454, arXiv:hep-ph/9401277 [hep-ph].

[102] M. Gell-Mann, R. Oakes, and B. Renner, "Behavior of current divergences under $SU_3 \times SU_3$," *Phys.Rev.* **175** (1968) 2195–2199.

[103] M. Dimou, J. Lyon, and R. Zwicky, "Exclusive Chromomagnetism in heavy-to-light FCNCs," *Phys.Rev.* **D87** (2013) 074008, arXiv:1212.2242 [hep-ph].

[104] H. Asatrian, H. Asatrian, C. Greub, and M. Walker, "Two loop virtual corrections to $B \to X(s) l^+ l^-$ in the standard model," *Phys.Lett.* **B507** (2001) 162–172, arXiv:hep-ph/0103087 [hep-ph].

[105] P. Colangelo and A. Khodjamirian, "QCD sum rules, a modern perspective," arXiv:hep-ph/0010175 [hep-ph].

[106] A. Khodjamirian, "$B \to \pi\pi$ decay in QCD," *Nucl.Phys.* **B605** (2001) 558–578, arXiv:hep-ph/0012271 [hep-ph].

[107] A. V. Smilga and M. A. Shifman, "Procedure of unitary Borelization in three point sum rules of QCD (in Russian)," *Sov.J.Nucl.Phys.* **37** (1983) 958.

[108] B. Ioffe and A. V. Smilga, "Meson Widths and Form-Factors at Intermediate Momentum Transfer in Nonperturbative QCD," *Nucl.Phys.* **B216** (1983) 373.

[109] S. Mandelstam, "Determination of the pion - nucleon scattering amplitude from dispersion relations and unitarity. General theory," *Phys.Rev.* **112** (1958) 1344–1360.

[110] G. Passarino and M. Veltman, "One-loop corrections for $e^+ e^-$ annihilation into $\mu^+ \mu^-$ in the Weinberg Model," *Nucl.Phys.* **B160** (1979) 151.

[111] T. Hahn and M. Perez-Victoria, "Automatized one loop calculations in four-dimensions and D-dimensions," *Comput.Phys.Commun.* **118** (1999) 153–165, arXiv:hep-ph/9807565 [hep-ph].

[112] A. Khodjamirian, T. Mannel, M. Melcher, and B. Melic, "Annihilation effects in $B \to \pi\pi$ from QCD light-cone sum rules," *Phys.Rev.* **D72** (2005) 094012, arXiv:hep-ph/0509049 [hep-ph].

[113] R. Eden, P. Landshoff, D. Olive, and J. Polkinghorne, *The Analytic S-Matrix*. Cambridge University Press, 1966.

[114] G. Källén and A. Wightman, "The analytic properties of the vacuum expectation value of a product of three scalar local fields," *Mat.-Fys. Skr. Danske Vid. Selsk.* **1** no. 6, (1958) 1–58. http://www.ams.org/mathscinet-getitem?mr=0112619.

[115] B. Andersson, "Dispersion relations for the vertex function from local commutativity. 1. one-dimensional dispersion relations," *Commun.Math.Phys.* **25** (1972) 283–307.

[116] C. Fronsdal and R. E. Norton, "Integral representations for vertex functions," *Journal of Mathematical Physics* **5** no. 1, (1964) 100–108. http://link.aip.org/link/?JMP/5/100/1.

[117] V. Chernyak and I. Zhitnitsky, "B meson exclusive decays into baryons," *Nucl.Phys.* **B345** (1990) 137–172.

[118] M. Beneke, G. Buchalla, M. Neubert, and C. T. Sachrajda, "QCD factorization for exclusive, nonleptonic B meson decays: General arguments and the case of heavy light final states," *Nucl.Phys.* **B591** (2000) 313–418, arXiv:hep-ph/0006124 [hep-ph].

[119] E. Bagan, P. Ball, V. M. Braun, and H. G. Dosch, "QCD sum rules in the effective heavy quark theory," *Phys.Lett.* **B278** (1992) 457–464.

[120] S. W. Bosch and G. Buchalla, "The Radiative decays $B \to V\gamma$ at next-to-leading order in QCD," *Nucl.Phys.* **B621** (2002) 459–478, arXiv:hep-ph/0106081 [hep-ph].

[121] E. Bagan, P. Ball, and V. M. Braun, "Radiative corrections to the decay $B \to \pi e\nu$ and the heavy quark limit," *Phys.Lett.* **B417** (1998) 154–162, arXiv:hep-ph/9709243 [hep-ph].

[122] T. Aliev and V. Eletsky, "On Leptonic Decay Constants of Pseudoscalar D and B Mesons," *Sov.J.Nucl.Phys.* **38** (1983) 936. [*Yad.Fiz.* **38** (1983) 1537–1541].

[123] **Particle Data Group** Collaboration, J. Beringer *et al.*, "Review of Particle Physics (RPP)," *Phys.Rev.* **D86** (2012) 010001. http://pdglive.lbl.gov/.

[124] **RBC-UKQCD Collaboration** Collaboration, C. Allton *et al.*, "Physical Results from 2+1 Flavor Domain Wall QCD and SU(2) Chiral Perturbation Theory," *Phys.Rev.* **D78** (2008) 114509, arXiv:0804.0473 [hep-lat].

[125] R. Arthur, P. Boyle, D. Brommel, M. Donnellan, J. Flynn, *et al.*, "Lattice Results for Low Moments of Light Meson Distribution Amplitudes," *Phys.Rev.* **D83** (2011) 074505, arXiv:1011.5906 [hep-lat].

[126] P. Ball and R. Zwicky, "SU(3) breaking of leading-twist K and K^* distribution amplitudes: A Reprise," *Phys.Lett.* **B633** (2006) 289–297, arXiv:hep-ph/0510338 [hep-ph].

[127] P. Ball and G. Jones, "Twist-3 distribution amplitudes of K* and phi mesons," *JHEP* **0703** (2007) 069, arXiv:hep-ph/0702100 [HEP-PH].

[128] P. Ball and R. Zwicky, "$|V_{td}/V_{ts}|$ from $B \to V\gamma$," *JHEP* **0604** (2006) 046, arXiv:hep-ph/0603232 [hep-ph].

[129] P. Ball, G. W. Jones, and R. Zwicky, "$B \to V\gamma$ beyond QCD factorisation," *Phys.Rev.* **D75** (2007) 054004, arXiv:hep-ph/0612081 [hep-ph].

[130] M. Galassi, J. Davies, J. Theiler, B. Gough, G. Jungman, P. Alken, M. Booth, and F. Rossi, *GNU Scientific Library Reference Manual*. Network Theory Limited, 3 ed., 2009. http://www.gnu.org/software/gsl/.

[131] A. V. Manohar and I. W. Stewart, "The Zero-Bin and Mode Factorization in Quantum Field Theory," *Phys.Rev.* **D76** (2007) 074002, arXiv:hep-ph/0605001 [hep-ph].

[132] J.-Y. Chiu, A. Jain, D. Neill, and I. Z. Rothstein, "A Formalism for the Systematic Treatment of Rapidity Logarithms in Quantum Field Theory," *JHEP* **1205** (2012) 084, arXiv:1202.0814 [hep-ph].

[133] C. Kim, A. K. Leibovich, and T. Mehen, "Nonperturbative Charming Penguin Contributions to Isospin Asymmetries in Radiative B decays," *Phys.Rev.* **D78** (2008) 054024, arXiv:0805.1735 [hep-ph].

[134] A. Khodjamirian, T. Mannel, and Y. Wang, "$B \to K\ell^+\ell^-$ decay at large hadronic recoil," *JHEP* **1302** (2013) 010, arXiv:1211.0234 [hep-ph].

[135] **CDF Collaboration** Collaboration, T. Aaltonen *et al.*, "Measurement of the difference of CP–violating asymmetries in $D^0 \to K^+K^-$ and $D^0 \to \pi^+\pi^-$ decays at CDF," *Phys.Rev.Lett.* **109** (2012) 111801, arXiv:1207.2158 [hep-ex].

[136] I. I. Bigi, A. Paul, and S. Recksiegel, "Conclusions from CDF Results on CP Violation in $D^0 \to \pi^+\pi^-, K^+K^-$ and Future Tasks," *JHEP* **1106** (2011) 089, arXiv:1103.5785 [hep-ph].

[137] A. Rozanov and M. Vysotsky, "$(\Delta A_{CP})_{LHCb}$ and the fourth generation," arXiv:1111.6949 [hep-ph].

[138] H.-Y. Cheng and C.-W. Chiang, "Direct CP violation in two-body hadronic charmed meson decays," *Phys.Rev.* **D85** (2012) 034036, arXiv:1201.0785 [hep-ph].

[139] H.-n. Li, C.-D. Lu, and F.-S. Yu, "Branching ratios and direct CP asymmetries in $D \to PP$ decays," *Phys.Rev.* **D86** (2012) 036012, arXiv:1203.3120 [hep-ph].

[140] J. Brod, A. L. Kagan, and J. Zupan, "Size of direct CP violation in singly Cabibbo-suppressed D decays," *Phys.Rev.* **D86** (2012) 014023, arXiv:1111.5000 [hep-ph].

[141] B. Bhattacharya, M. Gronau, and J. L. Rosner, "CP asymmetries in singly-Cabibbo-suppressed D decays to two pseudoscalar mesons," *Phys.Rev.* **D85** (2012) 054014, arXiv:1201.2351 [hep-ph].

[142] T. Feldmann, S. Nandi, and A. Soni, "Repercussions of Flavour Symmetry Breaking on CP Violation in D-Meson Decays," *JHEP* **1206** (2012) 007, arXiv:1202.3795 [hep-ph].

[143] E. Franco, S. Mishima, and L. Silvestrini, "The Standard Model confronts CP violation in $D^0 \to \pi^+\pi^-$ and $D^0 \to K^+K^-$," *JHEP* **1205** (2012) 140, arXiv:1203.3131 [hep-ph].

[144] M. Golden and B. Grinstein, "Enhanced CP Violations in Hadronic Charm Decays," *Phys.Lett.* **B222** (1989) 501.

[145] Y. Grossman, A. L. Kagan, and J. Zupan, "Testing for new physics in singly Cabibbo suppressed D decays," *Phys.Rev.* **D85** (2012) 114036, arXiv:1204.3557 [hep-ph].

[146] **LHCb collaboration** Collaboration, R. Aaij *et al.*, "Search for direct CP violation in $D^0 \to h^-h^+$ modes using semileptonic B decays," *Phys.Lett.* **B723** (2013) 33–43, arXiv:1303.2614 [hep-ex].

[147] **Heavy Flavor Averaging Group** Collaboration, Y. Amhis *et al.*, "Averages of B-Hadron, C-Hadron, and tau-lepton properties as of early 2012," arXiv:1207.1158 [hep-ex]. http://www.slac.stanford.edu/xorg/hfag/.

[148] G. Isidori, J. F. Kamenik, Z. Ligeti, and G. Perez, "Implications of the LHCb Evidence for Charm CP Violation," *Phys.Lett.* **B711** (2012) 46–51, arXiv:1111.4987 [hep-ph].

[149] G. Isidori and J. F. Kamenik, "Shedding light on CP violation in the charm system via D to V gamma decays," *Phys.Rev.Lett.* **109** (2012) 171801, arXiv:1205.3164 [hep-ph].

[150] G. F. Giudice, G. Isidori, and P. Paradisi, "Direct CP violation in charm and flavor mixing beyond the SM," *JHEP* **1204** (2012) 060, arXiv:1201.6204 [hep-ph].

[151] C. Greub, T. Hurth, M. Misiak, and D. Wyler, "The $c \to u\gamma$ contribution to weak radiative charm decay," *Phys.Lett.* **B382** (1996) 415–420, arXiv:hep-ph/9603417 [hep-ph].

[152] G. Burdman, E. Golowich, J. L. Hewett, and S. Pakvasa, "Radiative weak decays of charm mesons," *Phys.Rev.* **D52** (1995) 6383–6399, arXiv:hep-ph/9502329 [hep-ph].

[153] G. Burdman and I. Shipsey, "D^0 - $\bar{D}^0$ mixing and rare charm decays," *Ann.Rev.Nucl.Part.Sci.* **53** (2003) 431–499, arXiv:hep-ph/0310076 [hep-ph].

[154] V. Ezhela, S. Lugovsky, and O. Zenin, "Hadronic part of the muon $g-2$ estimated on the $\sigma^{2003}_{\rm total}(e^+e^- \to \text{hadrons})$ evaluated data compilation," arXiv:hep-ph/0312114 [hep-ph].

[155] **BaBar Collaboration** Collaboration, B. Aubert *et al.*, "Direct CP, Lepton Flavor and Isospin Asymmetries in the Decays $B \to K^{(*)}\ell^+\ell^-$," *Phys.Rev.Lett.* **102** (2009) 091803, arXiv:0807.4119 [hep-ex].

[156] **BELLE Collaboration** Collaboration, J.-T. Wei *et al.*, "Measurement of the Differential Branching Fraction and Forward-Backword Asymmetry for $B \to K^* l^+ l^-$," *Phys.Rev.Lett.* **103** (2009) 171801, arXiv:0904.0770 [hep-ex].

[157] F. Mahmoudi, "SuperIso: A Program for calculating the isospin asymmetry of $B \to K^*\gamma$ in the MSSM," *Comput.Phys.Commun.* **178** (2008) 745–754, arXiv:0710.2067 [hep-ph].

[158] J. Bijnens and N. Danielsson, "Electromagnetic Corrections in Partially Quenched Chiral Perturbation Theory," *Phys.Rev.* **D75** (2007) 014505, arXiv:hep-lat/0610127 [hep-lat].

[159] R. S. Chivukula and H. Georgi, "Composite Technicolor Standard Model," *Phys.Lett.* **B188** (1987) 99.

[160] A. Buras, P. Gambino, M. Gorbahn, S. Jager, and L. Silvestrini, "Universal unitarity triangle and physics beyond the standard model," *Phys.Lett.* **B500** (2001) 161–167, arXiv:hep-ph/0007085 [hep-ph].

[161] G. D'Ambrosio, G. Giudice, G. Isidori, and A. Strumia, "Minimal flavor violation: An Effective field theory approach," *Nucl.Phys.* **B645** (2002) 155–187, arXiv:hep-ph/0207036 [hep-ph].

[162] R. Zwicky and T. Fischbacher, "On discrete Minimal Flavour Violation," *Phys.Rev.* **D80** (2009) 076009, arXiv:0908.4182 [hep-ph].

[163] M. Albrecht, T. Feldmann, and T. Mannel, "Goldstone Bosons in Effective Theories with Spontaneously Broken Flavour Symmetry," *JHEP* **1010** (2010) 089, arXiv:1002.4798 [hep-ph].

[164] A. J. Buras, "Weak Hamiltonian, CP violation and rare decays," arXiv:hep-ph/9806471 [hep-ph].

[165] P. Ball, V. Braun, and N. Kivel, "Photon distribution amplitudes in QCD," *Nucl.Phys.* **B649** (2003) 263–296, arXiv:hep-ph/0207307 [hep-ph].

[166] **Fermilab Lattice Collaboration, MILC Collaboration** Collaboration, A. Bazavov *et al.*, "B- and D-meson decay constants from three-flavor lattice QCD," *Phys.Rev.* **D85** (2012) 114506, arXiv:1112.3051 [hep-lat].

[167] H. Na, C. J. Monahan, C. T. Davies, R. Horgan, G. P. Lepage, *et al.*, "The B and B_s Meson Decay Constants from Lattice QCD," *Phys.Rev.* **D86** (2012) 034506, arXiv:1202.4914 [hep-lat].

[168] M. Misiak, "QCD corrected effective Hamiltonian for the $b \to s\gamma$ decay," *Phys.Lett.* **B269** (1991) 161–168.

[169] M. Beneke and T. Feldmann, "Symmetry breaking corrections to heavy to light B meson form-factors at large recoil," *Nucl.Phys.* **B592** (2001) 3–34, arXiv:hep-ph/0008255 [hep-ph].

[170] B. Grinstein and D. Pirjol, "Exclusive rare $B \to K^* l^+ l^-$ decays at low recoil: Controlling the long-distance effects," *Phys.Rev.* **D70** (2004) 114005, arXiv:hep-ph/0404250 [hep-ph].

[171] C. Bobeth, G. Hiller, and D. van Dyk, "The Benefits of $\bar{B} \to \bar{K}^* l^+ l^-$ Decays at Low Recoil," *JHEP* **1007** (2010) 098, arXiv:1006.5013 [hep-ph].

[172] M. Beylich, G. Buchalla, and T. Feldmann, "Theory of $B \to K^{(*)} l^+ l^-$ decays at high q^2: OPE and quark-hadron duality," *Eur.Phys.J.* **C71** (2011) 1635, arXiv:1101.5118 [hep-ph].

[173] **LHCb Collaboration** Collaboration, R. Aaij *et al.*, "First observation of the decay $B^+ \to \pi^+ \mu^+ \mu^-$," *JHEP* **1212** (2012) 125, arXiv:1210.2645 [hep-ex].

[174] **Belle Collaboration** Collaboration, N. Taniguchi *et al.*, "Measurement of branching fractions, isospin and CP-violating asymmetries for exclusive $b \to d\gamma$ modes," *Phys.Rev.Lett.* **101** (2008) 111801, arXiv:0804.4770 [hep-ex].

[175] M. Beneke, T. Feldmann, and D. Seidel, "Exclusive radiative and electroweak $b \to d$ and $b \to s$ penguin decays at NLO," *Eur.Phys.J.* **C41** (2005) 173–188, arXiv:hep-ph/0412400 [hep-ph].

[176] W. Altmannshofer, P. Paradisi, and D. M. Straub, "Model-Independent Constraints on New Physics in $b \to s$ Transitions," *JHEP* **1204** (2012) 008, arXiv:1111.1257 [hep-ph].

[177] W. Altmannshofer and D. M. Straub, "Cornering New Physics in $b \to s$ Transitions," *JHEP* **1208** (2012) 121, arXiv:1206.0273 [hep-ph].

[178] R. Fleischer and R. Knegjens, "In Pursuit of New Physics with $B_s^0 \to K^+K^-$," *Eur.Phys.J.* **C71** (2011) 1532, arXiv:1011.1096 [hep-ph].

[179] M. Ciuchini, E. Franco, S. Mishima, and L. Silvestrini, "Testing the Standard Model and Searching for New Physics with $B_d \to \pi\pi$ and $B_s \to KK$ Decays," *JHEP* **1210** (2012) 029, arXiv:1205.4948 [hep-ph].

[180] B. Bhattacharya, A. Datta, and D. London, "Reducing Penguin Pollution," *Int.J.Mod.Phys.* **A28** (2013) 1350063, arXiv:1209.1413 [hep-ph].

[181] L. Hofer, D. Scherer, and L. Vernazza, "$B_s \to \phi\rho^0$ and $B_s \to \phi\pi^0$ as a handle on isospin-violating New Physics," *JHEP* **1102** (2011) 080, arXiv:1011.6319 [hep-ph].

[182] L. Hofer and L. Vernazza, "Status of the $B \to \pi K$ puzzle and its relation to $B_s \to \phi\pi$ and $B_s \to \phi\rho$ decays," arXiv:1212.4785 [hep-ph].

[183] M. Beneke, J. Rohrer, and D. Yang, "Branching fractions, polarisation and asymmetries of $B \to VV$ decays," *Nucl.Phys.* **B774** (2007) 64–101, arXiv:hep-ph/0612290 [hep-ph].

[184] T. Inami and C. Lim, "Effects of Superheavy Quarks and Leptons in Low-Energy Weak Processes $K_L \to \mu\bar{\mu}$, $K^+ \to \pi^+\nu\bar{\nu}$ and $K^0 \leftrightarrow \bar{K}^0$," *Prog.Theor.Phys.* **65** (1981) 297.

[185] B. Grinstein, Y. Grossman, Z. Ligeti, and D. Pirjol, "The Photon polarization in $B \to X\gamma$ in the standard model," *Phys.Rev.* **D71** (2005) 011504, arXiv:hep-ph/0412019 [hep-ph].

[186] P. Ball and R. Zwicky, "Time-dependent CP Asymmetry in $B \to K^*\gamma$ as a (Quasi) Null Test of the Standard Model," *Phys.Lett.* **B642** (2006) 478–486, arXiv:hep-ph/0609037 [hep-ph].

[187] D. Atwood, M. Gronau, and A. Soni, "Mixing induced CP asymmetries in radiative B decays in and beyond the standard model," *Phys.Rev.Lett.* **79** (1997) 185–188, arXiv:hep-ph/9704272 [hep-ph].

[188] L. Okun, M. A. Shifman, A. Vainshtein, and V. I. Zakharov, "On the $K^+ \to \pi^+ e^+ e^-$ Decay," *Sov.J.Nucl.Phys.* **24** (1976) 427.

[189] A. Khodjamirian, "Form-factors of $\gamma^* \rho \to \pi$ and $\gamma^* \gamma \to \pi^0$ transitions and light cone sum rules," *Eur.Phys.J.* **C6** (1999) 477–484, arXiv:hep-ph/9712451 [hep-ph].

[190] A. Bharucha, T. Feldmann, and M. Wick, "Theoretical and Phenomenological Constraints on Form Factors for Radiative and Semi-Leptonic B-Meson Decays," *JHEP* **1009** (2010) 090, arXiv:1004.3249 [hep-ph].

[191] B. Melic, "Nonfactorizable corrections to $B \to J/\psi K$," *Phys.Rev.* **D68** (2003) 034004, arXiv:hep-ph/0303250 [hep-ph].

[192] A. Khodjamirian, R. Ruckl, G. Stoll, and D. Wyler, "QCD estimate of the long distance effect in $B \to K^* \gamma$," *Phys.Lett.* **B402** (1997) 167–177, arXiv:hep-ph/9702318 [hep-ph].

[193] A. Grozin and M. Neubert, "Asymptotics of heavy meson form-factors," *Phys.Rev.* **D55** (1997) 272–290, arXiv:hep-ph/9607366 [hep-ph].

[194] A. Khodjamirian, T. Mannel, A. Pivovarov, and Y.-M. Wang, "Charm-loop effect in $B \to K^{(*)} \ell^+ \ell^-$ and $B \to K^* \gamma$," *JHEP* **1009** (2010) 089, arXiv:1006.4945 [hep-ph].

[195] A. Khodjamirian, T. Mannel, and N. Offen, "Form-factors from light-cone sum rules with B-meson distribution amplitudes," *Phys.Rev.* **D75** (2007) 054013, arXiv:hep-ph/0611193 [hep-ph].

[196] A. Ali and C. Greub, "A Profile of the final states in $B \to X_s \gamma$ and an estimate of the branching ratio BR($B \to K^* \gamma$)," *Phys.Lett.* **B259** (1991) 182–190.

[197] F. Muheim, Y. Xie, and R. Zwicky, "Exploiting the width difference in $B_s \to \phi \gamma$," *Phys.Lett.* **B664** (2008) 174–179, arXiv:0802.0876 [hep-ph].

[198] K. Anikeev, D. Atwood, F. Azfar, S. Bailey, C. Bauer, *et al.*, "B physics at the Tevatron: Run II and beyond," arXiv:hep-ph/0201071 [hep-ph].

[199] F. Kruger and J. Matias, "Probing new physics via the transverse amplitudes of $B^0 \to K^{*0} (\to K^- \pi^+) l^+ l^-$ at large recoil," *Phys.Rev.* **D71** (2005) 094009, arXiv:hep-ph/0502060 [hep-ph].

[200] **LHCb Collaboration** Collaboration, R. Aaij *et al.*, "Differential branching fraction and angular analysis of the decay $B^0 \to K^{*0}\mu^+\mu^-$," *JHEP* **1308** (2013) 131, arXiv:1304.6325 [hep-ex].

[201] P. Ball, "Theoretical update of pseudoscalar meson distribution amplitudes of higher twist: The Nonsinglet case," *JHEP* **9901** (1999) 010, arXiv:hep-ph/9812375 [hep-ph].

[202] R. Tarrach, "The Pole Mass in Perturbative QCD," *Nucl.Phys.* **B183** (1981) 384.

[203] M. A. Shifman and M. I. Vysotsky, "Form factors of heavy mesons in QCD," *Nucl.Phys.* **B186** (1981) 475.

[204] A. Vainshtein, V. I. Zakharov, and M. A. Shifman, "Right-Handed Currents and Sum Rule Delta T=1/2 in Nonleptonic Strange Particle Decays," *JETP Lett.* **23** (1976) 602. http://www.jetpletters.ac.ru/ps/1806/article_27604.shtml.

[205] D. Zwanziger, "Nonperturbative Faddeev-Popov formula and infrared limit of QCD," *Phys.Rev.* **D69** (2004) 016002, arXiv:hep-ph/0303028 [hep-ph].

[206] V. Gribov, "Quantization of Nonabelian Gauge Theories," *Nucl.Phys.* **B139** (1978) 1.